Cost-Effective Connection Details for Highway Sign, Luminaire, and Traffic Signal Structures

AUTHORS

BUY THIS BOOK

FIND RELATED TITLES

ACKNOWLEDGMENT

COPYRIGHT INFORMATION

DISCLAIMER

THE NATIONAL ACADEMIES
Advisers to the Nation on Science, Engineering, and Medicine

The **National Academy of Sciences** is a private, nonprofit, self-perpetuating society of distinguished scholars engaged in scientific and engineering research, dedicated to the furtherance of science and technology and to their use for the general welfare. On the authority of the charter granted to it by the Congress in 1863, the Academy has a mandate that requires it to advise the federal government on scientific and technical matters. Dr. Ralph J. Cicerone is president of the National Academy of Sciences.

The **National Academy of Engineering** was established in 1964, under the charter of the National Academy of Sciences, as a parallel organization of outstanding engineers. It is autonomous in its administration and in the selection of its members, sharing with the National Academy of Sciences the responsibility for advising the federal government. The National Academy of Engineering also sponsors engineering programs aimed at meeting national needs, encourages education and research, and recognizes the superior achievements of engineers. Dr. Charles M. Vest is president of the National Academy of Engineering.

The **Institute of Medicine** was established in 1970 by the National Academy of Sciences to secure the services of eminent members of appropriate professions in the examination of policy matters pertaining to the health of the public. The Institute acts under the responsibility given to the National Academy of Sciences by its congressional charter to be an adviser to the federal government and, on its own initiative, to identify issues of medical care, research, and education. Dr. Harvey V. Fineberg is president of the Institute of Medicine.

The **National Research Council** was organized by the National Academy of Sciences in 1916 to associate the broad community of science and technology with the Academy's purposes of furthering knowledge and advising the federal government. Functioning in accordance with general policies determined by the Academy, the Council has become the principal operating agency of both the National Academy of Sciences and the National Academy of Engineering in providing services to the government, the public, and the scientific and engineering communities. The Council is administered jointly by both Academies and the Institute of Medicine. Dr. Ralph J. Cicerone and Dr. Charles M. Vest are chair and vice chair, respectively, of the National Research Council.

The **Transportation Research Board** is one of six major divisions of the National Research Council. The mission of the Transportation Research Board is to provide leadership in transportation innovation and progress through research and information exchange, conducted within a setting that is objective, interdisciplinary, and multimodal. The Board's varied activities annually engage about 7,000 engineers, scientists, and other transportation researchers and practitioners from the public and private sectors and academia, all of whom contribute their expertise in the public interest. The program is supported by state transportation departments, federal agencies including the component administrations of the U.S. Department of Transportation, and other organizations and individuals interested in the development of transportation. **www.TRB.org**

www.national-academies.org

CONTENTS

ii

FIGURES

iii

iv

v

vi

vii

ix

TABLES

ACKNOWLEDGMENTS

Several figures developed under NCHRP Project 10-70 and presented in this report have been published previously:

- *Figure 56. Fatigue cracking in specimen IX-3 from the stool stiffener to tube weld toe at the termination of the vertical stiffener on the tube wall (with stool top plate removed).* (From Roy, S., Y.C. Park, R. Sause, and J. W. Fisher. Fatigue Resistance of Pole-to-Base Plate Connections in High Level Lighting Structures. In Proceedings ASCE Structures Congress 2010, Figure 7.)

- *Figure 58. Fatigue cracking in specimen XI-6 from termination of fillet weld toe on the tube wall of both the pole-to-transverse plate weld and the backing ring top weld* (From Roy, S., Y.-Chul Park, R. Sause, and J. Fisher. Fatigue Performance of Groove-Welded Tube-to-End-Plate Connections in Highway Sign, Luminaire, and Traffic Signal Structures. In Transportation Research Record: Journal of the Transportation Research Board, No. 2152, Figure 5.)

- *Figure 59. Fatigue cracking in specimen XII-8 – A: from the stiffener to tube weld toe at the termination of the stiffener on the tube wall; and B: from the socket weld toe on the tube wall at the base. (*From Roy, S., Y.C. Park, R. Sause, and J. W. Fisher. Fatigue Resistance of Pole-to-Base Plate Connections

xiii

ABSTRACT

This report documents the results of a comprehensive experimental and analytical study that evaluated fatigue performance of several critical welded connections in the highway sign, signal and high-level luminaire support structures. In this study, infinite life fatigue resistance of connection details in the existing inventory was established and new cost-effective fatigue resistant connections were developed. About 80 full size galvanized specimens of sign, signal and high-level luminaire support structures containing different welded connections were fatigue tested. Using parametric Finite Element Analyses (FEA) of 3D models verified by test data, fatigue performance of the connections in both finite and infinite life regimes were defined in terms of fatigue stress concentration factors over the range of applicable geometric dimensions. The study demonstrated that tube-to-transverse plate connections are the most fatigue critical details in the subject structures. Increasing the stiffness of the transverse plate is the most cost-effective means of improving fatigue resistance of this connection. Groove welded connections with smaller opening in the plate exhibits largest fatigue resistance. Sharper bend radius and less number of sides reduce fatigue threshold of connections in multi-sided sections. Based on these research findings, new specification recommendations were proposed for revision to the existing AASHTO specifications.

EXECUTIVE SUMMARY

Cost-effective fatigue resistant connections (details) for cantilevered highway sign, luminaire and traffic signal support (tubular) structures were developed by experimental and analytical research. Finite and infinite life resistances were established by fatigue testing of full-scale galvanized specimens. Effects of critical connection geometric parameters were determined and fatigue design provisions were developed by parametric Finite Element Analyses (FEA), verified by test data.

The fatigue resistance of connections in the subject structures depends on the geometry and in particular the relative flexibility of the components at the connection. Cross section shape, weld configuration, and weld profile have significant effects on the fatigue resistance. The existing *AASHTO Specification for Highway Signs, Luminaire and Traffic Signal Support Structures* does not recognize these effects, and specify inaccurate fatigue resistance. Implementation of the research results would enable safe and economic design of these structures.

Tube-to-transverse plate connections are the most fatigue critical details. Most of the reported fatigue cracking in service has been at unstiffened fillet-welded tube-to-transverse plate connections (socket connection), when a thin plate with a few discrete fasteners at a larger bolt circle was used. Increasing the plate thickness is often a cost-effective means of increasing the fatigue resistance. A minimum plate thickness of 2 in (51 mm) should be used. In larger diameter tubes, the thickness of transverse plate required to achieve the desired fatigue resistance may not be feasible. In such situations, a groove-welded tube-to-transverse plate connection or a stiffened connection should be explored.

Unstiffened full-penetration groove-welded tube-to-transverse plate connections often provide the most cost-effective design. A reduced opening in the transverse plate, in addition to increased plate thickness, reduces the transverse plate flexibility and increases the fatigue resistance. The opening size should be sufficient for draining liquid zinc during galvanizing and depositing the weld at the top of backing ring, if used. When the backing ring is welded to the tube, it provides a redundant load path after the tube to transverse plate weld develops fatigue cracking. However, fatigue cracking at the backing ring-to-tube weld is possible and therefore, this weld should specified and inspected as a structural weld. An adequately designed groove-welded connection can provide a constant amplitude fatigue threshold (CAFT) of 10.0 ksi (69 MPa), i.e., of AASHTO Category C. The existing specification defines the CAFT of this connection as 4.5 ksi (31 MPa), i.e., of AASHTO Category E.

In support structures employing larger diameter and thicker tubes, optimized stiffened tube-to-transverse plate fillet-welded connections often provide a cost-effective design. Fillet-welded tapered stiffeners with a wrapped-around weld at the terminus on the tube are cost-effective. A large stiffener thickness relative to the tube wall increases distortion of the tube and the potential for fatigue cracking at the stiffener terminus. A stiffener that is too thin or too short does not sufficiently reduce the stress at the tube-to-transverse plate weld. A ratio of stiffener thickness to tube thickness of 1.25 and a ratio of stiffener height to stiffener spacing of 1.6 were found to be optimum. A stiffener termination angle of 15^0 ensures the stiffener sections are fully effective in sharing load. An adequately designed stiffened tube-to-transverse plate fillet-welded

1

connection can provide a CAFT of 7.0 ksi (48 MPa), i.e., of AASHTO Category D. The existing specification defines the CAFT of this connection as 2.6 ksi (18 MPa), i.e., of AASHTO Category E´.

Fatigue cracking in multi-sided tube-to-transverse plate connections initiates at the bend corners due to higher stress concentration. With fewer sides and sharper bend corners, the stress concentration increases, reducing the CAFT of connections in multi-sided sections. A minimum of eight sides and 1 in (25 mm) bend radius should be used for multi-sided tubular structures.

Fatigue cracking can initiate from the edge of unreinforced handholes in sign/signal support structures. For reinforced handholes, fatigue cracking can initiate both from the root and the toe of the handhole frame-to-pole fillet-weld. Since the fatigue stress cycles in sign/signal support structures are primarily due to wind induced galloping oscillations in the plane containing the arm, handholes and other cutouts in these structures should be located in a low stressed area on the side normal to that containing the arm. The width of the handhole should be limited to 40% of the tube diameter.

Fillet-welded gusseted boxes or the ring-stiffened boxes at the mast-arm-to-pole connections did not develop any fatigue cracking in the tests. For all specimens fatigue cracking occurred at other critical details in the structure. Accordingly, standard details are proposed for these connections. For box connections, the width of the box should be the same as the diameter of the pole (i.e., the sides of the box are tangent to the sides of the pole). Ring-stiffened box connections are more fabrication intensive and should be employed in geographic regions where support structures are expected to experience significant wind induced oscillations. In other regions, gusseted-box connections are expected to provide satisfactory performance.

Fillet-welds for tube-to-transverse plate connections were specified as unequal leg welds, with the long leg at approximately 30º to the tube. Significant scatter was observed in the test results, which could be partially attributed to the variation in the fabricated weld profile. The weld geometry should be tightly controlled to reduce the scatter in fatigue performance of tube-to-transverse plate connections.

Detailed analytical and experimental protocols were developed for reliably and consistently assessing the fatigue resistance of tubular connections in the subject structures. A point measure of maximum principal stress on the tube surface ahead of the weld toe can adequately capture the geometric contribution of the components at a connection ("geometric stress"). The stress at a rounded weld toe captures the local effects of the weld toe notch and is appropriate for infinite life design ("notch stress").

Based on this research, recommendations are proposed for revision to *Chapter 11: Fatigue Design* of the existing *AASHTO Specification for Highway Signs, Luminaire and Traffic Signal Support Structures, 5th Edition*. The proposed specification provisions maintain infinite life design of new structures, and introduce finite life assessment of existing structures. The fatigue design provisions consider weld configuration, connection geometric parameters and cross-section shape. 3D sketches of the example connections identify the details and potential crack locations. The provisions retain the nominal stress based design philosophy and introduce detailed guidelines for computing nominal stress. The proposed specification also tabulates the details and fatigue resistances of specimens tested, which can be directly used for many new designs.

2

CHAPTER 1

INTRODUCTION AND RESEARCH APPROACH

PROBLEM STATEMENT

Over the past two decades, wind induced fatigue cracking of highway sign, luminaire and traffic signal support structures has been increasingly reported all over the United States. While fatalities associated with these failures have been limited, the nuisance of dealing with a large number of fatigue cracks in the sheer volume of these structures in the national inventory and the cost of inspecting, repairing and/or replacing the cracked structures have been substantial. As such, reliable assessment of fatigue performance of these structures and improved cost-effective design of fatigue critical details in these structures are of great importance.

Depending on their function and structural configuration, these support structures can be primarily divided into two groups: structures supporting high-level luminaires; and structures supporting highway signs and signals. Most of the highway sign, luminaire and traffic signal support structures are cantilevers. Compared to a bridge type sign or signal structure, the cantilevered structural configuration is desirable because it is cheaper, reduces the probability of vehicle collision with the vertical support member, and reduces clutter at an intersection. Accordingly, the span of signal structures has increased over the years to span across wider highways with increased number of lanes and to provide a greater setback distance. The high-level luminaires are generally used to illuminate larger areas adjacent to highways, such as interchanges and rest areas. The height of the pole structures supporting these luminaires has also increased significantly over the last couple of decades to provide illumination of larger areas with fewer structures. In service fatigue cracking has been mostly reported in the cantilevered support structures.

The cantilevered sign/signal and high-level luminaire support structures both have a single vertical column member (referred to as an upright, post, or pole). The sign/signal structures also include a horizontal member which is either a cantilevered beam (known as mast arm) or a cantilevered truss. The members are joined together by bolted connection between plates welded to the arm and the pole, or by direct welded connections. The members are usually built from thin-walled hollow shapes (i.e., tubes) of round or multi-sided cross section, rendering them extremely light weight as required for large spans. This, however, also makes these structures extremely flexible with a fundamental natural frequency of about 1.0 Hz. Damping in these steel structures is usually less than 1% of critical. As a result of their dynamic characteristics and cross-sectional shape, cantilevered support structures experience large-amplitude and long duration vibrations owing to wind induced aero-elastic effects such as galloping and vortex shedding, in addition to aerodynamic vibrations due to natural gusts and truck induced gusts. The vibrations can impart cycles of fatigue damage to the various welded connections in these structures. Most of the fatigue cracking in service has been reported from the weld toe on the tube either at the pole-to-base-plate connection, or the mast-arm-to-transverse plate connection. In addition fatigue cracking has been reported in handhole frame-to-pole

3

connection and the gusset-to-pole junction in the mast-arm-to-pole connection, also initiating at the weld toe.

Fatigue cracking at the weld toe precipitates from the existing stress concentration due to the weld bead geometry, presence of crack-like slag inclusion micro discontinuities that act as initial flaws, and high tensile residual stress inherent to the welding process, which promotes crack propagation. The primary load carrying mechanism in these thin tubular structures is in-plane membrane stresses. At a tube-to transverse plate connection or a tube-to-tube connection, however, compatibility requirements introduce out of plane flexural deformation that translates into out-of-plane stresses through the thickness of the tube wall. The superposition of large out-of-plane flexural stress on the in-plane membrane stress magnifies the local stress on the tube surface near the tube-to-plate junction. The out-of-plane deformation is further magnified by the deformation of the flexible base plate and discrete fastener locations. This boundary effect associated with the structure geometry, however, attenuates rapidly and the in-plane membrane stresses dominate in the rest of the structure.

In response to fatigue failure of sign, signal and luminaire support structures in the early 1990s, NCHRP Project 10-38: *Fatigue-Resistant Design of Cantilevered Signal, Sign and Light Supports* (*1*) was conducted, the findings of which were introduced as a new chapter — *Section 11: Fatigue Design* in the *AASHTO Standard Specification for Structural Supports for Highway Signs, Luminaires, and Traffic Signals, 4th Edition, 2001*. In Table 11-2 of this specification, the fatigue categories of typical connection details in the subject structures are defined. These fatigue design provisions are deemed to be either unrealistic or too stringent to be cost effective. One reason for this skepticism is that although some connection details in high-level (pole type) luminaire structures and cantilevered sign and traffic signal structures in the existing inventory have experienced fatigue cracking, others that do not meet the fatigue design provisions, are functioning satisfactorily. Another reason is the lack of conformity between the recommended fatigue categories for some details and the limited fatigue test data that were obtained after publication of the specification.

When the 2001 AASHTO Specification was prepared, very little fatigue test data was available for the various connection details in the cantilevered sign, signal and luminaire structures. Published large scale fatigue test data were available only for pole-to-base-plate and mast-arm-to-flange-plate socket connections (*2*), and for anchor bolts. NCHRP project 10-38 (*1*) focused on developing the fatigue design loads due to wind induced phenomenon and calibrating the load model. In addition, substantial research was carried out regarding fatigue performance of anchor bolts. Accordingly, the recommendations for other types of details were extrapolated from the provisions for: (1) the attachment details in the *AASHTO LRFD Bridge Design Specification*; (2) the tubular structure details in *AWS D1.1: Structural Welding Code – Steel*; and (3) similar structural details in the *Eurocode*. These provisions did not consider the out-of-plane deformation associated with the connection geometry and as such, nonconformities were noted between the recommended fatigue categories and the limited test results for some details (*3, 4*) that were obtained after publication of the specification.

To resolve the discrepancies, the National Cooperative Highway Research Program (NCHRP) initiated a research program NCHRP Project 10-70: *Cost Effective Connection Details for Highway Sign, Luminaire and Traffic Signal Structures*, which was performed by the ATLSS Engineering Research Center, Lehigh University.

4

OBJECTIVES

The objectives of the research project were as follows:

1) to develop protocols for reliably and consistently assessing the fatigue performance of connection details for high-level (pole type) luminaire and for cantilever (sign and traffic signal) structures,

2) to use the protocols for establishing the fatigue stress category of existing, retrofitted, and new cost effective connection details, and

3) to recommend revisions to the *AASHSTO Standard Specification for Structural Supports for Highway Signs, Luminaires, and Traffic Signals, 4th Edition* implementing the findings of the project

During the execution of this project, the 5th Edition of the AASHTO specification was published in 2009. Revisions based on the findings of NCHRP Project 10-70 were recommended to this edition of the specification.

RESEARCH APPROACH

To achieve the project objectives a research plan was developed with twelve primary tasks based on the guidelines provided in the NCHRP Request for Proposal (RFP). These tasks are summarized as follows.

Review of Connection Details

This task comprised reviewing connection details, performance data, existing specifications, research findings, and other information related to the cantilevered sign, signal and luminaire structures. This information was assembled from foreign and domestic technical literature and from unpublished experiences of engineers, owners, and manufacturers, and ongoing research. Special attention was paid to the available information on actual field performance of various connection details and to the identification of connection details that are in use but not included in the existing specification. This task contained three subtasks namely, literature review, survey of state *Departments of Transportation (DOT)* and other concerned agencies, and survey of manufacturers.

Identify Critical Parameters

Based on the literature review, analysis of survey results, review of research findings, and comparison of various specification recommendations accomplished in the previous task, and the understanding of the behavior and response of the subject structures in general, the critical parameters that influence the fatigue performance of the various connection details were identified.

Review of the Specification

Chapters 10 and 11 of the AASHTO specification were reviewed with respect to the information assembled in the previous tasks and deficiencies of the specifications that need to be addressed through further research were identified.

Develop Analytical and Experimental Protocols

Analytical and experimental protocols were prepared for reliably and consistently assessing fatigue performance of connection details in the subject structures. These protocols were validated by conducting analytical and experimental studies on full size specimens.

Conduct Analytical and Experimental Studies

Detailed analytical and experimental studies were carried out to develop cost-effective connection details in the subject structures and to establish their fatigue resistance. Seventy eight full size galvanized specimens of sign, signal and high-level luminaire support structures containing different welded connections were fatigue tested. In addition, fatigue performance of jacket retrofitted luminaire support structures was evaluated. Using parametric Finite Element Analyses (FEA) verified by test data, the fatigue performance of connections in both the finite and infinite life regimes was evaluated, optimized and extended over a practical range of geometric dimensions. Stress concentration equations involving the critical geometric parameters of a connection were developed for characterizing the fatigue performance of tube-to-transverse plate connections.

Develop Specification Recommendations and Commentary

Based on the research findings, a draft specification recommendation and commentary was developed and submitted for review by the AASHTO technical committee T-12: Structural Supports for Signs, Luminaires, and Traffic Signals.

SCOPE OF STUDY

The study reported herein pertains to cantilevered support structures for signs, signals and high-level luminaires that are used around highways. Only galvanized steel structures were considered as part of this study. This research mostly focused on developing cost-effective fatigue resistant designs of typical connections in the subject structures, rather than establishing the fatigue resistance of existing designs in the inventory, which exhibited less than desirable fatigue performance. All proprietary connection details such as scalloped collar, U-rib stiffeners etc, were excluded. Similarly, enhancement of fatigue resistance by post-weld treatments was excluded, including the proprietary Ultrasonic Impact Treatment (UIT).

6

CHAPTER 2

FINDINGS

REVIEW OF CONNECTION DETAILS

Literature Review

An extensive review of literature obtained from both domestic and foreign sources was carried out. Published and unpublished documents on fatigue performance of cantilevered sign, luminaire and traffic signal structures including recently completed/ongoing research and field investigations were collected and reviewed. A large number of references were available on dynamic wind-structure interaction, structural response characteristics, and assessment of loads causing fatigue in the subject structures. In view of the project objectives, however, the literature review was limited to the fatigue resistance of the relevant connection details. Publications on fatigue performance of tubular offshore structures, which are geometrically similar to the subject structures, and relevant specifications/design guides by organizations such as, American Welding Society (*AWS D1.1: Structural Welding Code – Steel, 2006*), American Petroleum Institute (*API RP 2A: Recommended Practice for Planning, Designing and Constructing Fixed Offshore Platforms, 19th Edition, 1991*), American Bureau of Shipping (*ABS Guide for the Fatigue Assessment of Offshore Structures, 2003*), Det Norske Veritas (*DNV-RP-C203: Fatigue Design of Offshore Steel Structures, 2005*), International Institute of Welding (*5*), European Committee for Standardisation (*Eurocode3: Design of Steel Structure — Part 1–9: Fatigue*), and Comité International pour le Développement et l'Etude de la Construction Tubulaire (*6*) were reviewed.

When this research project was initiated only limited published fatigue test results were available for a handful connection details in the subject structures. These tests were conducted in the United States and in Japan. No information could be found on fatigue test of the subject structures from Europe and other parts of the world. Fatigue tests in the United States were mostly conducted on full scale specimens and were reported by Fisher et al. (*2*), Alderson (*7*), Deschamp (*8*), Koenigs et al. (*3*) and Ocel et al. (*4*). Tests on tube-to-flange connection details on relatively small scale specimens were reported by South (*9*). Tests in Japan were conducted mostly on small scale specimens (*10, 11*). Another set of tests on tube to flange connection details were conducted by Archer and Gurney in the UK (*12*). Additional unpublished fatigue test results on full-size specimens were obtained from a major manufacturer of the subject structures in the United States.

Dimensions of the full-scale specimens that were tested in the United States were representative of typical sign, signal, and street light support structures used in different states. For example, Fisher et al. (*2*) conducted tests on round steel light pole structures used in California; Alderson (*7*) conducted tests on round signal pole structures used in Missouri; Deschamp (*8*) conducted tests on mast-arm and mast-arm-to-pole box connections in signal structures used in Wyoming; Koenigs et al. (*3*) conducted tests on round mast-arms used in Texas; and Ocel et al. (*4*) conducted tests on multi-sided signal structures used in Minnesota. Although variations existed between the details and specimen types used by these researchers,

7

the dimensions of the test structures were generally consistent for each type of cross section. Due to the large number of variables considered in some of the test programs, few replicates could be tested. As such, these test results provided very little conclusive evidence; only some general trends were noted and some of the test methods, conclusions and interpretation of results were questionable.

Nevertheless, the test results generally confirmed that the fatigue strength of fillet-welded welded tube-to-transverse plate connections (socket connections) commonly used in cantilevered sign structures were consistent with AASHTO Category E´. The socket connections in multi-sided cross section of octagonal shape exhibited fatigue resistance less than Category E´, particularly due to the stress concentration at the bend corners. Full-penetration groove-welded tube-to-transverse plate connections provided increased fatigue resistance compared to the socket connections. These connections achieved or exceeded AASHTO Category D fatigue resistance in round cross-sections and AASHTO Category E in octagonal cross-sections.

Mast-arm-to-pole connection in structures having octagonal cross section demonstrated fatigue resistance consistent with AWS Category K_2, irrespective of whether the mast-arm was connected to the pole via a mast-can or connected through a box connection (*4*). The ring-stiffened connection between the mast-arm and the pole with round tubes exhibited mixed results (*8*).

Stiffened socket connections demonstrated increased fatigue life, although the enhancement was not substantial for the stiffener configurations used (*3*, *4*). The limited experimental and analytical studies indicated that the fatigue performance of stiffened connections were dependent on the number, orientation, shape and size of the stiffeners and on the relative stiffness of the pole tube, the stiffener, and the base plate, in particular on the ratio of their thicknesses (*3*, *10*).

Increasing the thickness of the transverse plate appeared to be the most cost-effective means of improving the fatigue resistance of socket connections. This was indicated by tests conducted by Koenigs et al. (*3*), and internal tests by a fabricator on unstiffened socket connections in round tubes, and by Ocel et al (*4*) on unstiffened octagonal tube-to-transverse plate connections.

A few tube-to-transverse plate connection details, which are not currently included in the AASHTO specification, were investigated by Koenigs et al. (*3*) at the University of Texas at Austin, and by a fabricator (internal tests) as fatigue resistant cost-effective alternatives. Among the details tested at UT Austin, the performance of external collar and U-rib stiffener were noted for further evaluation. A fabricator also investigated external collar and patented a variant of it called the "scallop collar". The tests on a straight external collar at the UT Austin did not demonstrate any improvement in fatigue performance and exhibited a fatigue resistance of Category E´, the same as for unstiffened socket connections. Tests on straight external collars by the fabricator (information shared during manufacturers' survey) produced large spread in fatigue resistance ranging between Categories E and C. The reason for this scatter was attributed to large lack of fusion defects between the collars and the transverse plate and the tube walls. The tests on U-rib stiffeners at UT Austin exhibited fatigue resistance between Categories E and E´. These stiffeners are proprietary to Nippon Steel Corporation, Japan. Limited internal tests conducted on the external scallop collar by the fabricator indicated a wide scatter in fatigue resistance; two data points achieved fatigue resistance of Category C and two achieved a fatigue

8

resistance of Category B. This variability was attributed to lack of weld penetration between the collars and the transverse plate and tube walls.

Improvement of fatigue performance by post-weld Ultrasonic Impact Treatment (UIT) and pneumatic peening of the weld toe were investigated by the researchers at UT Austin, University of Minnesota and a fabricator (internal test results shared during manufacturers' survey). The level of improvement in fatigue performance by these treatment techniques is susceptible to the level of post-treatment sustained stresses and other processes such as heat treatment, including hot dipped galvanizing, which may eliminate the beneficial effect of the treatment. Substantial enhancement in fatigue performance of the fillet welded socket connections was obtained when the treatment was carried out with the weld subjected to sustained stress from permanent load.

The review of AWS specification recommendations for tubular structures revealed that these provisions were developed based on small scale test results conducted during the late 1960s and the early 1970s (*13*, *14*, *15*). The fatigue categories ET and K_2 were developed mostly based on limited test results and analytical extrapolation. The applicability of these results to the subject structures is questionable without adequate experimental verification.

The review of specifications and design guidelines from the offshore industry (API RP2A, ABS Guide, DNV-RP-C203, 5, 6) revealed that these specifications recommend using hot-spot stress design approach for tubular structures. For non-tubular structures use of S-N curves either based on nominal stress or stresses modified to include the effect of joint stress concentration is recommended. However, differences exist among these specifications regarding the definition of hot-spot stress and the lower bound design curves to be used with the hot-spot stress for assessment of fatigue resistance of a particular detail. A few publications provided formula for stress concentration factors in simple tube-to-tube connections (*16*, *17*); however, no solution was available for tube-to-transverse plate connections, which are critical for the sign, signal and high-level luminaire support structures.

Survey of State Departments of Transportation

A survey was sent to all state DOT, as well as the Federal Highway Administration (FHWA) and a few other owners of the subject structures. Altogether 40 agencies responded to the survey. The responses were followed-up by telephone interviews.

Most of the states maintained or were in the process of developing inventories of the subject structures. About 93% of the responding states used galvanized structures. Although 85% of the responding states experienced damage or failure of these structures, only 53% identified fatigue as the cause of damage of failure. The majority of the damage or failure was due to vehicle collision. About 95% of the responding states indicated that they implemented the 2001 AASHTO Specification for fatigue design of the subject structures.

In-service fatigue cracking of the high-level luminaire support structures was reported by Iowa DOT. The structures developed fatigue fracture from the tube-to-transverse plate weld toe on the tube. Fatigue cracks were also reported from reinforced hand holes in some of these structures. Fatigue cracking of cantilevered traffic signal structures was reported in Pennsylvania. These cracks developed at the weld toe on the tube of fillet-welded socket connection or at the termination of the gusset plate on the pole wall in a mast-arm-to-pole connection. Fatigue cracks from the end of the gusset attachment on the pole wall were reported

9

in Michigan. This detail was retrofitted by introducing a taper at the gusset termination and grinding the weld profile. Fatigue cracking from the weld toe of the bottom gusset-to-pole connection in the mast-arm-to-pole box connection was reported in a large number of signal structures in Wyoming and some in Kansas and Colorado. Failures of mast-arm socket connections were reported in Texas.

Many DOTs provided standard drawings, updated based on the existing specification, which were reviewed. Most DOTs did not have standard drawings for high-level luminaire support structures, and these structures are mostly designed by manufacturers/fabricators. Standard drawings for most states included sign and signal support structures of round cross-section. Members with multi-sided cross-section were shown on the standard plans of two states. North Carolina indicated multi-sided cross-sections with a minimum of 12 sides, and Colorado indicated multi-sided cross-sections with a ratio of inscribed to circumscribed circles of at least 0.98. Only the standard signal structures of Washington State had a square cross section.

Survey of Manufacturers

The responding state DOTs identified their manufacturers and fabricators of the sign, signal and luminaire structures. A total of 39 different companies were identified and a survey was sent to all of them. Only 10 manufacturers/fabricators responded to this survey. While a few of them suggested alternative fatigue resistant cost-effective connections, only one manufacturer provided a sketch of an alternative detail, test results, and sample drawings. Two manufacturers indicated that they have investigated the U-rib stiffener detail, patented by Nippon Steel, as a fatigue resistant connection detail. However, the fabrication process was quite complex and involved, and was not considered cost-effective.

IDENTIFICATION OF CRITICAL PARAMETERS

The two most important parameters that affect the fatigue performance of connection details are the stress history and the detail configuration. The stress history that is experienced by a particular detail is dependent on the loading condition, which in this case is primarily attributed to the wind loads. The stress history is also dependent on the dynamic characteristics of the structure, since a large number of fatigue stress cycles may be accumulated because of oscillations due to galloping or vortex shedding at the resonant frequency. Thus, there is an interaction between the loading and the structure at the global level, and the response characteristics of the structure can influence the stresses experienced by a connection detail at the local level. Measures for vibration mitigation add another level of variability in that interaction. In view of the scope of the project, however, the focus of the investigation on the fatigue performance of the connections was limited to the identification of critical parameters that affect the fatigue resistance of the details. The assessment of fatigue demand on these connections and its effect on their performance were excluded from this study.

Traditionally fatigue damage in a component is attributed to geometric stress raisers and microstructural discontinuities in the material. In welded connections, the conditions are further intensified by the rapid transition in cross section at the weld bead causing severe localized stress concentrations, the presence of crack like discontinuities at the weld toe, and the existence of tensile residual stresses, all of which are inherent to the welding process. Since the magnitude of

10

the residual stresses is usually close to the yield stress of the material, the severity of a detail becomes the function of the local geometry of the structural connection and the weld configuration.

As required for having large spans, the cantilevered sign, luminaire and traffic signal structures are mostly built with thin-walled hollow shapes of circular and polygonal cross section, rendering them extremely light weight. The primary load carrying mechanism in thin shells is in-plane membrane stresses. However, in the vicinity of the supports such as tube-to-flange connection, the boundary condition introduces out of plane flexural deformation. Due to thin section size and small section modulus this deformation introduces large out-of-plane bending stresses through the thickness of the section. The superposition of this out-of-plane bending stress on to the in-plane membrane stress magnifies the local stress in the section near the boundary. The out-of-plane deformation is further magnified by a flexible base plate and discrete fasteners locations. The boundary effects, however, attenuate rapidly, and the in-plane membrane stresses dominate in rest of the structure. Providing attachments such as longitudinal gusset plate or stiffeners between the transverse-end-plate and the tube-wall to control the out-of-plane deformation creates a different kind of perturbation in the in-plane stress field and changes the load transfer mechanism significantly. The relatively large stiffness of the stiffeners with respect to the tube wall attracts more stresses into the stiffeners and can increase distortion. A large portion of the in-plane membrane stresses in the tube deviate towards the stiffeners and are transferred to the base plate as in plane stresses in the stiffener. The stress at the pole-to-transverse-plate connection is reduced substantially and a concentration of stress occurs at the stiffener-to-tube connection. As a result, the fatigue critical detail is transferred from the tube-to-transverse-end-plate connection to the stiffener termination on the tube. In addition, the complex interaction between the stiffeners, base plate, and the tube promote secondary transverse bending of the tube wall in the hoop direction spanning between stiffeners. These response characteristics have been demonstrated by detailed FEA of cantilevered sign structures by various researchers.

Based on the review of performance of the connection details in the subject structures, and the understanding of the behavior and response of the subject structures in general, the critical parameters that influence the fatigue performance of various connection details were identified as follows.

Member Cross Section

Fatigue resistance of connection details in multi-sided tubular shapes is affected by the geometric stress concentration at the bend corners. This stress concentration is dependent on the roundness of the section, which is a function of the number of sides and the bend radius at the corners. Increasing the number of sides and/or the bend radius at the corner tends the section more toward a circular shape in the limit and hence reduces the stress concentration. The diminishing effect of multi-sided cross section on the fatigue strength was demonstrated by limited tests and parametric studies Ocel et al. (*4*).

Geometry of the Connection

Fatigue resistance of the connection details in the subject structures is dependent on their size and geometry and in particular the relative stiffness of the components at the connection such as the tube wall, the transverse plate, the gusset plates, and the stiffeners. Results from

11

limited fatigue tests and parametric studies conducted at the UT Austin (*3*), the University of Minnesota (*4*), and Nagoya University (*10*) support this observation. Increasing the thickness of the plate in an unstiffened tube-to-transverse plate connection reduced the stresses associated with the out-of-plane deformation in the tube wall and enhanced the fatigue performance of the connection in both round and multi-sided tubes. For a given plate thickness, increasing the thickness of the tube wall increased the stress concentration at the weld toe, which indicated an effect of relative stiffness of the tube and the plate on the fatigue performance. In stiffened tube-to-transverse plate connections, the fatigue performance depends on: the length and profile of the stiffener; relative thicknesses of the stiffener, the tube wall, and the transverse plate; and the number and orientation of the stiffener. Test results (3) indicated that increasing the ratio of the stiffener thickness to the tube thickness precipitated fatigue cracking. Also for a fixed stiffener thickness, increasing the thickness of the tube with respect to the transverse plate increased stress concentration. Tests conducted at UT Austin and by a fabricator (internal tests) on similar specimens and at similar stress ranges indicated that increasing the number of stiffeners from four to eight improved the fatigue performance of stiffened socket connections.

The flexibility of the transverse plate with respect to the tube seemed to have the most significant effect on the fatigue performance of stiffened and unstiffened tube-to-transverse plate connections. The flexibility of the transverse plate is a function of its thickness, the diameter of the bolt circle, the number of fasteners, and the size of opening. The flexibility of the tube is a function of its diameter, and thickness. The fatigue resistance of tube-to-transverse plate connections improves with decreasing relative flexibility of the transverse plate with respect to the tube. For a given tube diameter and thickness, the fatigue resistance of the detail will improve with increasing transverse plate thickness. For a given tube diameter and transverse plate thickness, the fatigue resistance of the detail will decrease with increasing tube thickness. With increased tube thickness, however, the stress at the detail may reduce below the reduced fatigue resistance of the detail, providing an acceptable fatigue performance of the connection. Parametric studies indicated that the relationship was nonlinear and seemed to taper off beyond a critical value of the stiffness ratio of the components.

Weld Configuration

The type of welded connection was found to be another important parameter. In all fatigue tests, a full-penetration groove-weld between the tube and the transverse plate provided better fatigue resistance compared to socket connections in similar geometry, whether the weld root was fused by continuously welding the backing bar to the plate or not. When the backing bar was welded to the tube in addition to the transverse plate, the fatigue performance was enhanced because the backing bar participated in sharing the stresses in the tube. Investigation on failure of high-level luminaire support structures in Iowa demonstrated that the backing bar welded both to the pole wall and the base plate provided alternate load path and redundancy against fatigue fracture. Subsequently, during the research under this project it was found that when the backing bar is welded to the tube, the weld quality becomes critical for the fatigue performance of the connection. In such situation, this weld should be specified as a structural weld (rather than seal weld as is the common practice) and inspected as such. Fatigue cracks in handholes sometimes initiate from the lack of fusion at the root of the weld between reinforcing frame and the tube. Some states recommended complete joint penetration weld at this connection to avoid this mode of failure.

12

Weld Geometry

In addition to weld configurations such as fillet weld and groove weld (full-penetration or partial-penetration), the weld profile is also an important parameter. Tests conducted by Fisher et al. (2) demonstrated that unequal fillet welds with long leg on the tube provided better fatigue resistance for socket welds by reducing the stress concentration. Following the same lines Alderson (7) proposed a bilinear weld configuration, which is being investigated as part of the Transportation Pooled Fund Study TPF-5(116) at UT Austin (18). Koenigs et al. (3) measured weld geometries on seventeen mast-arms and noted that a smaller local weld angle (the angle between the tangent to the weld at the weld toe and the mast arm surface) generally produced greater fatigue strength. All these welds were unequal leg fillet welds, where the local angle varied significantly from the global angle (calculated based on measured long and short leg dimensions). The global angle was generally consistent with the fabricator's specified angle of 30^0, although significant variability existed between measured leg dimensions across the specimens. The mode of fatigue cracking such as toe-crack versus root-crack was another significant parameter that could contribute to the fatigue performance of welded as well as post-weld treated connections.

REVIEW OF CHAPTERS 10 AND 11 OF THE SPECIFICATION

Chapters 10 and 11 of the 2003 Interim of the 4th edition of the AASHTO specification were reviewed with respect to the objectives of this research project, which was focused on defining fatigue resistance of various connection details in the subject structures. During the execution of this task in 2006, the 2003 Interim of the 4th edition of the specification was the latest version available. The 2006 Interim of the 4th edition and the 5th edition of 2009 were published after this review was completed. The relevant changes in these specifications have been noted as appropriate.

Chapter 10 of the specification addresses serviceability requirements such as deflection limitation, vibration mitigation, and camber requirements. Chapter 11 of the specification contains provisions for the fatigue design of cantilevered steel and aluminum structural supports for highway signs, luminaires, and traffic signals.

Review of Chapter 10

The serviceability limit state requirements of chapter 10 have no effect on the fatigue strength of the connection details. The deflection limits of this chapter are required to be satisfied with respect to the maximum static effect of dead and wind loads, while the dynamic load range is the cause of fatigue damage. The slope and deflection limits on vertical supports under dead load were developed based on aesthetic considerations. The deflection limit on high-level luminaires under combined dead and wind load is provided as a safeguard against design of highly flexible structures that may adversely affect proper functioning of luminaires. This requirement may have an indirect effect on the fatigue performance of the connections since controlling flexibility of the structure can affect the fatigue loading and hence the fatigue damage of the connection details. In chapter 10, no limitation is provided on the deflection of the horizontal members. In the commentary of chapter 11, however, it is suggested that the maximum vertical static deflection range at the free end of the horizontal members in single arm

13

cantilevered structures be limited to 8 in (204 mm) when subjected to the static design wind effect of galloping and truck induced gust loads as specified in that chapter. This requirement was proposed by Kaczinski et al. (*1*) to minimize: 1) complaints by motorists about difficulty in seeing the signs and the signals, and concerns about passing under; and 2) vibration damage to signal/sign attachments. No displacement limitation is imposed in the horizontal direction.

Vibration mitigation by using appropriate damping or energy-absorbing devices will reduce the fatigue loading on connection details and will affect the fatigue performance of the structure. This will not, however, affect the fatigue resistance of a particular connection detail. Similarly, camber requirements do not have any bearing on the fatigue resistance of the connection details. Permanent camber in addition to dead load camber is provided for the reasons of aesthetics, perception and geometric clearance. Providing camber by raking the vertical support may cause difficulty in tightening the anchor bolts at the base-plate. Since the vertical support is raked during construction by adjusting the leveling nuts at the base of the structure, it results in anchor bolts not perpendicular to the base-plate. Improper tightening of anchor bolts is known to be one of the primary reasons for fatigue failure of anchor bolts, and can adversely affect the fatigue performance of a tube-to-transverse plate connection by influencing the flexibility of the plate. Beveled washers should be used in such cases to achieve uniform contact with the base plate.

Review of Chapter 11

The fatigue design provisions of chapter 11 are based on a nominal stress approach. It requires that the cantilevered support structures designed for fatigue shall resist each of the following applicable equivalent static wind load effects acting separately — galloping, vortex shedding, natural wind gust, and truck induced wind gust. Several details in the subject structures are classified into different categories based on their notch severity, and fatigue resistance of each category is defined in terms of infinite life. These categories are consistent with the existing AASHTO and AWS specifications. One reason for adopting an infinite-life approach is that the wind induced loading spectra experienced by various connections over their life time is not well known. The other reason is that due to the inherent flexibility and low damping of the subject structures, the load cycles in the design life time may easily exceed 100 million cycles.

As indicated earlier, the current study focused on defining fatigue resistance of various connection details in highway sign, luminaire and traffic signal structures. Thus, issues such as fatigue loading and vibration mitigation by increased damping were excluded from this review.

Although the survey results indicated that most states implemented the fatigue design provisions and most of the manufacturers were using these provisions for new structures, the provisions were generally deemed to be either unrealistic or too stringent to be cost effective. One of the reasons for this skepticism was that some connection details in the subject structures in the national inventory experienced fatigue cracking, while others that did not meet the fatigue design provisions, functioned satisfactorily. Another reason was the lack of conformity between the recommended fatigue categories for some details and the limited fatigue test results that were obtained after publication of the specification.

When the 2001 *AASHTO* Specification was prepared, very little fatigue test data was available for the connection details in cantilevered structures for sign, signal and luminaire. Published large scale fatigue test data were available for the pole-to-base-plate or the mast-arm-

14

to-flange plate fillet-welded connections, and for anchor bolts. NCHRP Project 10-38 (1), which is the basis of the fatigue design provisions in the current specification, focused on developing the fatigue design loads due to wind induced phenomenon and calibrating the load model. In addition, substantial research was carried out regarding fatigue resistance of anchor bolts. Accordingly, the specification for other types of details was prepared based on the provisions for similar bridge details in the AASHTO Bridge Design Specification, AWS D1.1, and the Eurocode 3. This approach however failed to recognize the actual behavior of the thin tubular structures, and was the primary reason for the shortcomings of the current specification.

Fillet-welded Tube-to-transverse Plate Connections

Fatigue resistance of the fillet-welded tube-to-transverse plate connection is defined as Category E´ in the current specification. This recommendation was based on finite life tests conducted at Lehigh University (2) and was verified by tests conducted at UT Austin (3) on details having similar geometry. These tests involved round tubes. Tests conducted at the University of Minnesota (3) on octagonal tube-to-transverse plate fillet-welded connections exhibited fatigue resistance much lower than Category E´. The existing specification provisions do not distinguish between fatigue resistances of tubular connections based on the shape of the cross section. Moreover, limited experimental and analytical studies indicate that fatigue performance of fillet-welded tube-to-transverse plate connections depend on the thickness of the transverse plate. Increasing the plate thickness for particular tube geometry can improve the fatigue performance substantially. However, an optimum thickness for the transverse plate exists beyond which the improvement in fatigue performance for particular tube geometry may not be significant. More specifically, as discussed earlier fatigue resistance of a tubular connection is a function of the connection geometry and the relative stiffness of the components. The current specification does not recognize these effects.

Weld Geometry

Based on test results Fisher et al. (*2*) concluded that the fatigue resistance of equal leg fillet-welded tube-to-transverse plate connection was less than Category E´, and that of unequal leg fillet welded connection was equal to Category E´. The improved fatigue performance of the unequal leg fillet weld was attributed to the decreased stress concentration due to a decrease in the contact angle, which was about 30^0 at the termination on the tube wall. All tube-to-transverse plate connections in mast-arms tested at UT Austin (*3*) had unequal leg fillet welds similar in geometry to those tested at Lehigh University, and verified the classification of this detail. The 2003 Interim of the 4th edition of the specification (the specification that was available during execution of this task in 2006) did not take the geometry of the weld into consideration. Subsequently, in 2006 Interim of the specification, a requirement for unequal leg fillet welds for socket connections with the long leg on the column or mast-arm and a weld termination angle of 30^0 was introduced.

Groove-welded Tube-to-transverse Plate Connections

Limited test results on multi-sided tube-to-transverse plate connection employing full-penetration groove-weld with the backing bar not fused to the transverse plate indicated a fatigue resistance in excess of Category E´, which is consistent with the specification. Full penetration groove welded round tube-to-transverse plate connection with backing bar fillet welded to the transverse plate and tube wall exhibited fatigue resistance in excess of Category D, which was

15

one category higher than the recommendation. The same connection in multi-sided cross section also yielded similar results, although the backing bar was not welded to the base-plate and the tube. As suggested in the specification, the fatigue performance of a full-penetration groove-welded tube-to-transverse plate connection is not well established. As for fillet-welded tube-to-transverse plate connections, it is expected that the connection geometry and the relative stiffness of the components will have significant effect on the fatigue performance of this detail. The existing specification is deficient in that regard.

Stiffened Tube-to-transverse Plate Connections

One of the major shortcomings of the existing specification (2003 Interim of the 4th edition, the specification that was available during execution of this task in 2006) is regarding the fatigue resistance of longitudinal stiffeners or gussets attached to the tube. The specification acknowledges the deficiencies and recommends full scale fatigue testing to establish the fatigue resistance. In the specification, longitudinal stiffeners on a tube are limited to a length greater than 4 in (102 mm) and their fatigue strength is independent of the length of the attachment. Depending on the end condition at the termination on the tube, these details have been characterized as Categories C, D and E. For stiffeners with square ends at the termination on the tube, the thickness is limited to 1 in (25 mm). With flushed terminus, the fatigue strength is dependent on the transition radius and/or on the angle of incidence, and the potential for lack of penetration at the weld root. A limitation on the angle of incidence is recommended as 25^0. Limited test results and parametric studies, however, indicate that the fatigue performance of the stiffened tube-to-transverse plate fillet-welded connections is dependent on the ratio of thicknesses of the stiffener and the tube. The specification provisions related to stiffeners do not consider this effect.

One criticism of detail 21 in the 2003 Interim of the 4th edition, (detail 20 in the current specification) is that it uses a limiting length equal to 12 times the thickness of the stiffener, which is applicable to stiffeners in girders as a buckling limit state under compression loading. Correlation of the stress concentration at the end of the longitudinal attachment with this length parameter is unknown.

The specification allows grinding of the wrap-around weld at the termination of a longitudinal stiffener to a smooth transition with the tube face when a full-penetration weld is used. This is a major concern since it is difficult to grind the weld toe without grinding the thin tube wall, and since tubes of such small thicknesses are used. Any loss in cross section from grinding and/or residual grind marks will increase the stress concentration at the stiffener terminus and may precipitate fatigue cracking. Moreover, the grinding and its prerequisite full penetration weld introduce additional labor in the fabrication process and as such may not be cost-effective. Limited internal tests conducted by a fabricator (information shared during manufacturers' survey) on contoured gussets connected to the tube either with fillet welds stopping short of the termination or full penetration groove welds wrapped around the stiffener end and ground smooth did not produce any significant difference in fatigue performance. The specification classifies the former as Category D and the latter as Category C.

The specification is also silent about the effect of number and orientation of stiffeners on fatigue performance of stiffened socket connections. Tests conducted at the UT Austin and the University of Minnesota using four stiffeners evenly spaced between the fasteners demonstrated that the stiffeners were ineffective in providing protection to the fillet-weld at the tube to

16

transverse plate connection. However, tests conducted by a fabricator (information shared during manufacturers' survey) demonstrated that eight stiffeners evenly spaced around the tube were effective in protecting the socket welds.

It may be noted that in subsequent 5th edition of the specification (the current specification), the fatigue resistance of the of stiffeners against fatigue cracking from the weld toe at the termination on the tube is defined as Category E´, irrespective of the geometric parameters of the connection. Without any experimental and analytical efforts in determining the infinite life performance of the stiffened socket connections, this specification recommendation is premature. The specification still does not consider the effect of connection geometry on the fatigue resistance of stiffened connections. Recognizing these shortcomings, however, the specification allows a better fatigue classification at the discretion of the owner for connections in tubes thicker than ¼ in (6 mm) that have exhibited satisfactory field performance and employs a groove welded taper or transition radius at the terminus with weld termination ground smooth. The current specification also requires non-destructive inspection in the vicinity of weld termination and prohibits grinding of fillet or partial penetration weld to a smooth transition with the tube wall.

Punching Shear Check

Another questionable specification provision is the check of punching shear stress range for fillet welded tube to tube connections. This provision is recommended for built-up box as well as ring-stiffened mast arm connections. This provision was incorporated from the AWS D1.1, and requires that the stress range in the branch members should be less than the Category ET and the punching shear stress range in the main member should be less than the Category K_2. The CAFT for Category ET is 1.2 ksi (8.2 MPa) and the base CAFT for Category K_2 is 1 ksi (6.9 MPa), which is further reduced based on the radius/thickness ratio of the tubular member. The punching shear approach and the fatigue provisions for fillet welded tubes were developed decades ago primarily for offshore structures of typical geometry. As such, their applicability to the cantilevered sign, signal and luminaire structures is questioned. Recent limited full-scale fatigue tests of connection details similar to the box connections have produced mixed results. Dexter and Ricker (*19*) have reported fatigue test results where both of the above checks were conservative and the punching shear check was excessively conservative as it predicted only 11% of the experimental life. On the other hand, the tests conducted by Ocel et al. (*4*) on mast-arm-to-pole box connections in multi-sided cross sections exhibited fatigue resistance of Category ET for out of plane loading conditions. The preliminary results from an ongoing investigation at the University of Wyoming (*20*) on ring-stiffened box connections, however, indicate that the fatigue performance of the connection is better than Category D. Thus, it appears that this specification provision is not valid over the entire spectrum of application.

Needed Revisions

Based on the above discussion and the failures experienced in the subject structures, the following revisions to the AASHTO Specification were deemed necessary:

1. The specification provisions should be revised to take into consideration the effect of the cross section geometry — round and multi-sided.

17

2. The fatigue categories of connections should be established taking into account the geometric and cross-sectional parameters of the connected components. Dimensional limits should be set on the applicability of the provisions.

3. Finite life fatigue performance of the connections should be established for fatigue assessment of in–service structures.

4. Fatigue resistance of built-up box mast-arm-to-column connections and ring-stiffened mast-arm-to-column connections need to be determined.

5. Fatigue classification of T-, Y-, and K- tube to tube connections needs to be verified.

6. Provisions for in-service enhancement and retrofit of connection details should be included.

EXPERIMENTAL AND ANALYTICAL PROTOCOLS

Analytical Protocol

Review of the literature did not identify any unique analytical protocol that would reliably and consistently assess the fatigue performance of connection details in highway sign, signal and luminaire structures. Limited analytical evaluation of fatigue performance of the connection details in the subject structures had been conducted. Most of these analytical studies performed FEA to understand the overall behavior of the structures and to make a qualitative assessment of a particular connection component.

For analytical prediction of fatigue performance of a connection, the various parameters that affect its fatigue performance need to be individually assessed. Fatigue cracking in a welded connection originates from microstructural discontinuities primarily at weld toes abetted by local stress concentrations. Local stress analysis approaches that are often used in the literature are known as "hot-spot stress" approach, "structural stress" approach, and "notch stress" approach. "Fracture mechanics" can be used to model and compute fatigue life due to crack propagation from the stress singularity at the tip of a flaw or crack.

A review of the various specifications and design guides for offshore structures revealed that "hot-spot stress" based design for safe life and "fracture mechanics" based damage tolerant design approaches are generally recommended for analytical evaluation of fatigue performance of various connection details. Due to the geometric resemblance to offshore structures, these methods were considered useful for analytical assessment of fatigue performance of the connection details in subject structures.

Koenigs et al. (3) performed parametric finite element studies using hot-spot stress concentration as suggested in the DNV guidelines (DNV RP) for non-tubular structures. According to this approach, stress components on the plate surface were evaluated at distances 0.5 t and 1.5 t away from the hot-spot (which is the weld toe), where t is the plate thickness at the weld toe, and extrapolated linearly to the hot-spot. The ABS guidelines (ABS Guide), which also recommend a two point linear extrapolation, were also evaluated. In addition, refined meshing, and sub-model analysis techniques were studied, but the DNV guideline was adopted because of its simplicity in use. However, the fatigue performance of the connection details was not assessed and the validity of the analytical approach was not verified.

18

For developing a simple yet efficient analytical protocol that would reliably and consistently assesses the fatigue performance of a connection detail, a limited comparative study was conducted. In this study, the DNV guideline for tubular structures that recommends a point measure of principal stress at $0.1\sqrt{(rt)}$ from the weld toe as hot -spot stress, where r is the radius and t is the thickness of the tube, produced the best correlation with available experimental data in the finite life. An analytical protocol for infinite life could not be evaluated because of the lack of infinite life test data. While fracture mechanics has been used to establish fatigue crack growth threshold for welded details in steel bridges, this method was not pursued because of the complexities involved. Instead a notch stress based methodology developed in the automobile industry (*21*) and successfully used by Roy and Fisher (*22*) in establishing fatigue threshold of UIT details was proposed. This method uses the stress at a fictitiously rounded weld toe. These protocols were verified during execution of this project.

Analytical Protocol for Finite Life

The local stress in welded connections that can experience fatigue cracking at the weld toe should be determined from detailed linear FE analyses of a three dimensional (3D) model of the connection. The nominal weld geometry should be included in the model. Because of the steep geometric stress gradient associated with the connection geometry, a three dimensional FE model of the connection should be used. In thin tubular structures, the weld acts like a tiny stiffener and influences the geometric stress concentration. To achieve proper local stiffness and improved stress prediction, the nominal weld geometry should be modeled. The FE model should assume linear material properties.

The model should be large enough so the calculated results are not significantly affected by the assumptions made for modeling the boundary conditions and the application of loads. If the model is too large to be meshed at the required refinement, an analysis of a refined submodel driven by the analysis results of a less refined global model should be performed. Two dimensional (2D) shell elements may be used for modeling other parts of the support structures away from the connections to reduce computation costs.

20-node solid hexahedron elements incorporating isoparametric formulation and reduced integration should be used for modeling the connection. These are standard elements used for stress analysis. These elements, also known as serendipity elements, assume an incomplete quadratic polynomial as displacement and geometric shape functions resulting in linear strain and stress distributions. The element stiffness matrix is formed by assuming a reduced number of Gauss integration points for better correlation of FE results with true solution. In tubes a mesh size of $t \times t$ should be used for at least three rows of elements in front of the weld toe, where t is the tube wall thickness. At least two elements should be used in the thickness direction. To avoid numerical instabilities and inaccuracy in solutions, the elements should be well shaped and proportioned. All elements in the model should be limited to a maximum aspect ratio of 1:4. The elements should be well shaped having corner angles between 30^0 and 150^0.

The maximum (tensile) principal stress on the tube surface at $0\sqrt{(r \times t)}$ ahead of weld toe should be used as the local stress for fatigue design, where r and t are the outer radius and thickness of the tube respectively. For multi-sided cross sections, half of the outer opposite to flat distance should be substituted for r. This local stress is defined as the "geometric stress," and the ratio of this geometric stress with nominal stress is defined as the "geometric stress concentration factor (GSCF)."

19

When the weld toe is modeled with zero radius, the stress solution at the weld toe approaches infinity as the element size is decreased to zero. However, the effect of the connection geometry on the stress beyond the influence of the weld toe is of interest. The scatter associated with weld toe micro-discontinuities is included by using experimentally obtained S-N curves. It is well known from theory of thin tubes that the geometric stresses associated with secondary out-of-plane bending deformation at tube boundaries (arising from the need to maintain compatibility at the connections) is a function of the tube geometric parameter $\sqrt{(r \times t)}$. The coefficient 0.1 was determined empirically (*23*).

The geometric stress should be used with the experimentally obtained Category C design curve of the AASHTO LRFD Bridge Design Specifications in the finite life region to determine the expected fatigue life. The AASHTO C curve reflects fatigue cracking associated with the weld toe geometry, micro-discontinuities and the inherent variability.

Analytical Protocol for Infinite Life

The requirement for design against infinite life is that fatigue fracture must be avoided regardless of the duration of the service life. The possibility of cyclic crack initiation and that crack propagation must be suppressed. The underlying assumption is that no appreciable damage occurs at the weld toe notch and the notch stresses are purely elastic. This assumption is somewhat simplistic in that cracks may initiate at the weld toe notch but may not propagate, that is, "dormant cracks" may exist with limited damage from cyclic loading. To this end, the local stress at the weld toe notch should be determined.

The local stress for infinite life design against fatigue cracking from weld toe should be determined by 3D FEA considering the local effect of the weld toe notch. A notch of 0.04 in (1 mm) radius should be introduced at the toe of the nominal weld geometry. Determining the stresses at the weld toe notch is complicated by the significant scatter in local weld geometry and presence of micro discontinuities. Moreover, when the weld toe notch is modeled with zero radius, the stress solution approaches infinity as the element size in the FE model is decreased to zero. To obtain a fatigue effective stress at the weld toe notch, a radius of 0.04 in (1 mm) is introduced at the center of the notch, which has been verified to produce consistent results for structural steel.

The FE model should be large enough so the calculated results are not significantly affected by the assumptions made for modeling, the boundary conditions and the application of loads. If the model is too large to be meshed at the required refinement, an analysis of a refined submodel driven by the analysis results of a less refined global model shall be performed.

20-node solid hexahedron elements incorporating isoparametric formulation and reduced integration should be used for modeling the connection and the weld toe region. At least eight elements should be used along the rounded notch perimeter. All elements in the model shall be limited to a maximum aspect ratio of 1:4. To avoid numerical instabilities and inaccuracy in solutions, the elements should be well shaped having corner angles between 30^0 and 150^0.

The converged maximum (tensile) surface stress at the center of the rounded notch should be used as the local stress for fatigue design. This local stress is defined as the "notch stress," the ratio of this notch stress with respect to the nominal stress is defined as the "notch stress concentration factor (NSCF)."

The fatigue resistance for infinite life (constant amplitude fatigue threshold, CAFT) should be calculated as:

$$(\Delta F)_l = \frac{1}{22.4}\left[-F_y + \sqrt{F_y^2 + 4 \times F_u^2}\right] \text{ MPa}$$

$$(\Delta F)_l = \frac{1}{3.2}\left[-F_y + \sqrt{F_y^2 + 4 \times F_u^2}\right] \text{ ksi}$$

(1)

where F_y is the yield strength of the material (ksi, MPa); and F_u is the tensile strength of the material (ksi, MPa).

The above equation is simplified from a relationship developed by Roy and Fisher (*21*) for assessing the CAFT of welded connections using an effective notch stress. This relationship is a function of the stress ratio (the ratio of the stress range to the minimum stress), welding residual stress, the endurance limit of a smooth specimen and the NSCF. In as-welded connections, tensile residual stresses are approximately equal to the yield stress of the material near the weld, which results in a local stress ratio in excess of 0.5. An endurance limit of 0.5 of the tensile strength is assumed for structural steel. The fatigue effective notch stress concentration is then reduces to about 80% of the notch stress concentration of the rounded weld toe.

Experimental Protocol

Based on the review of experimental research conducted on the subject structures and from the experience of the research team in conducting large scale fatigue tests, the following test protocol was developed.

Experimental Protocol for Finite Life

The finite life fatigue resistance of a connection detail should be determined by full scale laboratory fatigue tests. The fatigue tests should be conducted at two stress range levels separated by at least 4 ksi (28 MPa). The stress range levels should be decided based on an assessment of the fatigue resistance of the test detail using the analytical protocol. At least three tests must be conducted at each level of stress range to provide sufficient replicates for a meaningful statistical analysis.

Specimens should be instrumented using encapsulated bonded electrical resistance strain gauges at locations of interest on the specimen surface to measure surface strains. For steel structures, these strains may be converted to stresses by multiplying with the modulus of elasticity of steel taken as 29000 ksi (200 GPa). The locations of the strain gauges should be decided based on analyses of the test specimen in accordance with the analytical protocol. Uniaxial strain gauges of $^1/_4$ in (6 mm) gauge length may be used for measuring nominal strains away from local stress raisers. These gauges should be placed a minimum of 5 in (127 mm) away from local stress raisers such as the weld toe of the tested detail, or as determined from the FE results. The strain gauges should be oriented in a direction in which the nominal strain is being measured. Uniaxial strain gauges of 0.04 in (1 mm) grid length may be used near the weld toe to capture the local stress. At least two strain gauges should be used to measure the variation of the

21

local stress gradient. These strain gauges in tubular connections should be located on the external surface of the tube at $0.1\sqrt{(r \times t)}$, but not less than 0.16 in (4 mm), and t away from the weld toe, where r is the external radius of the tube, and t is the thickness of the tube. These strain gauges should be oriented perpendicular to the weld toe.

All specimens should be tested under static loading (loading rate less than, 1 ksi/s [7 MPa/s]) prior to fatigue testing. Static tests should be conducted in a simple up-down pattern by loading the specimen up to the estimated maximum test load and complete unloading. The test should be repeated at least three times or until the residual strains at the strain gauges upon unloading become negligible. In each test, the strain at each gauge, the applied load, and the displacement at the load point should be recorded.

The fatigue tests should be conducted at a minimum 1 Hz frequency under constant amplitude loading. The tests should be monitored by maximum and minimum strains (or stresses) recorded at control strain gauges. To capture the nominal stresses, the control gauges should be located at a section beyond the influence of local stresses, as mentioned earlier.

The tests should be periodically monitored. The strains (or stresses) at the control and other gauges should be recorded. The test details should be inspected for fatigue crack growth with the aid of 10× magnifying glass and/or dye-penetrant or magnetic particle testing.

Fatigue failure of a detail will be defined by a visible through thickness crack of minimum 5 in (127 mm) length measured tip to tip. This crack length on a tube wall in a tubular connection should be taken as half the diameter of the tube. At an attachment detail on the tube wall (except at stiffeners in stiffened fillet-welded tube-to-transverse plate connections), the failure should be defined when the crack from the toe or the root of the attachment-to-tube weld branches into the tube wall. Failure criteria for stiffened tube-to-transverse plate connections should be the same as tubular connections described above.

The fatigue resistance of the test detail is defined by the nominal stress range and the number of cycles at failure. The nominal stress should be extrapolated from the stresses measured at the control gauge to the site of fatigue cracking according to the variation of loading and the respective section properties. The fatigue test results shall be plotted against the AASHTO fatigue design curves. The connection detail shall be classified by the fatigue design curve that is exceeded by the fatigue test result exhibiting the least fatigue life. The finite life constant for the connection detail should be determined accordingly.

Scatter in fatigue test data associated with uncontrolled variables such as the weld toe geometry and the micro discontinuities from the acceptable fabrication practice are expected. However, significantly larger scatter may arise in the fatigue test results owing to the variation in the fabricated weld geometry and particularly the weld angle from the specified nominal value. In the thin walled tubular support structures, the welds act as tiny stiffeners affecting the geometric stresses and contribute to the scatter in the test results. The detail classification based on the least fatigue life is expected to provide a lower bound estimate of the fatigue performance of the tested connection detail.

Experimental Protocol for Infinite Life

The infinite life fatigue resistance of a connection detail should be determined by full scale laboratory fatigue tests. At least four tests must be conducted for each detail type to determine the constant amplitude fatigue threshold (CAFT).

The first test should be conducted at a nominal stress range corresponding to a CAFT (as tabulated in the *AASHTO LRFD Bridge Design Specifications*) nearest to the estimated fatigue threshold of the particular detail type assessed by the analytical protocol. The nominal stress ranges corresponding to these fatigue thresholds (AASHTO CAFTs) in increasing severity of detail classes are: 16.0 ksi (110 MPa); 12.0 ksi (83 MPa); 10.0 ksi (69 MPa); 7.0 ksi (48 MPa); 4.5 ksi (31 MPa); and 2.6 ksi (18 MPa). As an approximation, the nominal stress range may be computed from Equation 1, by dividing the local stress-based fatigue resistance by an approximate stress concentration factor of 6.0.

The "run-out" life for infinite life fatigue test should be taken as: 12.5×10^6 cycles at 16.0 ksi (110 MPa); 7.0×10^6 cycles at 12.0 ksi (83 MPa); 8.2×10^6 cycles at 10.0 ksi (69 MPa); 14.7×10^6 cycles at 7.0 ksi (48 MPa); 20×10^6 cycles at 4.5 ksi (31 MPa); and 20×10^6 cycles at 2.6 ksi (18 MPa).

The infinite life tests should be conducted by a "step" method. If a specimen is run-out, it may be tested again at an increased stress range level corresponding to the next CAFT, provided it is verified by magnetic particle and dye-penetrant tests that no fatigue crack has initiated at the weld toe. On the other hand, if the specimen develops fatigue cracking before achieving the target number of cycles for infinite life, the subsequent specimen must be tested at a decreased stress range corresponding to the next lower CAFT.

Other aspects for infinite life tests including instrumentation, static and fatigue testing, and inspection, monitoring and recording, are the same as those stipulated for finite life tests.

EXPERIMENT DESIGN AND TEST MATRIX

The primary variables that were considered for experiment designs in this research were detail types, shapes of member cross-section, and stress parameters. The survey of the state DOT revealed that 37 states use galvanized sign, signal, and high-level luminaire support structures, and other states were planning to use only galvanized structures. As such, only galvanized specimens were considered for testing, and any detrimental effects of galvanizing on the fatigue performance of these structures were investigated by post-mortem fractographic analysis.

Twelve details were identified for investigation as shown in Table 1. These included unstiffened fillet- and groove-welded tube-to-transverse plate connections; stiffened tube-to-transverse plate connections; mast-arm-to-pole gusseted box and ring-stiffened box connections; mast-arm-to-pole pass-through connections; mast-arm-to-pole clamp connection; and unreinforced and reinforced handholes.

A test matrix indicating the distribution of specimens is presented in Table 2. All specimens were full-scale. All together 78 virgin specimens and two retrofitted specimens were tested. The specimens to be retrofitted were selected from previously fatigue cracked specimens. Each specimen included multiple details to optimize the output of the test program.

The specimens were primarily divided into two groups depending on the cross-section shape — round and multi-sided. Depending on the combination of test details included in a specimen, the specimens were distributed in 11 specimen types. The specimen types were identified by Roman numerals and each specimen of a type was identified by an Arabic numeral along with the type identification. Six specimen types, identified as I to VI, were of round cross-

section. The remaining five specimen types VII, IX, X, XI and XII were of multi-sided cross-section. All round specimens were representative of sign and signal support structures. All multi-sided specimens, except Type VII, were representative of high-level luminaire support structures. Specimen Type VII represented sign and signal support structures. The distribution of specimens along with key details is shown in Tables 3 and 4. Twelve specimens (three each of specimens Type I, II, VII and X) were tested in an early task to verify the analytical and experimental protocols.

Since the sign and signal structure specimens were pole and mast-arm assemblies, data from two tube-to-transverse plate connection details were available in each specimen. This provided the opportunity to simultaneously test connections of two different configuration and/or geometry. In high-level luminaire structure specimens, however, only one tube-to-transverse plate connection was available.

The test matrix was planned considering the test protocols, and distribution of specimens for validation of protocols and detailed experimental evaluation of finite and infinite life fatigue resistance. To obtain statistically significant results, multiple specimens of each type were tested. Generally six specimens were tested in the finite life region, equally distributed at two well separated stress range levels. The CAFT was determined in a Step fashion using four specimens. This protocol was followed for specimens Type III, VI, IX, XI and XII. Seven each of specimens Type I, and VII were tested to establish fatigue performance in the infinite life regime or at lower stress range levels, since fatigue test data at the higher stress range levels for the key details included in these specimens were available from other studies. Only three each of specimens Type II and X were tested. These tests were designed in the finite life regime for validation of protocols. The groove-welded tube-to-transverse plate connections included in Type II specimens were prone to fatigue cracking from the backing ring-to-tube weld at the top face due to poor weld quality arising from difficult fabrication. As such this detail was not pursued further and a more cost-effective and fatigue resistant variation of this detail was developed and included in other specimens. The fillet-welded tube-to-transverse plate connection in specimens Type X employed 16 fasteners, which were considered not cost-effective. Only four each of specimens Type IV and V were tested for limited evaluation.

The minimum stress was selected according to the structural application depending on whether the specimen represented a sign, signal or luminaire structure, as discussed in the test protocol. The stress ranges were decided progressively as the research program evolved based on analytical estimation of fatigue resistances of the details tested, and also based on the available and concluded fatigue tests.

All retrofitted specimens were tested for infinite life, as that would be intent of any repair/retrofitting. Only high-level luminaire support structures were considered for retrofit using steel jacket. Retrofitting of sign and signal structure specimens were not deemed cost-effective. The specimens for jacket retrofit were selected from previously fatigue cracked high-level luminaire structure specimens Type X and Type XI.

DESIGN OF SPECIMENS

Thirty eight of the test specimens were round and the other 40 were multi-sided. The round specimens and three of the multi-sided specimens comprised of pole and mast-arm

24

assembly representative of highway sign and traffic signal support structures. The remaining 37 multi-sided specimens were representative of high-level luminaire support structures. All specimens were full size and galvanized. The tubes had a taper of approximately 1 in 86 (0.14 in/ft or 11.6 mm/m). In all sign and signal structure specimen types, except in specimen Type VI, the arm had an inclination of 25^0 at the arm-to-pole connection.

The specimens were designed based on: (a) detailed study of available state DOT standard drawings and the range of parameters used in practice; (b) parametric finite element studies to optimize the connections and develop cost-effective designs; and (c) economic alternatives according to standard dimensions and practices of the fabricators to meet budgetary constraints. Considerations were also given to specimen sizes and results available from other previous experimental studies to create a basis for direct comparison by generating replicate data points and validating the results over a larger data base.

Round Specimens

When testing was initiated in this research, test results for round sign and signal structures were available from fatigue tests conducted at Lehigh University, at UT Austin, and at a fabricator's facility (internal test results shared during manufacturers' survey). The fatigue tests conducted at Lehigh University (*2*) used full size signal structures of $10^5/_8$ in (270 mm) diameter with $^5/_{16}$ in (8 mm) and 0.239 in (6 mm) tube thicknesses. The tests conducted at UT under both the Texas Mast-arm Study (*3*) and the TPF-5(116) Study (*18*) employed full size mast-arms of 10 in (254 mm) diameter and 0.179 in (4.5 mm) and 0.239 in (6 mm) tube thicknesses. The specimens tested by the fabricator had a diameter of 10 in (254 mm) with a thickness of 0.179 in (4.5 mm). The transverse plates for all studies were 1¾ in (45 mm) thick. Thus, for the round sign and signal structure specimens tested in this project, a mast-arm of 10 in (254 mm) diameter with a thickness of 0.179 in (4.5 mm) was selected, which was also the most commonly used mast-arm section in the DOT standard drawings.

A pole of 13 in (330 mm) diameter with a thickness of 0.239 in (6 mm) was selected to keep the cost of the specimens to a minimum, as tubes of this size were readily available from fabricators. Substantial savings in specimen price was realized when the pole diameter was reduced from 14 in (356 mm) to 13 in (330 mm).

As was determined from literature review, the most cost-effective means of improving fatigue resistance of the tube-to-transverse plate connection was by reducing the flexibility of the plate. One of the simplest ways of reducing this flexibility was to increase the plate thickness. The minimum transverse plate thickness in a tube-to-transverse plate connection that demonstrated this increase in fatigue performance in test results (*3*) was 2 in (51 mm). With the aim of developing cost-effective connection details under the current research, a minimum 2 in (51 mm) plate was used for all the tube-to-transverse plate connections at the pole and arm bases.

For the specimens that included handholes, a 5.2 in $\times$ 7.6 in (132 mm $\times$ 192 mm) handhole was provided in the pole in the plane of the mast-arm but on the "away" face. The handhole was located such as to produce the most critical stress condition in the handhole detail for fatigue. The size of the handhole was slightly larger than what is commonly used dimension of 4 in $\times$ 6½ in (102 mm $\times$ 165 mm), which was selected to suit the fabricator's standard size and thereby reduce the cost of the specimens.

Specimen Type I

Seven Type I specimens were tested. These specimens employed fillet-welded tube-to-transverse plate connections (socket connection) in the poles and the arms. The thickness of the transverse plates at the arm and pole bases was 2 in (51 mm). The specimens also contained a reinforced handhole and a ring stiffened box at the mast arm to pole connections. The details of this specimen are shown in Figure 1.

Specimen Type II

Three Type II specimens were tested as part of validation of protocols. The specimens were similar to specimens Type I in dimension, but the poles and the arms employed full-penetration groove-welded tube-to-transverse plate connections, where the backing ring was continuously fillet-welded to the plate and to the tube at the top face. The backing ring was $^1/_4$ in (6 mm) thick and approximately 2 in (51 mm) high. The groove-welds were provided with a fillet reinforcement similar to the fillet welds in the tube-to-transverse plate connections in specimen Type I. The other difference was that the Type II specimens had a fillet-welded gusseted box at the mast-arm-to-pole connections. Type II specimens also contained a reinforced handhole similar to the Type I specimens. The details of a Type II specimen are shown in Figure 2.

Specimen Type III

Ten Type III specimens were fatigue tested. These specimens were similar to Type II in overall size and shape. Specimens Type III differed from Type II as follows: (1) the arms and the poles had groove-welded tube-to-transverse plate connection with the backing ring continuously welded to the plate but not to the tube at the top face; (2) the openings in the transverse plates of the arms and the poles were reduced to reduce the transverse plate flexibility; and (3) the arm-to-pole connection employed a ring-stiffened box connection. The minimum size of the openings in the transverse plates was decided in discussion with the fabricator to be sufficient for flow of liquid zinc out of the arm and the pole tubes during galvanizing. A 4 in (102 mm) diameter opening with 1 in (25 mm) wide slotted ends was provided in the base plate of a 13 in (330 mm) diameter pole. In the transverse plates of 10 in (254 mm) diameter arms an opening of $7^5/_8$ in (194 mm) diameter without slots was provided. The other notable minor changes in the specimens Type III were the thicknesses of the pole and the arm, and an unreinforced hand hole that had similar opening size as the reinforced handholes in specimen Type II. The groove welds were also provided with a fillet-weld reinforcement similar to that in Type II specimens. Details of a Type III specimen are shown in Figure 3.

Specimen Type IVA and IVB

Two each of specimens Type IVA and IVB were tested. These specimens were similar to specimens Type III except the mast-arm-to-pole connections employed a fillet-welded gusseted box. In addition, specimens Type IVA did not have a handhole and specimens IVB had a reinforced handhole similar to specimens Type I and II. The other notable minor changes in these specimens compared to Type III were the thicknesses of the pole and the arm, which were similar to that in specimens Type I and II. Details of specimens Type IVA and Type IVB are shown in Figures 4 and 5.

26

Specimens Type IVA were loaded in the plane containing the arm and were tested to verify the results of Type III specimens. Specimens Type IVB were loaded out-of-plane at 45^0 to determine the effects of out-of-plane loading.

Specimen Type V

Four Type V specimens were tested. Details of this specimen type are shown in Figure 6. These specimens employed mast-arm-to-pole clamp connections. The arm tube was connected to the clamp plate with a fillet-weld. The tube-to-transverse plate connection at the pole base employed a groove welded connection identical to that in Type IV specimens.

Specimen Type VI

Ten Type VI specimens were tested. Details of this specimen type are shown in Figure 7. These specimens employed a novel partial-penetration groove-welded mast-arm-to-column pass-through connection. The connection involved a 25 in (635 mm) long pass-through sleeve that was welded to the pole (column) using a partial-penetration groove-weld. A 60 in (1524 mm) long and 0.179 in (4.5 mm) thick arm tube of matching diameter (called a starter piece) was inserted into the sleeve and a 0.179 in (4.5 mm) thick arm of matching diameter was slip fitted onto this starter piece. Alignment bolts were provided to prevent relative rotational slip between the arm, the starter piece and the sleeve about the arm axis. Because of the arm to pole connection geometry, the inclination of the arm was limited to 5^0. The pole was 0.239 in (6 mm) thick and had a 13 in (330 mm) diameter at the top of base plate similar to the poles in other round specimens. The pole base employed a full-penetration groove-welded tube-to-transverse plate connection with the backing ring continuously welded to the plate but not to the tube at the top face. The groove-weld was provided with a fillet-weld reinforcement similar to other groove-welded connections in round specimens. The base plate was 2.5 in (64 mm) thick and had an opening of 7 in (178 mm) diameter with 1 in (25 mm) slots. The pole base was designed with a larger opening for easier drainage of liquid zinc, but with a thicker plate to provide a consistent performance similar to groove welded tube-to-transverse plate connections in Type III, Type IV and Type V specimens that had poles of same diameter and thickness, but a 2 in (51 mm) thick base plate with a 4 in (102 mm) diameter opening.

The arm sleeve to pole connection was different from a typical tube-to-tube connection in that the sleeve passed continuously through the pole. The weld between the arm sleeve and the pole was a partial-penetration groove-weld with the joint preparation done on the pole wall. Due to tolerances and lack of complete fit between the pass-through sleeve and the pole, a non-uniform root gap is possible, and complete fusion of the weld root cannot be ensured. Accordingly, fatigue cracking could be experienced from this lack of fusion at the weld root.

Multi-sided Specimens

Specimen Type VII

When the testing under this research was initiated, the only fatigue test data available for multi-sided signal and pole structures were from tests conducted at the University of Minnesota (*4*). These specimens were eight sided with bend radius of about $^9/_{16}$ in (14 mm). The outer opposite to flat dimension of the poles was 14 in (356 mm), and that for the arms was 11.6 in (295 mm). However, the transverse plate thickness in these specimens was 1¼ in (32 mm),

which was responsible for the poor fatigue performance of these structures. An increase in fatigue resistance was obtained in similar pole specimens when the transverse plate thickness was increased to 2½ in (64 mm). The multi-sided sign and signal structure specimen Type VII was designed to provide a comparison with the previous test results as well as with the specimens with round cross sections that were tested in this research. An octagonal cross section was chosen similar to the UM study but with an increased bend radius of 1 in (25 mm). The bend radius was increased as FEA results showed that a radius as sharp as the UM test specimens would cause severe stress concentration and early fatigue cracking. Increasing the bend radius to a maximum allowed by the fabrication process, depending on the specimen size and configuration, is a cost-effective means of enhancing fatigue performance of multi-sided tubular structures. It is, therefore, rational to specify a minimum bend radius so that a reasonable fatigue resistance is obtained. It was also necessary to investigate the validity of the protocols over a wide range of values of the critical parameters. In view of these considerations, the bend radius of 1 in (25 mm) was chosen such that it was not too large compared to the previous test specimens to confound the effects of other geometric changes.

Seven Type VII specimens were tested. These specimens employed fillet-welded tube-to-transverse plate connections (socket connections) in the pole and the arm. These specimens also contained a reinforced handhole and a fillet-welded gusseted box at the mast-arm-to-pole connections.

The flat to flat dimensions of the poles and the mast-arms were selected respectively as 13 in (330 mm) and 10 in (254 mm) to be comparable with the round test specimens. A transverse plate of 2 in (51 mm) thickness was also provided at the pole and arm bases similar to the round specimens. Although a bend radius of 1 in (25 mm) was specified, the as-received specimens had a bend radius of about 0.5 in (13 mm). The details of this specimen are shown in Figure 8.

Specimen Type IX

Ten Type IX specimens were tested. These specimens employed stool-type stiffeners at the fillet-welded tube-to-transverse plate connection at the pole base, similar to the high-level luminaire support structures in Iowa. Details of this specimen type are shown in Figure 9. According to Iowa DOT (personal communication with Mr. Bruce Brakke of Iowa DOT), these details performed extremely well in service. The stool type stiffeners were used for 90 structures in Iowa. The tube diameter in the bottom section of these structures ranged between 22 in (559 mm) and 34½ in (876 mm) and the thickness in this section ranged between $^5/_{16}$ in (8 mm) and $^{11}/_{16}$ in (17 mm). The base-plate thickness ranged from 1¾ in (44 mm) to 3 in (76 mm) and the base-plates had a central hole ranging between 8 in (203 mm) and 10 in (254 mm) diameter. The tube-to-transverse plate connections at the pole base were full penetration groove welds with a backing ring. The handhole was reinforced with a doubler plate fillet welded to the tube. The structures used twelve, eight and four anchor bolts. None of these structures developed fatigue cracking in service.

Except for the in-service performance history, no test data on stool type stiffened connections existed. A limited number of specimens tested at UT Austin as part of the TPF-5(116) Study (*18*) included similar stool type stiffened connections, but had a significant difference from the detail employed in the Iowa structures. In the Iowa structures, the plate at the top of the stiffeners that served as the anchorage for the anchor rods was not welded to the tube.

28

Only the vertical stiffener plates were welded to the tube and the base plate. Two of the test specimens in the UT Austin study had the top plate also welded to the tube wall. In the other four specimens, a continuous annular plate was provided around the pole at the top of the stiffeners, which was welded to the stiffeners and the tube. Fatigue cracking occurred from the toe of the top plate weld on the tube demonstrating mixed performance.

In this research, information about the Iowa high-level luminaire support structures with stool type stiffened connections were gathered and parametric studies conducted to optimize their fatigue performance. The parameters considered were the thickness and height of stiffeners, the number of anchor rods, and the thickness of the tube wall. For ease of comparative evaluation, the geometric parameters of specimens Type IX were generally maintained the same as the other high-level luminaire support structures tested under this study and under the TPF-5(116) Study (*18*). The pole had a 16-sided cross section with an outer dimension of 24 in (610 mm) between the opposite flat faces at the top of base plate. Due to the limitation of available tooling with the fabricator, only a 1 in (25 mm) inner bend radius could be provided at the corners instead of an inner bend radius of 4 in (102 mm) that was provided for the other specimen types. Because the fillet-welded tube-to-transverse plate connection at the pole base is protected by the pre-stress introduced in the pole wall by the anchor rods, the effect of the sharper bend radius on the local stress in the pole corners at the base connection was insignificant. The critical location in this specimen was the weld toe at the termination of the vertical stiffener on the pole wall, where the local stresses were not significantly affected by the reduced bend radius. Since stiffeners were used to protect the socket connection, a 2 in (51 mm) base plate was used (as a minimum). Eight stool-stiffeners were provided at alternate bend corners, along with eight anchor rods on a 30 in (762 mm) bolt circle spaced equally between the vertical stiffeners. The vertical stiffener plates were 18 in (457 mm) high and $^3/_8$ in (10 mm) thick, the same as the conventional stiffened socket connections in the specimen Type XII. Like the detail in Iowa structures, the plate at the top of the stiffeners that served as the anchorage for the anchor rods, was not welded to the tube. The vertical stiffener plates were welded to the tube and the base plate, and the welds were wrapped around the vertical stiffeners at top.

Specimen Type X

At the time of designing the multi-sided high-level luminaire support structures Type X, the only standard drawings for these structures were available from Wyoming DOT. This standard used a minimum of 16 sides for a multi-sided pole section with a bend radius not less than ¾ in (19 mm) at the corners. The maximum outside corner-to-corner dimension for the base section was suggested as 24¼ in (616 mm) with a wall thickness of $^3/_8$ in (10 mm). A reinforced hand hole with a clear opening of 30 in × 10 in (762 mm × 254 mm) and a 1 in (25 mm) thick framing was recommended. A groove-welded tube-to-transverse plate connection was specified in the WYDOT standard drawing.

After initiation of testing in this research, the test results from the first phase of the TPF-5(116) Study (*18*) became available. Under this test program, ten unstiffened fillet welded connections with five different combinations of base-plate thicknesses and number of bolts, and four unstiffened groove welded tube-to-transverse plate connections (two each of Texas and Wyoming standard details) were tested in multi-sided high-level luminaire specimens. These specimens were 16 sided having an outer opposite to flat distance of 24 in (610 mm) with a inner bend radius of 4 in (102 mm) at the corners. The base-plate thicknesses used were 1½ in (38

29

mm), 2 in (51 mm) and 3 in (76 mm). The fastener arrangements were either eight or 12 bolts on a bolt circle of 30 in (762 mm) diameter. The wall thickness was $^5/_{16}$ in (8 mm).

As part of validating the analytical and experimental protocols, it was decided to test fillet-welded tube-to-transverse plate connections (socket connection) in specimens Type X, which showed relatively early cracking in the TPF-5(116) Study (*18*) for the base-plate thicknesses considered. This also allowed validating the analytical protocols on a common connection detail over a wide range of cross sectional parameters. For ease of comparison with available fatigue test results from the TPF-5(116) Study (*18*), it was decided to design the Type X specimens with the same tube size and shape. However, a 3 in (76 mm) thick base-plate fastened with 16 bolts evenly spaced on a bolt circle of 30 in (762 mm) diameter was used to explore the effect of the transverse plate flexibility on improving the fatigue performance of fillet-welded tube-to-transverse plate connections. This specimen configuration was not tested in the TPF-5(116) Study (*18*), and provided an extreme combination of the critical geometric parameters. The selected specimen size was also similar to that specified in the WYDOT standard drawings. A handhole of same size and location, as shown in WYDOT standard drawings, was included in specimen Type X. The detail of this specimen is shown in Figure 10. Three Type X specimens were tested.

Specimen Type XI

Ten Type XI specimens were tested. This specimen type employed a full-penetration groove-welded tube-to-transverse plate connection at the pole base, where the backing ring was continuously fillet-welded to the plate and to the tube at the top face. The groove-weld was provided with a fillet reinforcement that was of the same size as the fillet-welded tube-to-transverse plate connection in specimen Type X. The detail was similar to that shown in WYDOT standard drawings for high-level luminaire support structures.

Experimental and analytical evaluation of socket connections demonstrated that the fatigue resistance of tube-to-transverse plate connections is a function of the relative flexibility of the tube and the transverse plate. Reducing the relative flexibility of the transverse plate can significantly increase the fatigue resistance of the connection. Since the groove welded tube-to-transverse plate connections in specimen Type XI were geometrically similar to the fillet-welded tube-to-transverse plate connections in specimen Type X, it was expected that their performances would exhibit similar trends. The hole in the transverse plate matching the tube diameter, and the transverse plate thickness were the primary contributors to the large flexibility of the transverse plate in socket connections. In groove welded connections, this hole is not necessary except for the flow of liquid zinc in galvanized tubes and access for welding the backing ring to the tube wall. Thus, the base plate in the Type XI specimen was provided with a 14 in (356 mm) diameter opening with two 1 in (25 mm) wide slots, in discussion with the fabricator, for sufficient access during welding the backing ring to the tube wall and easy flow of liquid zinc during galvanizing.

For ease of comparison with other high-level lighting support specimens, the pole cross-section in Type XI specimens was maintained the same as Type X and Type XII specimens. A 2.5 in (64 mm) thick base plate was provided, which was fastened with 8 bolts evenly spaced and aligned with alternate corners on a bolt circle of 30 in (762 mm) diameter. The backing ring at the pole base groove-welded connection was $^1/_4$ in (6 mm) thick and approximately 2 in (51 mm) high. The base plate thickness, the opening diameter and the number of bolts were decided based on a parametric study such as to match the fatigue performance of the fillet-welded tube-to-

30

transverse plate connection in specimen Type X, which had a 3 in (76 mm) thick base plate with 16 bolts. The specimen included a reinforced handhole. Details of this specimen type are shown in Figure 11.

Specimen Type XII

Ten Type XII specimens were tested. This specimen type represented a multi-sided high-level luminaire support structure having a conventional stiffened fillet-welded tube-to-transverse plate connection (socket connection) at the pole base.

For direct comparison of the fatigue performance with Type X and Type XI specimens, having fillet-welded and groove-welded tube-to-transverse plate connections respectively, the pole cross section of specimen Type XII was maintained the same. Eight fillet-welded tapered stiffeners with wrapped around weld at the stiffener terminus on the tube were provided at alternate corners, as a cost-effective optimized design. Stiffeners with a transition radius at the terminus on the tube are fabrication intensive and are expected to be costlier than a tapered alternative. To avoid exposing the lack of fusion at the weld root in fillet and partial penetration groove welds, a stiffener terminus with a transition radius needs to be groove welded. In addition, it is difficult to carry out controlled grinding of weld toe without grinding the tube at the transition, which is a concern for these thin tubes. Since stiffeners were used to protect the socket connection, a 2 in (51 mm) base plate was used as a minimum. Eight bolts were provided on a 30 in (762 mm) bolt circle spaced equally between the stiffeners (aligned with the middle of flat sides).

The stiffened tube-to-transverse plate socket connection in specimen Type XII was designed parametrically based on 3D FEA. The parameters considered were: the tube thickness; the stiffener thickness; the height of the stiffener; and the angle of the stiffener at the termination on the tube. An optimum solution with equal likelihood of fatigue cracking at the stiffener terminus and the socket weld toe on the tube was obtained with: (1) a stiffener height of about 16 in (406 mm); (2) a stiffener termination angle of about 14^0; and (3) a stiffener thickness of about 1.25 times the tube thickness. Accordingly, 18 in (457 mm) tall and $^3/_8$ in (10 mm) thick stiffeners with a termination angle of 15^0 on the tube were provided. Details of the specimen are shown in Figure 12.

Jacket Retrofitted Specimens JRX and JRXI

Retrofitting fatigue-cracked high-level luminaire support structures using steel jackets was investigated on specimens X-3 and XI-9 that had developed fatigue cracking at the tube-to-transverse plate weld toe on the tube at the pole base. The retrofitted specimens were identified by attaching the prefix JR to the respective specimen type.

Similar steel jacket retrofits encompassing the pole base and the hand hole were designed and implemented by Wiss Janney Elstner Associates (WJE) for high-level luminaire structures in Iowa (*22*). Since fatigue cracking in the subject structures in service mostly occurred at the tube-to-transverse plate weld, while the other welded connections in the structure remained un-cracked, the bolted jacket retrofits provided a cost effective solution by eliminating the need for replacing the bottom section of the structure, which would have involved complete removal of the structure from the foundation, section separation and unit replacement, and internal disassembly and assembly of mechanical and electrical equipments.

31

The steel jacket for this research used a split tube design with a full-penetration groove-welded connection between the jacket shell (tube) and the base (transverse) plate that did not employ a backing ring. The groove weld was deposited from both sides with the weld root back gouged and the weld quality was ascertained by Ultrasonic Testing. A cut out matching the hand hole was provided in the jacket shell. The jacket was non-galvanized and was fastened to the retrofitted specimens by bolted connections. Details of the jacket retrofit are shown in Figure 13. The design philosophy of the retrofitted jacket specimens was to ensure infinite life without further growth of existing fatigue cracks.

Specimens Type X had a fillet-welded tube-to-transverse plate connection at the pole base. Specimens Type XI had a groove-welded connection at the pole base, with the backing ring welded at the top to the pole wall. Both specimens included a reinforced hand hole. Specimen X-3 had developed a 17 in (432 mm) long fatigue crack in the tube at the tube-to-transverse plate weld toe on the tube, on the same side as the hand hole. Specimen XI-9 had developed fatigue cracks in the tube on the hand hole side at the toes of the tube-to-transverse plate weld and the backing ring to tube weld at the top face. These cracks were respectively 19 in (483 mm) and 25¾ in (654 mm) long at the time of retrofit. On the opposite side, the specimen had developed a 17 in (432 mm) long fatigue crack in the tube at the tube-to-transverse plate weld toe on the tube.

Only one set of jacket was fabricated. After testing of JRXI was completed, the jacket was taken off the specimen XI-9 and was put on specimen X-3. The bottom of the hand hole frame in specimen XI-9 was 14 in (356 mm) above the base plate, whereas in specimen X-3 the hand hole frame was only 12 in (305 mm) above the base plate. The cutout in the jacket for the hand hole was modified accordingly. In addition, specimen XI-9 used 8 anchor rods for fastening to the foundation plate, whereas specimen X-3 used 16 anchor rods. Locations of the additional holes in the base plate of X-3 interfered with locations of some of the tapped and drilled bolt holes for connecting the jacket to the base plate. Clamped connections were devised for these situations.

EXPERIMENTAL STUDIES

Test Setups

The tests were conducted at the multi-directional testing facility in the ATLSS Engineering Research Center, and at the dynamic testing bed in the Fritz Engineering Laboratory.

Four setups were built in the Fritz Laboratory capable of testing sign and signal structure specimens that were loaded vertically at the tips of the mast-arms and in the plane containing the arms, simulating galloping oscillation. In the ATLSS Center, two setups were built for testing sign and signal structure specimens loaded vertically in the plane containing the arm. Two other setups were built for testing high-level lighting support structure specimens that were loaded laterally simulating vortex shedding oscillation in the first mode. Accordingly, specimens Type IX, X, XI and XII were tested in the ATLSS Center.

The specimens were loaded using hydraulic actuators. Suitable fixtures were provided at the arm tips of the sign and signal structure specimens and at the loading point of the high-level lighting structure specimens to receive actuators.

32

All specimens were supported on washers under the bolt holes and were fastened to a foundation plate which in turn was anchored to the rigid laboratory floor. The specimens were supported such as to simulate the discrete supports to these structures in the field, where the pole base-plates are supported on leveling nuts at the anchor locations and are restrained in position by a pair of locking nuts at each anchor. Although the test setup did not replicate the free up-stand of the anchors between the bottom of the leveling nut and the top of concrete pedestal, which is usually limited to one nut height, the setup accurately reproduced the boundary conditions for the fatigue tests. The small up-stands do not introduce any appreciable flexibility to the base-plate and therefore does not significantly affect the stresses driving fatigue cracking of the tube-to-transverse plate welded connections at the pole base. The flexibility of the base-plate from differential deformation of the transverse plate due to discrete supports, however, can influence the stresses driving fatigue cracking of the pole tube-to-transverse plate welded connection, which was incorporated by discretely supporting the poles on the washers.

Test Setups in the Fritz Laboratory

The schematics of test setups in the Fritz Engineering Laboratory are shown in Figure 14. Four independent test setups were prepared in the east and west dynamic test beds for testing four specimens simultaneously. Each setup consisted of a test frame accommodating one specimen at a time.

The specimens were supported on washers under the bolt holes and were fastened to a foundation plate which in turn was anchored to the rigid laboratory floor. The foundation plate was 2 in (51 mm) thick. Upward flexural deflection of this foundation plate during fatigue tests was limited by a hold down beam laid across this plate behind the pole (the opposite side of arm), which was anchored to the laboratory floor (Figure 15).

The specimens were loaded vertically in the plane of the arm by actuators supported from overhead reaction frame. The testing equipment used at Fritz Laboratory was manufactured by Amsler. The Amsler system comprised a variable stroke hydraulic pump (called a pulsator) to load the jacks. The jacks used for this test program had a maximum dynamic capacity of 22 kips (98 kN)

Test Setups in the ATLSS Center

The test setups in the ATLSS Center are shown in Figure 16. Four independent test setups were prepared for testing two high-level luminaire support structure and two sign and signal support structure specimens simultaneously. One specimen could be tested at each setup at a time.

The test setups for the high-level lighting support structures were designed to load the specimens laterally (horizontally) by supporting the actuators against reaction walls. The specimens were supported on washers under the bolt holes and were fastened to a foundation plate which in turn was anchored to the rigid laboratory floor. The foundation plate was 4 in (102 mm) thick. The maximum upward deflection of the foundation plate during testing was insignificant, which was verified by both measurements and FEA. The actuators were attached to specimens using two plates on the opposite faces of the specimens that were tied together by anchor rods passing through the specimen. Wooden shims and neoprene pads were used for uniform contact between the specimen and loading plates.

33

The test setups for the sign and signal structures were designed to load the specimens vertically in plane of the arm from underside by supporting the actuators off the laboratory floor. The specimens were supported on washers under the bolt holes and were fastened to a foundation plate that was supported on a pair of wide flange sections and was anchored to the rigid laboratory floor. The foundation plate was 6 in (152 mm) thick. The supporting assembly was very rigid to allow any noticeable flexing of the foundation plate.

In the ATLSS Center, the tests were conducted using a computer controlled closed loop electro-hydraulic system manufactured by Vickers. Initially Hannon fatigue rated actuators having maximum capacity of 132 kips (587 kN) were used for the sign/signal structure setup and Vickers TJ actuators having a capacity of 30 kips (133 kN) were used for the high-level luminaire structure specimens. Subsequently to increase the frequency of testing, all specimens were loaded using Vickers TJ actuators and MTS actuators having a capacity of 22 kips (100 kN) respectively.

Instrumentation and Data Acquisition

Encapsulated metallic bonded resistance strain gauges of 0.04 in (1 mm) and ¼ in (6 mm) gauge length were used to measure strains during static and fatigue tests. The loads and displacements were measured using load cells and tempasonics. The data were collected using Campbell Scientific CR 9000 digital data logger. In addition, the spatial distribution of surface strain at critical areas of interest was measured using a 3D-image correlation photogrammetry (3D ICP) technique in one specimen of each type.

Static Tests

As per the test protocol, prior to the fatigue tests all specimens were loaded at a slow rate (static) up to the estimated maximum test load followed by complete unloading to: (a) evaluate the response of the structure compared to the analytical prediction; (b) determine the dynamic load and displacement limits for the fatigue tests; and (c) shake down residual stresses. This up-down loading was repeated at least three times or until the residual strains at the strain gauges were negligible.

One specimen of each type was instrumented extensively using conventional strain gauges and tested under static loading to capture the overall response of the structure and to determine the stresses near the critical details. The surface stresses near the critical details in these structures were also determined by 3D ICP. The FEA results were compared with the static test measurements to assess the quality of the analytical models and to verify the applicability of the FEA models in predicting the fatigue performance of the test specimens based on the analytical protocol. All static tests were conducted following the proposed test protocols.

Details of Conventional Measurements

Strains at discrete locations of interest were measured using bondable strain gauges. The locations of strain gauges were decided based on FEA results of the test specimen and the history of fatigue cracking in these structures in service. Multiple gauges were placed at or near the weld toe on the tube surface of the pole and the arm, where the stress concentration was the most severe and where most of the fatigue cracking was exhibited by these structures in service. Additional gauges were provided away from the weld toe for controlling nominal stresses.

34

Gauges were provided both on the outer and the inner surfaces of the tube. Load cells were provided to control the load applied on the structure. In addition, displacements of the specimens in the direction of loading were measured at the point of load application. In the Fritz Laboratory, either a tempasonic or a Linear Voltage Differential Transformer (LVDTs) was used for measuring displacements. In the ATLSS Center, the displacement sensors (tempasonic or LVDT) of the servo-hydraulic actuators were used for measuring displacements.

Typical arrangement of strain gauges in specimens at a few critical regions on the tension side (under static loading) outer face of the pole and the arm are shown in Figures 17-20 for the specimens Type I, II, VII and X respectively.

Details of 3D ICP Measurements

The surface stresses at the critical details were also measured using 3D ICP technique in one specimen of each type that was instrumented extensively for static test. Displacements and strain fields at four critical regions (identified as Regions 1, 2, 3 and 4) of the signal structures were measured by this technique.

3D ICP is a non-contact discrete point optical measurement technique that combines the principles of photogrammetry with an image correlation algorithm to generate a displacement field at discrete points. A fairly fine pattern with good contrast, such as a black spray paint on a white background, is applied to the measured object. Based on triangulation principles, photogrammetry uses a series of photographs taken of the measured object from different angles to recreate the exact coordinates of the target points on the pattern. Image correlation algorithms engage in pattern recognition. With an image processing software, unique sub-regions called facets of the applied pattern are identified and tracked under load deformation at sub-pixel accuracy, yielding displacements. The system can provide a displacement resolution to the order of about 1-2 μm over a viewing area of about 10 in × 10 in (254 mm × 254 mm). The displacement resolution of this technique thus scales somewhat linearly with the area to be measured.

The 3D ICP measurements were conducted by Trilion Quality Systems. The measuring device or the photogrammetry camera consisted of a pair of lenses mounted on a frame and tripod and controlled by a laptop computer (Figure 21). Capturing of pictures, analysis and processing of data was conducted by proprietary software called ARAMIS. The working distance was approximately 40 in (1 m). The camera angle, i.e., the total angle between two lines from one point on the specimen to each camera was 15.6^0. The lenses were of 50 mm focal length. The field of view was 5.5 in (140 mm) wide × 3.5 in (90 mm) high. A white background encompassing the field of view was spray painted at the region of interest. A pattern was created on this background by speckles of black spray paint. Calibration was performed by using standard templates of regularly spaced white dots on a black background. The measurement accuracy was of the order of 50~75 με.

Fatigue Tests

Details of Fatigue Tests

Fatigue testing of the specimens was conducted at constant amplitude fatigue loading following the test protocol. The loading cycles were sinusoidal. Minimum stress (S_{min}) and the stress range (S_r) were the two design stress variables considered for the fatigue tests. The sign

35

and signal structure specimens Type I, II, III, IV, V, VI and VII, were tested under a high level of minimum stress, representing the dead load effects from the overhanging weight of the signs and signal attachments. The details in the high-level luminaire structure specimens Type IX, X, XI, and XII were tested under complete stress reversal, reproducing the typical in-service loading of these structures.

The tests were controlled by strain gauge data. The control strain gauge in the sign and signal structure specimens was located on the outer tensile surface of the arm (top surface) on the major axis of symmetry of the cross section at 6 in (152 mm) from the tube-to-transverse plate weld toe on the tube at the arm base. In the high-level luminaire structure specimens the control gauge was located on the outer surface of the pole wall on the axis of symmetry at about 70 in (1778 mm) from the tube-to-transverse plate weld toe at the pole base. The control gauge locations were decided based on FEA results as presented earlier, beyond the effect of any secondary stresses, to capture only the nominal stress. In addition, a few gauges were provided near the weld toes where fatigue cracking was anticipated from the FEA results.

Static tests were performed prior to fatigue tests to determine the dynamic load and displacement limits during fatigue tests to achieve desired stresses at the control gauges and to shake down residual stresses from fabrication. These static tests were conducted following the static test protocols.

RESULTS OF EXPERIMENTAL STUDIES

Static Test Results

The stress measurements at discrete points are compared with the stresses obtained from the FEA results in Figures 22 through 35 for a few specimen types. Good correlation was noted between the FEA stresses and the measured stresses away from the regions of geometric discontinuity. Near the weld toes, the surface stress profiles were similar to the FEA results; however, the measured peak stresses were lower. One of the reasons for this is the difference between the modeled and the actual global weld geometry and local weld toe profile. While the weld toe was modeled as a notch with zero toe radius, in reality each weld toe has a finite radius and thus a smaller peak stress develops at the weld toe. Also as will be discussed later, metallographic examinations of the welds revealed that the global weld profile particularly the weld angle in many cases was significantly smaller than the specified weld angle of 30^0. Limited FEA results with a reduced weld angle showed significant reduction in stresses particularly near the weld where the FEA results exceeded the strain gauge measurements. Thus, the static tests verified the FEA results and provided credence to analytical predictions based on the FEA models.

A typical surface stress contour obtained by the 3D ICP technique in Region 1 of specimen Type I near the pole-to-base plate weld is shown in Figure 36. The contour is overlaid on the actual region in the measured structure, where the spray painted pattern is visible. Also shown in this figure is the contour plot obtained from FEA. Both the pictures correspond to an applied load of 6 kip (27 kN) at the arm tip and the stresses are plotted over the same range. Both analysis and the measurements indicate similar stress contours. A similar comparison for the handhole detail (Region 3) is shown in Figure 37.

The stresses obtained by 3D ICP technique in specimens Type I and II are plotted along with the stresses obtained from FEA and bondable strain gauges (Figures 22 through 29). Comparison of the stresses obtained by bondable strain gauges and by 3D ICP technique produced mixed results. While in some cases the 3D ICP measurements produced a reasonable agreement with the bondable strain gauges within the accuracy of the system, in other cases the data were quite different. Measurement of stresses by 3D ICP provided a spatial distribution of surface stresses over the region of measurement. In addition, it provided surface topography of the measurement area. The accuracy in measurement was 50~75 με, which is equivalent to about 2~3 ksi (14~21 MPa). Compared to strain gauge measurements the 3D ICP measurements were inaccurate.

Fatigue Test Results

A summary of fatigue test results is presented in Table 5.

Specimen Type I

Seven Type I specimens were fatigue tested. These specimens represented round sign and signal support structures and employed fillet-welded tube-to-transverse plate connections in the poles and arms. These specimens also contained a reinforced handhole and ring stiffened box at the mast arm to pole connections.

Specimens I-1, I-2 and I-3 were tested as part of validation of protocols. These specimens were fatigue tested to determine the finite life fatigue performance of the connections. The other four specimens (I-4, I-5, I-6 and I-7) were tested to determine the CAFT of the connections.

Specimens I-1, I-2 and I-3 were tested at 12 ksi (83 MPa) nominal stress range at the tube-to-transverse plate weld toe on the tube at the arm base. These specimens developed fatigue cracking at the arm tube-to-transverse plate weld toe on the tube (Figure 38).

After failure of the arms, fatigue testing of the poles in specimens I-1, I-2 and I-3 were continued by replacing the failed arms with previously delivered arms that were rejected because of a mismatch between design and fabrication. Multiple fatigue cracks developed from the un-fused root of the handhole frame-to-pole fillet weld (Figure 39). Holes were drilled at the crack tips to arrest crack growth as the cracks advanced into the pole wall (Figure 41), and the tests were continued. These tests were terminated when fatigue cracks initiated from the edge of these arrest holes and the tests could not be continued. No fatigue cracks were detected at the tube-to transverse plate fillet-weld at the pole base or in the ring stiffened box connections.

Specimens I-4 and I-5 were tested under a nominal stress range of 7.0 ksi (48 MPa), the CAFT of AASHTO Category D, at the tube-to-transverse plate fillet-weld toe on the tube at the arm base. Using the analytical protocol the CAFT of this detail was assessed to be about 6 ksi (41 MPa). Both specimens developed fatigue cracks in the mast-arms at the tube-to-transverse plate fillet-weld toe on the tube. The weld toe on the tube at the pole base was subjected to a nominal stress range of 4 ksi (28 MPa), where no fatigue cracks was detected. Accordingly, it was decided to test specimens I-6 and I-7 at a nominal stress range of 4.5 ksi (31 MPa), corresponding to the CAFT of AASHTO Category E, at the weld toe on the tube at the arm base, and these tests were run-out. Specimens I-6 and I-7 were re-tested under an elevated nominal stress range of 7 ksi (48 MPa) at the weld toe on the tube at the arm base. Typical fatigue crack growth was detected in these specimens at the arm tube-to-transverse plate fillet weld toe on the tube.

37

Since no fatigue cracking was detected at the pole base, at the handhole, or at the arm-to-pole ring-stiffened box connections in specimens I-4, I-5, I-6, and I-7, it was decided to continue testing these poles using a specially fabricated arm. The poles in specimens I-4, I-5 and I-6 were run-out when tested under a nominal stress range of 4 ksi (28 MPa) at the tube-to-transverse plate fillet-weld toe on the tube at pole base (corresponding to 10 ksi [69 MPa] in the replacement arm). The pole in specimen I-7, however, developed typical fatigue cracking at the tube-to-transverse plate fillet-weld toe on the tube, when tested at the same nominal stress range at the crack site.

A crack was discovered from the root of the handhole frame-to-pole fillet-weld in specimen I-6, which was arrested by drilling a hole ahead of the crack tip in the pole wall. The poles in specimens I-4, I-5, and I-6 were re-tested at an elevated stress range of 5.7 ksi (39 MPa) at the tube-to-transverse plate fillet-weld toe on the tube at the pole base (corresponding to 10 ksi [69 MPa] in the arm). The pole in I-4 developed fatigue cracking from the root of the handhole frame-to-pole weld. Testing of the pole in I-5 resulted in typical fatigue cracking at the pole base weld toe on the tube. Fatigue testing of the pole in I-6 was terminated when a fatigue crack initiated from the edge of crack arrest hole.

No cracking was found in the arm-to-pole ring stiffened connection or any other welded details in the Type I specimens.

Specimen Type II

Three Type II specimens were fatigue tested as part of validation of protocols. These specimens represented round sign and signal support structures. The poles and the arms employed full-penetration groove-welded tube-to-transverse plate connections, where the backing ring was continuously fillet-welded to the plate and to the tube at the top face. The groove-welds were provided with a fillet reinforcement. These specimens also contained a reinforced handhole and fillet-welded gusseted box at the mast-arm-to-pole connections.

All Type II specimens were tested at a stress range of 12 ksi (83 MPa) at the tube-to-transverse plate groove-weld toe on the tube at the arm base, and developed fatigue cracks in the arm tube, either at the arm-to-transverse plate groove-weld toe or, at the backing ring top weld toe, or both (Figures 42 and 43).

In addition, multiple fatigue cracks developed in these specimens from the unfused root of the handhole frame-to-pole fillet-weld similar to the specimen Type I. In specimen II-2, the crack originating from the handhole grew almost half the pole perimeter and fractured the hand hole frame before it was detected, thereby terminating the fatigue test. The crack in the arm of II-2 grew to 4.5 in (114 mm) when testing of this specimen was terminated. In other specimens, the crack growth from the handhole was detected at an early stage and arrest holes were drilled at the crack tips as the cracks advanced into the pole wall to continue fatigue tests.

After failure of the arms, fatigue testing of the poles in specimens II-1 and II-3 were continued with the replacement arms. Only specimen II-1 developed fatigue cracking at the tube-to-transverse plate groove-weld toe on the tube at the pole base.

None of the built-up box mast-arm-to-column connections or other connections in these specimens developed any fatigue cracking.

38

Specimen Type III

Ten Type III specimens were fatigue tested. These specimens represented round sign and signal support structures. The arms and poles in these specimens had groove-welded tube-to-transverse plate connection with the backing ring welded to the plate but not to the tube at the top face. The groove-weld was provided with a fillet reinforcement. This specimen type also included an unreinforced hand hole and a ring-stiffened arm-to-pole connection.

Six specimens (III-1, III-2, III-3, III-8, III-9, and III-10) were fatigue tested to determine the finite life fatigue performance of the connections. The other four specimens (III-4, III-5, III-6 and III-7) were tested to determine the CAFT of the connection details.

Specimens III-1, III-2 and III-3 were tested at a nominal stress range of 12 ksi (83 MPa) at the tube-to-transverse plate groove-weld toe on the tube at the arm base. Specimens III-8, III-9 and III-10 were tested at a nominal stress range of 16 ksi (110 MPa).

Fatigue testing of specimen III-4 was run-out thrice when tested at nominal stress ranges of 7 ksi (48 MPa), 10 ksi (69 MPa), and 12 ksi (83 MPa) respectively at the tube-to-transverse plate groove-weld toe on the tube at the arm base. When retested at an elevated nominal stress range of 16 ksi (110 MPa), the arm experienced fatigue failure from the weld toe on the tube.

The arms in specimens III-5 and III-6 experienced fatigue cracking at a nominal stress range of 10 ksi at the tube-to-transverse plate groove-welded connection at the arm base. The fatigue cracks developed from the tack welds between the top face of the backing ring and the tube. Figure 44 shows the fatigue cracking in the arm of III-5 from the toe of the tack weld between the backing ring and the tube. Figures 45 and 46 show the fatigue crack growth in the arm of specimen III-6 from a lack of fusion between the tack weld and the tube. Although the tack welds were not shown in the fabrication drawings, they were used despite the fabricator being instructed not to use tack welds that were not incorporated in the final welds.

Fatigue testing of specimen III-7 was run-out twice when tested at nominal stress ranges of 10 ksi (69 MPa) and 12 ksi (83 MPa) respectively at the tube-to-transverse plate groove-weld toe on the tube at the arm base. When retested at an elevated nominal stress range of 16 ksi (110 MPa), the arm experienced fatigue cracking through the throat of the weld.

After the arms failed, fatigue testing of the poles in the Type III specimens was continued with special replacement arms to determine the CAFT of the groove welded connection at the pole base. The run-out specimens were retested at progressively elevated stress ranges until fatigue cracking prevented further testing. None of the groove-welded connections at the pole base developed fatigue cracking. All tests were terminated by fatigue crack growth from the edge of the unreinforced handhole. Only in specimen III-1, a 1 in (25 mm) arrest hole was drilled at the crack tip for continued testing, when the crack grew into the pole wall by $^3/_8$ in (10 mm). This attempt to arrest crack growth was, however, unsuccessful as a fatigue crack initiated soon (within another 60,000 cycles) from the edge of the arrest hole, terminating the test. It was evident that arrest holes were not effective at the high stress ranges at which the tests were conducted.

Fatigue testing of the poles were run-out as follows: in specimens III-5, and III-6 at a nominal stress range of 5.4 ksi (37 MPa) at the tube-to-transverse plate groove-weld toe on the tube at the pole base (corresponding to a nominal stress range of 10 ksi [69 MPa] at the arm base);. in specimens III-1, III-2, III-3, III-4, III-5, III-6 and III-7 at a nominal stress range of 6.5

39

ksi (45 MPa) at the pole base (corresponding to a nominal stress range of 12 ksi [83 MPa] at the arm base); in specimens III-4, III-5, III-7, III-8 and III-10 at a nominal stress range of 8.7 ksi (60 MPa) at the pole base (corresponding to a nominal stress range of 16 ksi [110 MPa] at the arm base); in specimens III-2, III-4, III-5, and III-7 at a nominal stress range of 10 ksi (69 MPa) at the pole base; and in specimen III-4 at a nominal stress range12 ksi (83 MPa) at the pole base.

Fatigue cracking from the unreinforced handhole occurred as follows: in specimens III-1, III-3, III-6, III-8, and III-10 subjected to a nominal stress range of 10.5 ksi (72 MPa) on the net section (corresponding to a nominal stress range of 10 ksi [69 MPa] at the pole base); in specimens III-2, III-5 and III-7 subjected to a nominal stress range of 12.6 ksi (87 MPa) on the net section (corresponding to a nominal stress range of 10 ksi [69 MPa] at the pole base); and in specimen III-4 subjected to a nominal stress range of 16.7 ksi (115 MPa) on the net section (corresponding to a nominal stress range of 16 ksi [110 MPa] at the pole base).

No cracking was found in the arm-to-pole ring-stiffened connection or any other welded details in these specimens.

Specimen Type IVA and IVB

Two each of specimens Type IVA and IVB were tested. These specimens represented round sign and signal support structures. Similar to specimens Type III, the arms and poles in these specimens had a groove-welded tube-to-transverse plate connection with the backing ring welded to the plate but not to the tube at the top face. The groove-weld was provided with a fillet reinforcement. The specimens employed a fillet-welded gusseted box at the mast-arm-to-pole connections. Specimens IVA did not contain any handhole and specimens IVB were provided with a reinforced handhole similar to specimens I and II. Specimens IVA were loaded in the plane containing the arm, and specimens IVB were loaded out-of-plane at 45^0. The Type IV specimens were tested to determine CAFT of the various welded connections in these structures.

Fatigue testing of specimens IVA-1 and IVA-2 was initiated at a nominal stress range of 7 ksi (48 MPa) at the tube-to-transverse plate weld toe on the tube at the arm base. These tests were run-out and also subsequently when tested at an elevated nominal stress range of 10 ksi (69 MPa) at the arm base. Specimen IVA-1 developed fatigue cracking at the tube-to-transverse plate weld toe on the tube at the arm base when retested at an elevated stress range of 12 ksi (83 MPa) at the arm base. Fatigue testing of specimen IVA-2, however, was run-out successively at nominal stress ranges of 12 ksi (83 MPa) and 16 ksi (110 MPa) at the arm base. The connection at the arm base developed fatigue cracking at the weld toe on the tube when tested under a nominal stress range of 24 ksi (165 MPa).

After failure of the arms, fatigue testing of the poles in these specimens was continued with a special replacement arm. Testing of the pole in specimen IVA-1 was run-out subsequently under nominal stress ranges of 6.5 ksi (45 MPa) corresponding to a nominal stress range of 12 ksi (83 MPa) at the arm base, and 10 ksi (69 MPa) at the tube-to-transverse plate weld toe on the tube at the pole base. This connection experienced fatigue cracking at the weld toe on the tube, when retested for the fourth time at an elevated nominal stress range of 12 ksi (83 MPa). The tube-to-transverse plate connection at the pole base in specimen IVA-2 developed fatigue cracking at the weld toe on the tube when tested under a nominal stress range of 13.1 ksi (90 MPa) corresponding to a nominal stress range of 24 ksi (165 MPa) at the arm base.

Fatigue testing of specimen IVB-1 was initiated under out-of-plane loading at a nominal stress range of 10 ksi (69 MPa) at the tube-to-transverse plate weld toe on the tube at the arm base. This test was run-out. When retested at an elevated nominal stress range of 12 ksi (83 MPa), a fatigue crack developed from the root of the side gusset to pole weld at the bottom corner (Figure 47). Testing of this specimen was continued after drilling holes at the crack tips on the pole wall and the test was run-out without further crack growth. The specimen was retested at an elevated stress range of 16 ksi (110 MPa) at the arm base and the test was terminated due to fatigue cracking from the root of handhole frame-to-pole weld that grew into the tube. A hole was drilled at the crack tip on the tube to continue testing, but with limited success, as a fatigue crack initiated from the edge of the hole within another 58,000 cycles. The nominal stress range at the handhole was 9.3 ksi (64 MPa) on the net section.

Fatigue testing of specimen IVB-2 was also conducted under out-of-plane loading at a nominal stress range of 10 ksi (69 MPa) at the tube-to-transverse plate weld toe on the tube at the arm base. This test was also terminated due to fatigue cracking from the root of handhole frame-to-pole weld that grew into the tube. The nominal stress range at the handhole was 5.8 ksi (40 MPa) on the net section.

Specimen Type V

Four Type V specimens were tested. These specimens employed mast-arm-to-pole clamp connections. The arm tube was connected to the clamp plate with a fillet-weld. Fatigue testing of two specimens V-1 and V-2 was conducted at a nominal stress range of 12 ksi (83 MPa) at the arm tube-to-clamp plate weld toe on the tube. Specimens V-3 and V-4 were tested at a nominal stress range of 7 ksi (48 MPa). All tests were terminated by fatigue cracking at the arm tube-to-clamp plate weld toe on the plate (Figure 48).

Subsequently, fatigue testing of the groove welded connection at the pole base in specimens Type V were continued by testing the poles as vertical members under lateral loading (similar to the high-level luminaire structure specimens, but under a sustained minimum load). The poles were tested at nominal stress range of 12 ksi (83 MPa) at the tube-to-transverse plate weld toe on the tube. The higher stress range was selected since none of the groove welded tube-to-transverse plate connections at the pole bases in specimens Type III and IV with equivalent estimated stress concentration had developed fatigue cracking below a nominal stress range of 12 ksi (83 MPa). Three specimens (V-1, V-2, and V-3) developed fatigue cracking at the tube-to-transverse plate weld toe on the tube.

Specimen Type VI

Ten Type VI specimens were tested. These specimens represented round sign and signal support structures. The specimens employed a novel partial-penetration groove-welded mast-arm-to-column pass-through connection. The pole base was provided with a groove-welded tube-to-transverse plate connection, with the backing ring welded to the plate but not to the tube at the top face. The groove-weld was provided with a fillet reinforcement.

Using the analytical protocol, the CAFT of both the arm-to-pole pass-through connection and the tube-to-transverse plate connection at the pole base was estimated as approximately 12 ksi (83 MPa). Due to lack of any previous fatigue test data on this type of arm connection and the complex distribution of stresses between the pole and the arm-sleeve, an incremental approach was taken in deciding the test stress range for these specimens consistent with the proposed test

41

protocols. Fatigue testing of specimens VI-1, VI-2 and VI-3 was initiated simultaneously under a nominal stress range of 7.7 ksi (53 MPa) in the pole at the intersection with the arm sleeve, which resulted in a nominal stress range of 6.3 ksi (43 MPa) at the pole base. These stress ranges corresponded to a stress range of 12 ksi (83 MPa) in the arms of sign and signal structure specimens Type I, II, III, IV and VII employing a gusseted box or ring-stiffened mast-arm-to-pole connection. Since the specimens VI-1, VI-2, and VI-3 exhibited mixed results (see discussion later), another specimen (VI-4) was also tested at the same stress range. Fatigue testing of specimens VI-8, and VI-10 was conducted at a nominal stress range of 16 ksi (110 MPa) in the pole at the intersection with the arm sleeve, resulting in a nominal stress range of 13.1 ksi (90 MPa) at the pole base. This higher stress range was considered since none of the groove welded tube-to-transverse plate connections at the pole base in specimens Type III and IV with equivalent estimated stress concentration had developed fatigue cracking below a nominal stress range of 12 ksi (83 MPa). Specimen VI-9 was tested at nominal stress ranges of 12 ksi (83 MPa) in the pole at the intersection with the arm sleeve and 9.8 ksi (68 MPa) at the pole base respectively. Testing of specimens VI-5, VI-6 and VI-7 were conducted at a nominal stress range of 4.5 ksi (31 MPa) in the pole at the intersection with the arm sleeve, resulting in a nominal stress range of 3.7 ksi (26 MPa) at the pole base. These specimens were considered for infinite life tests.

All Type VI specimens developed fatigue cracking at the arm-sleeve-to-pole weld towards the free end of the sleeve (opposite to the arm side) — at the toe of the groove weld on the sleeve wall in the lower quadrants (see Table 5 and footnote for easy identification of crack locations), initiating closer to the upper ends. In specimens VI-4, VI-5, VI-6, VI-8, VI-9, and VI-10, the toe cracks developed in both the lower quadrants. One of the weld toe cracks in specimens VI-4, and VI-9, and the toe crack in specimen VI-2 initiated at a weld start-stop and progressed along the weld toe (Figure 49). In all but specimen VI-6, the cracks also branched into the pole and/or the arm-sleeve. In specimens VI-1, VI-2, VI-3 and VI-5, the cracks that branched into the pole and/or the arm-sleeve were arrested by drilling holes for continuing fatigue tests (Figure 50).

Fatigue tests were terminated when the total crack length along the arm sleeve-to-pole weld toe was at least 5 in (127 mm). The only exception was specimen VI-3, where the crack was 1¾ in (44 mm) long when the test was terminated at 20×10^6 cycles, as fatigue cracking of the starter piece prevented further testing. Two fatigue cracks developed at the arm-sleeve-to-pole weld toe in specimen VI-3. The upper crack branched into the pole and the sleeve, and was found after 11.1×10^6 cycles. Holes were drilled at the crack tips in the pole and the sleeve for continuing fatigue tests. The lower crack grew at a slow rate along the weld toe.

Specimens VI-5, VI-6, and VI-7 were run-out at 20×10^6 cycles, when tested under nominal stress ranges of 4.5 ksi (31 MPa) in the pole at the intersection with the arm-sleeve and 3.7 ksi (26 MPa) at the pole base. Upon retesting at an elevated stress range of 7.7 ksi (53 MPa) at the arm sleeve-to-pole intersection and 6.3 ksi (43 MPa) at the pole base, specimens VI-6 and VI-7 developed fatigue cracking. Testing of specimen VI-5, however, was run-out. Specimen VI-5 was again tested at an elevated nominal stress range of 10.3 ksi (71 MPa) at the arm sleeve-to-pole intersection and 8.2 ksi (57 MPa) at the pole base. The test was terminated by fatigue cracking of the arm-sleeve-to-pole weld.

In specimens VI-1, VI-3, VI-4 and VI-8 additional fatigue cracks were found in the starter piece from the edge of the alignment bolt hole at the top that grew around the tube

42

perimeter and interrupted fatigue testing. Alignment bolts were provided to prevent relative rotational slip between the arm, the starter piece and the sleeve about the arm axis. The bolt holes were located at top and bottom (at the maximum tensile/compressive fibers under flexural loading) and were drilled after the specimens were fully assembled. As such, the edges of the holes could not be completely ground smooth. The as-drilled edges coupled with high tensile stress range (including the stress concentration due to the hole) precipitated fatigue cracking from the lateral edges of the top hole in the starter piece at the arm junction. To reduce the applied stress range without losing any functionality, these holes were relocated on the neutral axis in subsequent specimens, which eliminated fatigue cracking from these holes in subsequent tests. Additional fatigue cracking of the starter pieces occurred in specimens VI-5, VI-6, VI-8 and VI-10 from surface scribes at the interface with the arm that grew around half of the perimeter before it was discovered. The surface scribes in the starter pieces were formed during slip fitting the arm on to the starter piece. On closer inspection it was determined that lumps of zinc deposits on the inside surface of the arm tube were causing these scratches and were preventing an uniform fit-up between the arm tube and the starter piece. These zinc deposits were ground off during assembly of subsequent specimens that eliminated further surface scribes and fatigue cracking of the starter pieces. The starter pieces were replaced once each in VI-3, VI-10, and twice in VI-8 for continuing fatigue tests.

None of the tube-to-transverse plate connections at the pole base developed fatigue cracking when the tests were terminated due to fatigue cracking of arm-to-pole connection. Subsequently, fatigue testing of the groove welded connection at the pole base in specimens Type VI were continued by testing the poles as vertical members under lateral loading (similar to the high-level luminaire structure specimens, but under a sustained minimum load), after the fatigue cracked arm-sleeve-to-pole connections were cut-off. No fatigue cracking was detected by magnetic particle and dye-penetrant testing at the tube-to-transverse plate weld toe on the tube at the pole base. The test setups for high-level luminaire support structure specimens were modified for testing these specimens.

Testing of poles in specimens VI-1, VI-2, VI-3, VI-4, VI-6, and VI-7 were initiated at a nominal stress range of 12 ksi (83 MPa) at the tube-to-transverse plate weld toe on the tube at the pole base. This connection in the assembled pole and arm specimens was subjected to a nominal stress range of 6.3 ksi (43 MPa). The higher stress range of 12 ksi (83 MPa) was considered since none of the groove welded tube-to-transverse plate connections at pole bases in specimens Type III and IV with equivalent estimated stress concentration had developed fatigue cracking below a nominal stress range of 12 ksi (MPa).

Only the pole of specimen VI-7 developed fatigue cracking at the tube-to-transverse plate weld toe on the tube at the pole base. Fatigue testing of poles in specimens VI-1, VI-2, VI-3, VI-4, and VI-6 were run-out. Upon re-testing at an elevated nominal stress range of 16 ksi (110 MPa), the poles of specimens VI-1, VI-4 and VI-6 developed fatigue cracking at the weld toe on the tube. Fatigue testing of specimens VI-2 and VI-3 were run-out when tested at an elevated nominal stress range of 16 ksi. When retested at a further elevated stress range of 24 ksi (165 MPa), the pole in specimen VI-3 failed by fatigue cracking; the testing of pole in specimen VI-2, however, was run-out.

Testing of poles in specimens VI-8, VI-9 and VI-10 were continued at the nominal stress range of 13.1 ksi at the tube-to-transverse plate weld toe on the tube at the pole base. The pole in specimen VI-9 developed fatigue cracking at the weld toe on the tube. The poles in specimens

43

VI-8 and VI-10, however, were run-out. Upon retesting at a nominal stress range of 16 ksi, the tube in specimen VI-10 developed fatigue cracking at the weld toe on the tube. The pole in specimen VI-8, however, was run-out at 12.5×10^6 cycles. This specimen finally failed by fatigue cracking at the weld toe on the tube, when tested at a nominal stress range of 24 ksi (165 MPa).

Specimen Type VII

Seven Type VII specimens were fatigue tested. This specimen type represented multi-sided sign and signal support structures and employed fillet-welded tube-to-transverse plate connections (socket connections) in the pole and the arm. These specimens also contained a reinforced handhole and a fillet-welded gusseted box at the mast-arm-to-pole connection.

Specimens VII-1, VII-2 and VII-3 were tested as part of validation of protocols. These specimens were fatigue tested to determine the finite life fatigue performance of the connections. The other four specimens (VIII-4, VII-5, VII-6 and VII-7) were tested to determine the CAFT of the details in multi-sided specimens.

Specimens VII-1, VII-2 and VII-3 were tested at 12 ksi (83 MPa) nominal stress range at the tube-to-transverse plate weld toe on the tube at the arm base and experienced fatigue cracking in the arm.

Specimens VII-4 and VII-5 were tested under a nominal stress range of 4.5 ksi (31 MPa), the CAFT of AASHTO Category E, at the tube-to-transverse plate fillet-weld toe on the tube at the arm base and experienced fatigue cracking in the arm. Using the analytical protocol, the CAFT of this detail was assessed to be about 4.5 ksi (31 MPa). An additional crack was discovered at the hand hole detail in specimen VII-4 (Figure 51). This crack initiated from the seam weld root of the handhole frame and progressed through the frame into the pole wall. A hole was drilled in the pole wall for continued testing.

In view of the result of specimens VII-4 and VII-5, it was decided to fatigue test specimens VII-6 and VII-7 at a nominal stress range of 2.5 ksi (17 MPa), corresponding to the CAFT of AASHTO Category E´, at the tube-to-transverse plate weld toe on the tube at the arm base. In specimen VII-7, a small crack was detected at one of the outermost bend corners on the tension face at a very early age of 70,000 cycles (Figure 52). However, this crack did not demonstrate any significant growth. Fatigue testing of specimens VII-6 and VII-7 was run-out. When re-tested at an elevated nominal stress range of 4.5 ksi (31 MPa) in the arm, both specimens developed fatigue cracking from the hand hole frame to pole weld. Growth of this crack was arrested by drilling hole at the crack tip in the pole, and the fatigue testing was continued. Testing of specimen VII-6 was again run-out, without further fatigue cracking from the other welded details. Specimen VII-7, however, experienced fatigue cracking in the arm. Specimen VII-6 experienced fatigue cracking in the arm when re-tested at an elevated stress range of 7 ksi (48 MPa) at the tube-to-transverse plate fillet-weld toe on the tube at the arm base.

All Type VII specimens failed by fatigue cracking in the arm at the tube-to-transverse plate fillet-weld toe on the tube at the arm base (Figure 53). These cracks initiated at the at the bend corners on the tension face at an early age due to high stress concentration, precipitated by sharp bend radius (~0.5 in [13 mm]), and were detected very early into the fatigue tests. The cracks then progressed through the thickness and grew as a through thickness crack on two fronts. Once the cracks developed out of the bends into the flat face, the crack propagation rate

reduced. Specimens VII-1, VII-2 and VII-3 also experienced similar fatigue crack growth at the tube-to-transverse plate fillet-weld at the pole base (Figure 54).

After failure of arms in specimens VII-4, VII-5, VII-6, and VII-7, fatigue testing of the poles in these specimens were continued with a special replacement arm. The pole base in specimen VII-6 was tested at a nominal stress range of 3.9 ksi (27 MPa) corresponding to a nominal stress range of 7 ksi (48 MPa) in the arm at the tube-to-transverse plate weld to on the tube. The poles in specimens VII-4, VII-5 and VII-7 were tested at a nominal stress range of 2.5 ksi (17 MPa) corresponding to a nominal stress range of 4.5 ksi (31 MPa) in the arm at the tube-to-transverse plate weld to on the tube. The pole of specimen VII-6 developed fatigue cracking at the tube-to-transverse plate weld toe on the tube. This test was, however, terminated by fatigue cracking from the root of the handhole frame-to-pole weld after 15.4×10^6 cycles. At that time, the fatigue crack at the pole base weld toe on the pole wall grew to $6^3/_8$ in (162 mm), which was slightly less than the failure criteria of half the tube diameter (6.5 in [165 mm]). Fatigue testing of poles in specimens VII-4, VII-5, and VII-7 was run-out. The pole in specimen VII-7 was re-tested at an elevated nominal stress range of 3.9 ksi (27 MPa) as a replicate fatigue test of the pole in specimen VII-6, and developed fatigue cracking at the tube-to-transverse plate weld toe on the tube at the pole base.

The poles in specimens VII-4 and VII-5 were re-tested at an elevated nominal stress range of 4.5 ksi (31 MPa), corresponding to the CAFT of AASHTO Category E. In specimen VII-4, a fatigue crack initiated in the pole wall from the hole that was drilled to arrest crack growth from the hand hole, which terminated the fatigue test. The pole base of specimen VII-5 developed a fatigue crack at the tube-to-transverse plate weld toe on the tube.

No fatigue cracking was detected in the fillet-welded gusseted box at the mast-arm-to-pole connections.

Specimen Type IX

Ten Type IX specimens were tested. This specimen type represented multi-sided high-level luminaire support structures having stool type stiffeners at the tube-to-transverse plate connection at the pole base. This specimen did not include any handhole. The specimens were tested under reversal loading applied in the plane of a stiffener pair.

Three specimens (IX-1, IX-2 and IX-3) were fatigue tested under a nominal stress range of 12 ksi (83 MPa) at the stiffener-to-tube weld toe on the tube at the termination of the vertical stiffeners. Considering the larger section modulus provided by the stiffeners, the nominal stress range at the tube-to-transverse plate weld toe on the tube at the pole base was 3.3 ksi (23 MPa). Three other specimens IX-8, IX-9 and IX-10 were fatigue tested under a nominal stress range of 16 ksi (110 MPa) at the stiffener-to-tube weld toe on the tube at the termination of the vertical stiffeners.

Specimens IX-4, IX-5, IX-6 and IX-7 were tested to determine the CAFT of the stool type stiffened socket connections. Using the analytical protocol, the CAFT of this detail was assessed to be about 12 ksi (83 MPa). The specimens were tested respectively at nominal stress ranges of 10 ksi (69 MPa), 7 ksi (48 MPa), 4.5 ksi (31 MPa), and 4.5 ksi (31 MPa) at the weld toes on the tube at the termination of the vertical stiffeners, as they sequentially developed fatigue cracking.

45

All Type IX specimens developed fatigue cracks from the vertical stiffener-to-tube weld toe on tube at the termination of the stiffeners (Figure 55). Multiple cracks developed at this section from each stiffener termination, which grew away from the stiffeners in the pole wall as through thickness cracks on two fronts and coalesced (Figure 56).

No cracks were detected at the tube-to-transverse plate fillet-weld toe on the tube at the pole base.

Specimen Type X

Three Type X specimens were tested. This specimen type represented a multi-sided high-level luminaire support structure and employed a fillet-welded tube-to-transverse plate connection (socket connection) at the pole base. This specimen also included a reinforced handhole. The specimens were tested under reversal loading, loaded laterally in a plane of symmetry containing the handhole.

Specimen X-1 was tested at a stress range of 5.4 ksi (37 MPa) at the tube-to-transverse plate weld toe on the tube at the pole base. This stress range was decided based on the FEA results and in view of the poor performance of this connection in high-level lighting support structures of similar cross section in TPF-5(116) Study (*18*) that were fatigue tested at a stress range of 10 ksi (69 MPa). Specimen X-1, however, was run-out. The specimen was subsequently retested at an elevated stress range of 8 ksi (55 MPa). This test was also run-out and the specimen finally developed fatigue cracks when tested at a stress range of 10 ksi (69 MPa). Specimens X-2, and X-3 were tested at a stress range of 8 ksi (55 MPa) at the tube-to-transverse plate weld toe on the tube at the pole base, and experienced fatigue cracking.

The Type X specimens developed fatigue cracking at the tube-to-transverse plate fillet-weld toe on the tube at the pole base (Figure 57). These cracks initiated at the bend corners, grew through the thickness, and progressed along the weld toe towards the sides as a through thickness crack on two fronts. In most cases, multiple cracks initiating at different corners coalesced to form one large crack.

No fatigue cracks developed at the handhole detail in the Type X specimens.

Specimen Type XI

Ten Type XI specimens were tested. This specimen type represented a multi-sided high-level luminaire support structure having full-penetration groove-welded tube-to-transverse plate connection at the pole base, where the backing ring was continuously fillet-welded to the plate and to the tube at the top face. The specimen included a reinforced handhole. The specimens were tested under reversal loading, loaded laterally in a plane containing the handhole. Six specimens (XI-1, XI-2, XI-3, XI-8, XI-9, and XI-10) were fatigue tested to determine the finite life fatigue performance of the groove-welded tube-to-transverse plate connection at the pole base and the handhole details. The remaining four specimens (XI-4, XI-5, XI-6, and XI-7) were tested to determine the CAFT of the connection details.

Specimens XI-1, XI-2, and XI-3 were tested at a nominal reversal (total) stress range of 12 ksi (83 MPa) at the tube-to-transverse plate weld toe on the tube at the pole base. The nominal test stress range for specimens XI-8, XI-9, XI-10 was intended to be 16 ksi (110 MPa) at the tube-to-transverse plate weld toe on the tube at the pole base. Specimen XI-8, however, was

inadvertently tested at a nominal stress range of 14 ksi (96 MPa). Specimens XI-9 and XI-10 were tested as planned.

Using the analytical protocol, the CAFT of the groove-welded detail against crack growth from the weld toe on the tube was estimated to be about 10.9 ksi (75 MPa). Specimens XI-5, XI-6, XI-7 and XI-8 were tested at a nominal stress range of 7 ksi (48 MPa), the CAFT of AASHTO Category D, at the tube-to-transverse plate weld toe on the tube at the pole base. No fatigue cracks were detected in the specimens by dye-penetrant and magnetic particle tests when the tests were run-out. Subsequently, the specimens developed fatigue cracks when retested at an elevated nominal stress range of 10 ksi (69 MPa), corresponding to the CAFT of AASHTO Category C.

In all specimens fatigue cracking occurred at the toes on the tube of both the tube-to-transverse plate weld and the backing ring top weld (Figure 58). The cracks initiated at the groove weld toe on the tube in the outermost or adjacent bend corners, grew through the tube thickness and progressed towards the sides as through thickness cracks on two fronts. Cracks at the toe of the backing ring top weld appeared after the cracking at groove-weld toe, when the backing ring acted as an alternate path for the stresses to the base plate. These cracks also initiated at the weld toe in the outermost corner, grew through the tube thickness and progressed towards the sides as a through thickness cracks on two fronts. In most cases, multiple cracks initiating at different corners coalesced to form one large crack. The crack growth rate at the groove-weld toe diminished after the cracking at the backing ring top weld toe, as this crack acted as a relief for the groove-weld. Attempts were made to continue fatigue testing until the crack at the weld toe at top of the backing ring grew to the failure criteria of half the tube diameter (12 in [305 mm]), unless the crack at the groove-weld toe grew so large that it prevented further testing.

No fatigue cracks were detected at the hand hole detail in the Type XI specimens.

Specimen Type XII

Ten Type XII specimens were tested. This specimen type represented a multi-sided high-level luminaire support structure having a stiffened fillet-welded tube-to-transverse plate connection (socket connection) at the pole base. The specimens were tested under reversal loading applied in the plane of a stiffener. Six specimens (XII-1, XII-2, XII-3, XII-8, XII-9, and XII-10) were fatigue tested to determine the finite life fatigue performance of the stiffened socket connection at the pole base. The remaining four specimens (XII-4, XII-5, XII-6, and XII-7) were tested to determine the CAFT of the connection details.

Specimens XII-1, XII-2, and XII-3 were tested at a nominal reversal (total) stress range of 12 ksi (83 MPa) at the stiffener-to-tube fillet-weld toe on the tube at the termination of the stiffener. The nominal stress range at the tube-to-transverse plate fillet-weld toe on the tube at the pole base was 8.5 ksi (57 MPa). Three other specimens (XII-8, XII-9, and XII-10) were tested at a nominal stress range of 16 ksi (110 MPa) at the stiffener-to-tube weld toe on the tube at the termination of the stiffener. The nominal stress range at the tube-to-transverse plate fillet-weld toe on the tube at the pole base was 11.3 ksi (78 MPa).

Using the analytical protocol, the CAFT of this stiffened socket connection against crack growth from the stiffener-to-tube weld toe on the tube at the stiffener termination was estimated to be about 10.2 ksi (70 MPa). Specimens XII-4, XII-5, XII-6, and XII-7 were initially tested at a

47

nominal stress range of 7 ksi (48 MPa), the CAFT of AASHTO Category D, at the stiffener-to-tube weld toe on the tube at the termination of the stiffener. Only specimen XII-6 developed fatigue cracking from the weld at the stiffener termination. No fatigue cracks were detected in specimens XII-4, XII-5 and XII-7 by dye-penetrant and magnetic particle tests when the tests were run-out. Subsequently, the specimens were retested at an elevated nominal stress range of 10 ksi (69 MPa), corresponding to the CAFT of AASHTO Category C, when fatigue cracking occurred at the stiffener termination.

All specimens failed by fatigue cracking at the stiffener-to-tube weld at the termination of the stiffener. In all but XII-6, these cracks originated at the weld toe on the tube. In specimens XII-1, XII-8, and XII-10, additional fatigue cracking occurred at the tube-to-transverse plate fillet-weld toe on the tube. Photograph of typical fatigue cracking in specimens Type XII is shown in Figure 59. In specimen XII-6, the crack initiated at the weld root and proceeded through the weld throat and into the tube wall. The exposed fracture surface (Figure 60) indicated that the fatigue crack grew from a relatively large lack of fusion at the stiffener-to-tube weld root, causing failure at the lower stress range.

Jacket Retrofitted Specimens JRX and JRXI

Two multi-sided high-level luminaire support structure specimens (X-3 and XI-9) that experienced fatigue cracking earlier were fatigue tested after retrofitting with a steel jacket. The steel jacket used a split tube design with a full penetration groove-welded connection between the jacket shell (tube) and the base (transverse) plate that did not employ a backing ring. The jacket was fastened to the retrofitted specimens by bolted connections

Using the analytical protocol, the CAFT of the groove-welded tube-to-transverse plate connection in the jacket was estimated to be about 12 ksi. Both the jacket retrofitted specimens XI-9 (identified as JRXI) and X-3 (identified as JRX) were fatigue tested at a nominal stress range of 10.0 ksi (69 MPa), the CAFT of the AASHTO Category C, at the tube-to-transverse plate groove-weld toe on the jacket tube. Both tests were run-out after 8.2×10^6 stress cycles without any visible cracking at the jacket tube-to-transverse plate weld. In specimen XI-9, however, fatigue cracks were found at the bottom corners of the handhole frame-to-pole weld at about 5.3×10^6 cycles (Figure 61) Originating from the lack of fusion at the root of this weld, the crack progressed into the handhole frame and into the pole wall. This crack growth stopped as it propagated into the compressive stress field of a bolted connection between the jacket and the pole. No growth of the cracks at the tube-to-transverse plate weld toe on the tube was observed.

PARAMETRIC STUDIES

The fatigue test results demonstrated that the tube-to-transverse plate connections were the most critical details in the sign, signal and high-level luminaire support structures. Fatigue cracking in these connections precipitated due to local out-of-plane bending or geometric stresses in the tube from the need to maintain compatibility between the tube and other elements at the connection. Thus, fatigue resistance of tube-to-transverse plate connections depends on the relative flexibility of the components at a connection or the connection geometry. This geometric stress concentration affects the fatigue resistance of the connections for both finite and infinite life performance. In addition, the resistance of the connections against any fatigue crack growth

48

for infinite life is also affected by the notch stress concentration related to local geometry of the weld.

The geometric parameters that can affect the relative flexibility of the components at an unstiffened tube-to-transverse plate connection are: the thickness of the transverse plate; the opening in the transverse plate (in groove-welded connections); the number of fasteners; the bolt circle ratio, defined as the ratio of the bolt circle diameter to the tube diameter; the tube diameter and thickness; the height and thickness of the backing ring (in groove-welded connections); and the number of sides and internal bend radius (in multi-sided sections). In stiffened connections additional geometric parameters are: the stiffener shape and size (thickness, height and angle); and the number of stiffeners (or stiffener spacing). While experimental studies would be the best way to establish the fatigue performance of welded connections, it is not feasible to conduct fatigue tests of all possible combination of the geometric parameters due to limited time and budget. As such, fatigue performance of the connections in both finite and infinite life regimes were evaluated and optimized over the range of applicable geometric dimensions using parametric FEA verified by limited test data. These analyses were conducted as per the analytical protocols presented earlier. Since a large number of models or parameter combinations had to be analyzed, pre- and post-processing of models were automated using Python scripting. About 10% of models were randomly selected for manual verification of the results.

Identification of Parameters

Unstiffened Fillet-welded Tube-to-Transverse Plate Connections in Round Tubes

Figure 62 shows the geometric parameters of an unstiffened fillet-welded tube-to-transverse plate connection in round tubes. These are: the thickness of the transverse plate (t_{TP}); the number of fasteners (N_B); the bolt circle or the ratio of the bolt circle diameter (D_{BC}) to the tube diameter (C_{BC}); the tube diameter (D_T) and thickness (t_T). The nomenclature of the parameters is tabulated in Table 6.

Unstiffened Groove-welded Tube-to-Transverse Plate Connections in Round Tubes

Figure 63 shows the geometric parameters of an unstiffened groove-welded tube-to-transverse plate connection in round tubes. In addition to the parameters identified for the fillet welded connections, the diameter of the opening in the transverse plate (D_{OP}) is a significant geometric parameter for an unstiffened groove-welded tube-to-transverse plate connection in round tubes. Nomenclature of the parameters is tabulated in Table 6.

The size of the backing ring was assumed as 2 in × ¼ in (51 mm × 6 mm). The backing ring was not welded to the tube. When the backing ring is welded to the tube, fatigue cracking can occur at the backing ring-to-tube weld toe, as the backing ring participates in transferring forces from the tube to the transverse plate. To ensure adequate performance, this weld should be specified and inspected as a structural weld, the quality of which can only be ensured in larger diameter tubes. The force shared by the backing ring depends on the diameter and thickness of the tube, and the height and thickness of the backing ring. FEA results, using a 2 in × ¼ in (51 mm × 6 mm) backing ring welded to the tube in both 24 in (610 mm) and 10 in (254 mm) diameter tubes, showed that the GSCF at the backing ring weld toe was much less than the GSCF at the groove-weld toe on the tube. Test results in larger diameter Type XI specimens and smaller diameter Type II specimens confirmed this finding, as fatigue cracking in almost all

49

cases developed first at the groove-weld toe on the tube, when the backing ring weld was of adequate quality. As such, it was decided not to include the weld at the top of backing ring in the models of unstiffened groove-welded tube-to-transverse plate connections.

Stiffened Fillet-welded Tube-to-Transverse Plate Connections in Round Tubes

The geometric parameters for stiffened fillet-welded tube-to-transverse plate connections in round tubes are shown in the Figure 64. The nomenclature of the additional parameters relevant to stiffened connections is also listed in Table 6.

The shape and size of a stiffener is defined by the thickness of stiffener (t_{ST}), height of stiffener (h_{ST}), and stiffener angle at the termination on the tube. The stiffener angle, however, was kept constant at 15^0, which was determined by a preliminary parametric study conducted when the optimized specimen Type XII was designed. The optimum design was obtained at a stiffener angle of about 14^0, when the stresses at the stiffener termination and the fillet-weld were the same, creating equal possibility of fatigue crack growth from either of these details.

Tube-to-Transverse Plate Connections in Multi-sided Tubes

Two additional geometric parameters, the number of sides (N_S) and the internal bend radius at the corner (r_b), were considered for multi-sided tubes as shown in Figure 65. The nomenclature of these additional parameters is also listed in Table 6. The outer opposite flat-to-flat distance of the tube was considered as its diameter. The outer opposite flat-to-flat distance and the thickness of a tube were varied from 10 in (254 mm) to 24 in (610 mm) and 0.179 in (4.5 mm) to 0.5 in (13 mm), respectively. The thickness of the transverse plate was kept constant at 2 in (51 mm). The number of sides was varied from 8 to 20, and bend radius was varied from 0.5 in (13 mm) to 6 in (152 mm).

Factorials for Parametric Study

Figures 66 through 69 show the partial factorials for the parametric studies of unstiffened and stiffened tube-to-transverse plate connections. These factorials are two level (two dimensional) projections of multi-dimensional or multi-level factorials that are possible from various combinations of the parameters. The factorials are, however, partial and developed based on realistic combination of geometric parameters over the applicable range of dimensions of these structures in service.

The range of parameters considered for parametric studies are shown in Tables 7 through 10.

Finite Element Modeling

The parametric FEA were conducted using a global model and multi-level sub-models to determine the local stresses accurately. The global model and the first level sub-model were developed for determining the geometric stresses for finite life assessment. The subsequent sub-models were developed to determine the notch stress at the weld toe for estimating the CAFT of the detail. Typical global and first level sub-models of the analyzed structures are shown in Figures 70 and 71. The size of each level of sub-model and respective mesh density was verified by convergence tests. The solution of the sub-model was driven by the displacement solutions at

the interface with the global model. All analyses were performed as per the analytical protocols presented earlier.

Global Model

Realistic three dimensional global models of the structures were developed including the nominal weld geometry and the fasteners. A tube with a transverse plate was modeled, where the tube and the transverse plate parameters were varied over a range of dimensions. Unstiffened connections were modeled in round tubes, and stiffened connections were modeled in multi-sided tubes. The length of the tube was defined as eight times the tube diameter.

Square transverse plates were used with four fasteners. Four fasteners were commonly used in models representing mast-arms and poles (columns) of sign and signal support structures. Initially, two fastener arrangements and transverse plate shapes were considered for four fasteners. A rectangular transverse plate was considered, where the fasteners were located at 30^0 from the loading plane. A square transverse plate was considered, where the fasteners were located at 45^0. These two cases were typical of connections in mast-arms and poles, respectively. Figure 72 shows the effects of these two fastener arrangements over a range of transverse plate thicknesses, and two bolt circle ratios, for a 10 in (254 mm) diameter tube, 0.179 in (4.5 mm) thick. The difference in the GSCFs for these two fastener arrangements was insignificant. Any small difference at smaller transverse plate thicknesses diminished asymptotically at larger plate thicknesses. As is evident, the bolt circle ratio has more significant effect on the GSCF for all transverse plate thicknesses. The effect was more pronounced at smaller plate thickness (i.e., more flexible plate). Accordingly, a square plate was assumed for all analyses with four fasteners.

An annular transverse plate was modeled when the plate was anchored by six or more number of fasteners, representing poles of sign, signal and high-level luminaire support structures.

The structure model was supported discretely at the fasteners, which were modeled as separate parts and were assembled with the structure. All fasteners were pre-stressed to the yield load. A rigid contact interface was defined between the fasteners and the transverse plate to simulate the realistic condition (Figure 73). Fasteners were fixed at their base. A rigid loading plate was tied to the tube end opposite to the transverse plate.

The model was analyzed as a cantilever, subjected to a concentrated load applied at the center of the loading plate. The applied load was scaled such as to produce a nominal stress of 12 ksi (83 MPa) at the most fatigue critical section (where fatigue cracking is expected) in each model. For example, in fillet-welded tube-to-transverse plate connections, the section through the weld toe on the tube was considered as the critical section. In groove-welded tube-to-transverse plate connections, the section through the weld toe of the fillet reinforcement was considered as the critical section. In stiffened connections, the section through the toe of the wrap-around weld at the stiffener termination on the tube was considered as the critical section. To obtain the most critically stressed location in a section, the loading direction was varied.

For structures with only four fasteners, the load was applied in the middle plane between fasteners. Four fasteners are typically used for mast-arms or poles of sign and signal support structures, which experience fatigue damage due to wind-induced galloping oscillation in this plane. Where the four fasteners were used, the load was applied in the middle plane in between

51

the fasteners. The models with more than four fasteners were loaded in a plane containing a fastener (Figure 74), as the stress concentration was higher compared to the case where the structure was loaded in middle plane between the fasteners. Because of the two different critical sections in a stiffened tube-to-transverse plate connection, all models containing this connection were analyzed for two loading directions (Figure 75 (a) and (b)) to produce the critical stress concentration at each section. The more severe stress concentration occurred at the toe of the wrap-around weld on the tube at a stiffener termination when the structure was loaded in the plane of a stiffener. The critical stress concentration at the fillet-weld toe on the tube at the base occurred when the structure was loaded in the middle plane between the stiffeners.

Level 1 Sub-model

For the first level sub-model, only the tube-to-transverse plate connection was considered including a tube length of 1.5 times the tube diameter above the top of transverse plate (Figure 76). The fasteners and the loading plate were removed from the model. Two layers of elements were provided through the tube thickness.

Level 2 Sub-model

The second level sub-model contained only half of the tube on the tension side of the neutral axis, including the weld and part of transverse plate as shown in Figure 77. The height of the tube was only one half of the tube diameter. Four layers of elements were used through the tube thickness.

Level 3 Sub-model

A third level sub-model was analyzed to determine notch stresses for evaluating the fatigue threshold. For this sub-model, a 10^0 segment of the tube and the weld was modeled as shown in Figure 78. A height of the tube equal to the weld height was modeled. The weld toe was rounded by 0.04 in (1 mm) radius to obtain a converged finite stress at the weld notch. Eight elements were used along the rounded notch perimeter, and ten elements were used through thickness.

Analysis

The analyses were conducted using a commercial FEA package ABAQUS (*23*). Three dimensional solid hexahedral quadratic serendipity elements C3D20R with twenty nodes were used. The elements used isoparametric formulation and reduced integration. All analyses were linear elastic.

Effect of Geometric Parameters

Unstiffened Fillet-welded Tube-to-Transverse Plate Connections in Round Tubes

Figures 79 through 83 present the typical effects of geometric parameters on GSCFs at unstiffened fillet-welded tube-to-transverse plate connections. Figure 79 shows the effect of transverse plate thickness for a 13.0 in (330 mm) diameter tube with thicknesses of 0.179 in (4.5 mm), 0.239 in (6 mm), $^5/_{16}$ in (8 mm), $^3/_8$ in (10 mm), and 0.5 in (13 mm). The transverse plate was fastened with four bolts with a bolt circle ratio of 1.5. Five transverse plate thicknesses were considered: 2.0 in (51 mm), 2.5 in (64 mm), 3.0 in (76 mm), 3.5 in (89 mm) and 4.0 in (102 mm). As is evident, the GSCF decreased exponentially with increasing transverse plate thickness

and asymptotically approached a constant value for all tube thicknesses. The reductions were more pronounced for thinner plate thicknesses and for thicker tubes. As the transverse plate thickness increased, the reduction in stress concentration diminished. For a given transverse plate thickness, thicker tubes produced higher GSCF, except for larger transverse plate thicknesses where the stress concentration almost became constant. The plots exhibited that the GSCF at unstiffened tube-to-transverse plate connections depended on the thickness or the flexibility of the transverse plate. Decreasing plate thickness increased the transverse plate flexibility and increased the GSCF. The plot also showed that the stress concentration was dependent on the relative flexibility of the tube and the transverse plate. For a given plate thickness, increasing tube thickness will increase the GSCF, unless both the plate and the tube thicknesses are increased to extreme values.

Figure 80 shows the effect of bolt circle ratio for a 10.0 in (254 mm) diameter tube, 0.179 in (4.5 mm) thick, and transverse plate thicknesses of 2.0 in (51 mm), 2.5 in (64 mm), 3.0 in (76 mm), and 3.5 in (89 mm). The transverse plate was fastened with six bolts. The bolt circle ratios considered were: 1.25, 1.5, 1.75, and 2.1. As is evident, the GSCF increased asymptotically with increasing bolt circle ratio for all transverse plate thicknesses. For a given bolt circle ratio, thinner transverse plates produced higher stress concentrations.

Figure 81 shows the effect of number of fasteners for a 18.0 in (457 mm) diameter tube, $^5/_{16}$ in (8 mm) thick and transverse plate thicknesses of 2.5 in (64 mm), 3.0 in (76 mm), 3.5 in (89 mm), and 4.0 in (102 mm). The bolt circle ratio was 1.25. The number of fasteners considered was 6, 8, 12, and 16. As is evident, the GSCFs reduced exponentially and approached a constant value asymptotically for all transverse plate thicknesses. For a given number of fasteners, the thinner plates produced higher stress concentration. Also, the effect of number of fasteners was pronounced in thinner plates and for lesser fasteners.

Figures 82 and 83 show the effects of tube geometry on the GSCF. Figure 82 shows the effect of tube thickness in a 24.0 in (610 mm) diameter tube for transverse plate thicknesses of 2.0 in (51 mm), 2.5 in (64 mm), 3.0 in (76 mm), 3.5 in (89 mm) and 4.0 in (102 mm). The transverse plate was fastened with eight bolts at a bolt circle ratio of 1.75. Four tube thicknesses were considered: 0.239 in (6 mm); $^5/_{16}$ in (8 mm); $^3/_8$ in (10 mm); and 0.5 in (13 mm). The figure shows that the GSCF increased linearly for all transverse plate thicknesses. The effect was more pronounced for thinner transverse plates. For a transverse plate thickness of 4.0 in (102 mm) the effect was practically negligible. Also for a particular tube thickness, the thinner plates produced larger stress concentrations.

Figure 83 shows the effect of tube diameter in a 0.179 in (4.5 mm) thick tube for transverse plate thicknesses of 2.0 in (51 mm), 2.5 in (64 mm), 3.0 in (76 mm), 3.5 in (89 mm), and 4.0 in (102 mm). The transverse plate was fastened with four bolts at a bolt circle ratio of 1.5. Four tube diameters were considered: 10.0 in (254 mm); 13.0 in (330 mm); 18.0 in (457 mm); and 24.0 in (610 mm). As is evident, the GSCF increased almost linearly with increasing tube diameter for all transverse plate thicknesses. The increase was more pronounced for thinner transverse plates. Also for a given tube diameter, the thinner plates produced larger stress concentrations.

The parametric study results demonstrate that reducing the flexibility of the transverse plate by increasing the transverse plate thickness, and/or decreasing the bolt circle ratio, and/or increasing the number of fasteners reduces the GSCF. This reduction is, however, asymptotic

53

and levels off beyond a certain reduction of transverse plate flexibility. The plots also show that the stress concentration is dependent on the relative flexibility of the tube and the transverse plate. As the tube thickness and diameter increase, the tube flexibility reduces and the GSCF increases (almost linearly). It may also be noted that in an unstiffened tube-to-transverse plate fillet welded connection, increasing the tube diameter also increases the matching opening in the transverse plate, which reduces the plate flexibility.

Unstiffened Groove-welded Tube-to-Transverse Plate Connections in Round Tubes

Figures 84 through 89 present the effects of geometric parameters on GSCFs at unstiffened full-penetration groove-welded tube-to-transverse plate connections. The effects of plate thickness, the bolt circle ratio, the number of fasteners, tube diameter, and tube thickness exhibit similar trend as the fillet-welded connection presented earlier. The additional geometric parameter in groove-welded connection is the size of opening in the transverse plate, which need not be as large as the fillet-welded connections.

Figure 86, shows the effect of transverse plate opening in a 18.0 in diameter tube, 0.179 in (4.5 mm) thick, for transverse plate thicknesses of 2.0 in (51 mm), 2.5 in (64 mm), 3.0 in (76 mm), and 3.5 in (89 mm). The transverse plate was fastened with six bolts at a bolt circle ratio of 1.25. Five transverse plate openings were considered, which are presented as a normalized opening ratio obtained by dividing the opening diameter with the tube diameter. As is evident from the figure, the GSCF reduces exponentially as the transverse plate opening ratio reduces for all transverse plate thicknesses, and asymptotically approaches a constant number at a small opening ratio. The decrease in stress concentration is more pronounced in thinner plates. For a given opening ratio, the thinner plates produce higher stress concentration. The parametric study results show that the opening in the transverse plate has a significant effect on the GSCF at an unstiffened tube-to-transverse plate groove-welded connection, as it influences the transverse plate flexibility. A smaller opening size reduces the transverse plate flexibility. This reduction is, however, asymptotic and levels off beyond a certain reduction in the opening ratio.

Stiffened Fillet-welded Tube-to-Transverse Plate Connections in Multi-sided Tubes

Figure 90 shows typical contour plot of maximum principal stresses in stiffened tube-to-transverse plate fillet-welded connections. With adequately designed stiffener-to-transverse plate weld against root cracking, fatigue cracking can occur at the stiffener termination on the tube and/or at the tube-to-transverse plate fillet-weld toe on the tube (exhibited by high stress concentrations at these locations in the figure), depending on the various geometric parameters of the connection.

Figures 91 through 96 exhibit the effects of the various parameters on the GSCF at the stiffener termination on the tube. Figure 91 shows that the transverse plate thickness does not affect the geometric stress at stiffener termination. Figures 92 and 93 show that the stress concentration increases with increased stiffener thickness and/or less stiffeners. The increases are asymptotic and are respectively functions of the tube thickness and the tube diameter. A thicker stiffener with respect to the tube exhibits higher stress concentration at the stiffener terminus on the tube as it increases local distortion of the tube. Similarly, when fewer stiffeners are used, each stiffener carries more stress and the stress concentration at the stiffener terminus increases. The height of the stiffener does not show any significant effect on the stress concentration at the

54

stiffener terminus over a range of tube diameters and stiffener thicknesses (Figure 94), with the tube thickness and the number of stiffeners kept constant.

The effects of tube geometry are shown in Figures 95 and 96. A thinner tube and a larger tube diameter tend to increase the stress concentration at the stiffener terminus. The effect of the tube thickness is more pronounced and a similar trend is seen for all tube diameters. The number of stiffeners shows a significant effect on the stress concentration. For a given tube diameter the stress concentration increases with lesser number of stiffeners. The increase in stress concentration with respect to the tube diameter is less when more stiffeners are used, which indicates that the stiffener spacing is a significant parameter. Figure 97 shows the GSCF at the stiffener termination with respect to the distance between stiffeners or stiffener spacing, which is determined by dividing tube perimeter by number of stiffeners. As is evident, the stress concentration increases almost linearly with increasing stiffener spacing.

As discussed earlier, the ratio of stiffener to tube thicknesses appears to have a significant effect on the GSCF at the stiffener terminus. Figure 98 plots the stress concentration with respect to the ratio of stiffener thickness and tube thickness raised to an exponent. A distinct correlation is evident for a range of stiffener and tube thicknesses.

The primary objective of attaching longitudinal stiffeners to a fillet-welded tube-to-transverse plate connection is to protect or eliminate fatigue cracking at the tube-to-transverse plate fillet-weld toe. The effect of the various geometric parameters on the effectiveness of this protection was investigated by examining the ratio of the geometric stresses at the tube-to-transverse plate fillet-weld in stiffened and unstiffened connections. The local stresses at the unstiffened and stiffened connections were determined with respect to the same nominal stress at the toe of the fillet-weld. The nominal stress for the stiffened connection was computed based on the section property of the tube section only. The effects of geometric parameters on the ratio of stress concentrations are presented in Figures 99 through 104. It is evident from the plots that the height and the number of stiffeners are the significant geometric parameters that affect the extent of protection provided by the stiffeners to the tube-to-transverse plate weld. Increasing the height and/or number of stiffener increases the protection. The effects of other geometric parameters such as the stiffener thickness, the transverse plate thickness, the tube thickness and the tube diameter are not significant.

Tube-to-Transverse Plate Connections in Multi-sided Tubes

For multi-sided sections, number of sides and bend radius are the two parameters in addition to geometric parameters for round tube-to-transverse plate connections. The results of parametric study for the fillet-welded tube-to-transverse plate connections in multi-sided sections are presented in Figures 105 and 106 for varying number of sides and bend radius respectively. The results are presented in terms of ratio of GSCF in multi-sided tubes with respect to that in round tubes of same cross-sectional dimensions. As is evident, both number of sides and bend radius have significant effect on the GSCF. The stress concentration ratios decrease as bend radius and number of sides increase, and approach to that of round pole-to-transverse plate connections.

To define the combined effect of bend radius and number of sides, a "roundness" factor was defined that quantifies the geometric similarity of a multi-sided section to a round section:

55

$$R = \frac{\cos\left(\dfrac{\pi}{N_S}\right)}{1.0 - \dfrac{r_b}{R_{Ti}}\left(1.0 - \cos\left(\dfrac{\pi}{N_S}\right)\right)} \tag{2}$$

The definition consists of three factors — the internal bend radius (r_b), the radius of inside inscribed circle (R_{Ti}), and the number of sides (N_S). The factor was determined as a ratio of the distance from the center of tube to the inside face of bend corner and the radius of inscribed circle of the multi-sided tube section. The factor can vary from 0.5 to 1.0, where 0.5 indicates three-sided tube with zero bend radius, and 1.0 indicates a perfectly round tube. For a given number of sides, the length of flat face will reduce with increasing bend radius, and the shape will approach to that of a round tube. On the other hand, with increasing number of sides the shape of a multi-sided tube will approach to round tube, even with a sharp bend radius. Fouad et al. (26) proposed a "roundness" factor, defined as the ratio of the inside bend radius to the radius of inscribed circle of the multi-sided tube, which varied from 0.0 to 1.0, where 0.0 denoted perfectly sharp corner and 1.0 denoted perfectly round tube. However, this definition did not include the effect of number of sides, one of the primary and independent geometric parameter, and as such was incomplete.

Figure 111 shows the variation in ratio of GSCFs in multi-sided and round sections with respect to roundness for different tube diameters (outer opposite flat-to-flat distance). The ratio decreases with higher roundness and approaches 1.0 for a perfectly round section. The ratios are clearly grouped by different tube diameters, and a small variation caused by variation in tube thickness is evident within each group. It is apparent that the stress concentration ratio is a function of the tube flat-to-flat distance, and the variation with respect to roundness factor for each tube diameter exhibits similar trend. For a given roundness, a tube with larger diameter exhibits larger stress concentration. The figure also demonstrates that for a tube with a larger diameter, the roundness should be increased to reduce stress concentration, which can be achieved by increasing number of sides and/or increasing bend radius.

Notch Stress at the Weld Toe

Figure 107 presents the notch stresses computed in all models. The notch stresses were normalized by the corresponding geometric stresses and plotted against the GSCFs to investigate their relationship. The plots show that the ratios of notch stress to geometric stress are functions of the tube thickness. For all thicknesses, the ratio of notch and geometric stress increases with GSCF at lower values and approaches a constant number asymptotically with increasing GSCF.

Equations of Geometric Stress Concentration Factors

Equations of GSCFs at the tube-to-transverse plate welded connections for the various connection configurations were developed by performing regression on the various geometric parameters of the connection. In view of the non-linear relationships between GSCF and many of the significant geometric parameters at a connection, nonlinear regression models were established considering one parameter at a time. Since a large number of geometric parameters were involved for a connection, the nonlinear regression were performed using built-in nonlinear regression tool in the commercial program SigmaPlot version 10.0, which implements the

56

Marquardt-Levenberg algorithm (24, 25). The regressed equations for GSCFs are denoted as K_F (fatigue stress concentration factor for finite life), and are used in subsequent chapters while developing the fatigue design guidelines.

Unstiffened Fillet-welded Tube-to-Transverse Plate Connections in Round Tubes

The equation of GSCF for an unstiffened fillet-welded tube-to-transverse plate connection in round tubes is given as:

$$K_F = 2.16 + \left(0.908 - 0.924 \frac{C_{BC}^{0.0474}}{N_B^{0.0105}} \right) \times \left(4.54 + 52.1 \times t_T \right)$$
$$\times \left(14.6 - 1.17 \times D_T^{1.15} \right) \times t_{TP}^{-2.36} \tag{3}$$

Figure 108 compares the stress concentration factors obtained from the above equation and the FEA results of each model. The correlation coefficient was 0.994, with estimated errors of average 1.9 % and maximum 9.2%.

Unstiffened Groove-welded Tube-to-Transverse Plate Connections in Round Tubes

The equation of GSCF for unstiffened groove-welded tube-to-transverse plate connections in round tube included an additional term associated with the opening in the transverse plate, and is given as:

$$K_F = 1.35 + \left(0.982 - \frac{C_{BC}^{0.0674}}{N_B^{0.0029}} \right) \times \left(1.0 + 17.3 \times t_T \right) \times \left(2.60 - \frac{D_T^{1.12}}{2.24} \right)$$
$$\times \left(\frac{1.0}{C_{OP}^{-0.689} - 0.764} \right) \times t_{TP}^{-1.95} \tag{4}$$

Comparison of the stress concentration factors obtained from the above equation and the FEA results for each model is shown in Figure 109. The correlation coefficient was 0.994, with estimated errors of average 1.5 % and maximum 5.1%.

Stiffened Fillet-welded Tube-to-Transverse Plate Connections in Round Tubes

The equation of GSCF for a stiffened fillet-welded tube-to-transverse plate connection at the stiffener termination on round tubes is given as:

$$K_F = \left(\frac{4.36 \times \frac{t_{ST}}{t_T^{0.334}} - 1.0}{2.26 \times \frac{t_{ST}}{t_T^{0.707}}} \right) \times \left(0.519 + 0.257 \frac{D_T}{N_{ST}^{1.60} \times t_T^{1.42}} + \frac{0.870}{t_T^{0.797}} + \frac{0.0293}{t_{ST}^{2.91}} \right)$$
$$\times \left(\frac{0.160 + 0.864 \times h_{ST}}{1.0 + 1.12 \times h_{ST}} \right) \tag{5}$$

Figure 110 compares the stress concentration factors obtained from the above equation and the FEA results of each model. The correlation coefficient was 0.996, with estimated errors of average 0.9 % and maximum 3.5%.

The equation of GSCF at the tube-to-transverse plate fillet-weld of the stiffened connection was determined in terms of the GSCF of an unstiffened connection and the reduction in GSCF due to the presence of stiffeners. The reduction factor was primarily dependent on the number, height and thickness of the stiffeners. The equation of the reduction factor is given as:

$$\frac{K_{F,stiffened\ fillet-weld}}{K_{F,unstiffened\ fillet-weld}} = \begin{bmatrix} \left(9.84 - \dfrac{D_T}{1.82} + 4.89\dfrac{D_T^{1.03}}{N_{ST}^{0.914}}\right) \times \left(\dfrac{0.129}{h_{ST}+6.56}\right) \\ \times \left(0.859 + \dfrac{2.79}{t_{ST}^{0.631}}\right) \times \left(0.802 + \dfrac{t_{TP}}{12.9}\right) \end{bmatrix} \tag{6}$$

Tube-to-Transverse Plate Connections in Multi-sided Tubes

The GSCFs in multi-sided tube-to-transverse plate connections were determined in terms of ratio of GSCF in multi-sided tubes with respect to that in round tubes. Stress concentration in multi-sided tube-to-transverse plate connections approach that of a round tube as the bend radius and number of sides increase. A roundness parameter was defined earlier, which quantifies the geometric similarity of a multi-sided section with a round section. Also, as presented in Figure 111 the ratio of GSCF in a multi-sided tube to that in a round tube exhibited clear dependence with tube diameter (outer opposite flat-to-flat distance), along with some scatter due to tube thickness. To collapse the effects of tube diameter and tube thickness into one single curve, a factor α is defined as follows:

$$\alpha = \frac{\left[K_{F,MS}/K_{F,Round} - 0.923\right]}{(0.25 - 0.15 \times t_T) \times (1.97 + \dfrac{D_T^{2.44}}{828})} \tag{7}$$

where 0.923 is the value of roundness for an eight sided tube with zero bend radius.

Figure 112 shows the variation of α with roundness for the parametric study models. As is evident, α values clustered quite well for roundness greater than 0.94 and decayed monotonically as roundness approached 1.0. A nonlinear regression provided the following relationship between the upper bound of reduced data set (α) and roundness, which is also plotted on the figure:

$$\alpha = 0.745e^{\left(\frac{0.028}{R-1}\right)} \tag{8}$$

Thus, the equation for the ratio of the geometric stress concentrations in a multi-sided tube to that in a round tube was established as:

$$\frac{K_{F,MS}}{K_{F,Round}} = \left[e^{\left(\frac{0.028}{R-1.01}\right)} \times \left(0.186 - \frac{t_T}{8.93}\right) \times \left(1.97 + \frac{D_T^{2.44}}{828}\right) + 0.923\right] \tag{9}$$

Equation of Notch Stress Concentration Factor

The equation of the NSCF at the weld toe of tube-to-transverse plate connections was determined with respect to their respective GSCF. As shown in Figure 107, the ratio of notch and geometric stresses clustered with respect to the tube thickness for all models and asymptotically

58

approached a constant for increasing GSCF. Figure 113 presents variation of normalized ratio of notch stress and geometric stress with GSCF for all models, where the ratio is normalized with respect to tube thickness to eliminate the thickness dependence of the ratios. A nonlinear upper bound regression to the normalized data produced the equation for NSCF in tube-to-transverse plate connections. This equation, as shown in the following, is denoted as K_I (fatigue stress concentration factor for infinite life), and is used in the subsequent chapters while developing the fatigue design guidelines:

$$K_I = \left[(1.76 + 1.83 \times t_T) - 4.76 \times 0.22^{K_F} \right] \times K_F \tag{10}$$

59

60
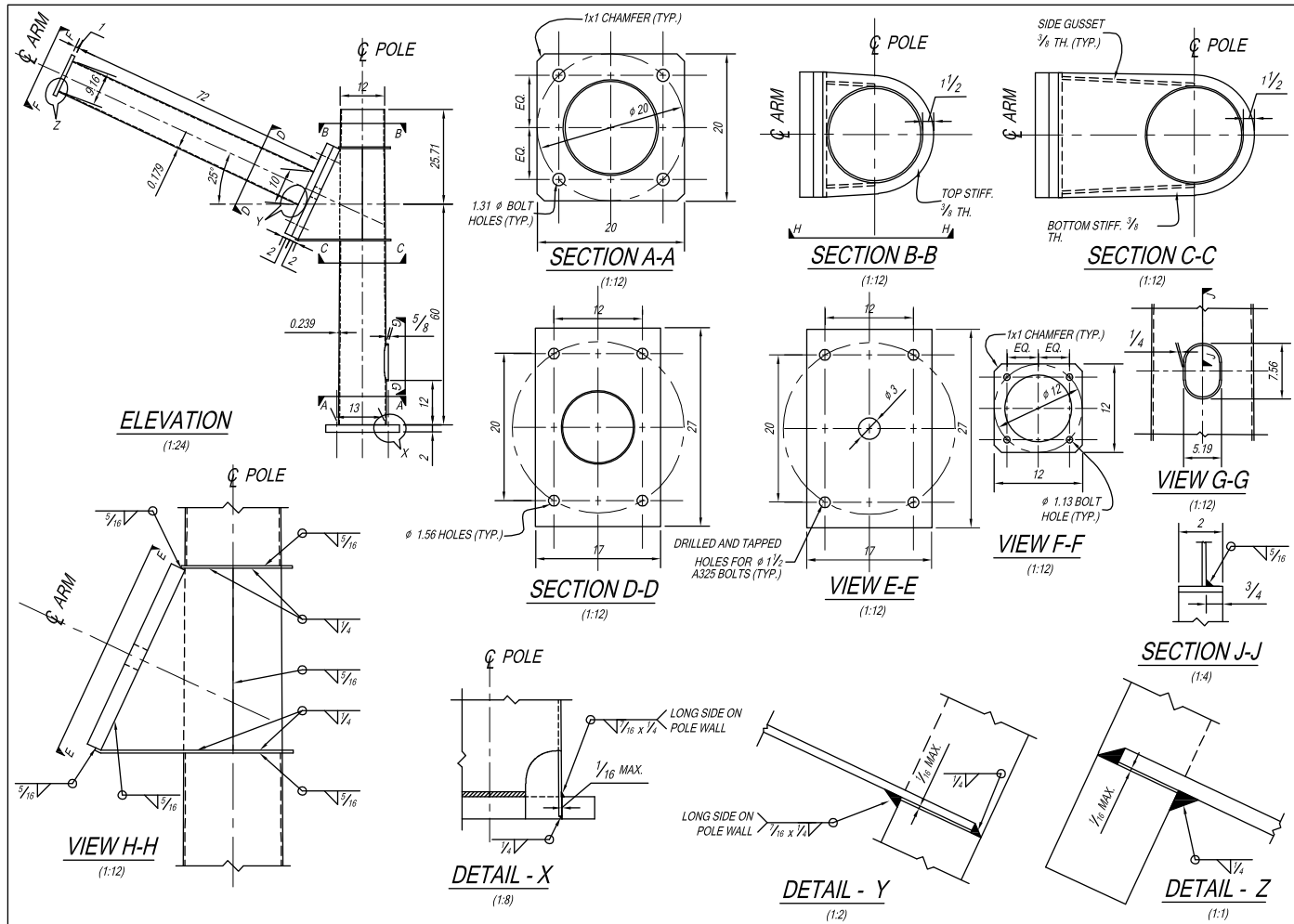
Figure 1 Details of specimen Type I
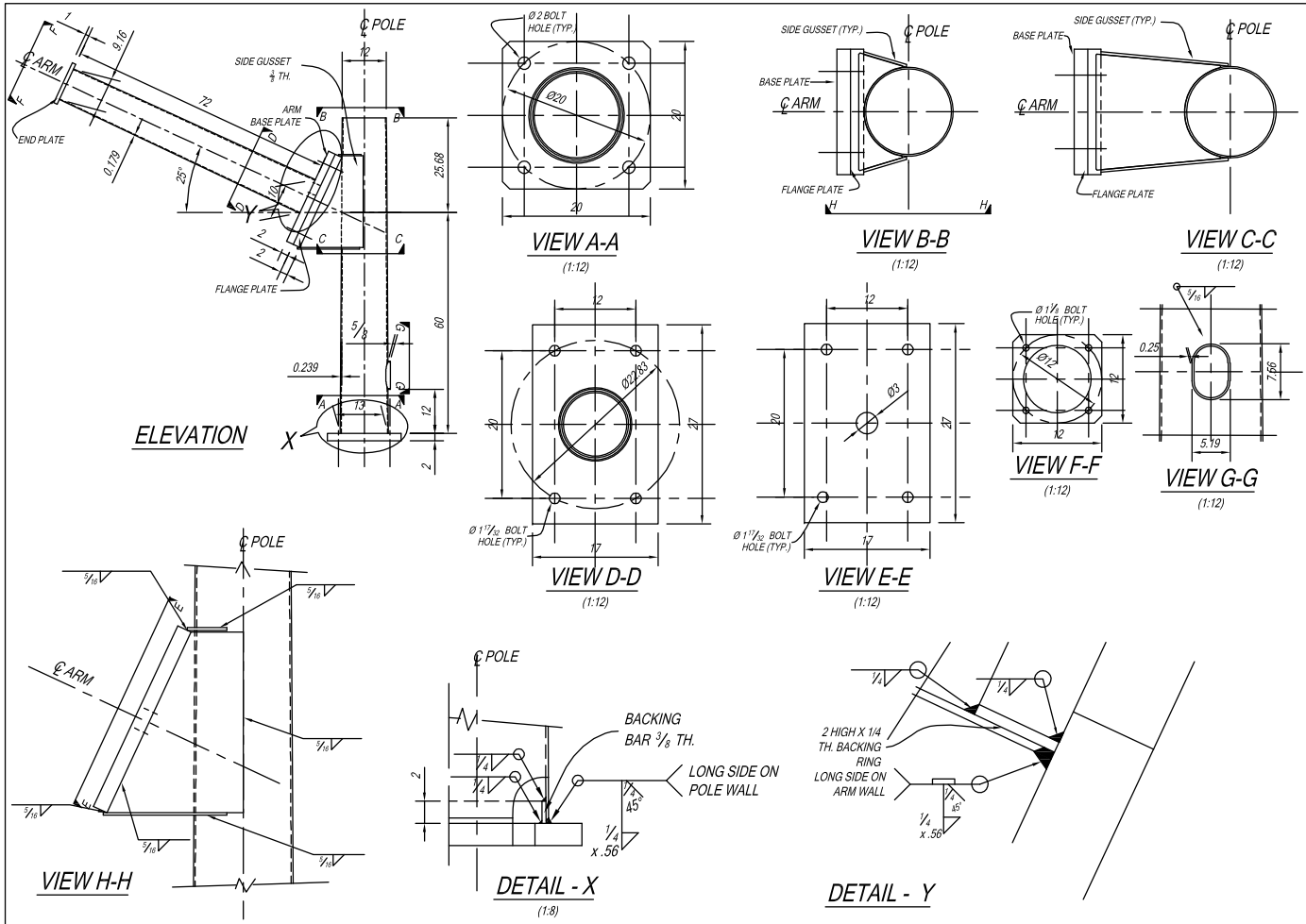
Figure 2 Details of specimen Type II
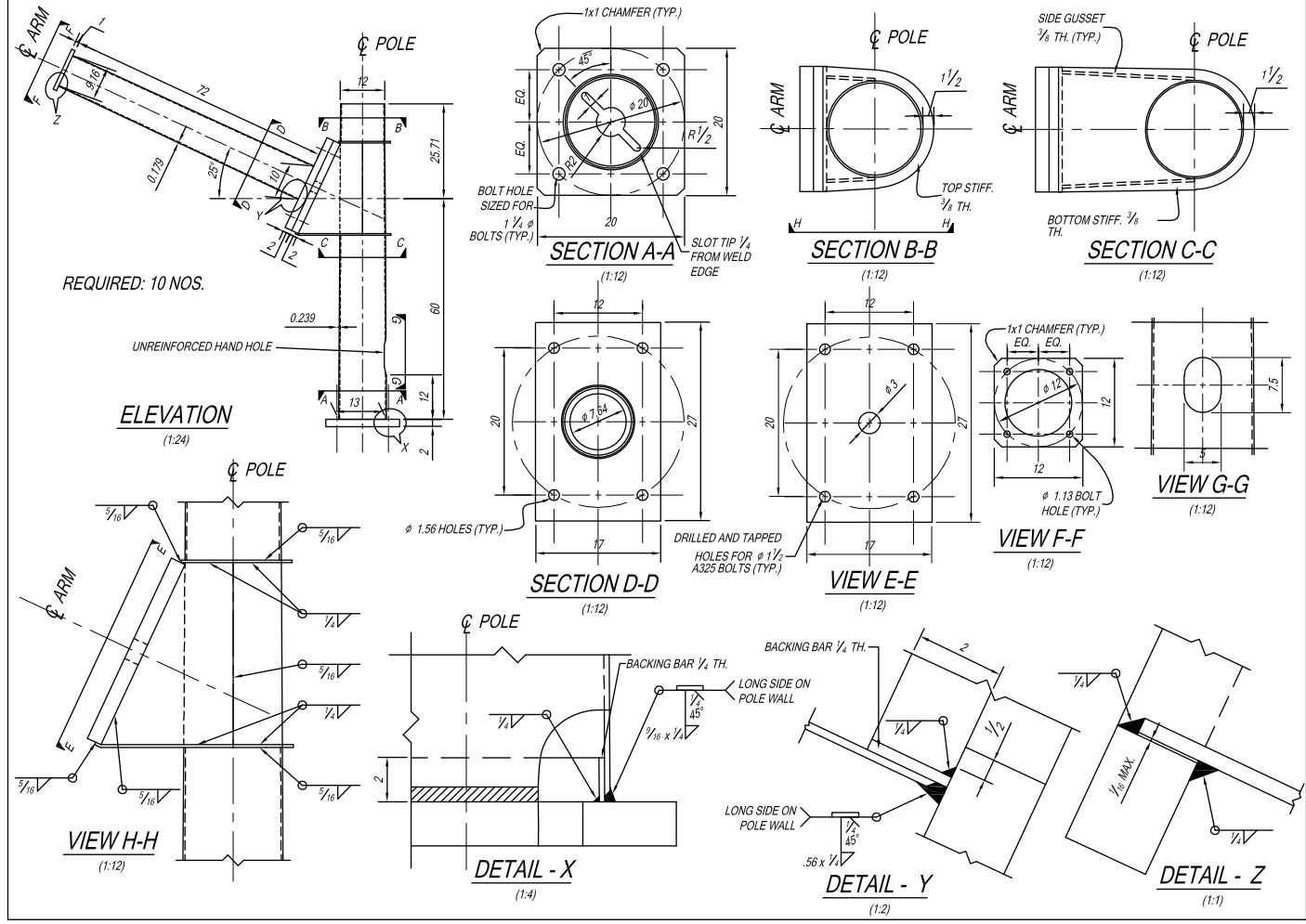
Figure 3 Details of specimen Type III
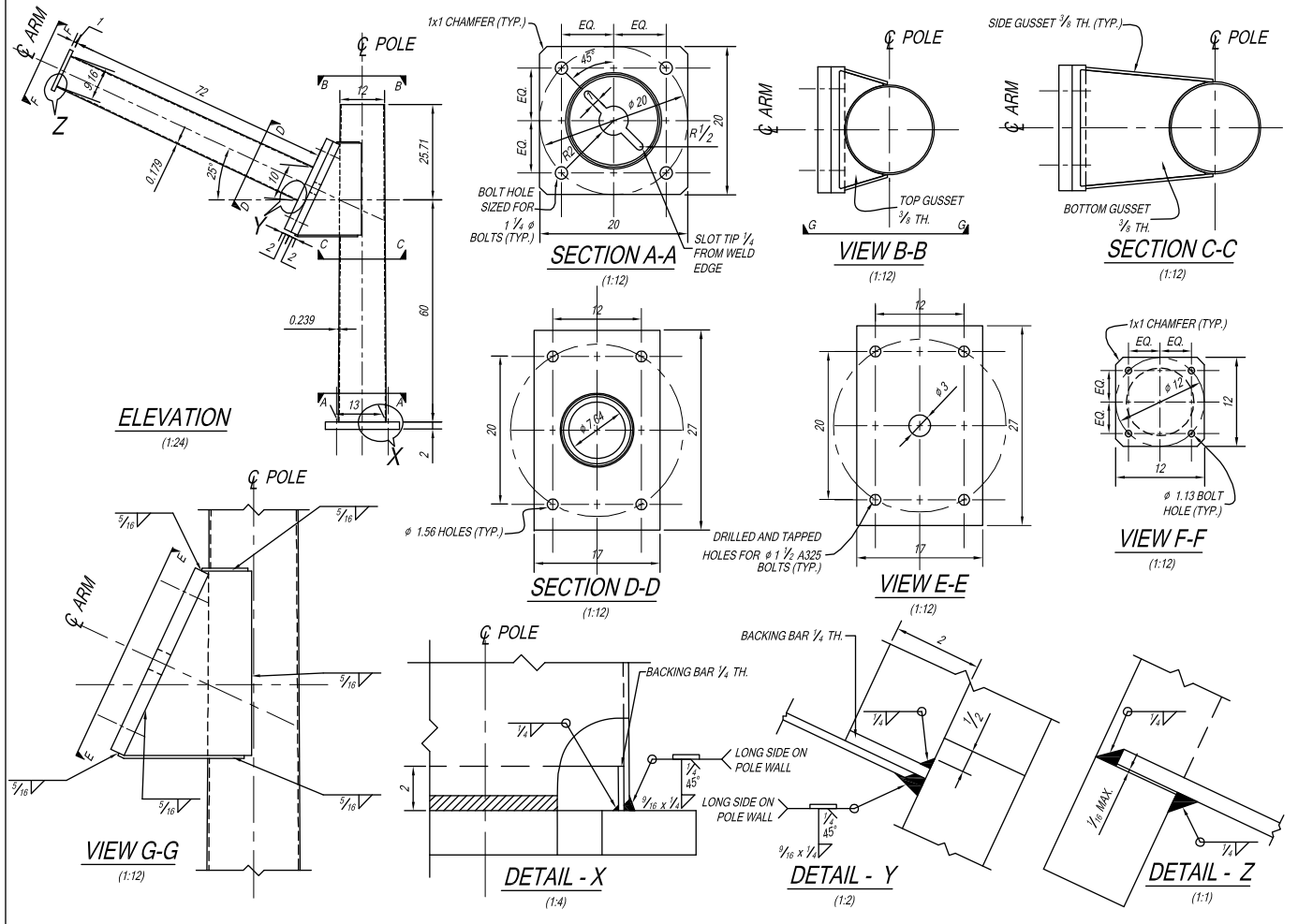
Figure 4 Details of specimen Type IV-A

64
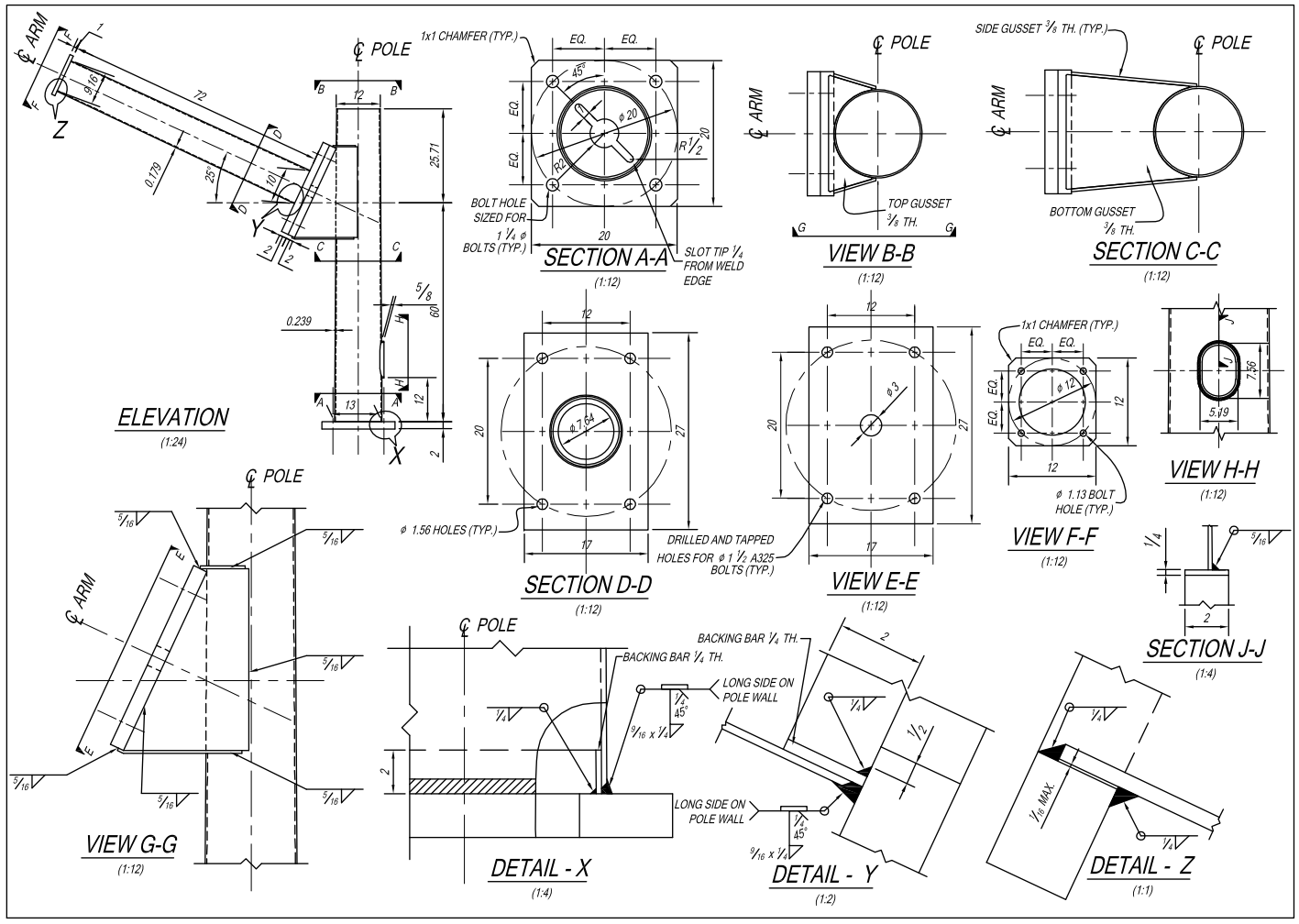
Figure 5 Details of specimen Type IV-B
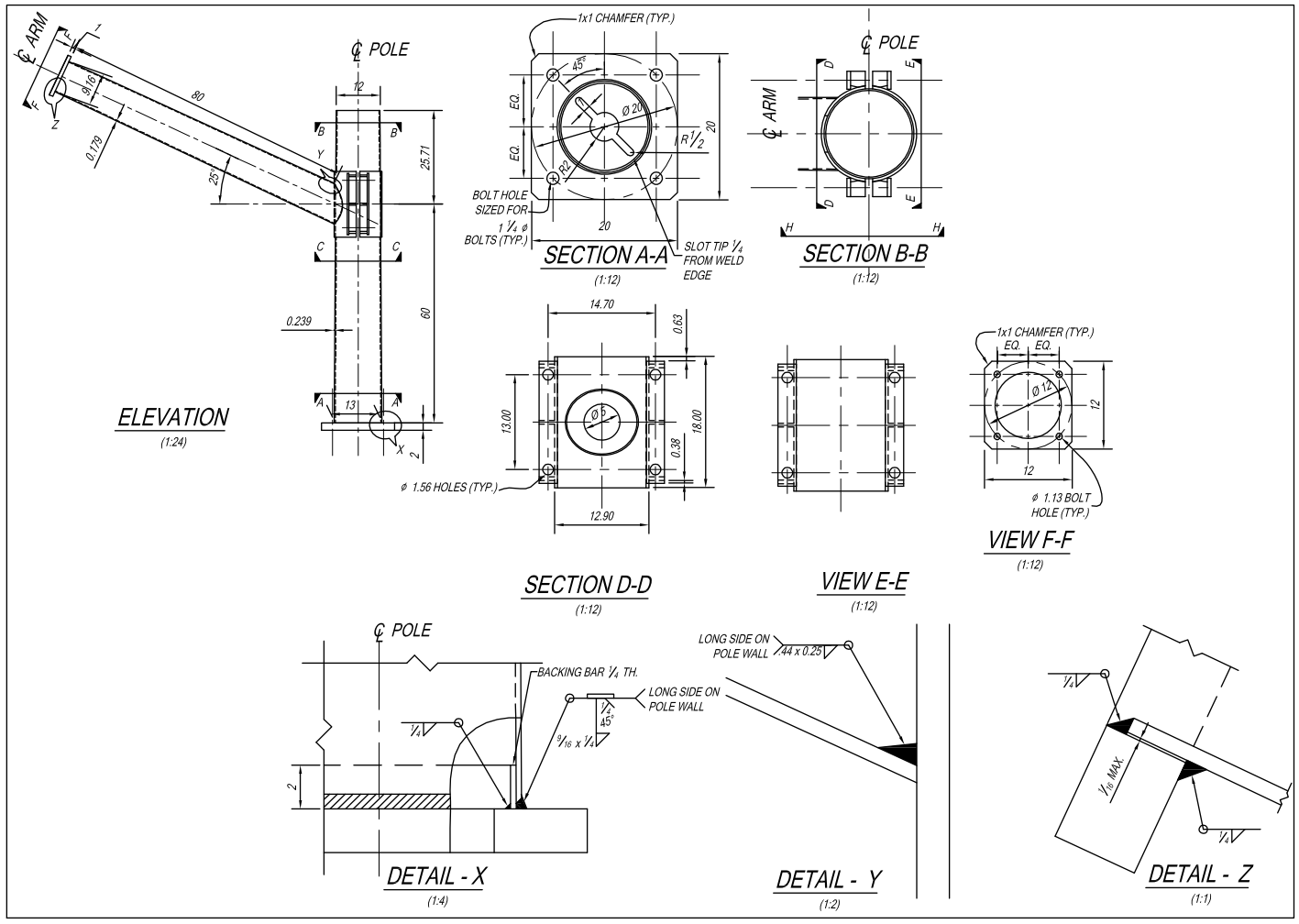
Figure 6 Details of specimen Type V

66
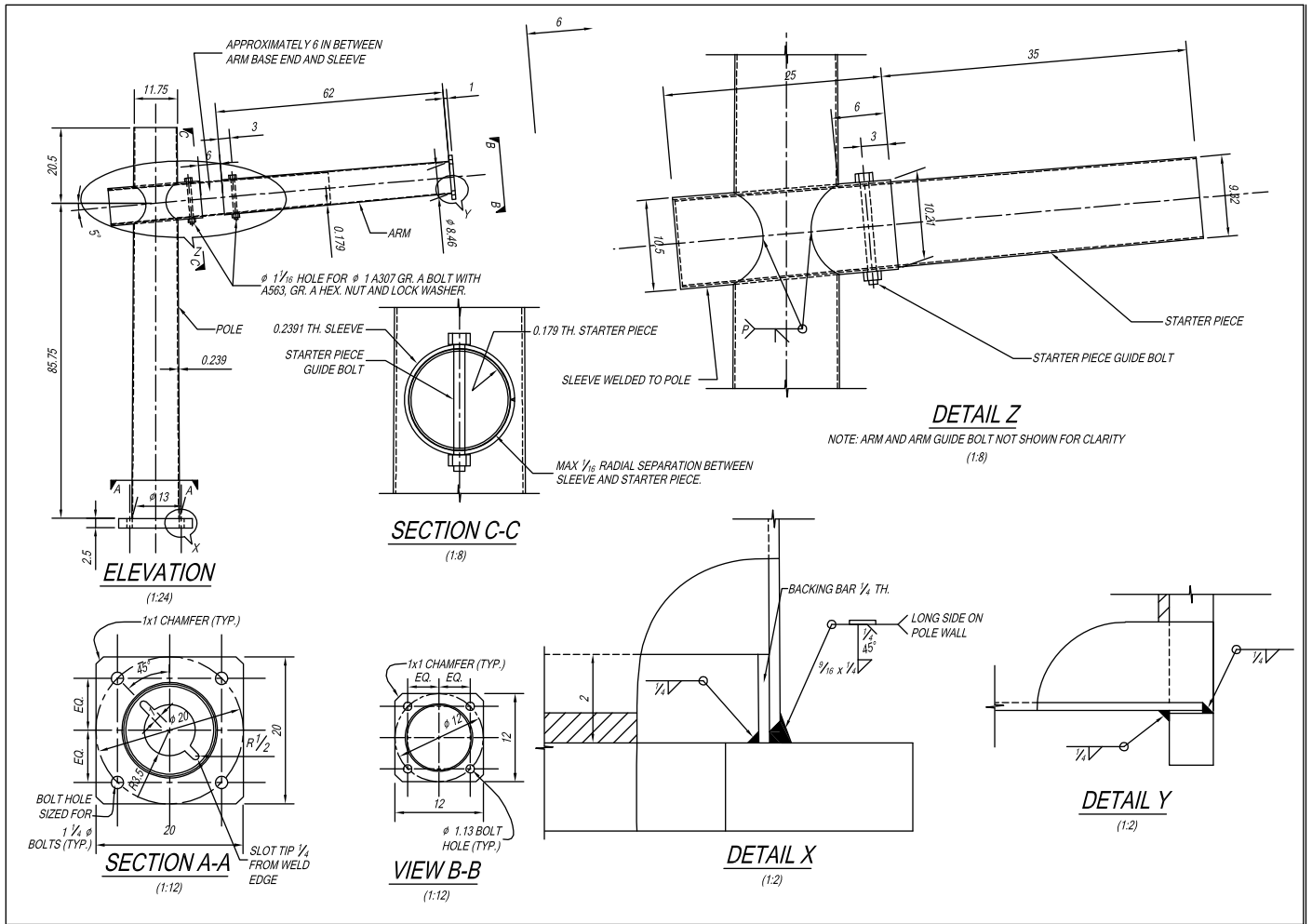
Figure 7 Details of specimen Type VI
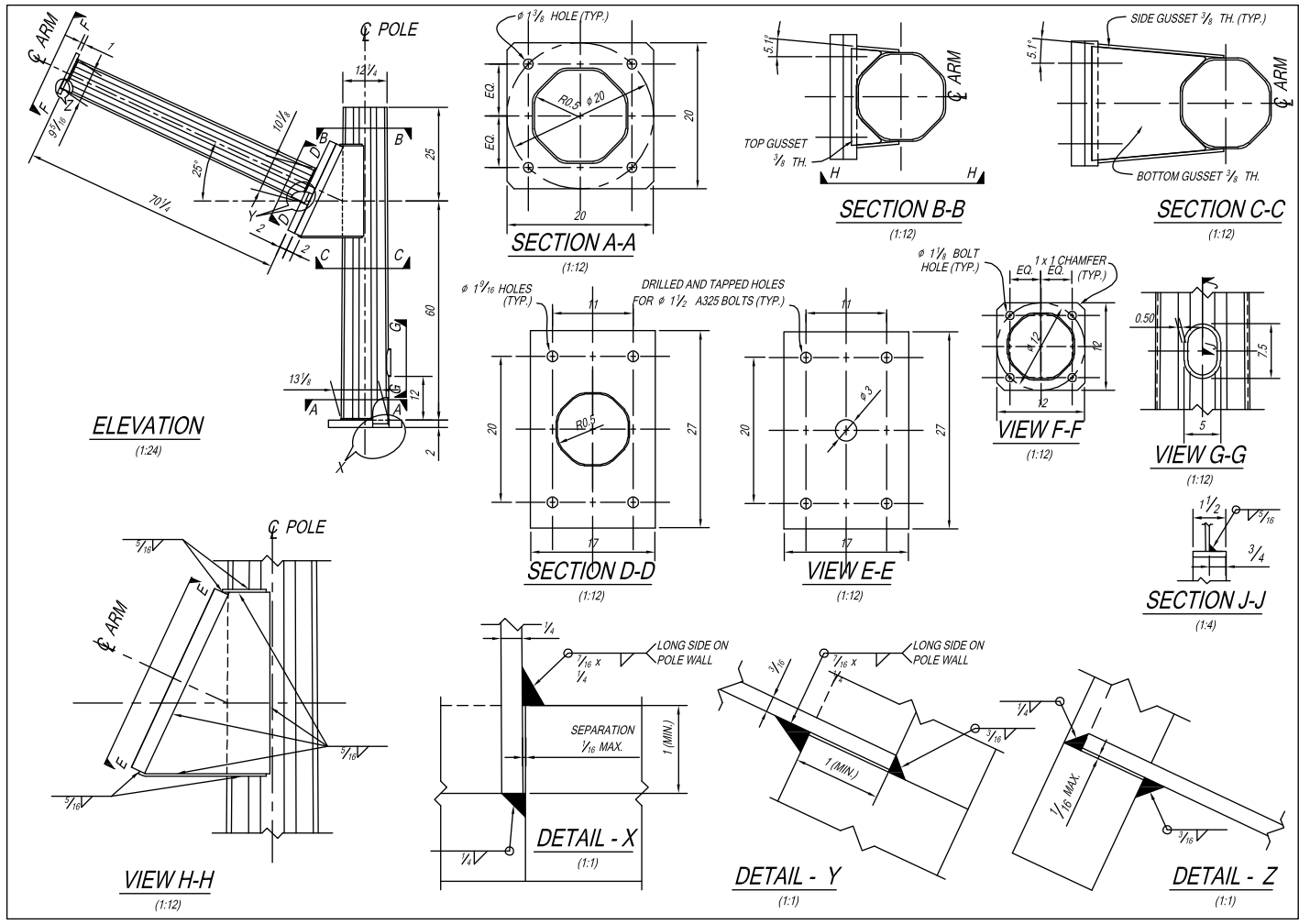
Figure 8 Details of specimen Type VII
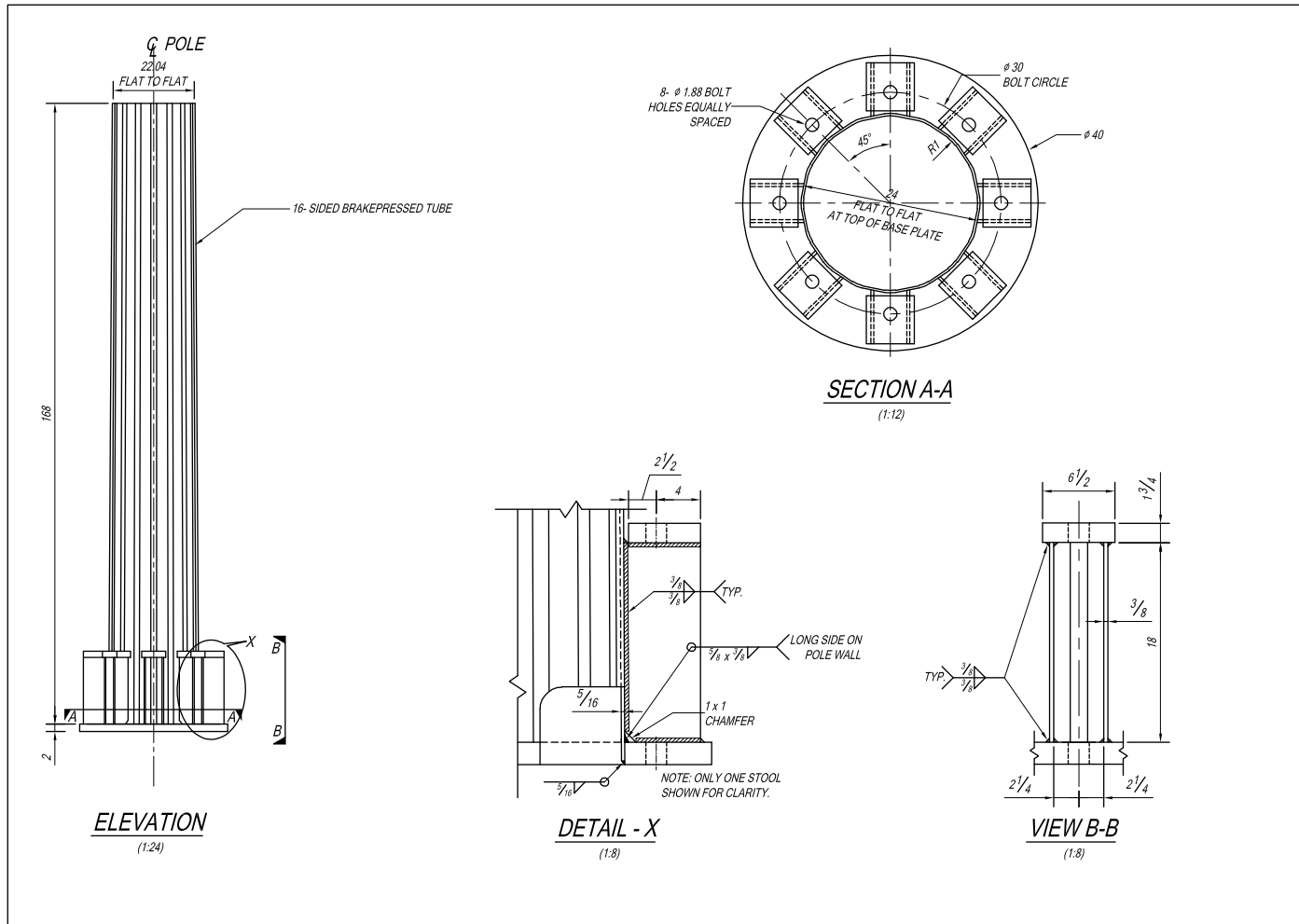
Figure 9 Details of specimen Type IX
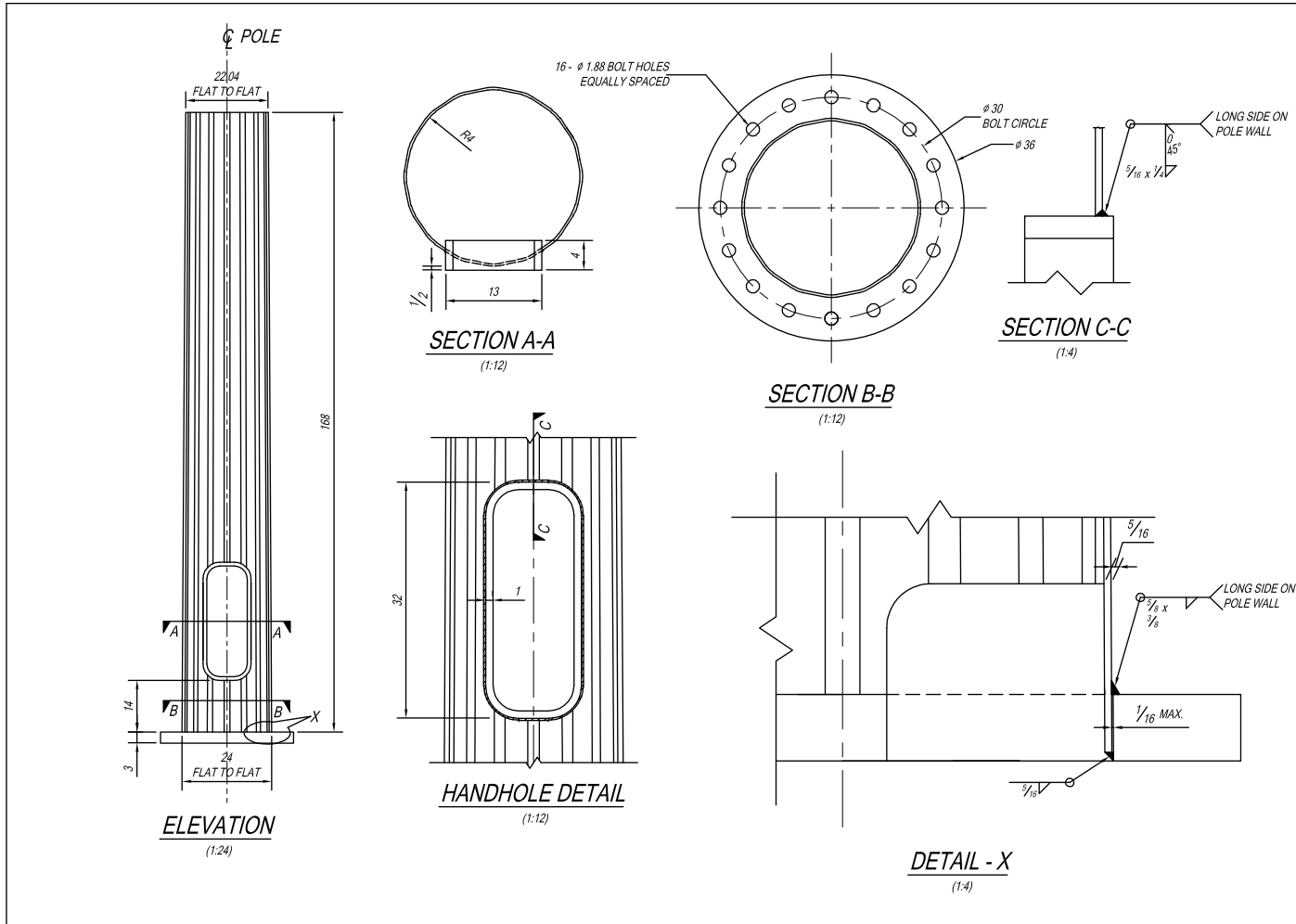
Figure 10 Details of specimen Type X
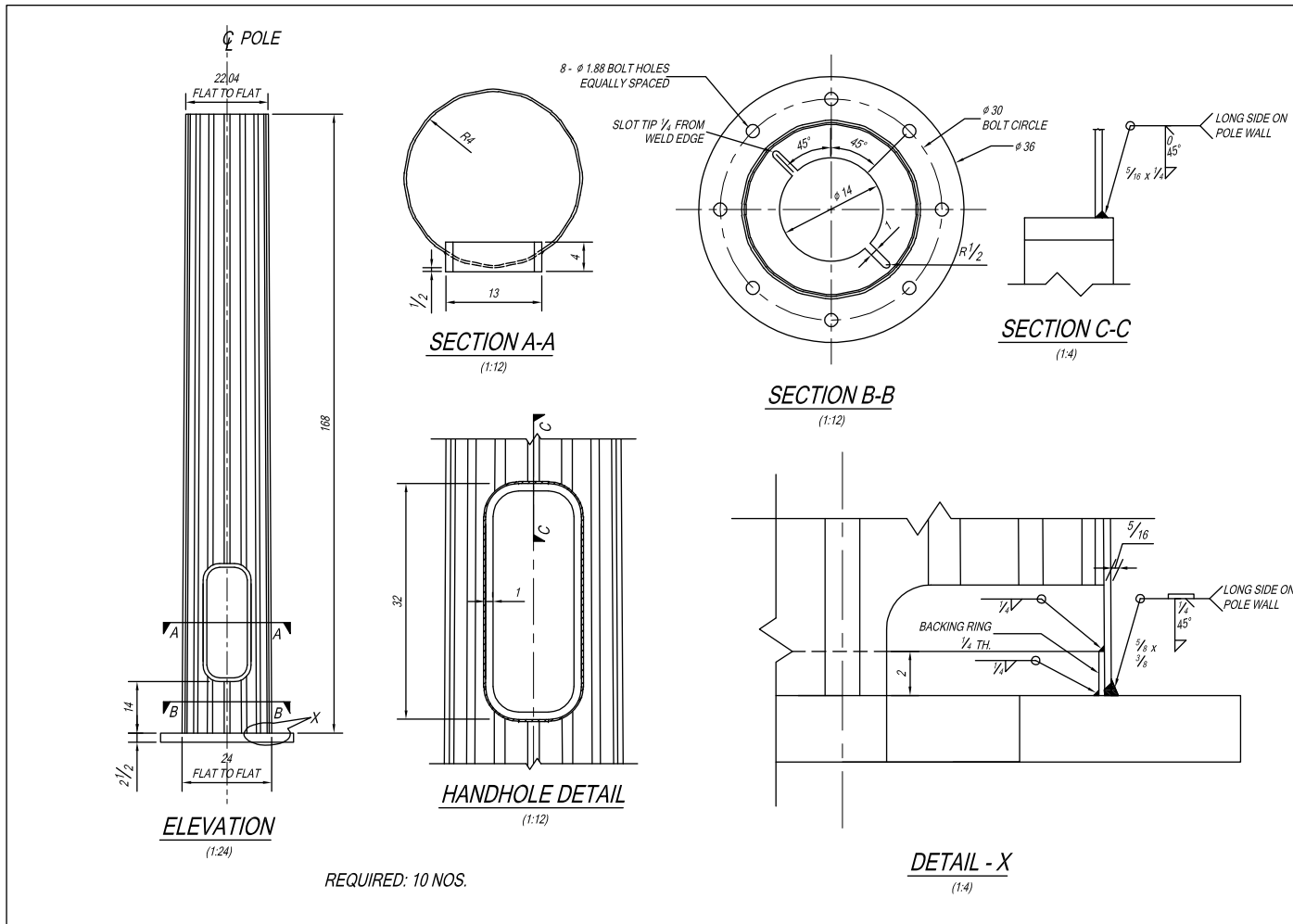
Figure 11 Details of specimen Type XI
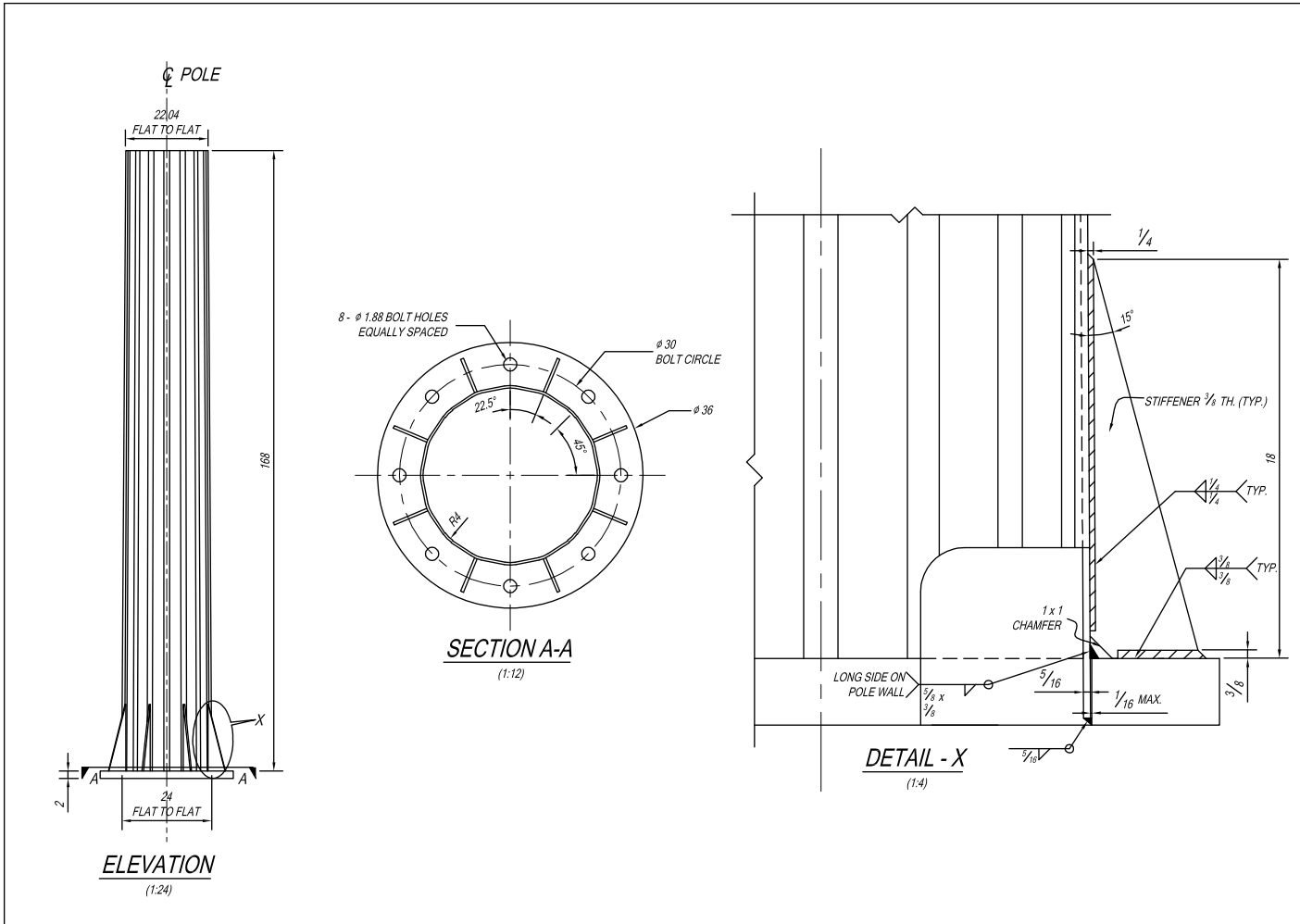
Figure 12 Details of specimen Type XII
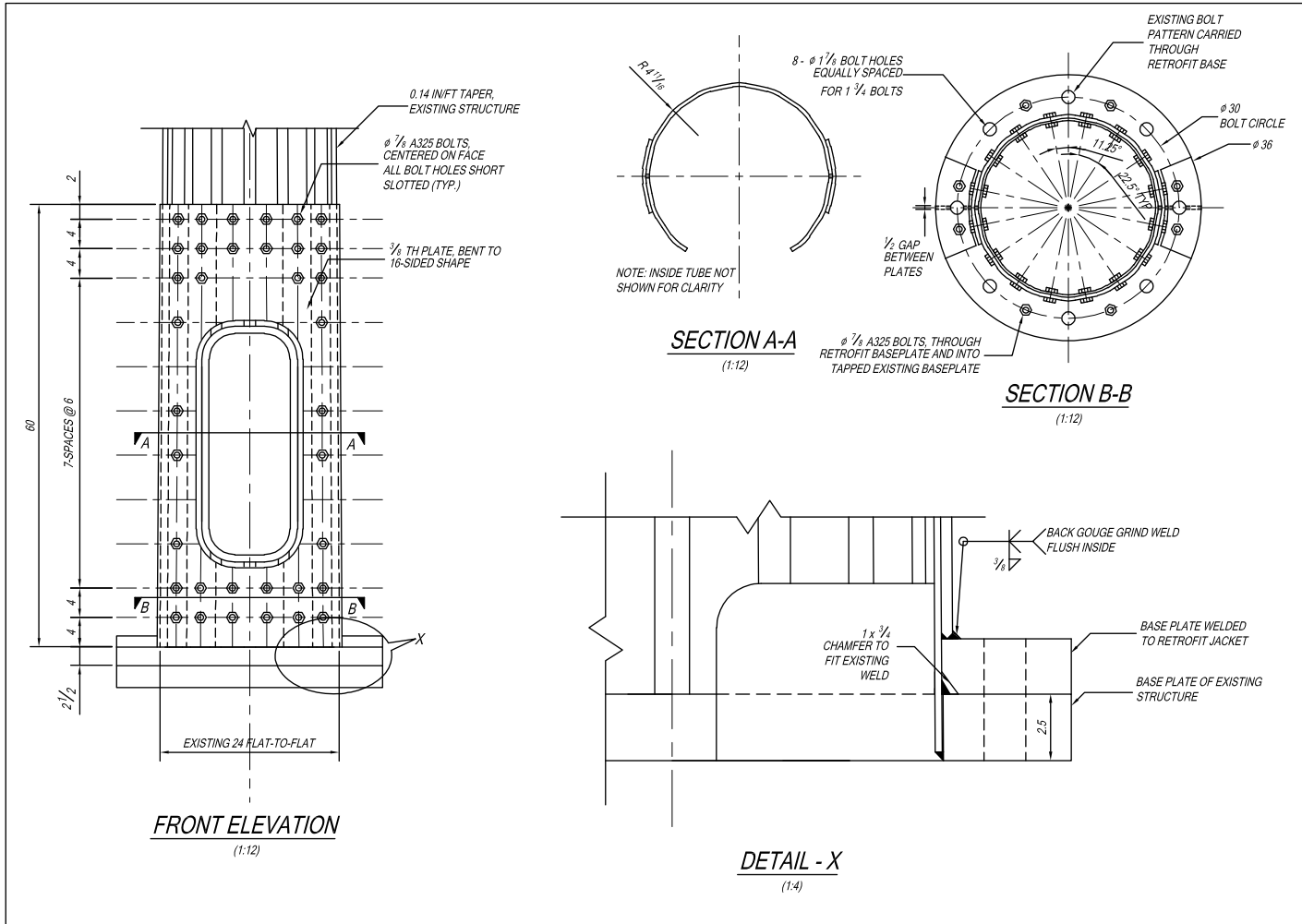
Figure 13 Details of retrofit jacket
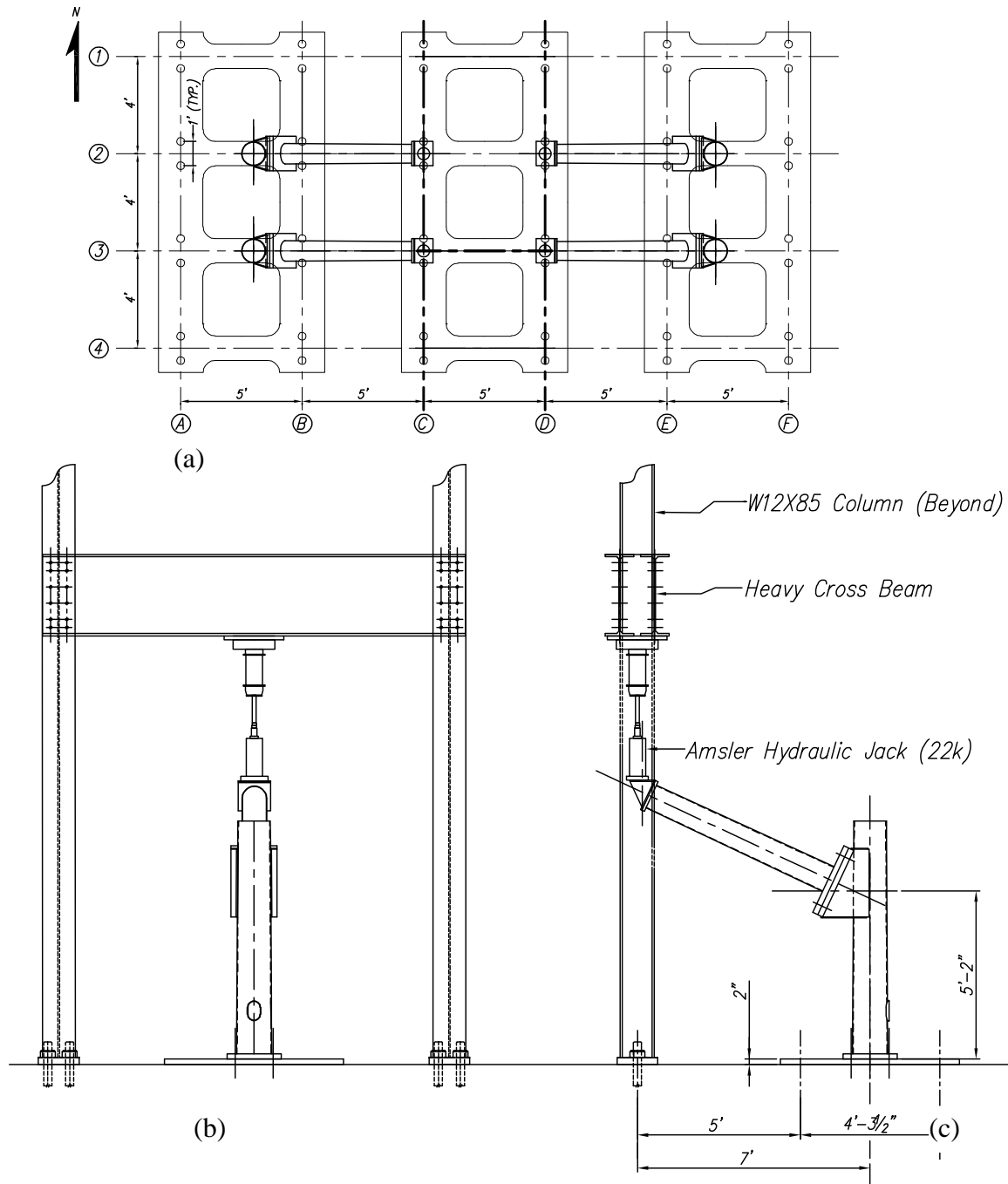
Figure 14 Schematic of test setups at Fritz Laboratory: (a) Plan; (b) Front Elevation; (c) Side Elevation

73

Figure 15 Hold down beam to reduce flexing of foundation plate

74

Figure 16 Test setups in the ATLSS Center

75
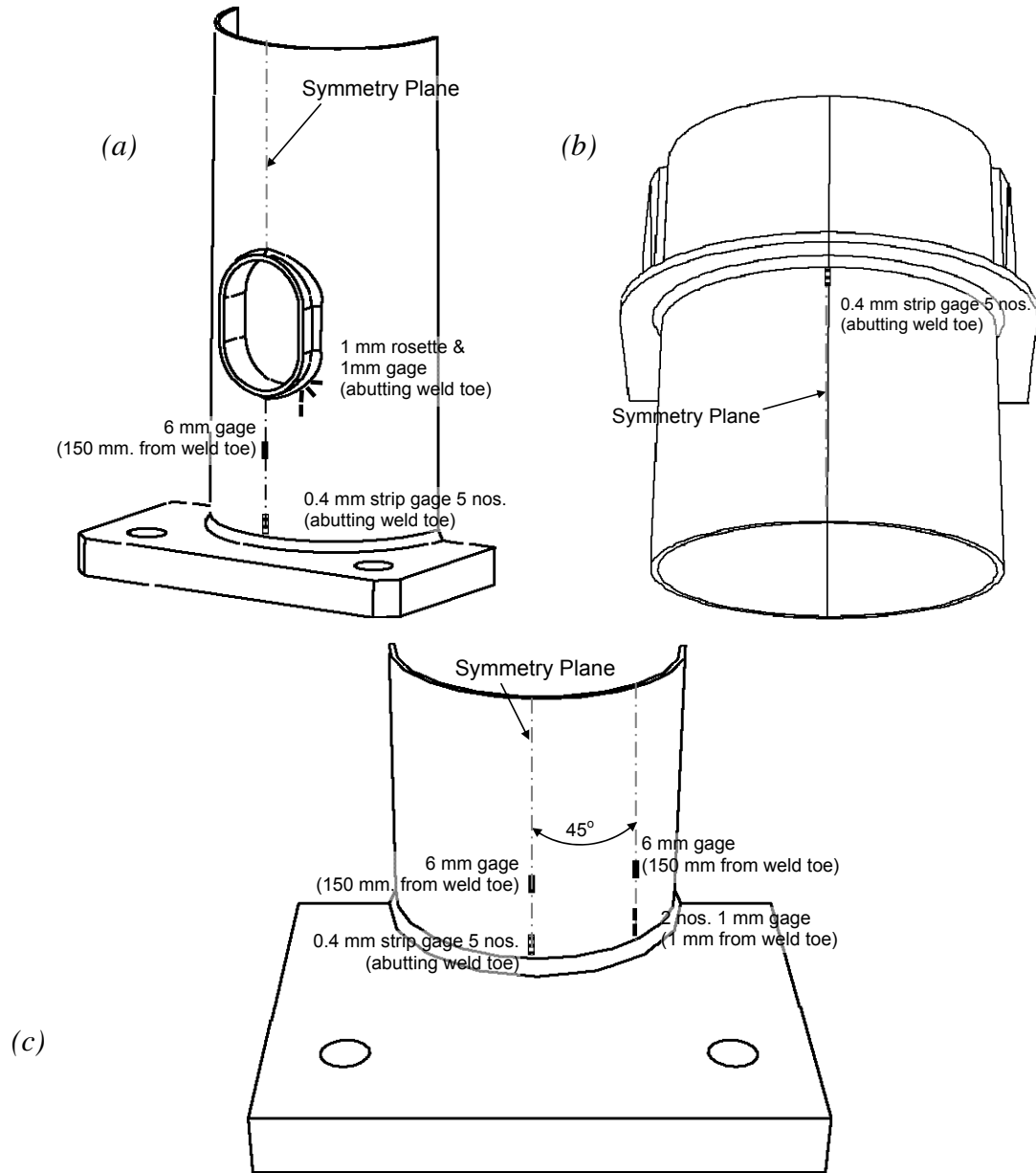
Figure 17 Strain gauge layout in specimen Type I: (a) pole base and hand hole; (b) side gusset top; (c) arm base

76
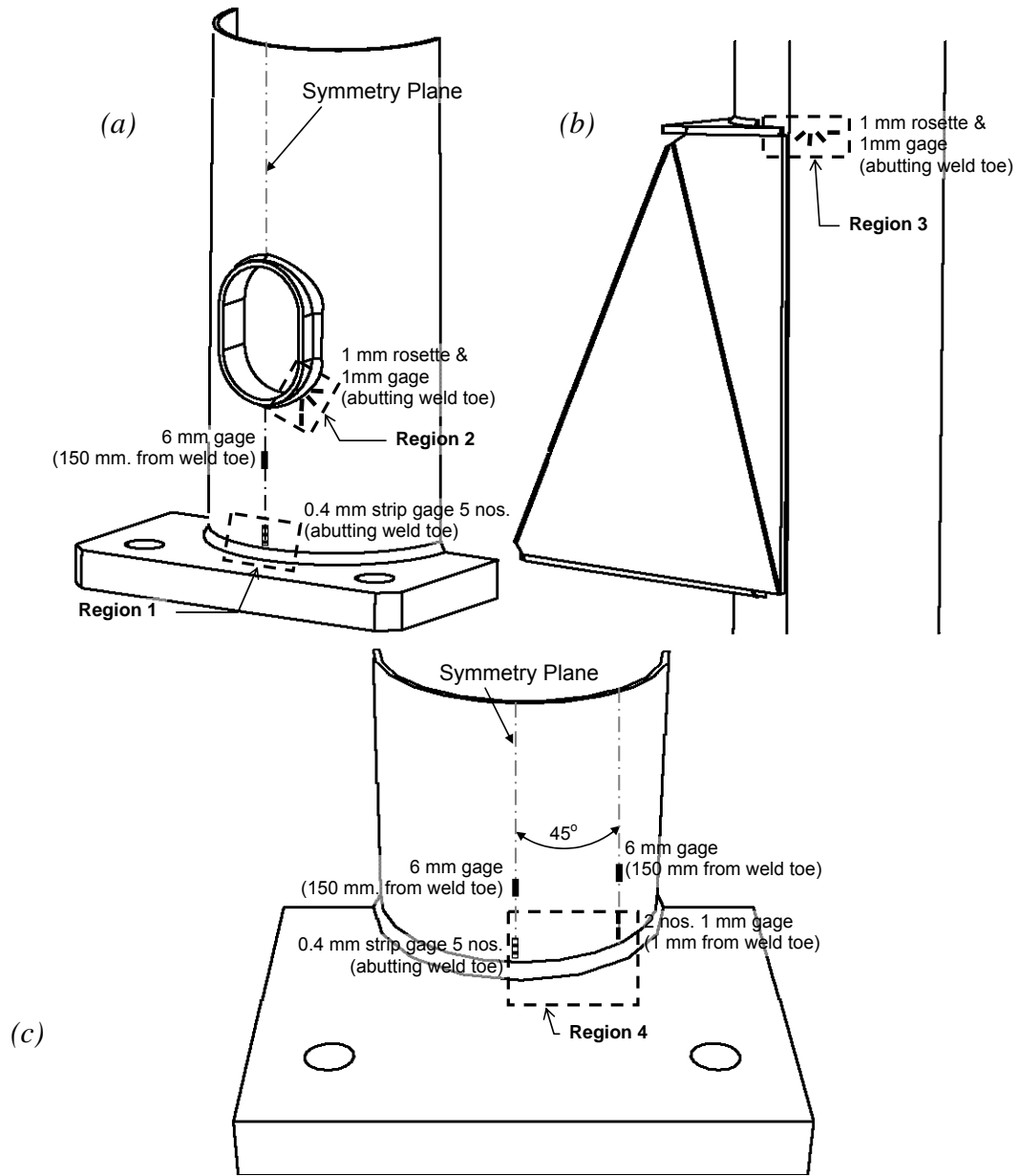
Figure 18 Strain gauge layout in specimen Type II: (a) pole base and hand hole; (b) side gusset top; (c) arm base

77
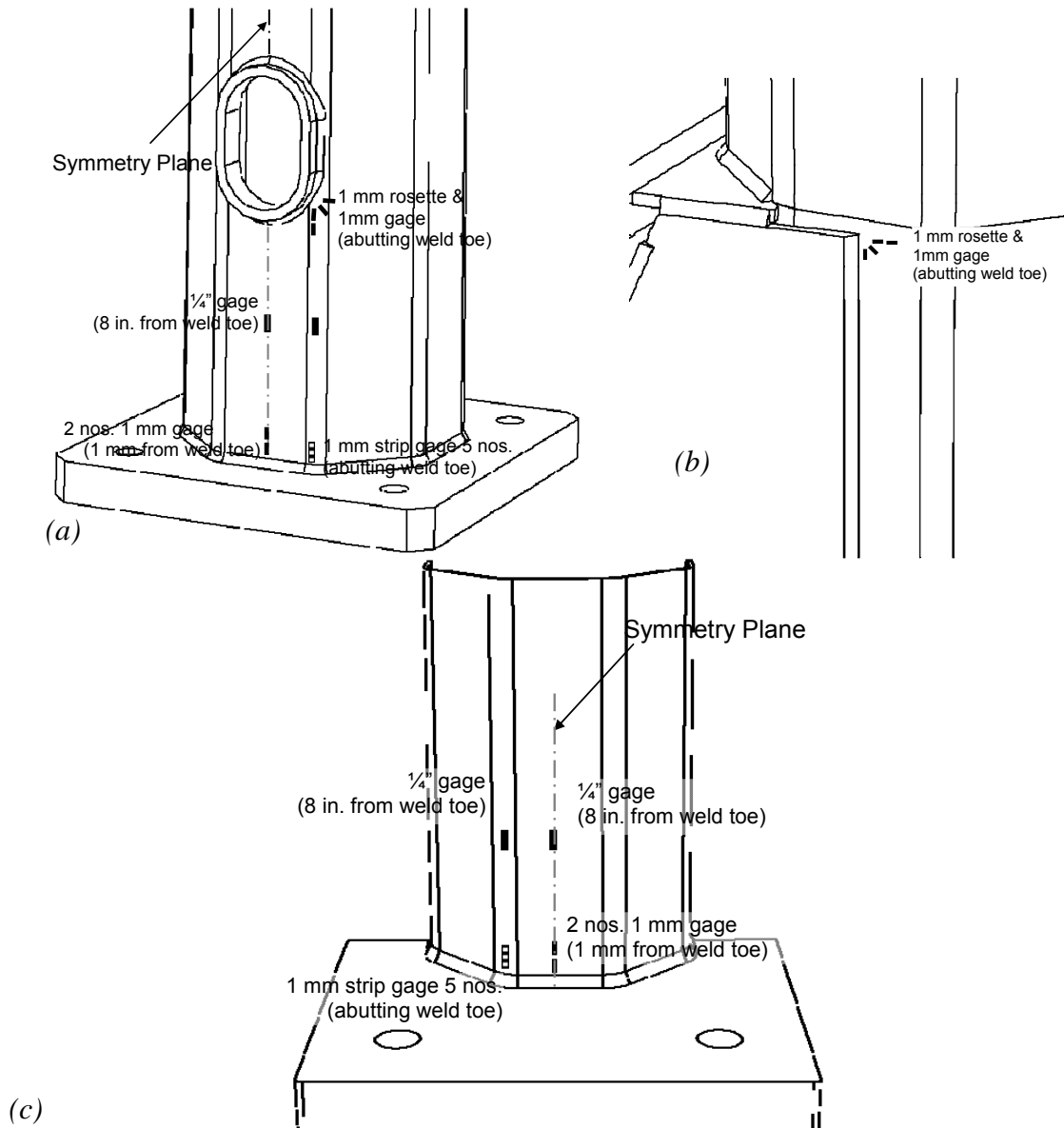
Figure 19 Strain gauge layout in specimen Type VII: (a) pole base and hand hole; (b) side gusset top; (c) arm base

78
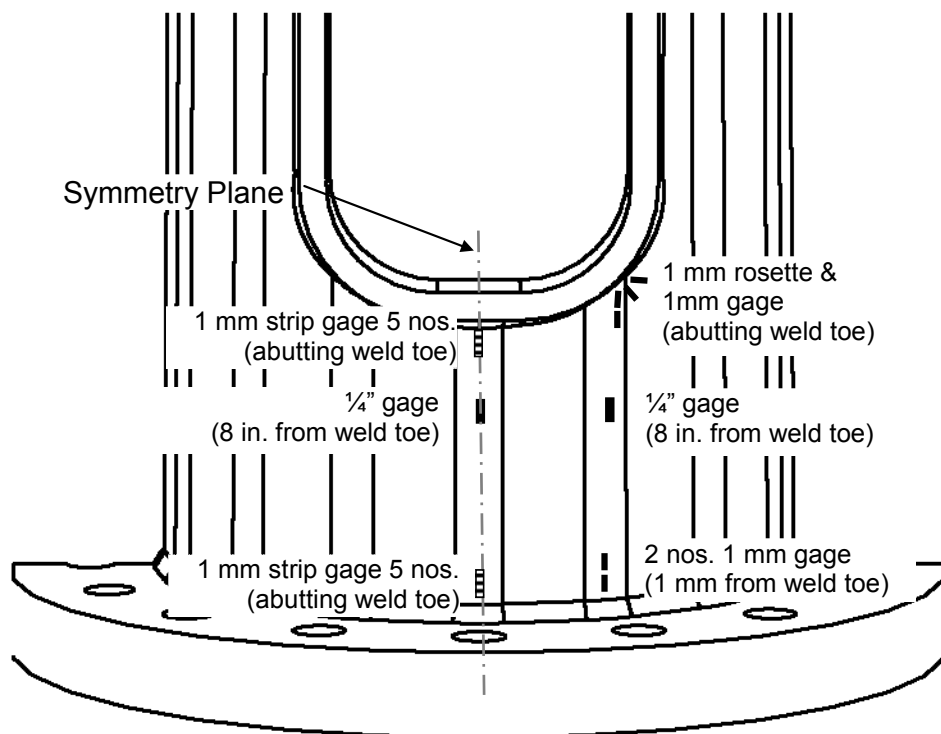
Figure 20 Strain gauge layout in specimen Type X near pole base and hand hole
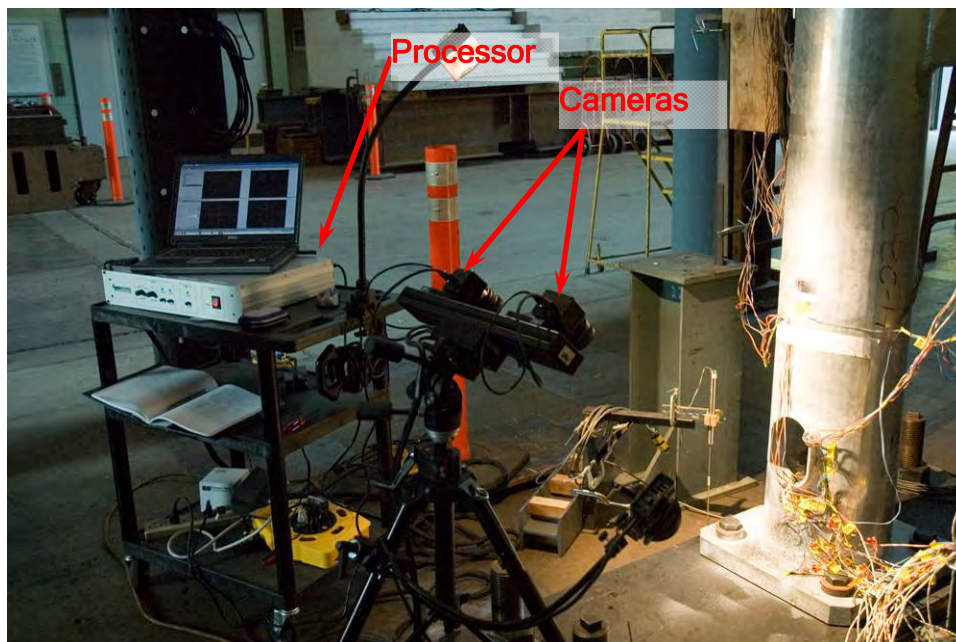
Figure 21 Strain measurements by 3D image correlation / photogrammetry technique

79
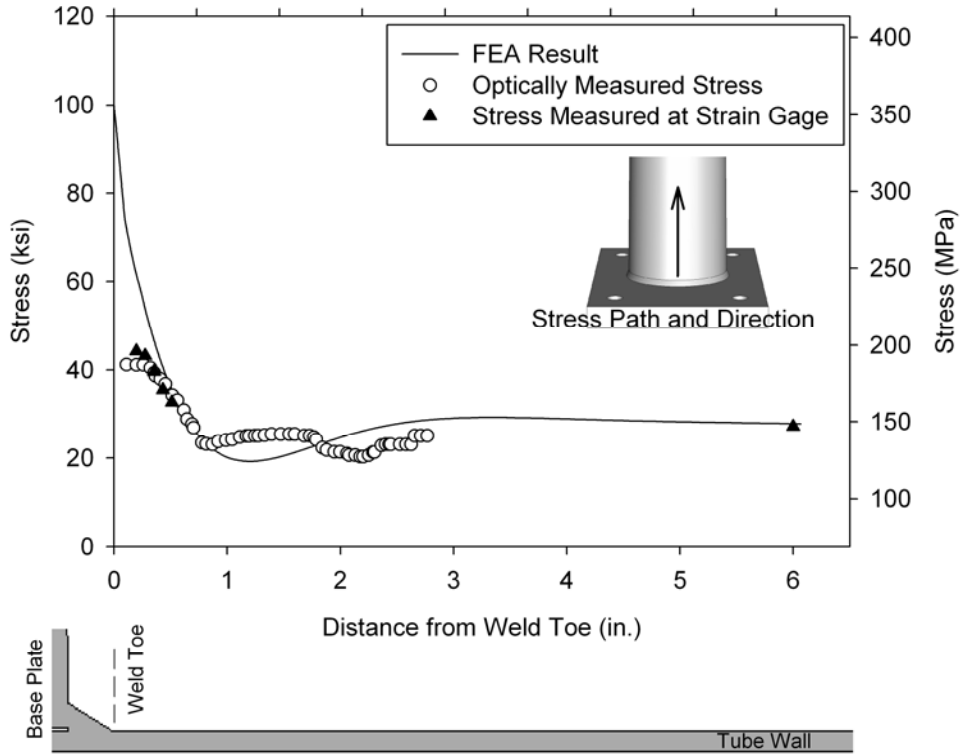
Figure 22 Stress profile near arm tube-to-transverse plate connection (Region 1) in specimen Type I
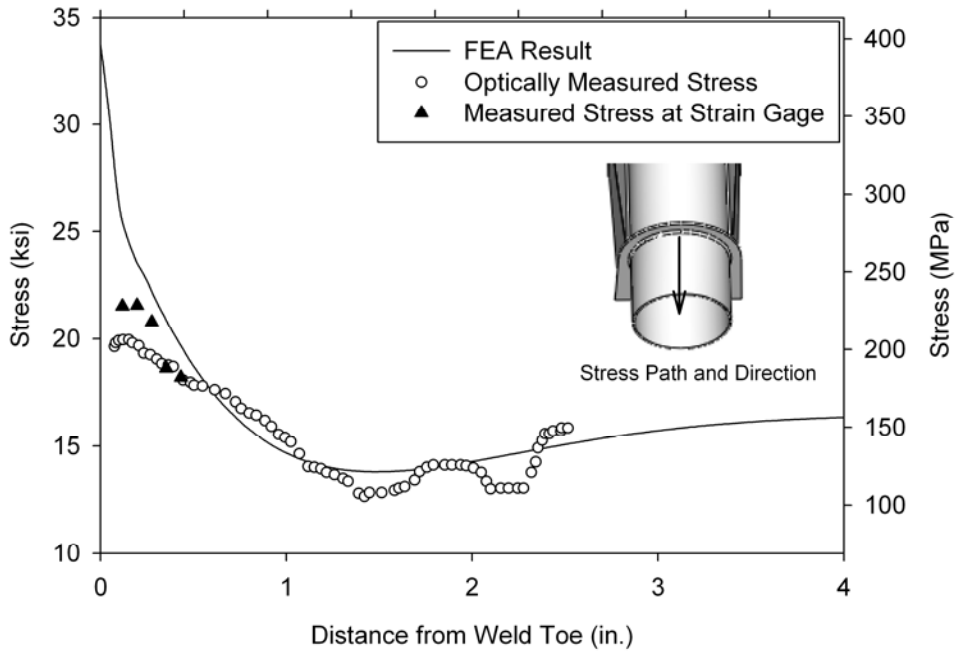
Figure 23 Stress profile underside of bottom ring stiffener (Region 2) in specimen Type I

80
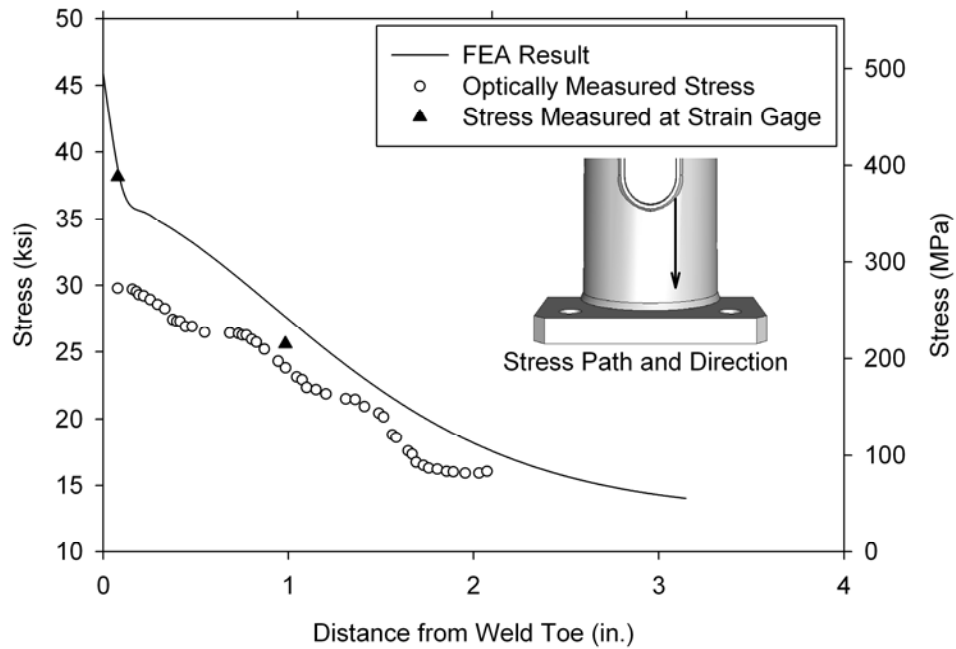
Figure 24 Stress profile near bottom right corner of hand-hole (Region 3) in specimen Type I
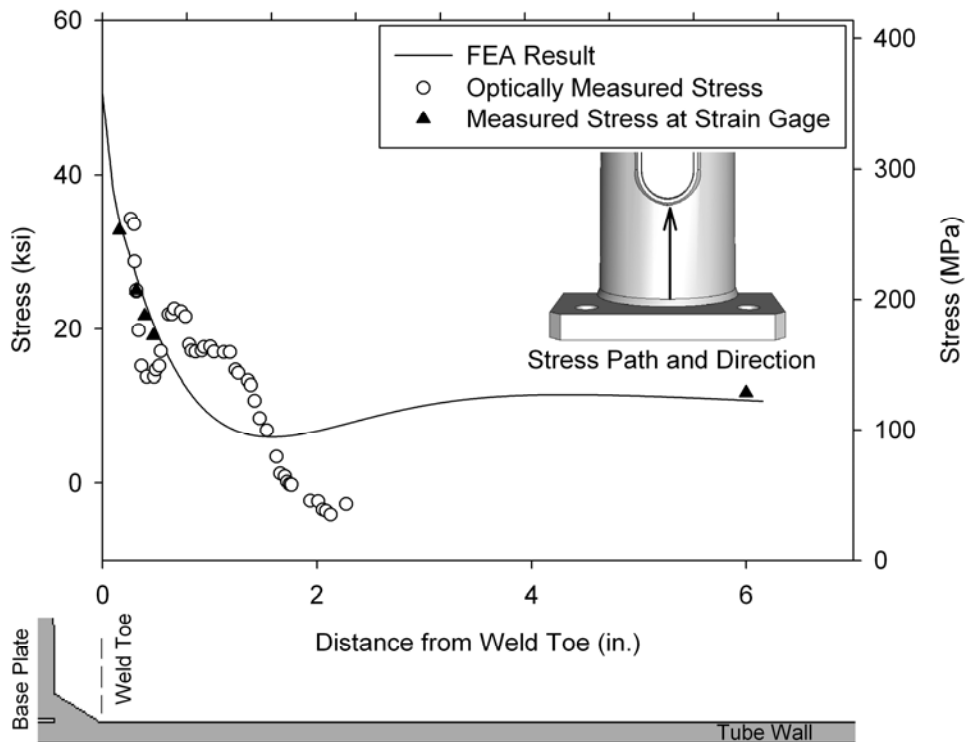
Figure 25 Stress profile near pole-to-base plate connection weld (Region 4) in specimen Type I

81
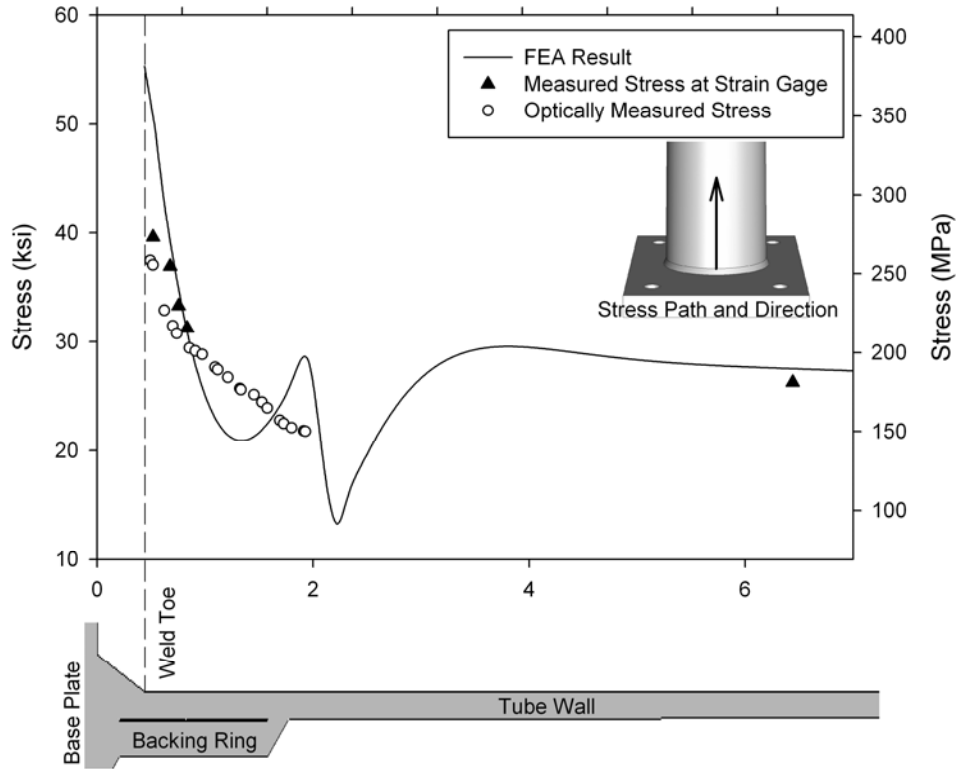
Figure 26 Stress profile near arm tube-to-transverse plate connection (Region 1) in specimen Type II
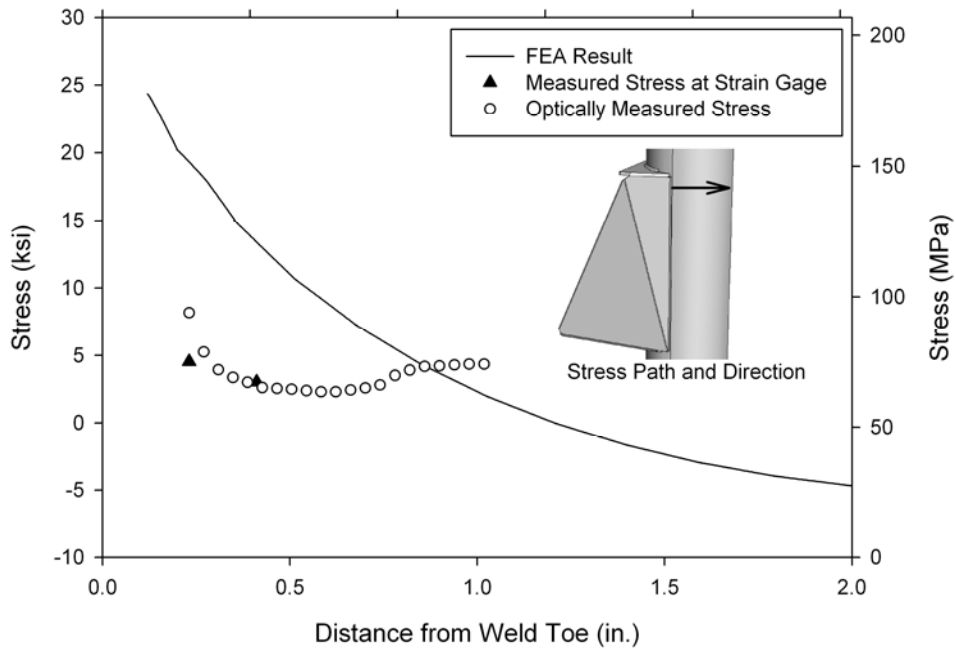
Figure 27 Stress profile near top corner of side gusset (Region 2) in specimen Type II

82
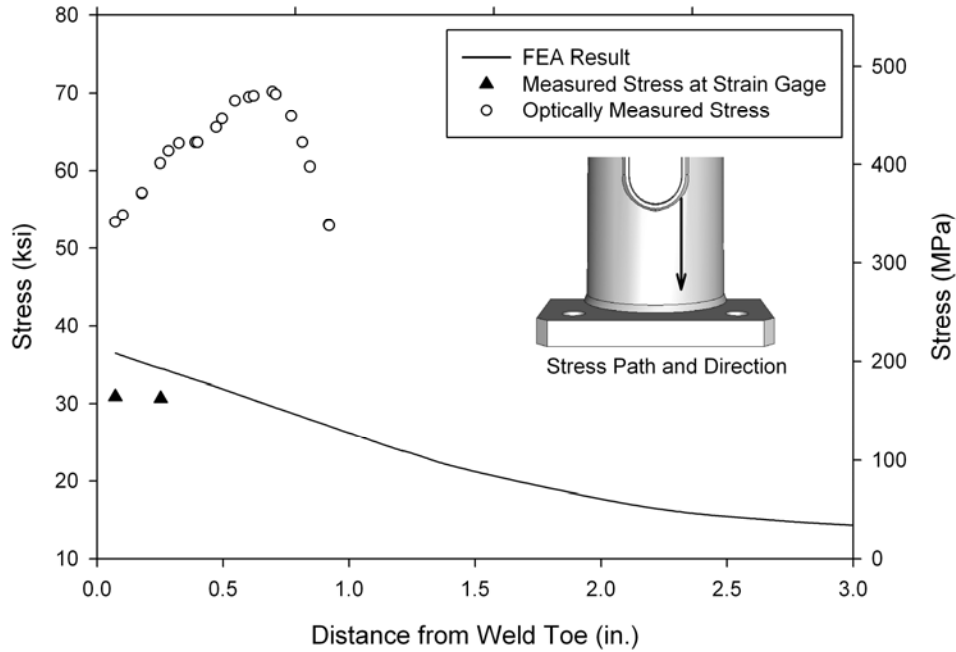
Figure 28 Stress profile near bottom right corner of hand-hole (Region 3) in specimen Type II
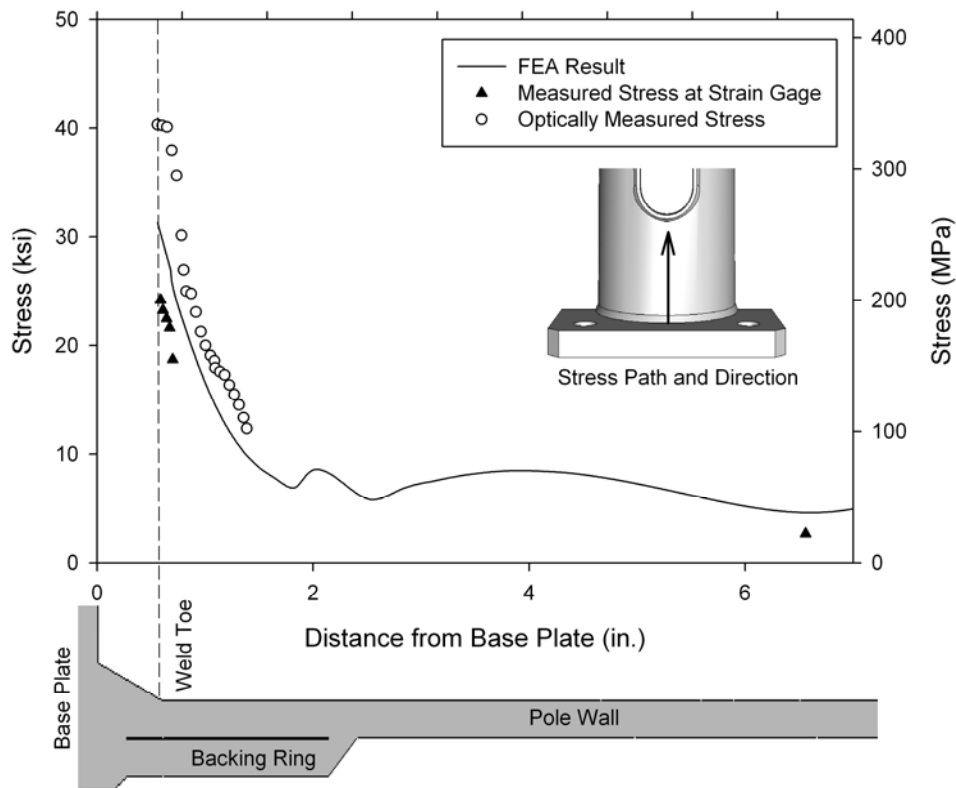
Figure 29 Stress profile near pole-to-base plate connection weld (Region 4) in specimen Type II

83
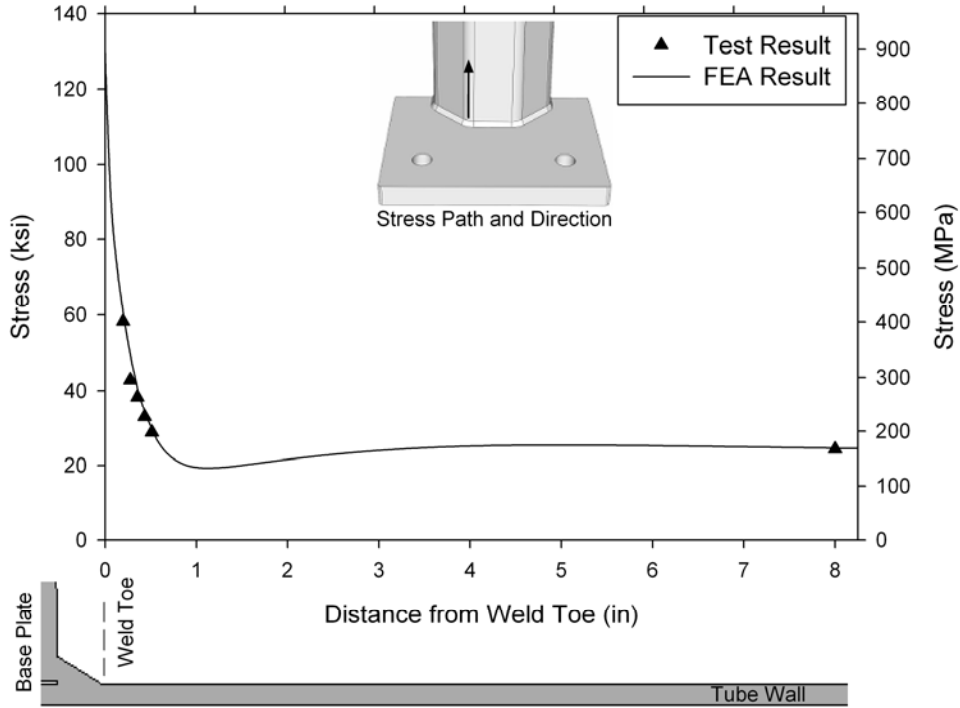
Figure 30 Stress profile near corner of arm tube-to-transverse plate connection in specimen Type VII
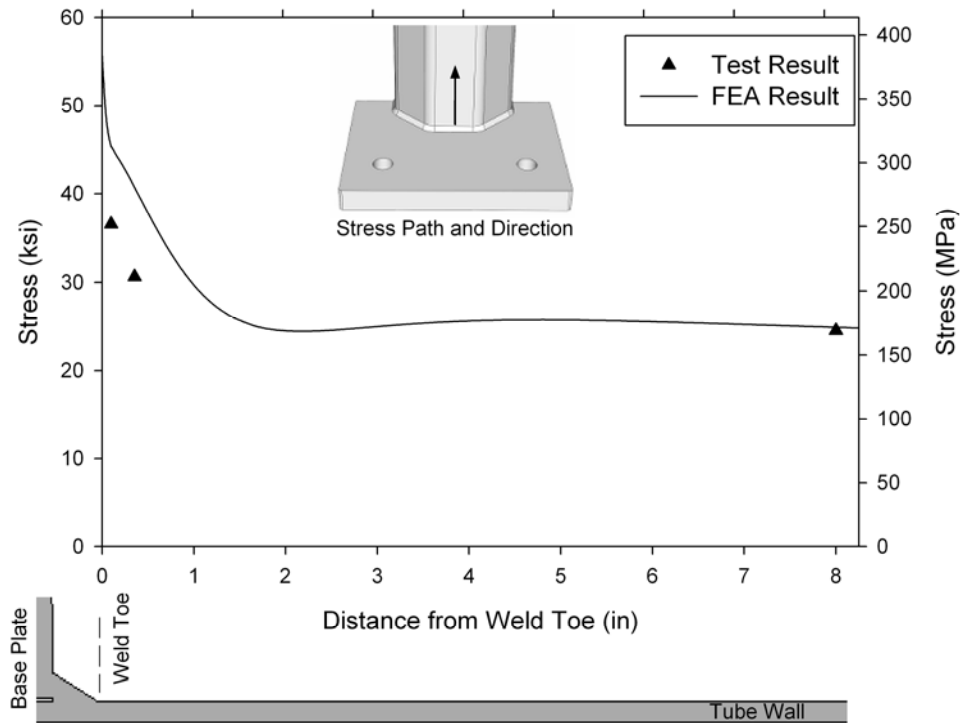
Figure 31 Stress profile near middle of flat of arm tube-to-transverse plate connection in specimen Type VII

84
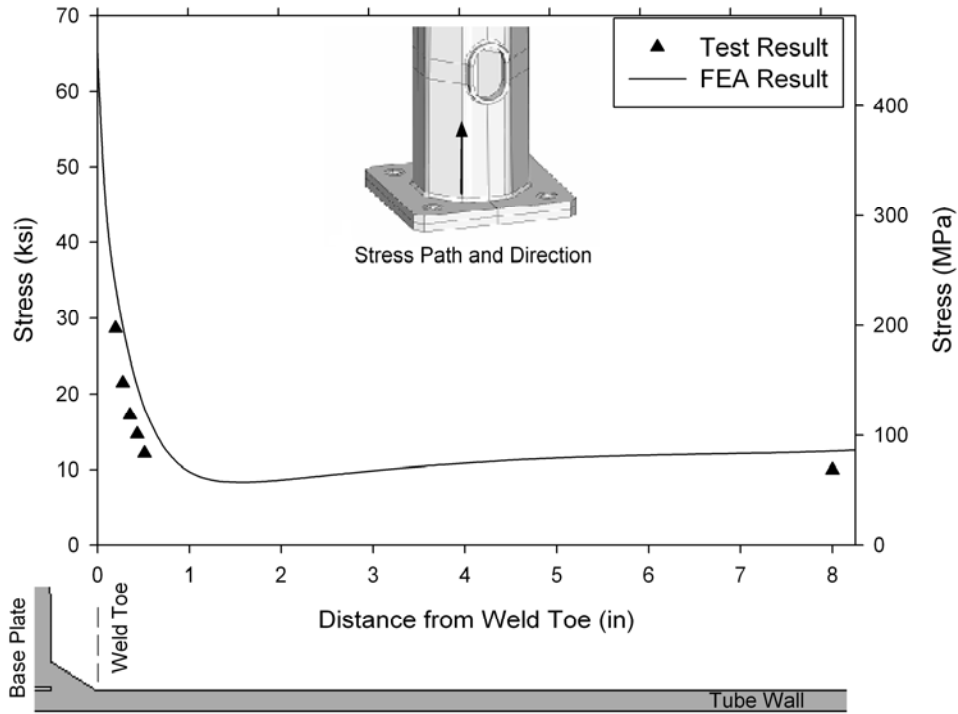
Figure 32 Stress profile near corner of pole-to-base plate connection in specimen Type VII
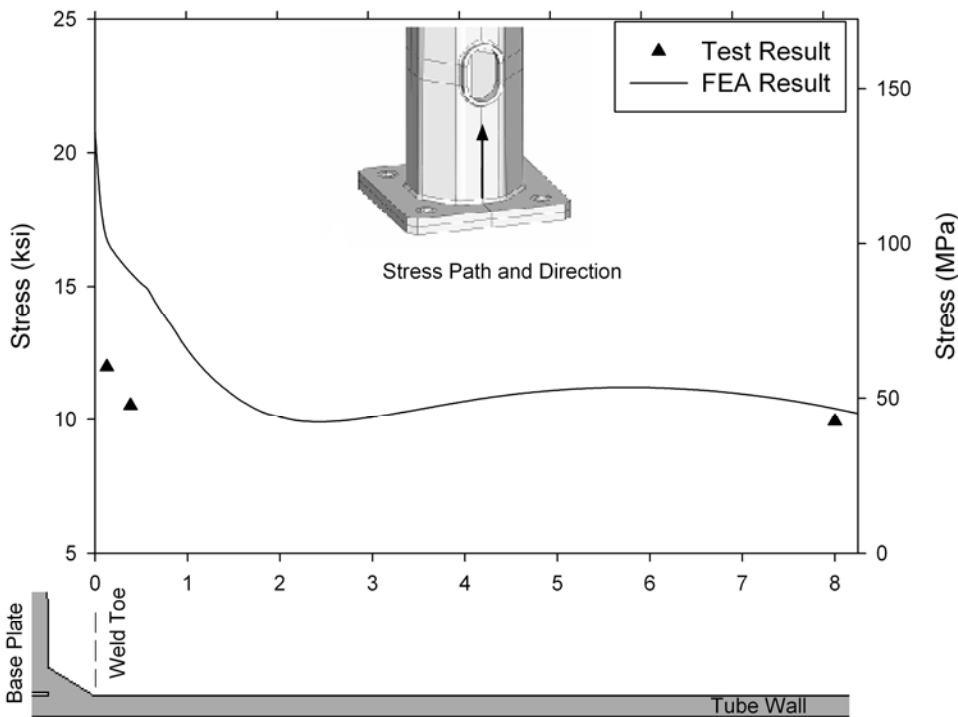
Figure 33 Stress profile near middle of flat of pole-to-base plate connection in specimen Type VII

85
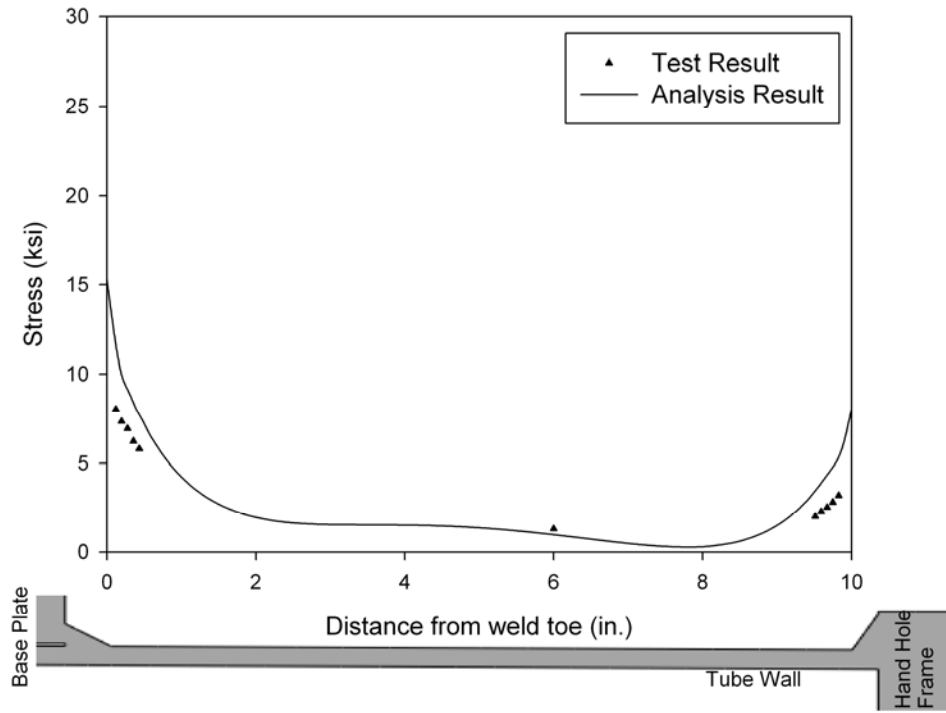
Figure 34 Stress profile near pole-to-base plate connection weld and hand hole in specimen Type X

86
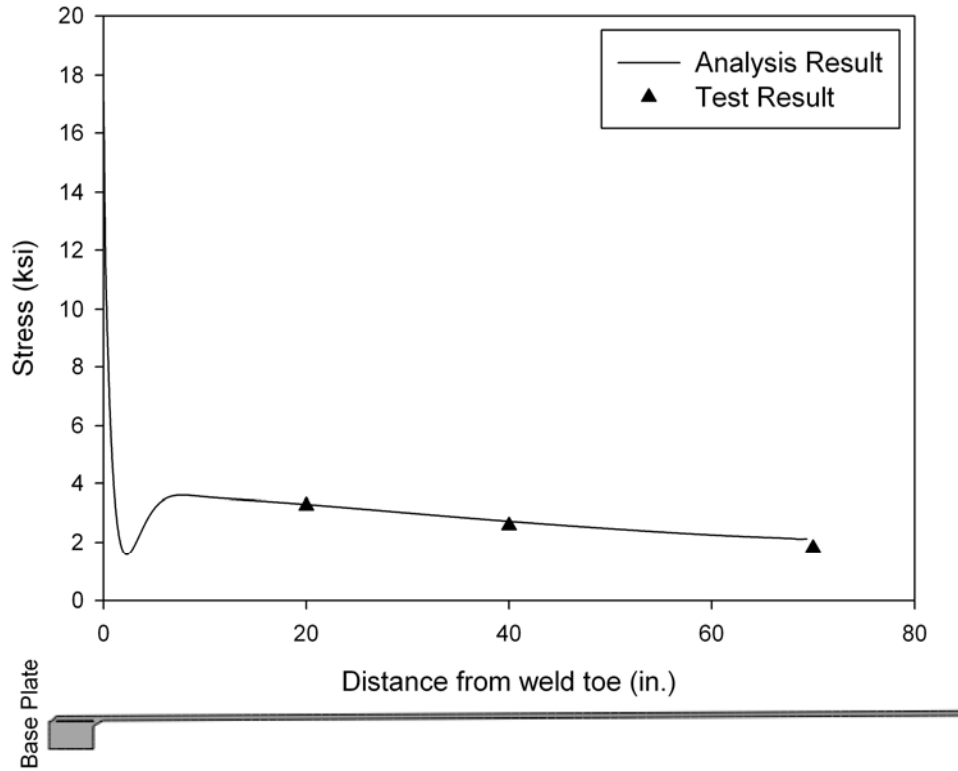
Figure 35 Stress profile in pole wall opposite to hand hole in specimen Type X
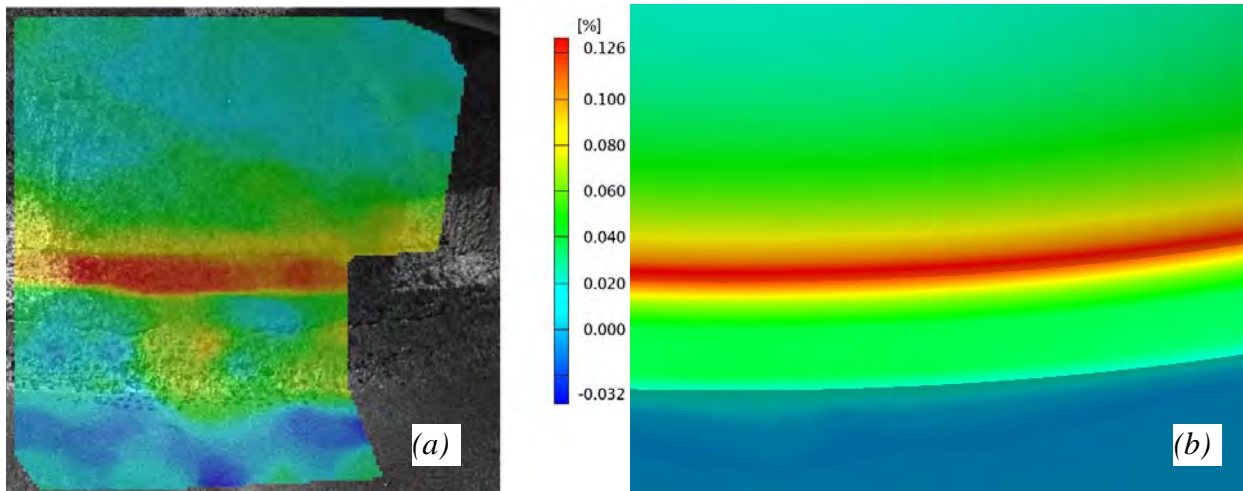
Figure 36 Principal stress contour near base of pole in Specimen Type I: (a) 3D ICP measurement; (b) FEA result

87
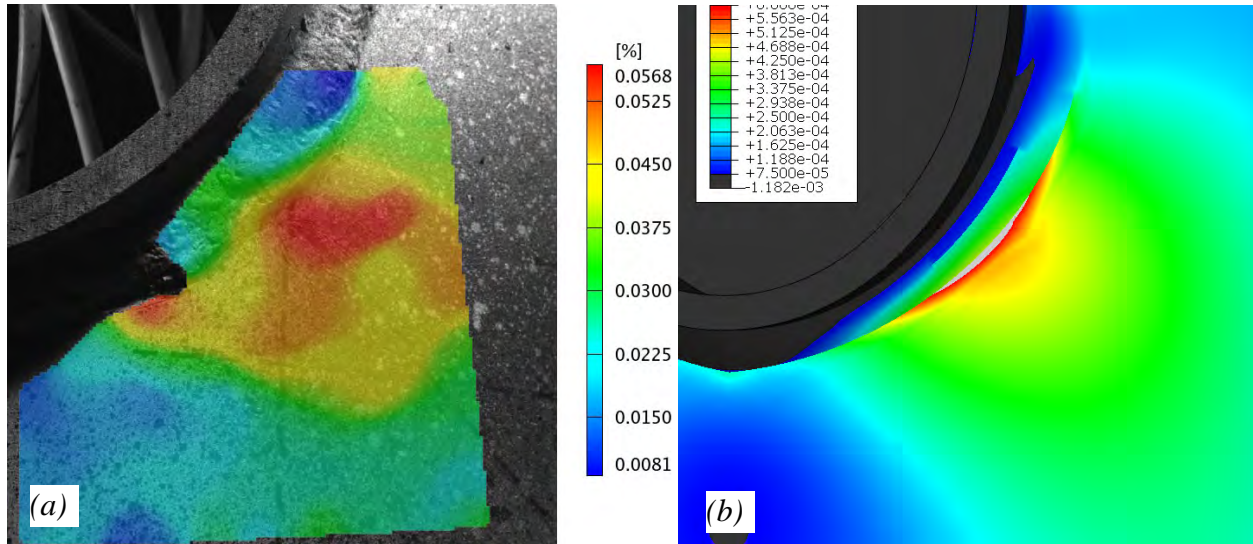
Figure 37 Principal stress contour near hand hole in Specimen Type I: (a) 3D ICP measurement; (b) FEA result
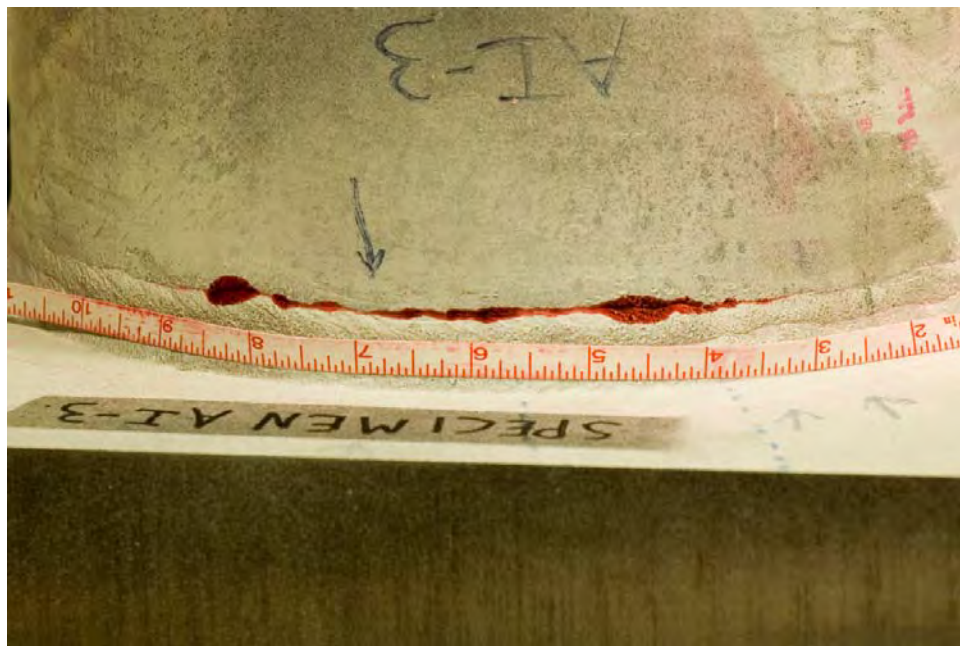
Figure 38 Fatigue crack from the fillet weld termination on the tube wall in arm pole-to-transverse plate socket connection in Specimen Type I

88

Figure 39 Fatigue crack from un-fused root of hand hole frame to pole weld
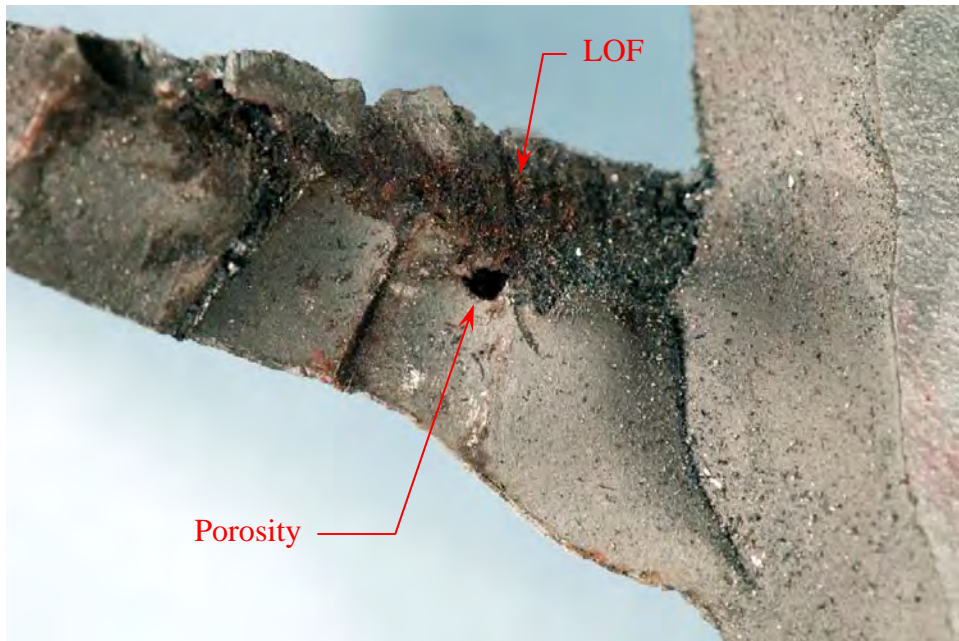
Figure 40 Fracture surface of hand hole frame to pole fillet weld revealing the origin of fatigue crack from the lack of fusion and porosity at the weld root

89

Figure 41 Holes drilled at the crack tip for continuing fatigue tests

Figure 42 Fatigue cracking in arm from the toe of backing ring to tube weld (inside)

90
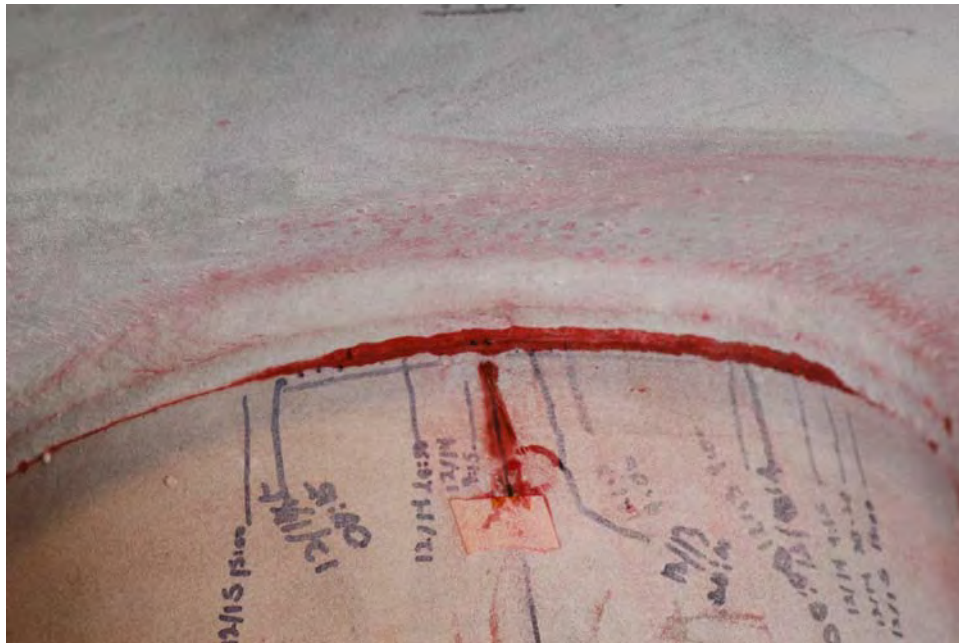
Figure 43 Fatigue cracking in arm from the toe of pole-to-transverse plate groove-weld

Figure 44 Fatigue cracking in arm of specimen III-5 from tack weld between the backing ring and the tube wall

91
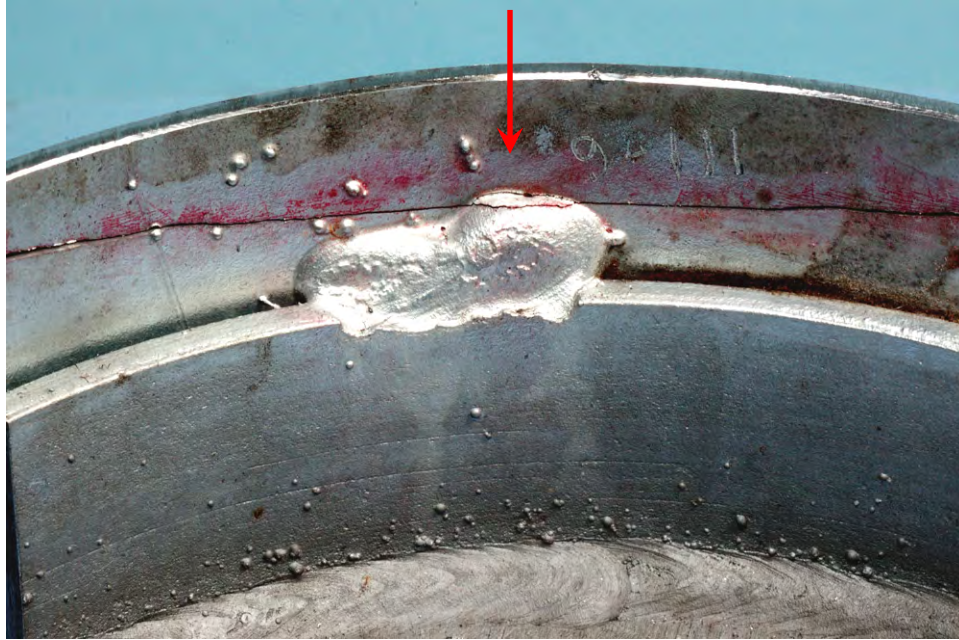
Figure 45 Fatigue cracking in arm of specimen III-6 from tack weld between the backing ring and the tube wall
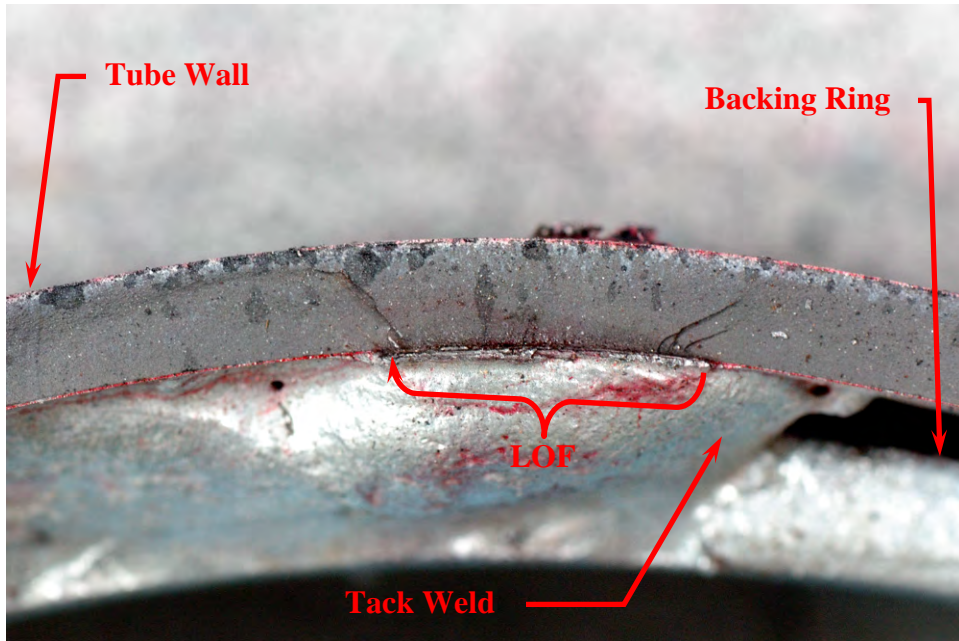
Figure 46 Exposed fatigue fracture surface in the arm of specimen III-6 showing crack origin at the lack of fusion (LOF) between the tack weld and the tube wall (refer Figure 45 for view direction)

92

Figure 47 Fatigue cracking from gusset-to-pole fillet-weld in specimen IVB-1

93

Figure 48 Fatigue cracking in specimen V from arm-to-clamp weld toe on the clamp
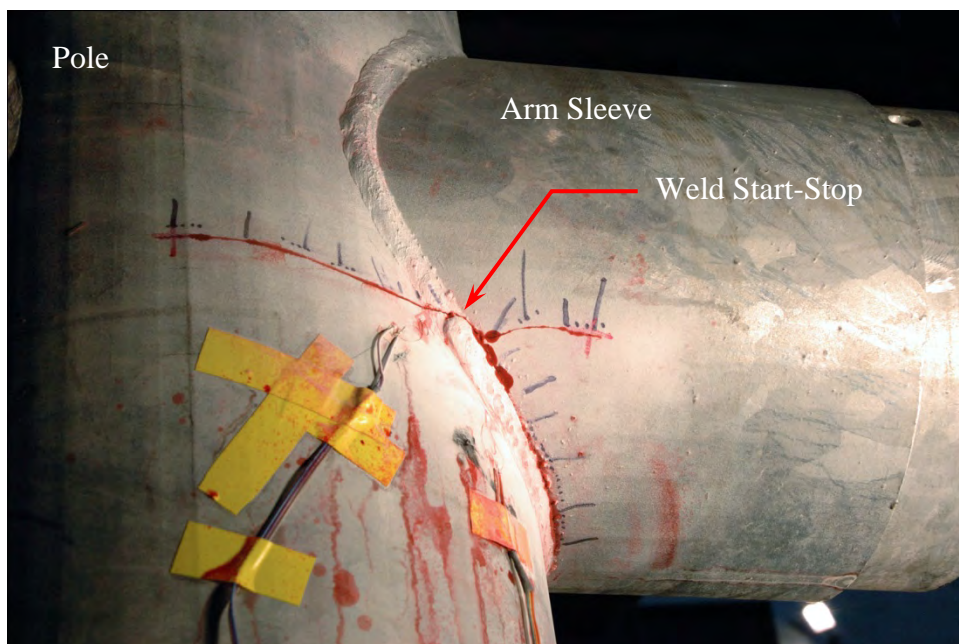
Figure 49 Fatigue cracking in specimen VI-2 from a weld start-stop

94

Figure 50 Fatigue cracking in specimen VI-1 from weld root arrested by hole drilling in the arm sleeve
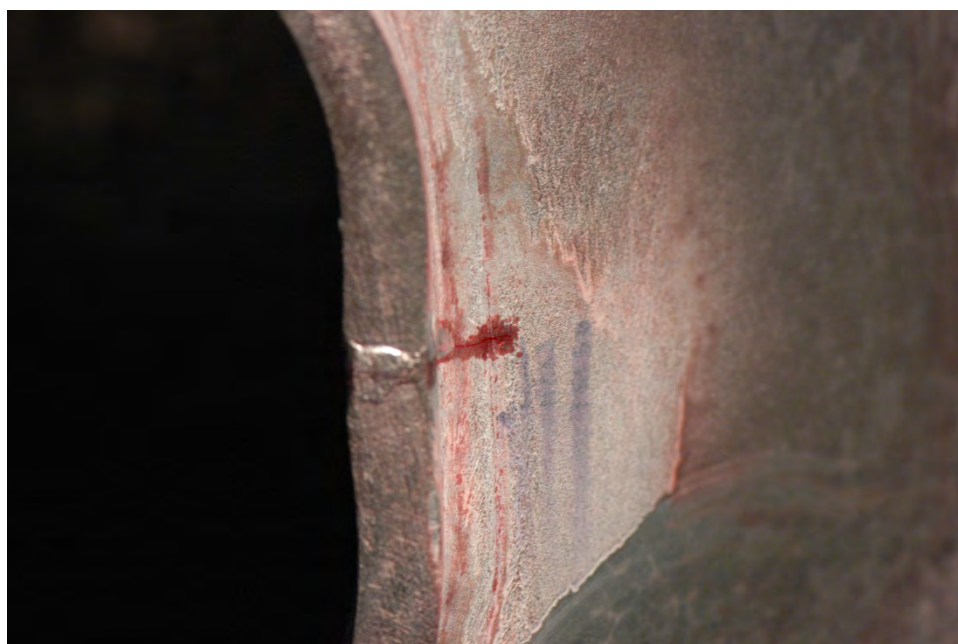
Figure 51 Fatigue cracking from seam weld in the hand hole frame of specimen VII-4

95
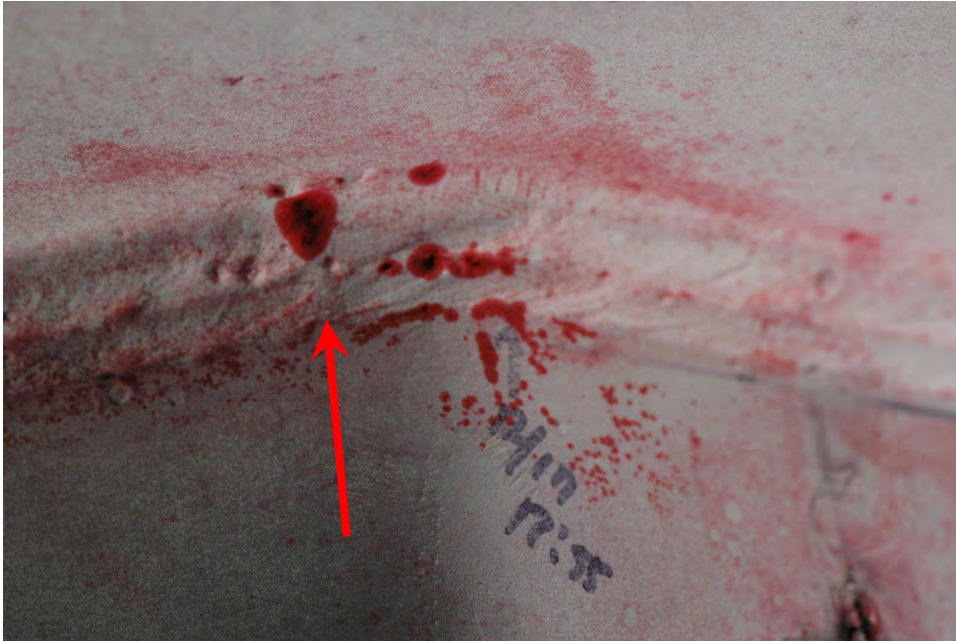
Figure 52 Fatigue cracking from bend corner in the arm of specimen VII-7

Figure 53 Fatigue cracking in arm of specimen VII-5, from the fillet weld toe on the tube in tube-to-transverse plate connection

96

Figure 54 Fatigue cracking from toe of pole-to-transverse plate weld in pole of specimen Type VII
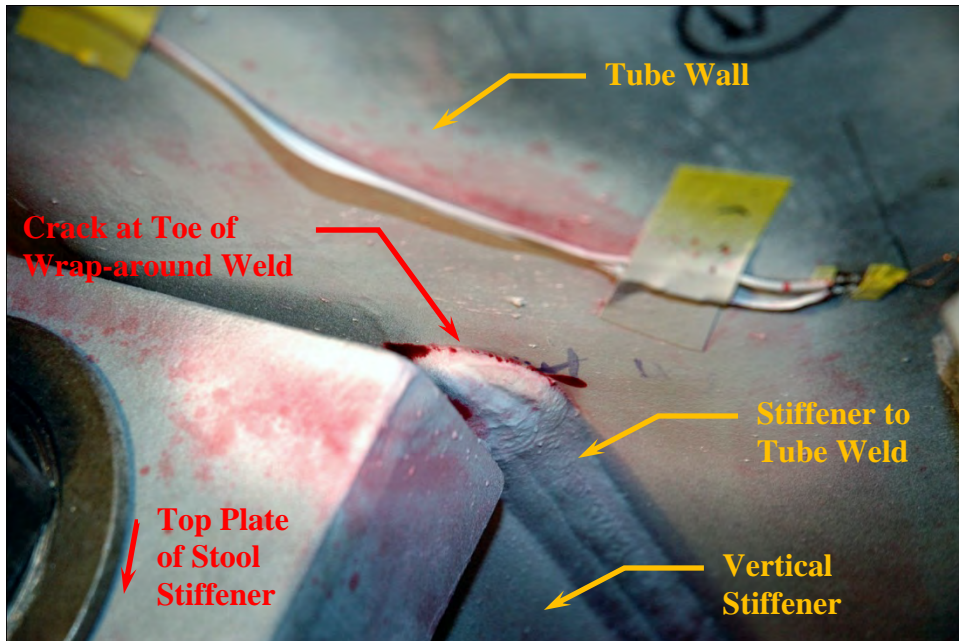
Figure 55 Fatigue crack initiation in specimen IX-2

97

Figure 56 Fatigue cracking in specimen IX-3 from the stool stiffener to tube weld toe at the termination of the vertical stiffener on the tube wall (with stool top plate removed)

Figure 57 Fatigue cracking at pole-to-base plate fillet weld toe in high-level luminaire structure specimens
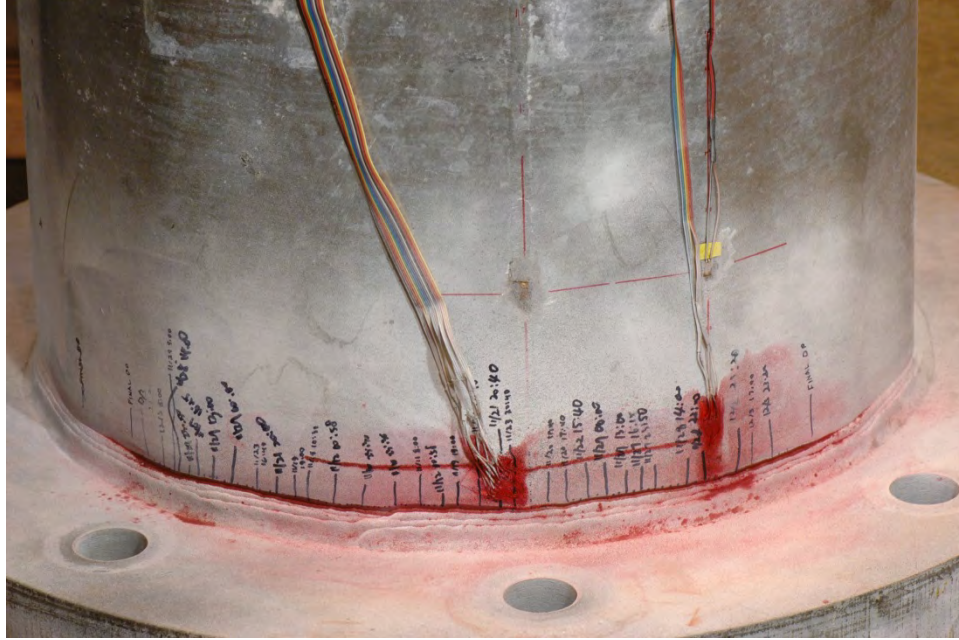
98

Figure 58 Fatigue cracking in specimen XI-6 from termination of fillet weld toe on the tube wall of both the pole-to-transverse plate weld and the backing ring top weld

Figure 59 Fatigue cracking in specimen XII-8 – A: from the stiffener to tube weld toe at the termination of the stiffener on the tube wall; and B: from the socket weld toe on the tube wall at the base

99
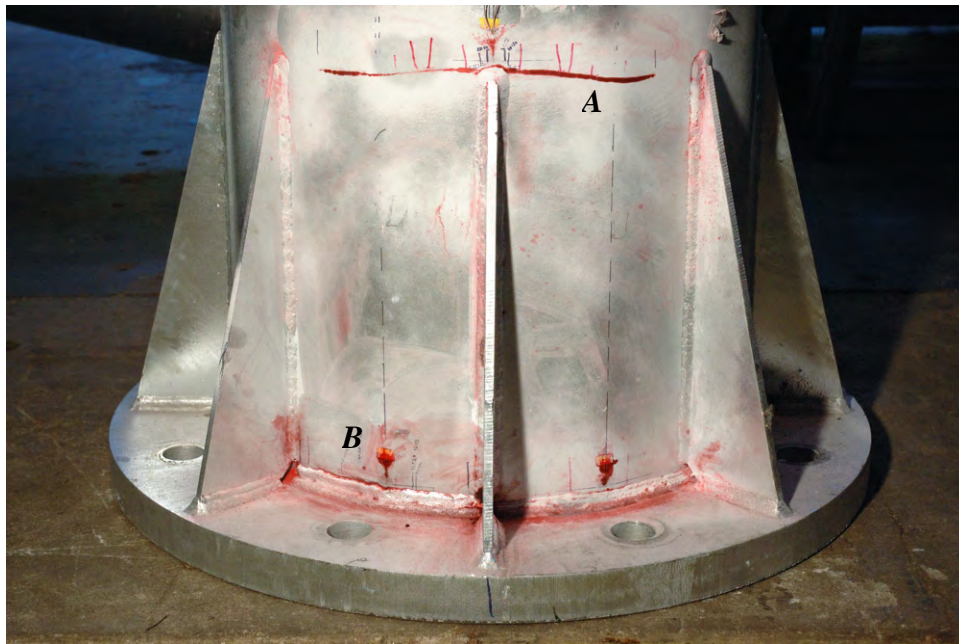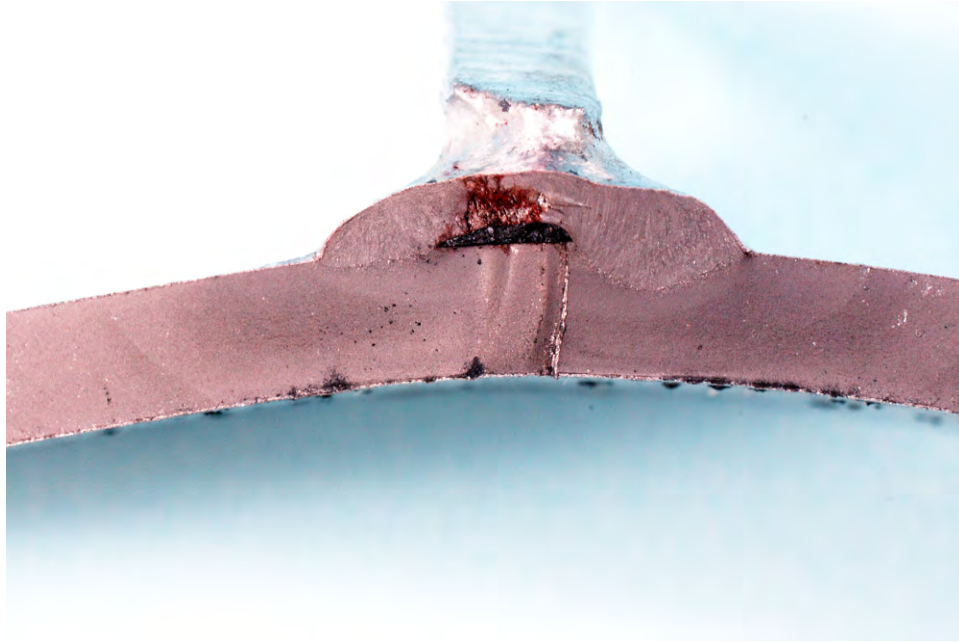
Figure 60 Fatigue crack growth from the lack of fusion at the stiffener to tube weld root in specimen XII-6
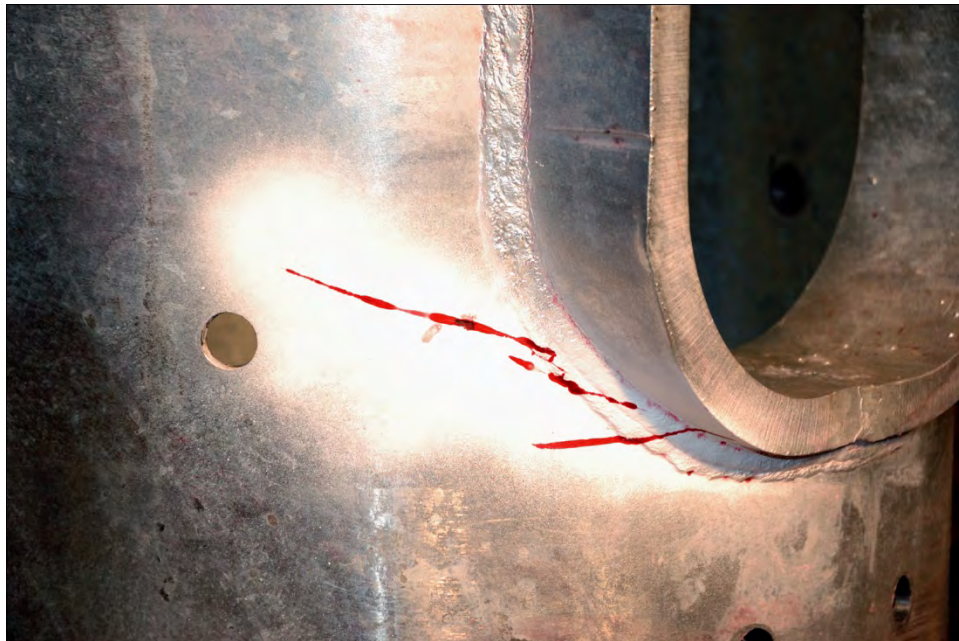
Figure 61 Fatigue crack initiation in specimen JRXI from the root of hand hole frame to pole weld (photographed after jacket removed)

100
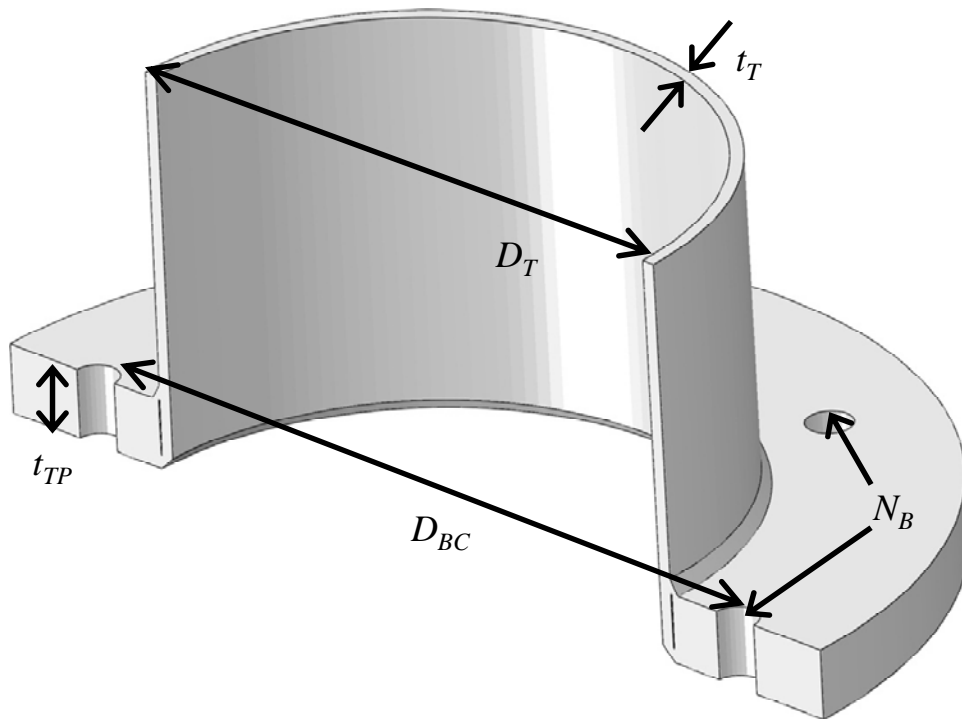
Figure 62 Geometric parameters for unstiffened fillet-welded tube-to-transverse plate connection
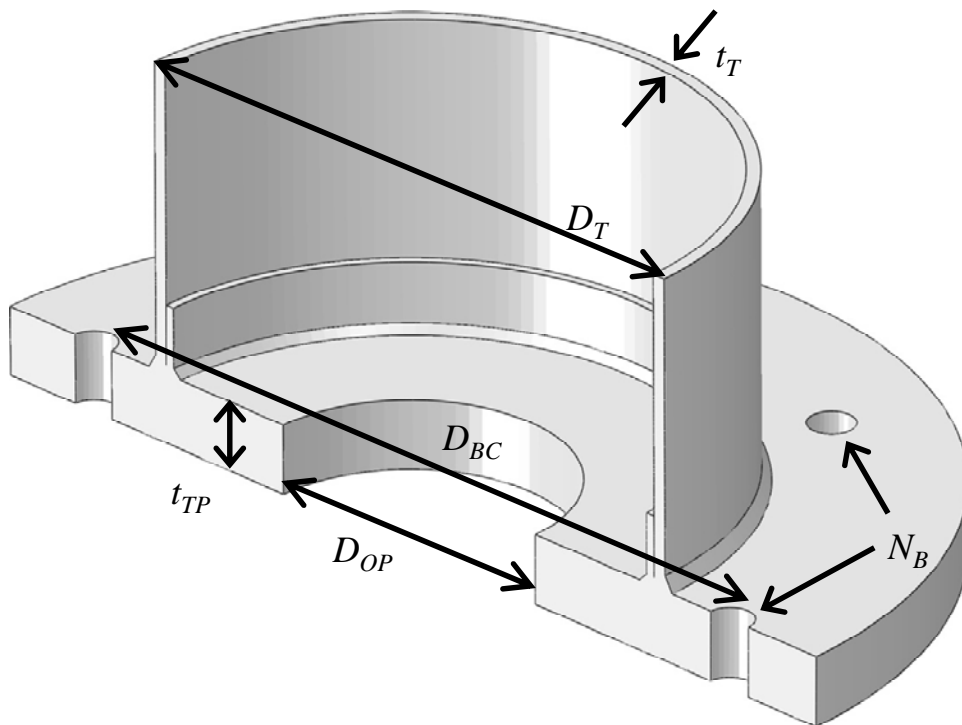
Figure 63 Geometric parameters for unstiffened groove-welded tube-to-transverse plate connection

101
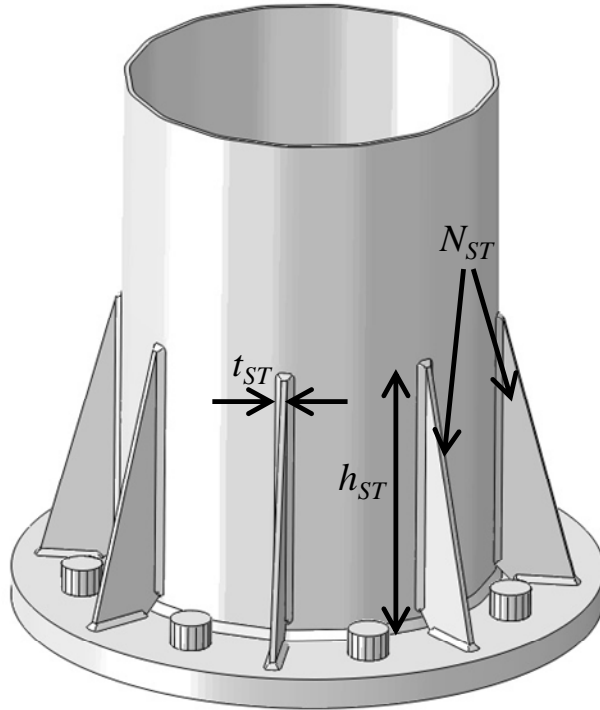
Figure 64 Geometric parameters for stiffened tube-to-transverse plate connection
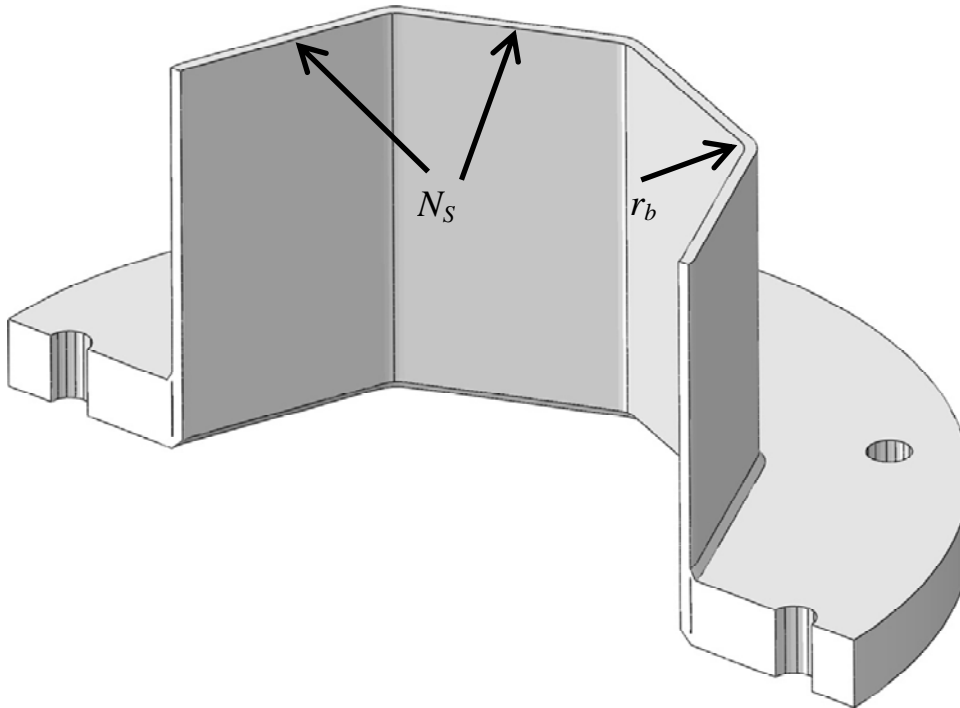
Figure 65 Geometric parameters for multi-sided tube
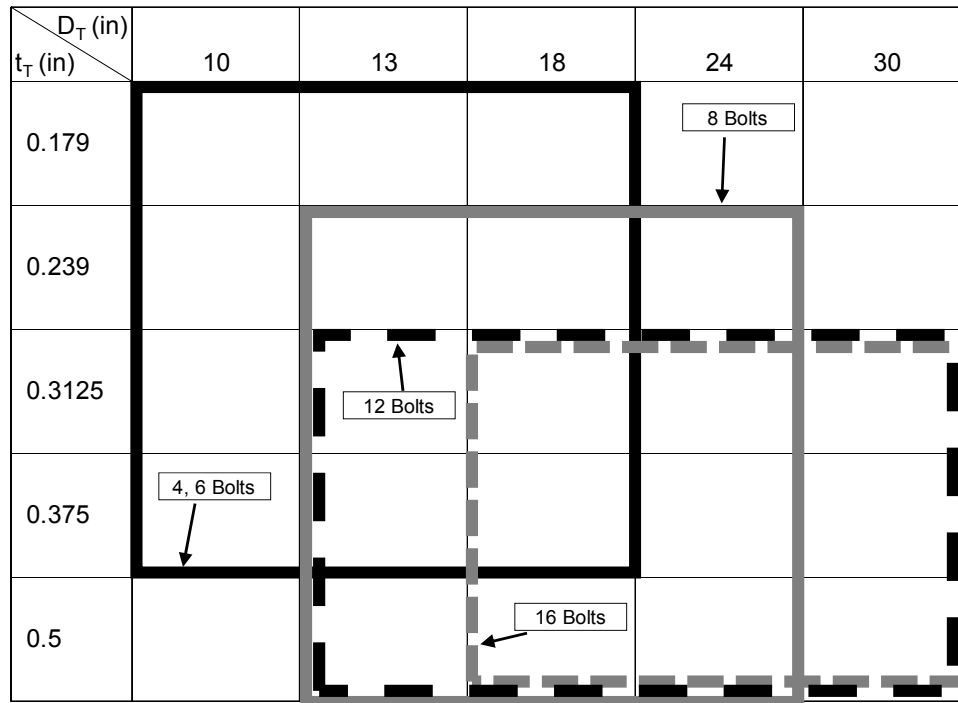
102

D_T (in) t_T (in)	10	13	18	24	30
0.179				8 Bolts	
0.239					
0.3125		12 Bolts			
0.375	4, 6 Bolts				
0.5			16 Bolts		

$C_{OP} = (D_{OP}) / (D_T)$: max., 85%, 70%, 55%, 40%

max. = max$(D_{OP})/(D_T)$; max$(D_{OP}) = D_T - 2x$(backing ring thickness+backing ring weld size)

Figure 66 Partial factorial for unstiffened fillet- and groove-welded connections in terms of tube diameter and tube thickness

103

C_{BC} t_{TP} (in)	1.25	1.50	1.75	2.10
2.0				8 Bolts
2.5			12 Bolts	
3.0	16 Bolts			4 Bolts
3.5				6 Bolts
4.0				
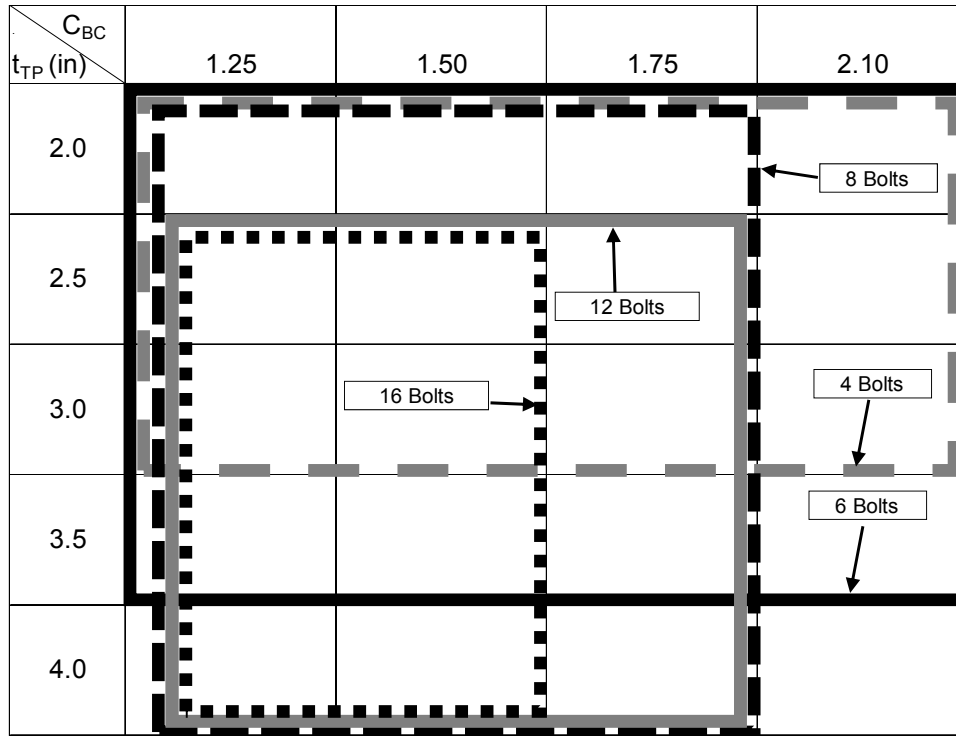
$C_{OP} = (D_{OP}) / (D_T)$: max., 85%, 70%, 55%, 40%

max. = max$(D_{OP})/(D_T)$; max$(D_{OP}) = D_T - 2$x(backing ring thickness+backing ring weld size)

Figure 67 Partial factorial for unstiffened fillet- and groove-welded connections in terms of transverse plate thickness and bolt circle ratio

D_T (in) h_{ST} (in)	24	30	36
12			
18			
24			
30			
36			
42			

N_{ST} : 6, 8, 12 for all combinations

Figure 68 Partial factorial for stiffened fillet welded connections in terms of tube diameter and stiffener height

104

t_T (in) / t_{ST} (in)	0.3125	0.375	0.5	0.625
0.25				
0.3125				
0.375				
0.5				
0.625				
0.75				
0.875				

N_{ST} : 6, 8, 12 for all combinations

Figure 69 Partial factorial for stiffened fillet welded connections in terms of tube thickness and stiffener thickness

105

Figure 70 Global model of analyzed structures: (a) with unstiffened tube-to-transverse plate connection; (b) with stiffened tube-to-transverse plate connection

106
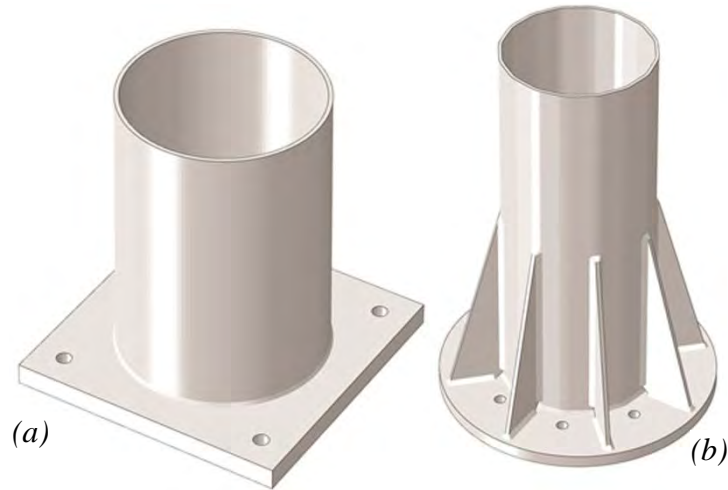
Figure 71 Sub-model of analyzed structures: (a) with unstiffened tube-to-transverse plate connection; (b) with stiffened tube-to-transverse plate connection
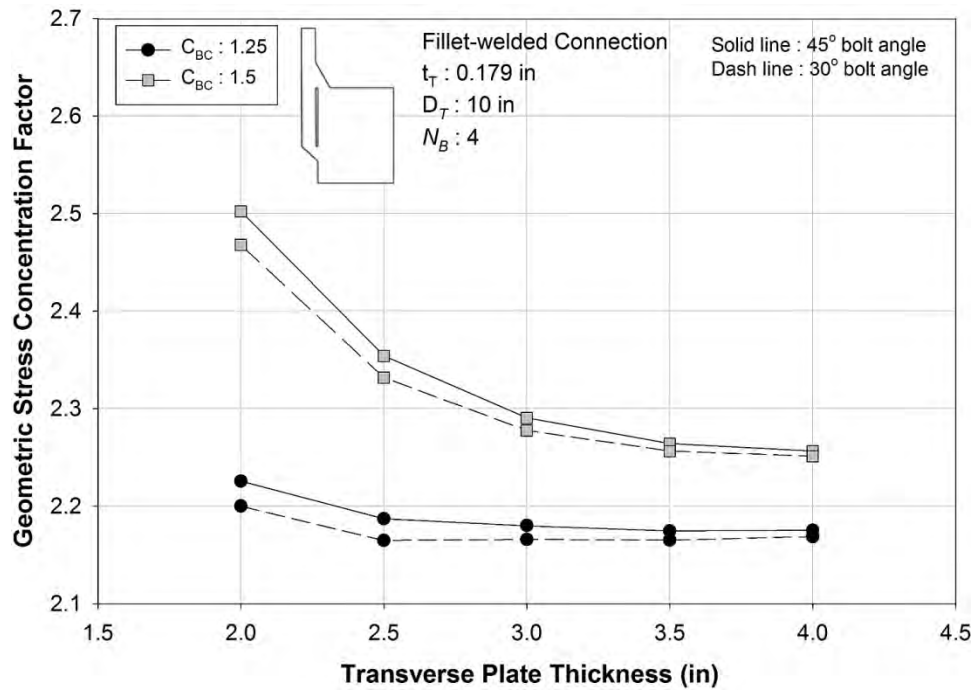
Figure 72 Effect of fastener arrangement with four fasteners

107
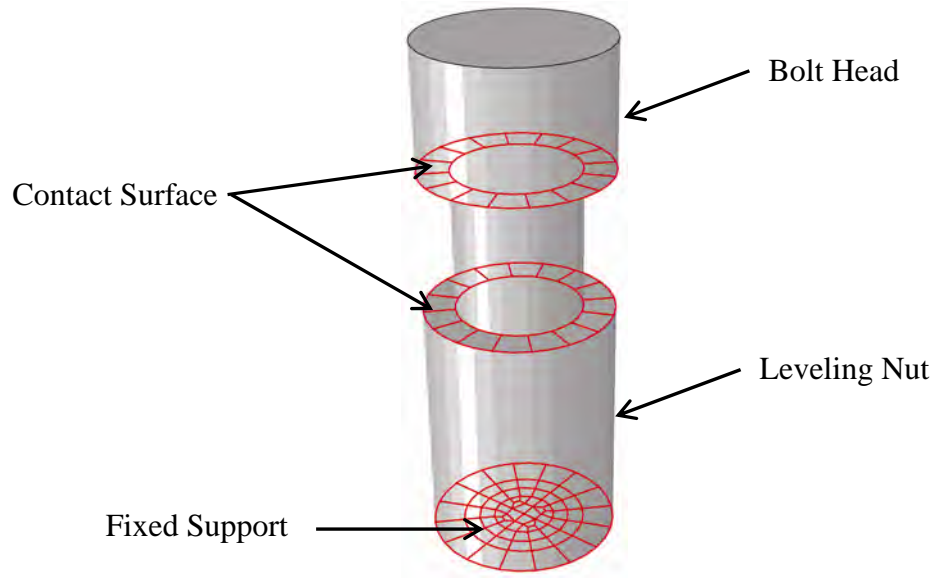
Figure 73 Shape of fasteners, contact surfaces, and location of fixed support
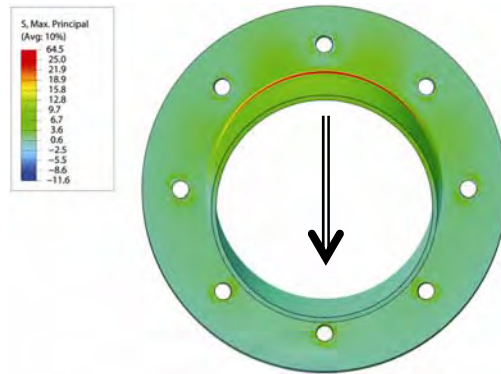
Figure 74 Loading direction considered for unstiffened tube-to-transverse plate connection

108
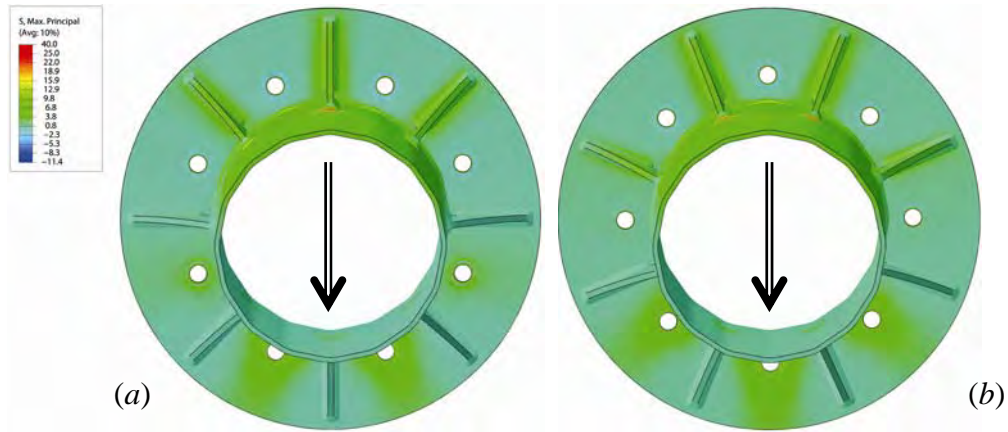
Figure 75 Loading directions considered for parametric study of stiffened tube-to-transverse plate fillet-welded connections: (a) load case 1; (b) load case 2

109

Figure 76 1ˢᵗ level sub-model

110
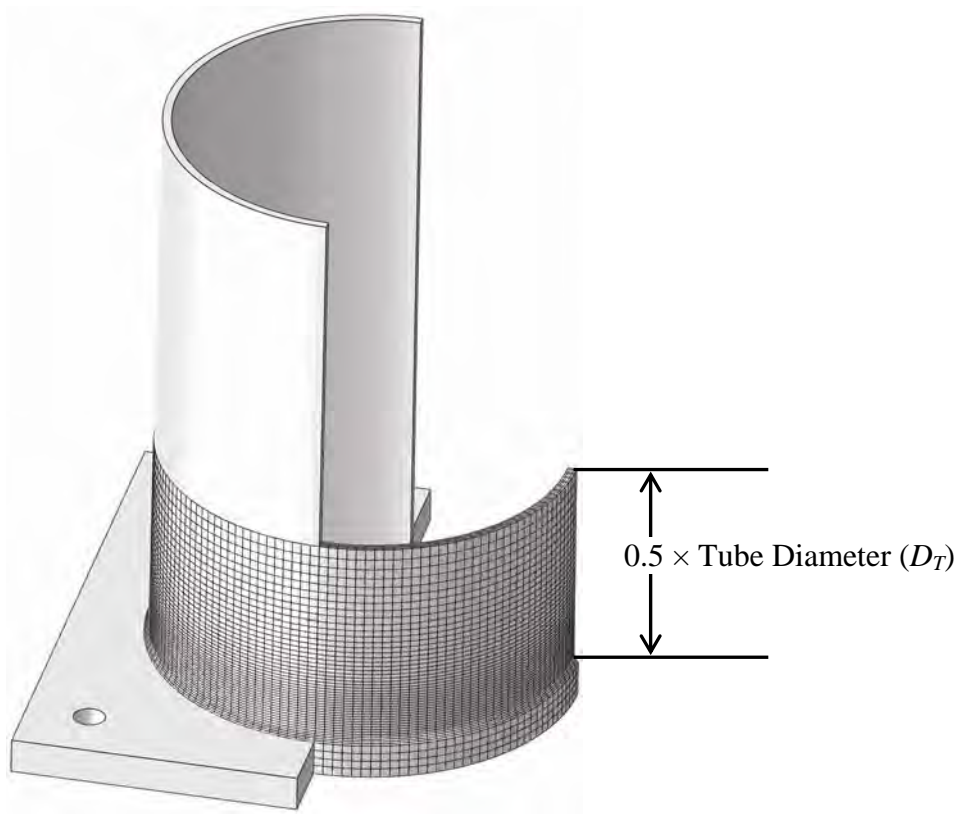
Figure 77 2nd level sub-model

111

Tube Center

10°

Height of Weld
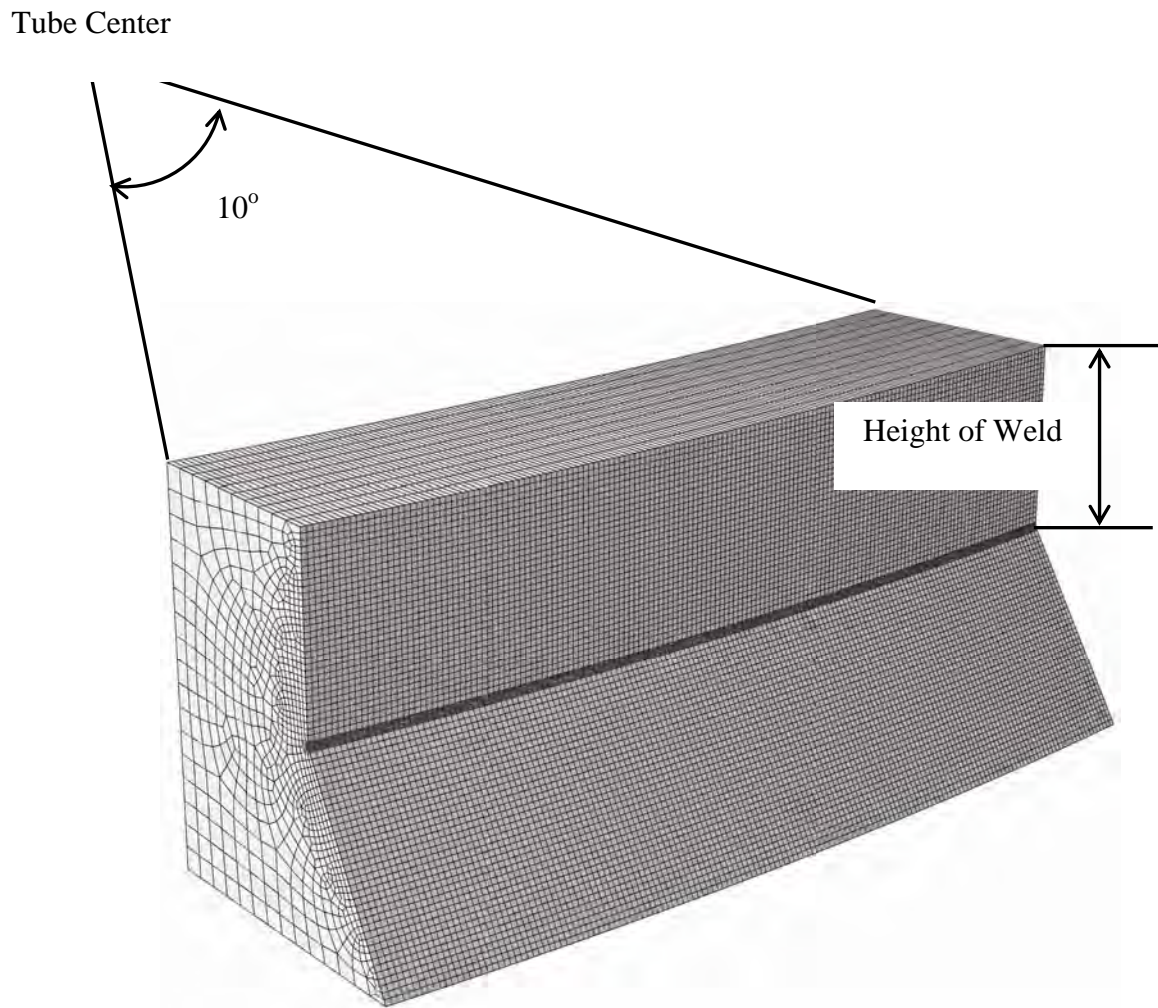
Figure 78 3rd level sub-model
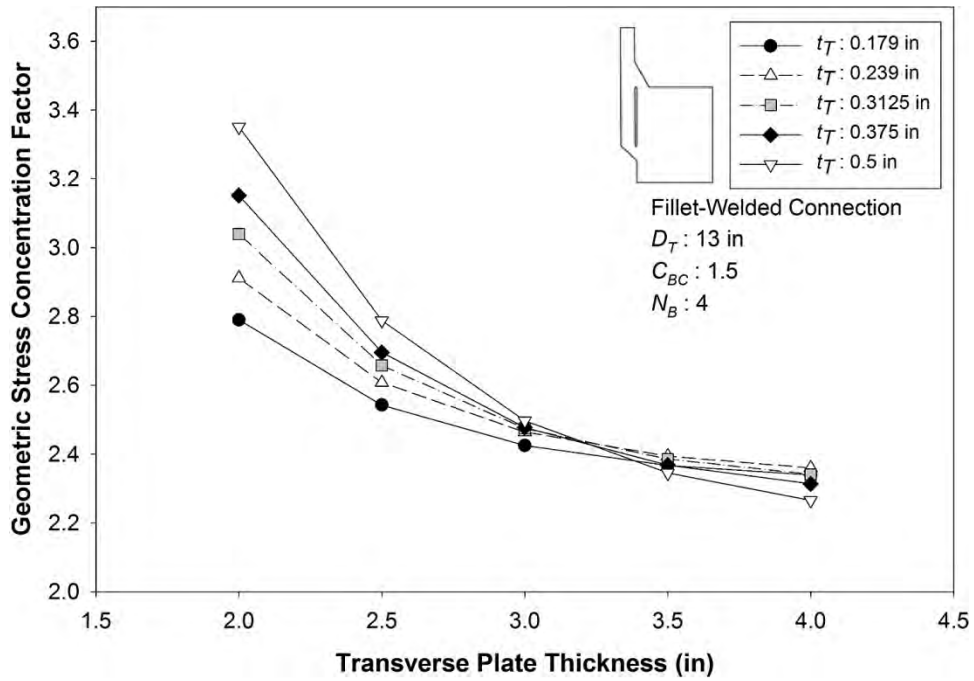
Figure 79 Effect of transverse plate thickness in unstiffened round tube-to-transverse plate fillet-welded connection
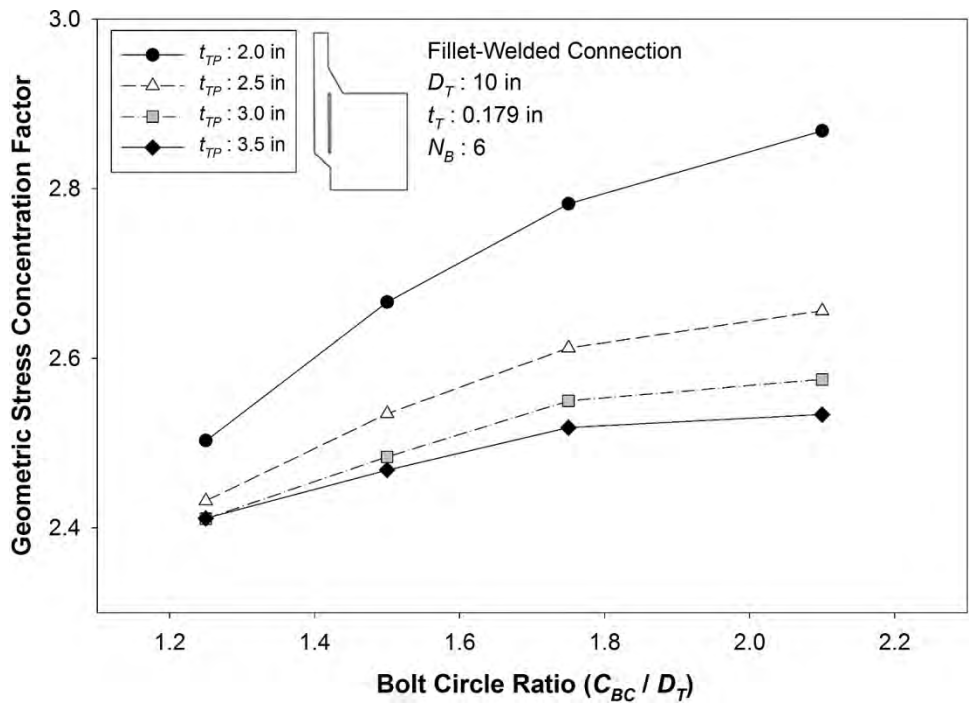
Figure 80 Effect of bolt circle ratio in unstiffened round tube-to-transverse plate fillet-welded connection

113
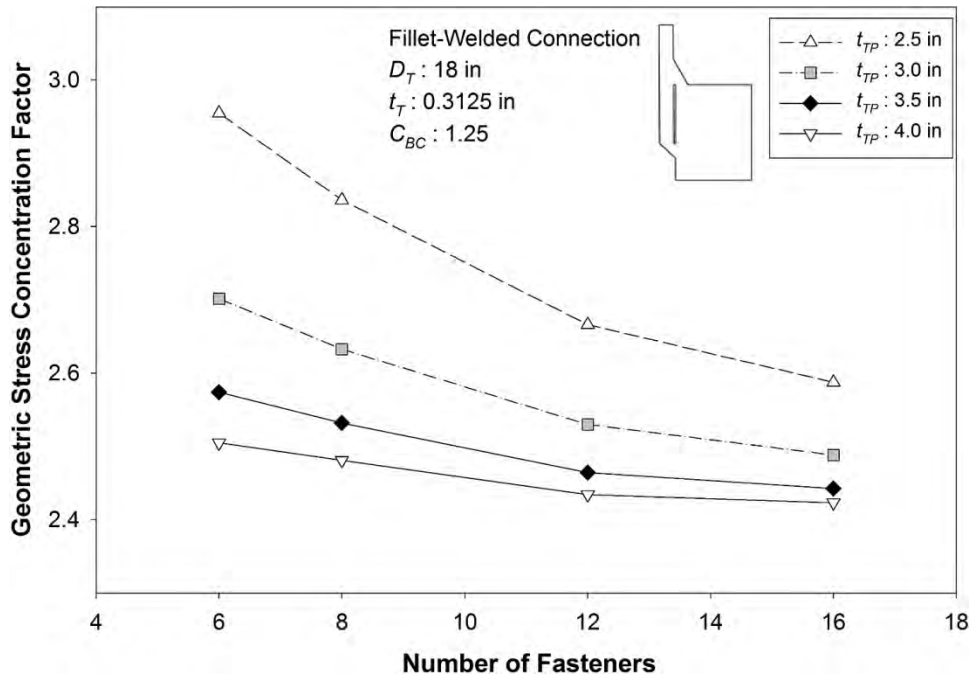
Figure 81 Effect of number of fasteners in unstiffened round tube-to-transverse plate fillet-welded connection
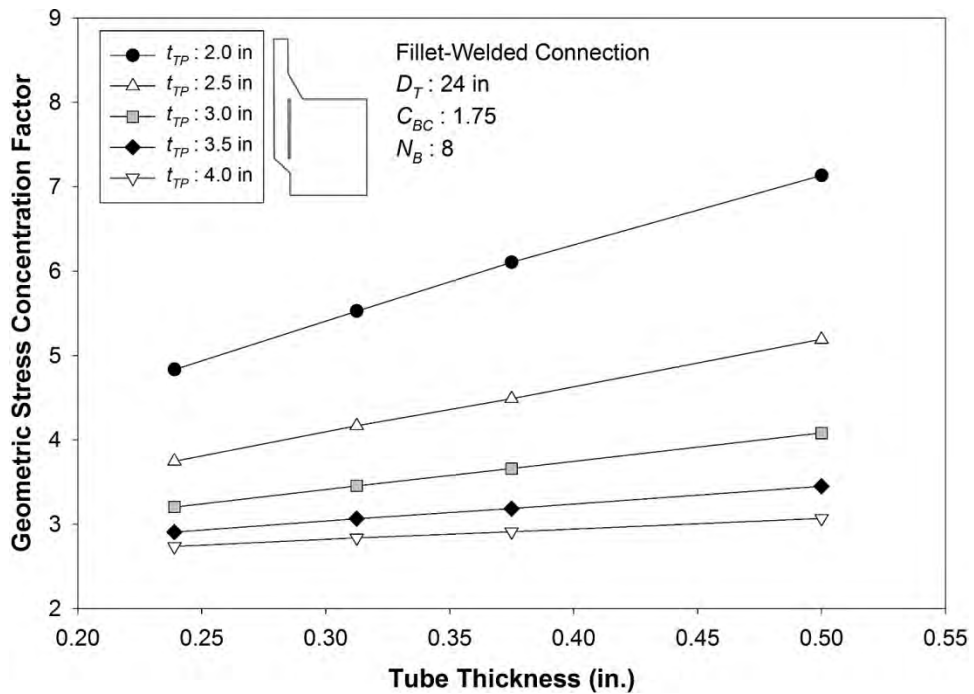
Figure 82 Effect of tube thickness in unstiffened round tube-to-transverse plate fillet-welded connection

114
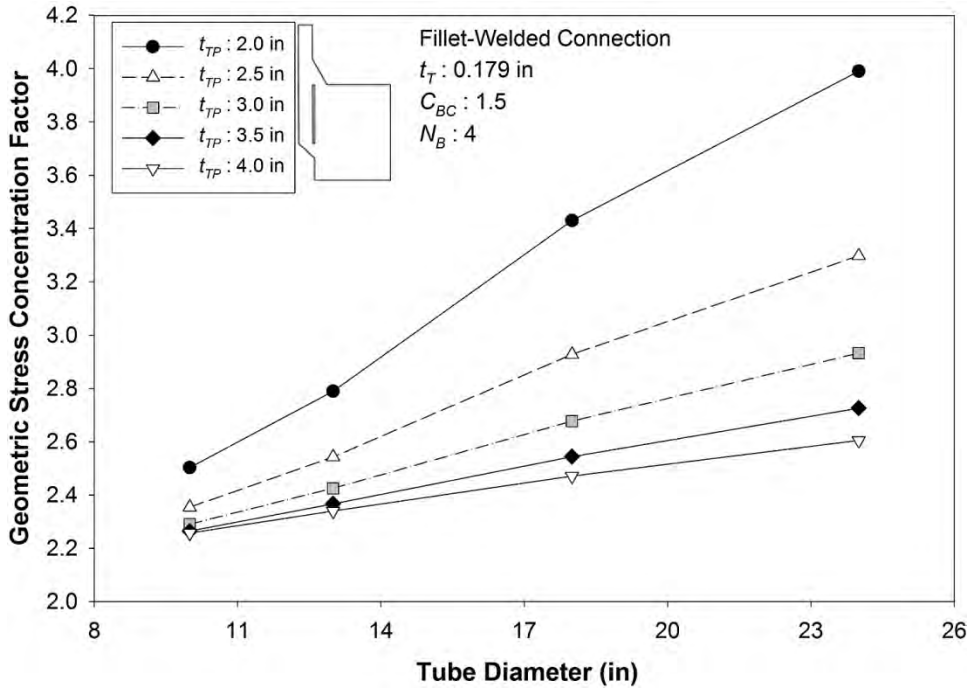
Figure 83 Effect of tube diameter in unstiffened round tube-to-transverse plate fillet-welded connection
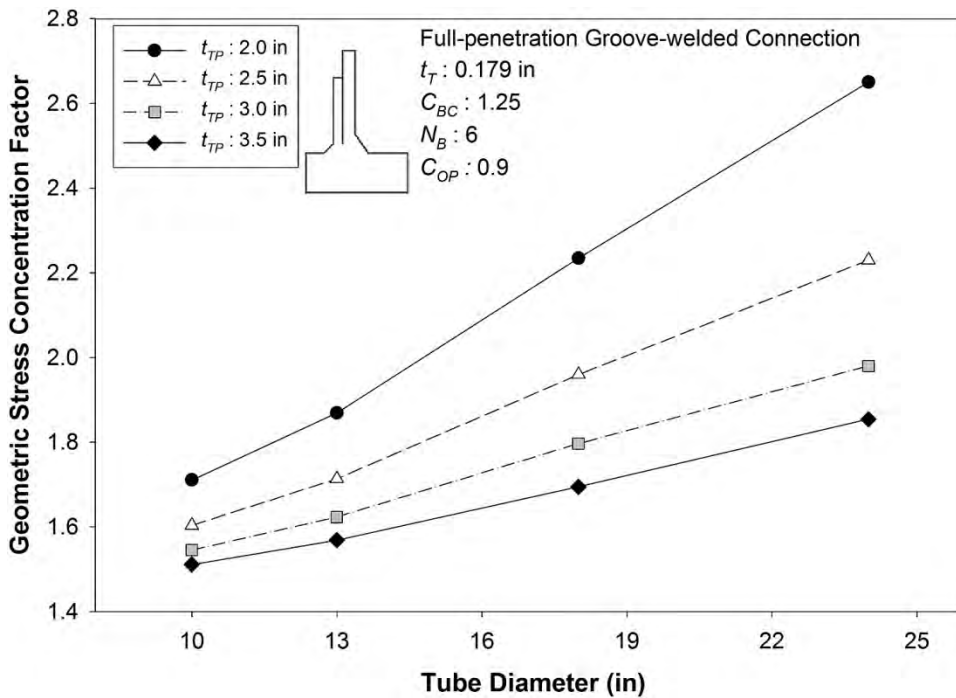
Figure 84 Effect of tube diameter in unstiffened round tube-to-transverse plate groove-welded connection

115
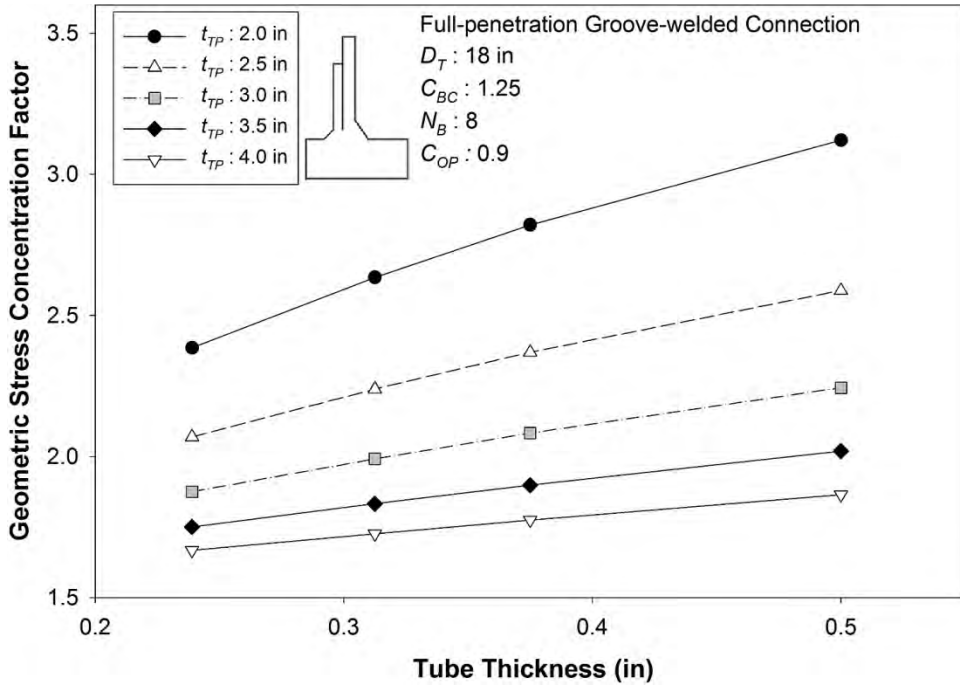
Figure 85 Effect of tube thickness in unstiffened round tube-to-transverse plate groove-welded connection
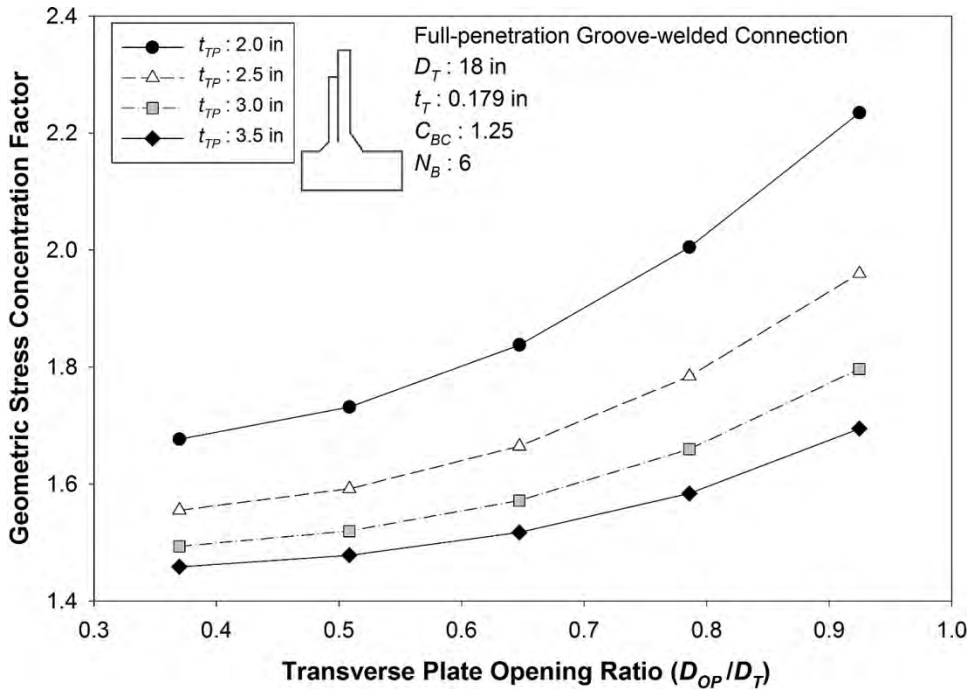
Figure 86 Effect of transverse plate opening in unstiffened round tube-to-transverse plate groove-welded connection

116
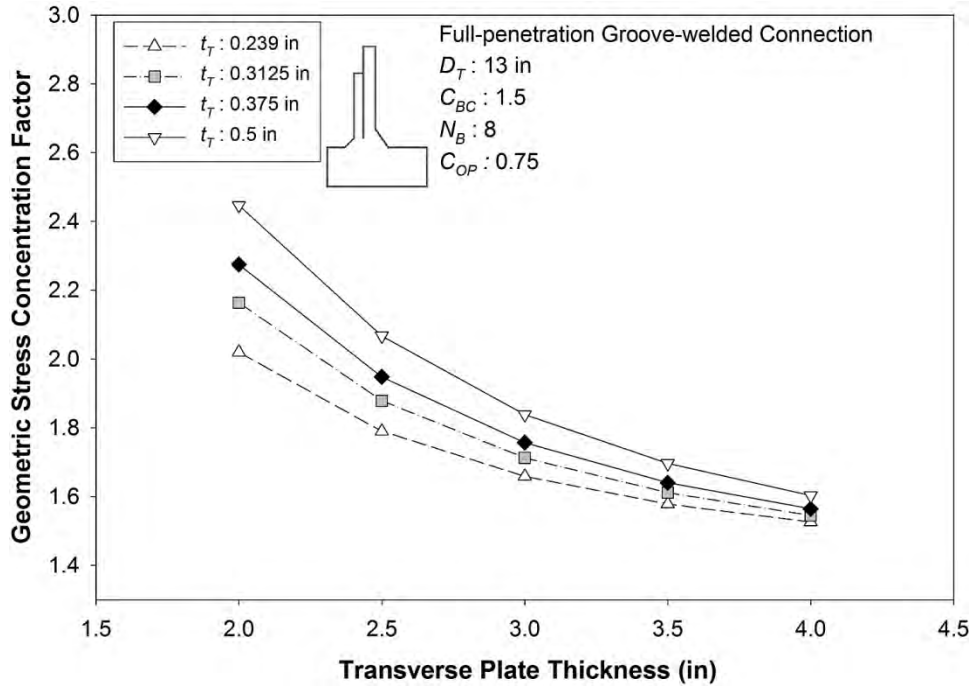
Figure 87 Effect of transverse plate thickness in unstiffened round tube-to-transverse plate groove-welded connection
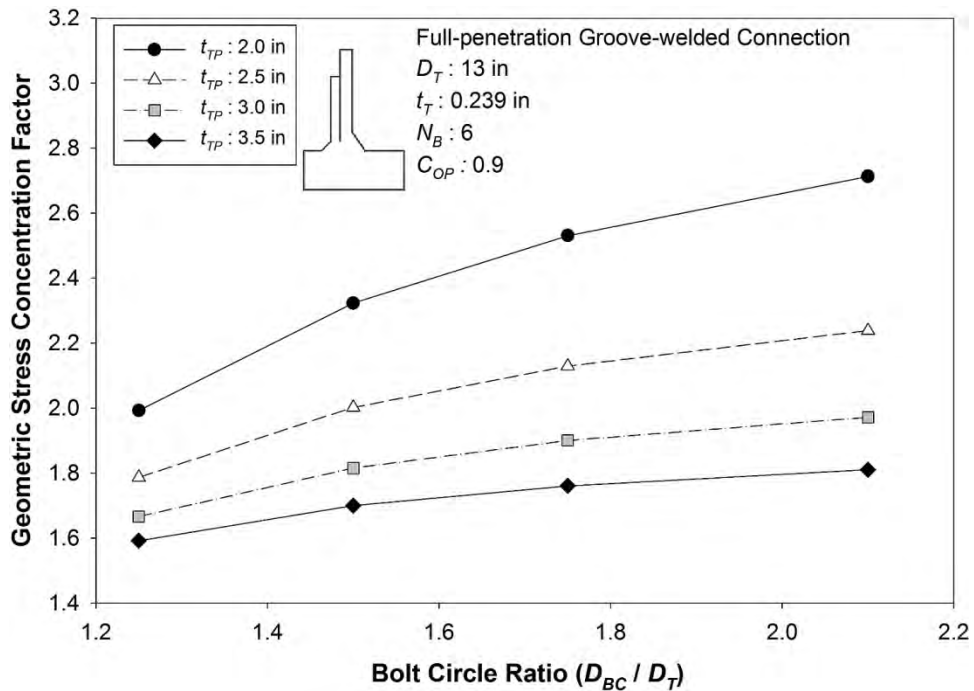
Figure 88 Effect of bolt circle ratio in unstiffened round tube-to-transverse plate groove-welded connection

117
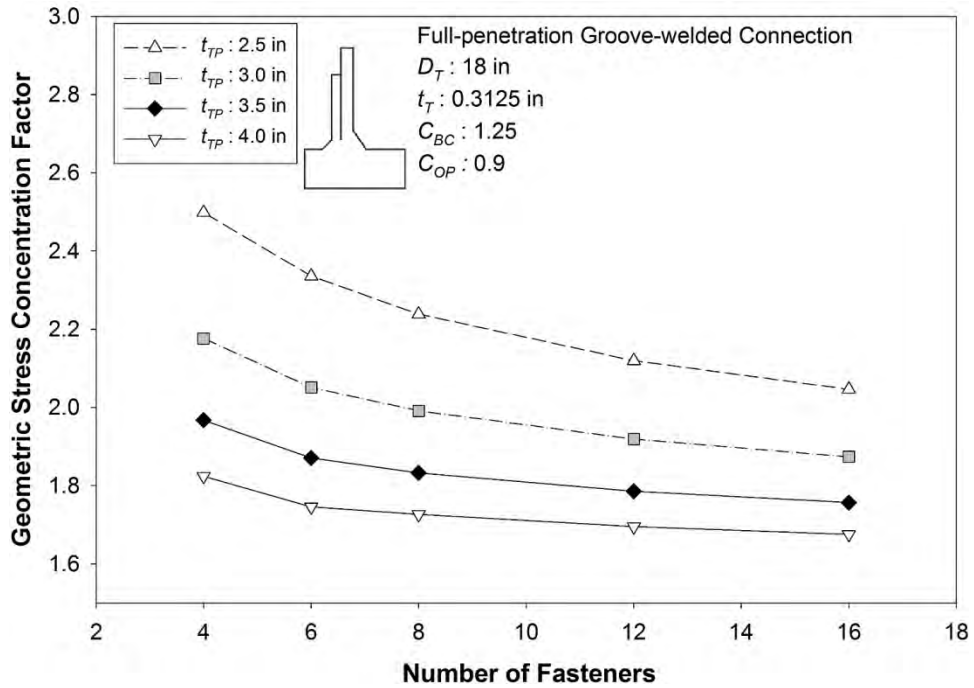
Figure 89 Effect of number of fasteners in unstiffened round tube-to-transverse plate groove-welded connection
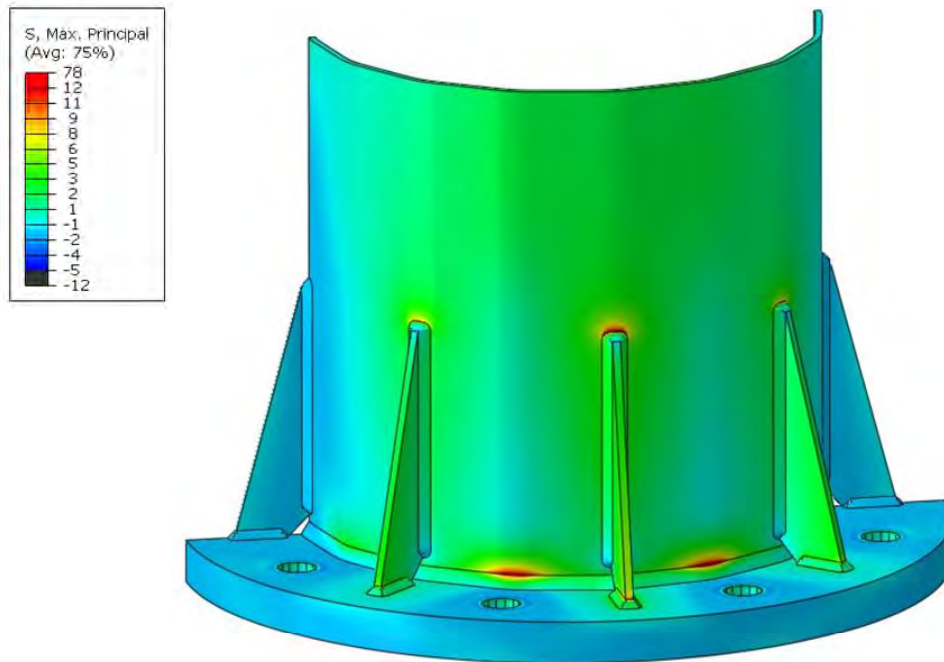
Figure 90 Typical contour of maximum principal stress in stiffened tube-to-transverse plate fillet-welded connections

118
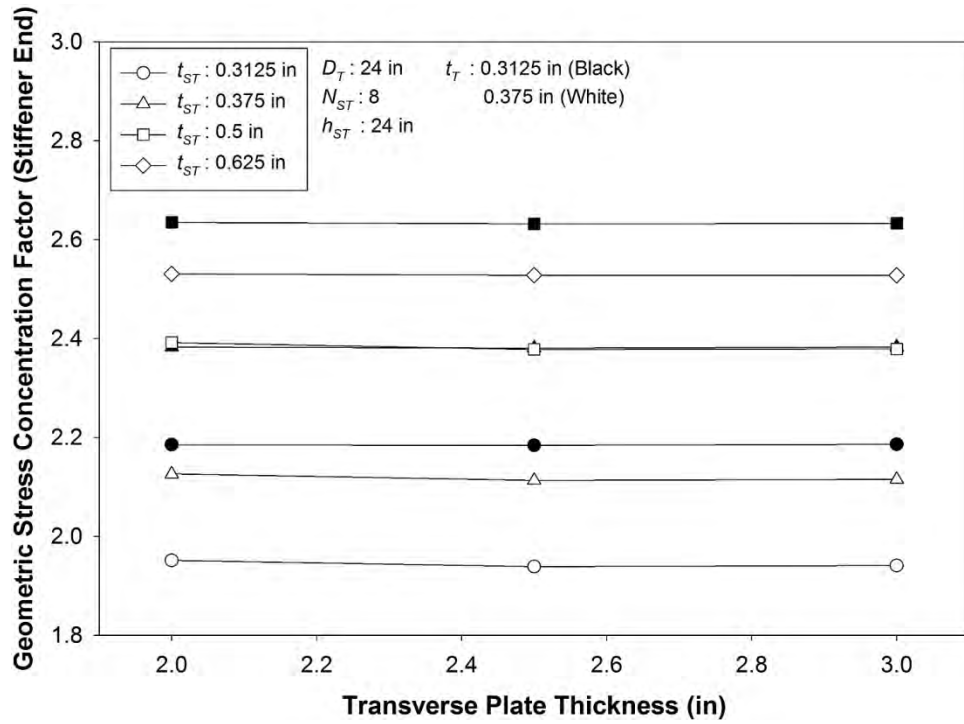
Figure 91 Effect of transverse plate thicknesses in stiffened fillet-welded tube-to-transverse plate connection
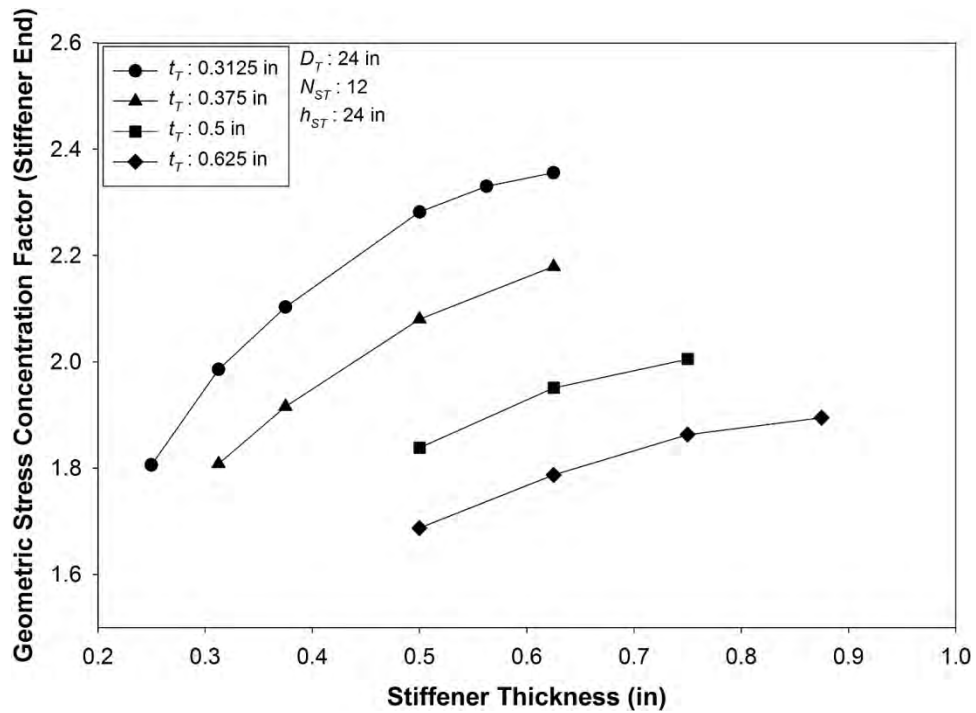
Figure 92 Effect of thicknesses of stiffeners in stiffened fillet-welded tube-to-transverse plate connection

119
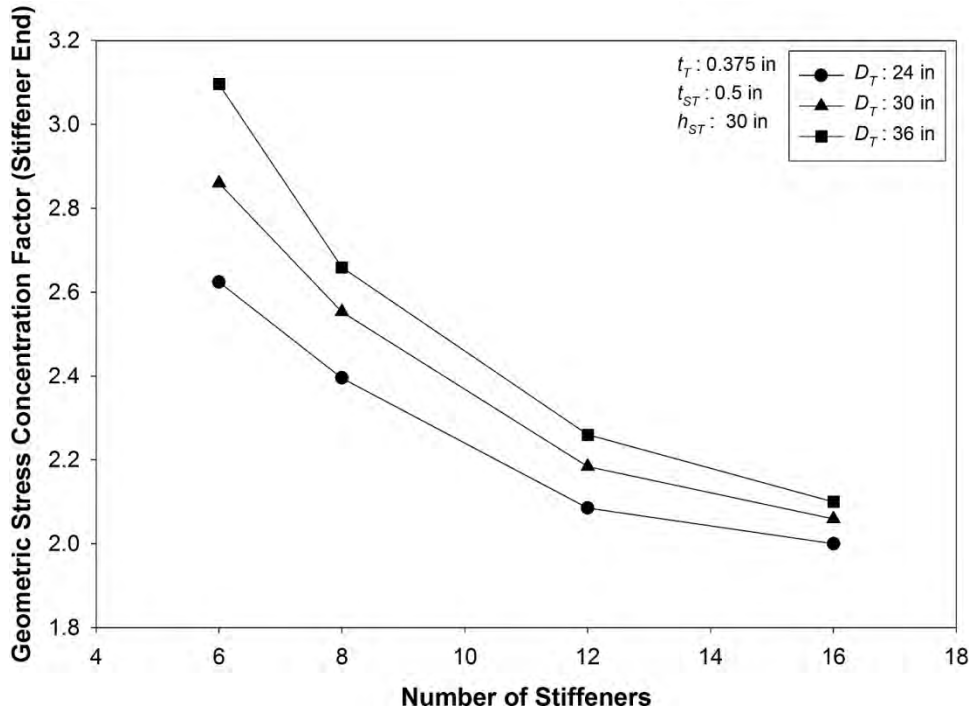
Figure 93 Effect of number of stiffeners in stiffened fillet-welded tube-to-transverse plate connection
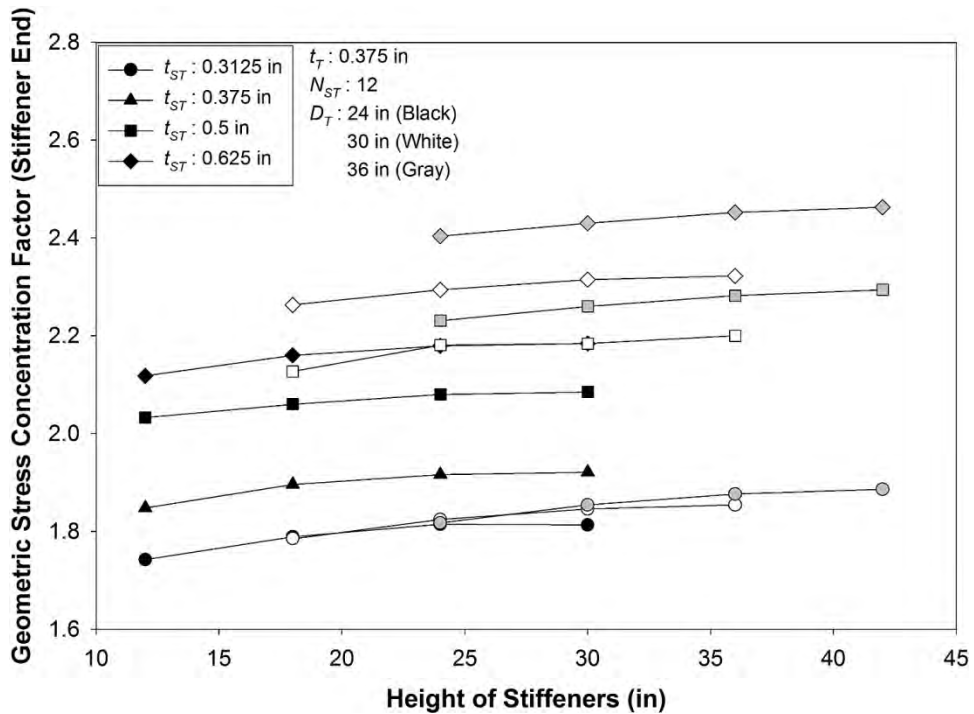
Figure 94 Effect of height of stiffeners in stiffened fillet-welded tube-to-transverse plate connection

120
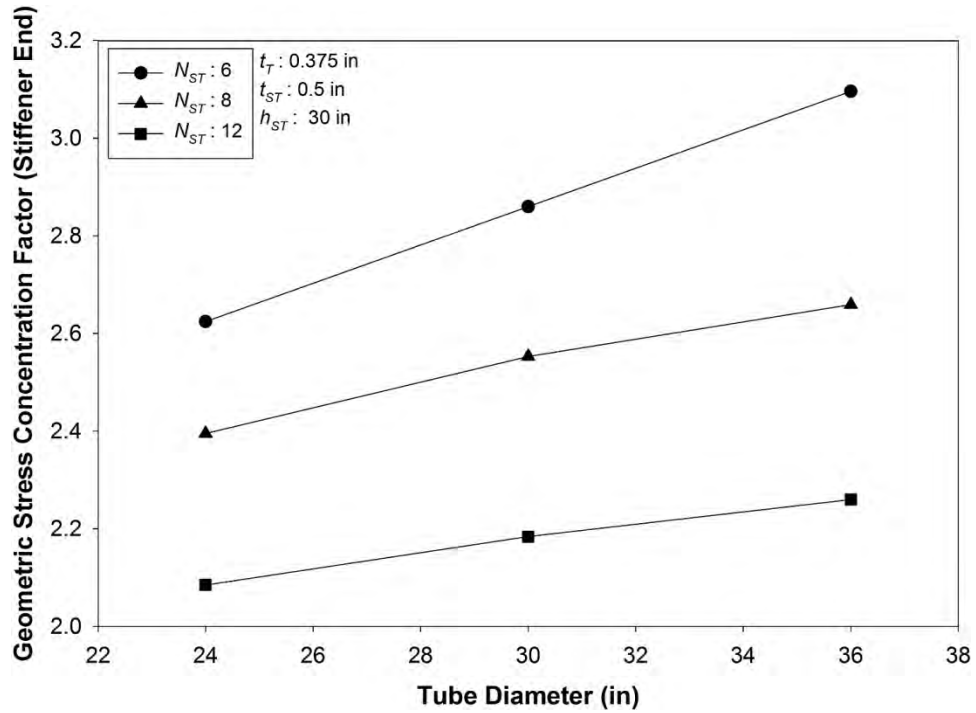
Figure 95 Effect of tube diameter in stiffened fillet-welded tube-to-transverse plate connection
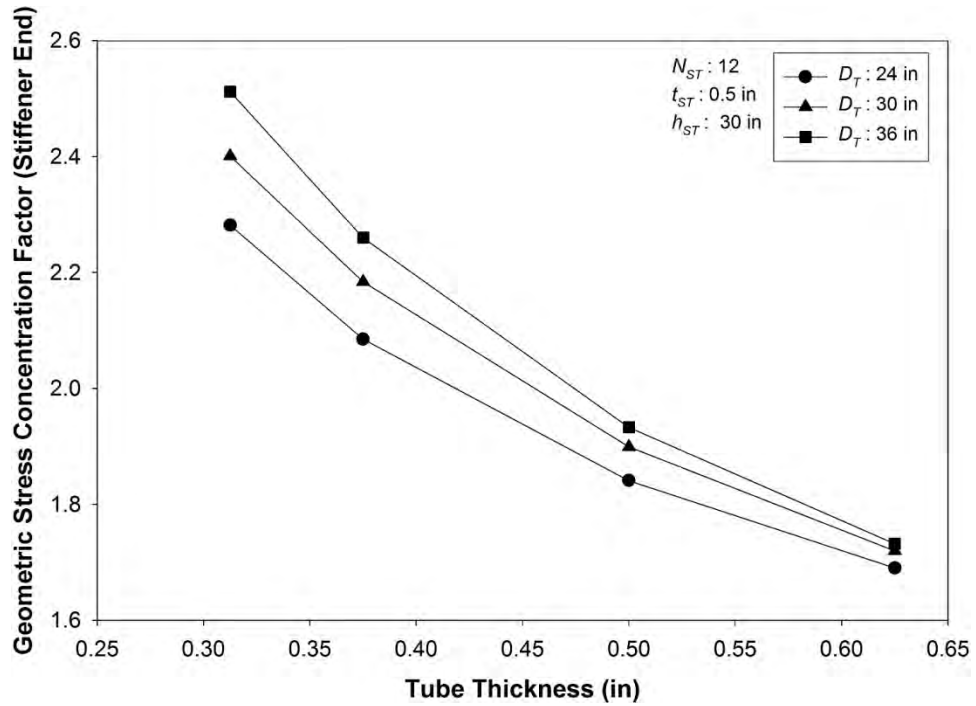
Figure 96 Effect of tube thickness in stiffened fillet-welded tube-to-transverse plate connection

121
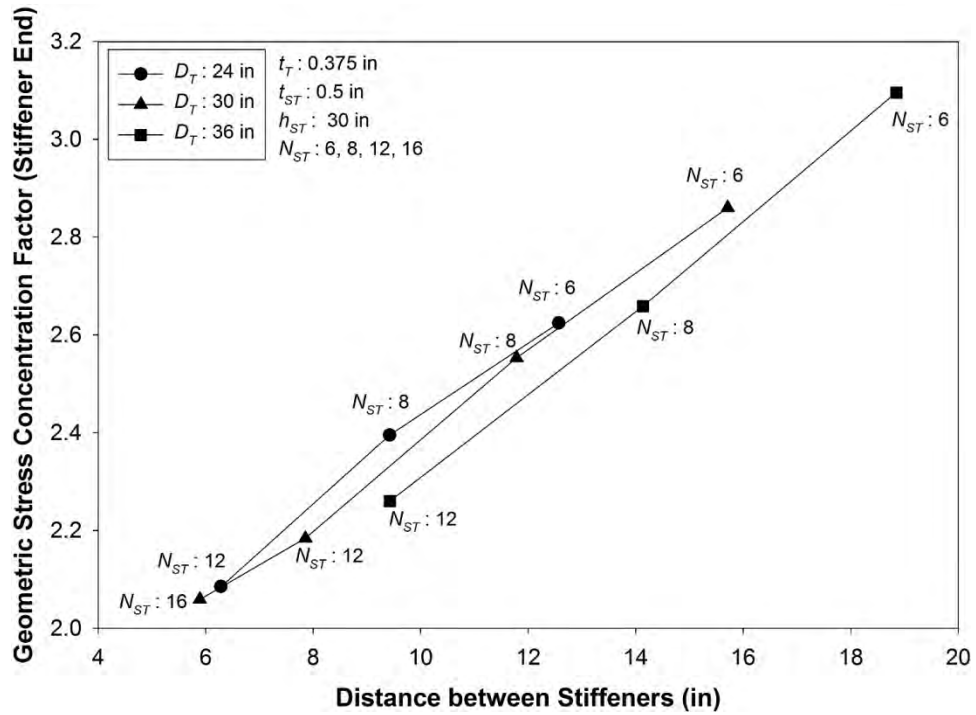
Figure 97 Effect of distance between stiffeners in stiffened fillet-welded tube-to-transverse plate connection
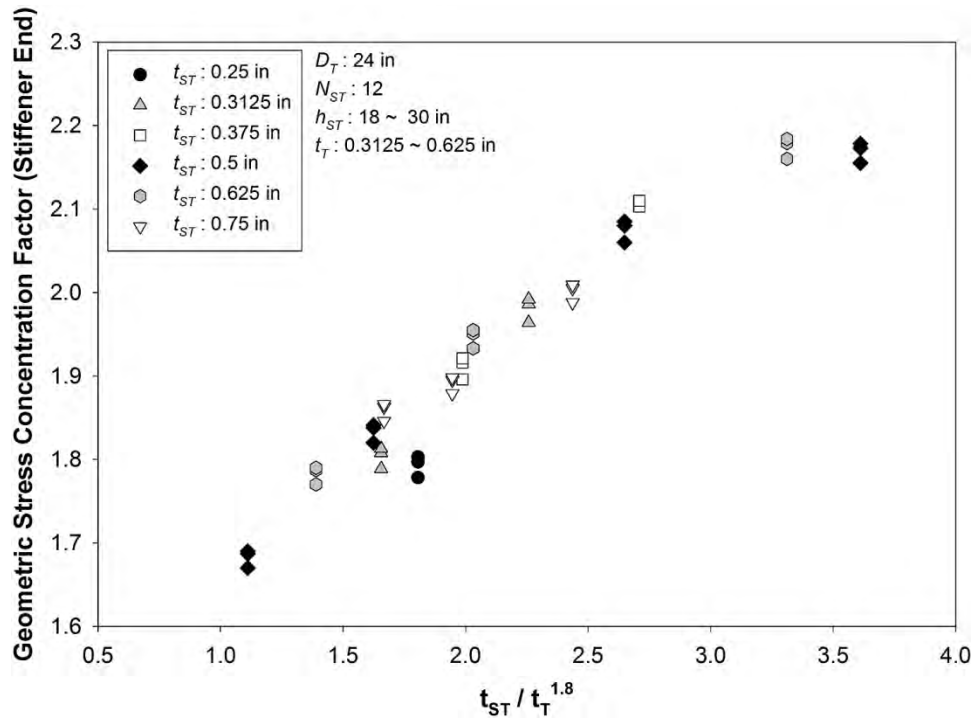
Figure 98 Effect of derived ratio of tube and stiffener thickness in stiffened fillet-welded tube-to-transverse plate connection

122
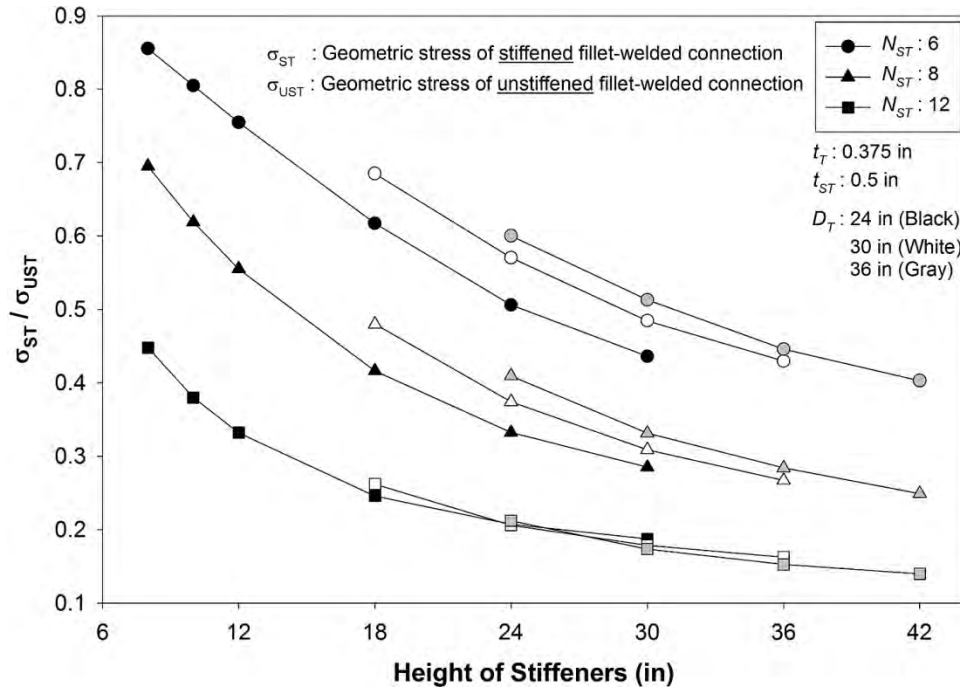
Figure 99 Effect of stiffener height on local stress ratio in stiffened fillet-welded tube-to-transverse plate connection
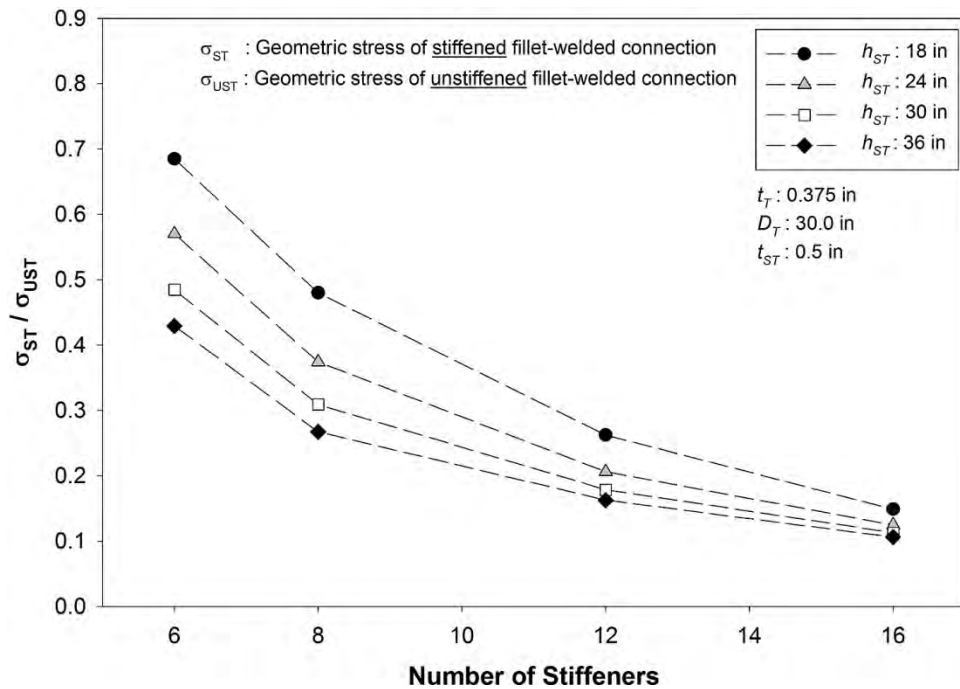
Figure 100 Effect of number of stiffeners on local stress ratio in stiffened fillet-welded tube-to-transverse plate connection

123
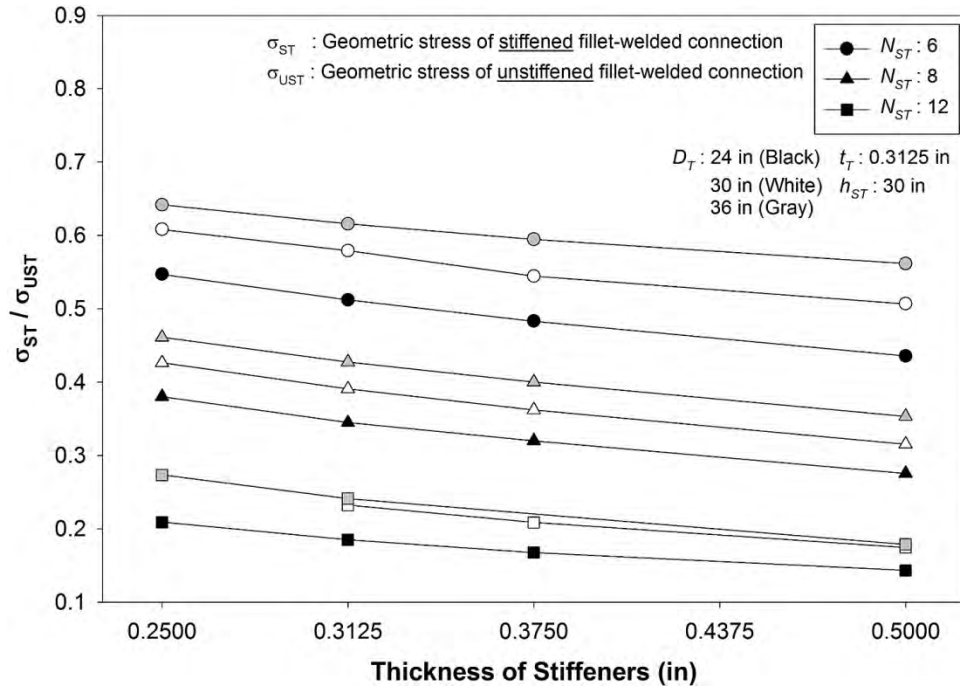
Figure 101 Effect of thickness of stiffener on local stress ratio in stiffened fillet-welded tube-to-transverse plate connection
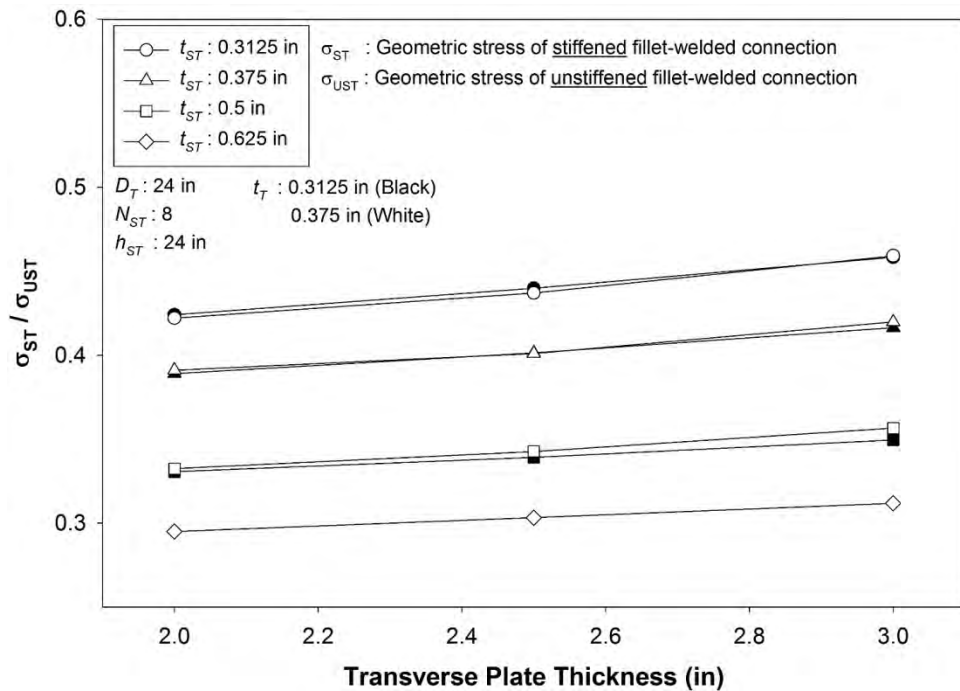
Figure 102 Effect of transverse plate thickness on local stress ratio in stiffened fillet-welded tube-to-transverse plate connection

124
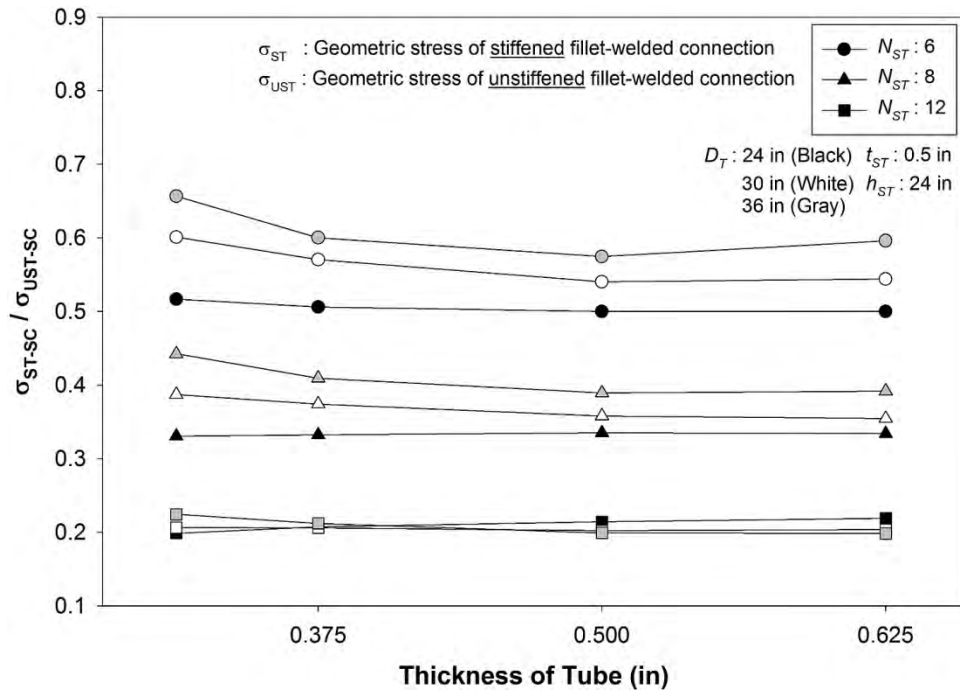
Figure 103 Effect of tube thickness on local stress ratio in stiffened fillet-welded tube-to-transverse plate connection
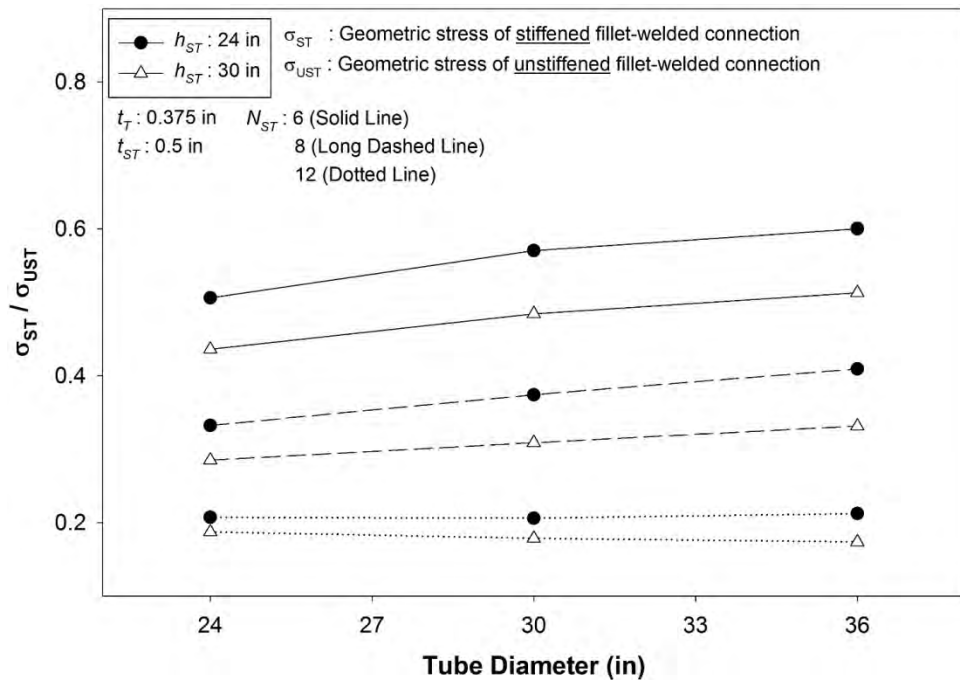
Figure 104 Effect of tube diameter on local stress ratio in stiffened fillet-welded tube-to-transverse plate connection

125
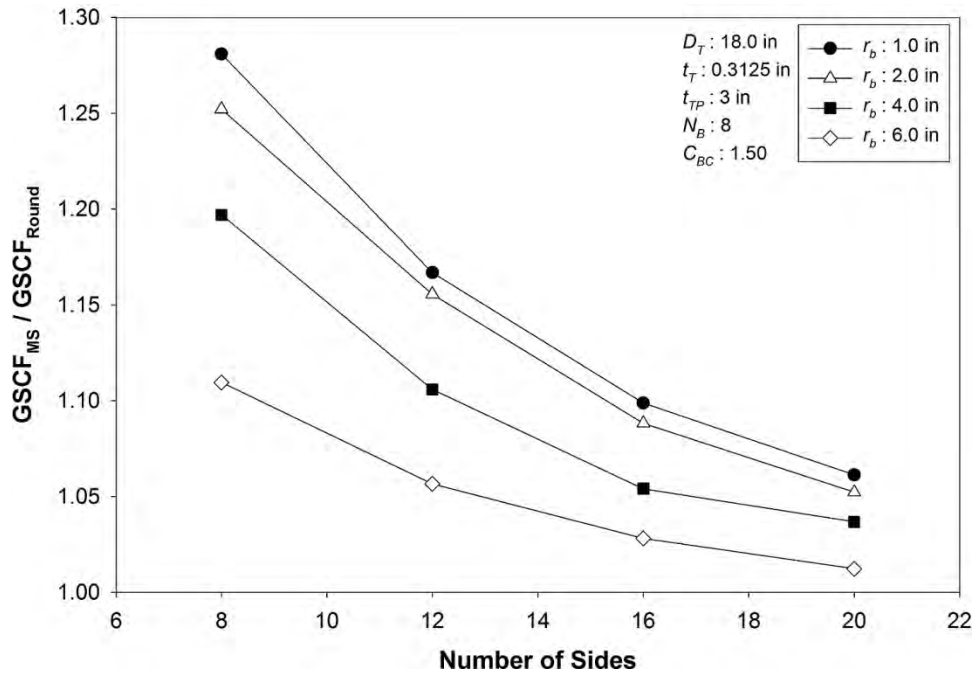
Figure 105 Effect of number of sides on local stress ratio in stiffened fillet-welded tube-to-transverse plate connection
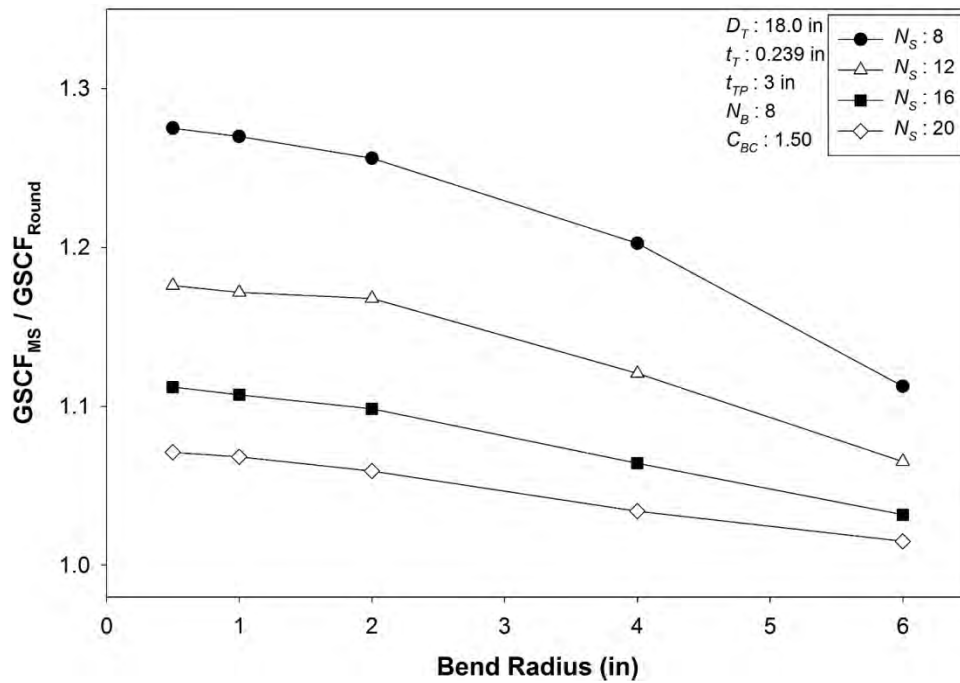
Figure 106 Effect of bend radius on local stress ratio in stiffened fillet-welded tube-to-transverse plate connection

126
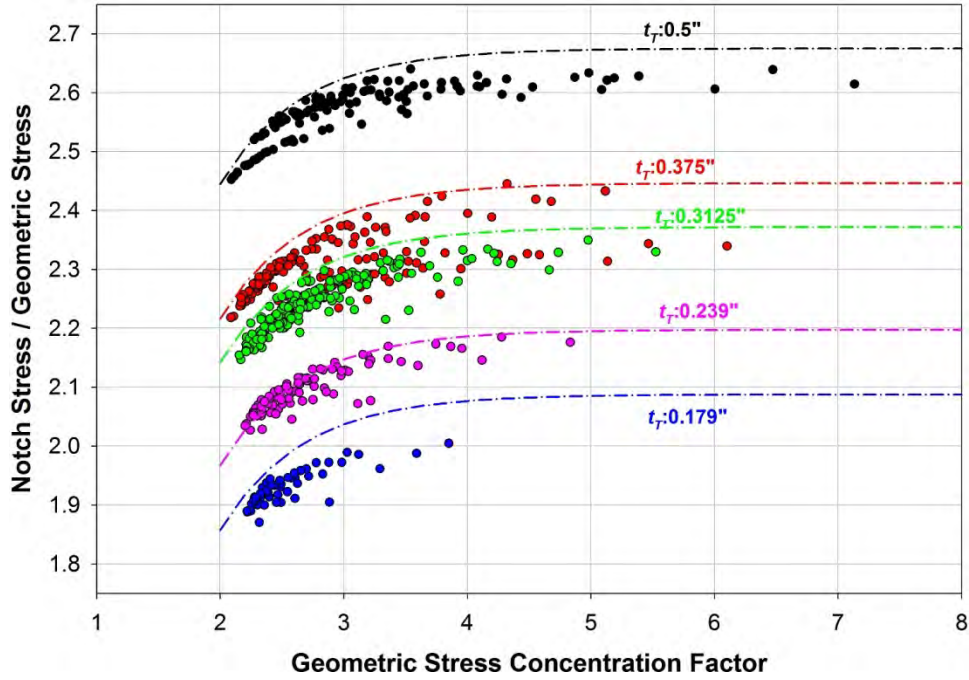
Figure 107 Relationship between normalized notch stress and GSCF
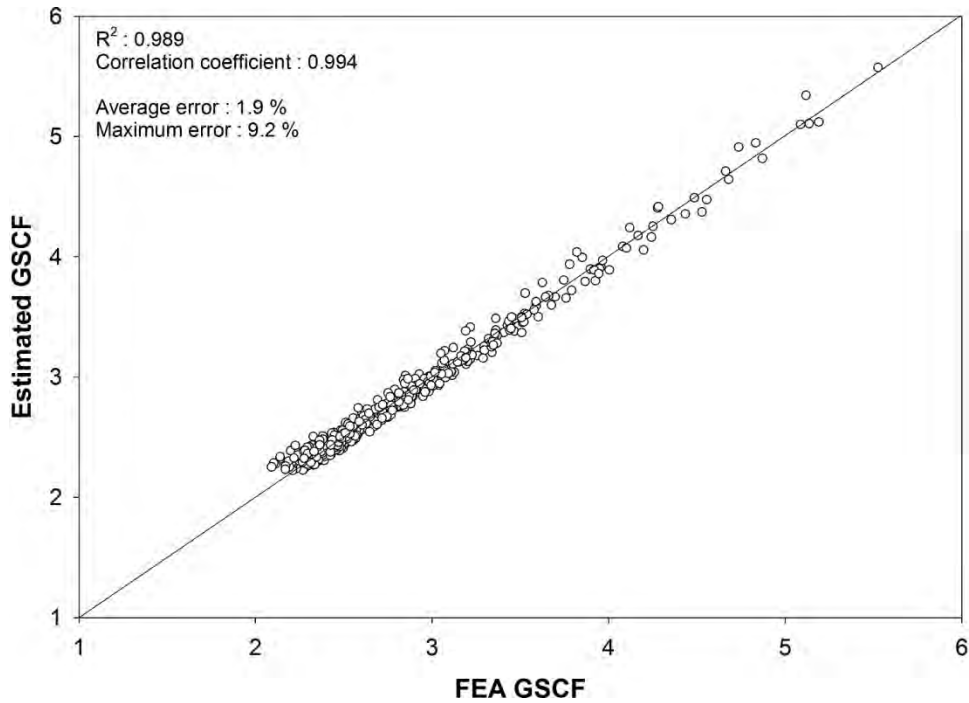
Figure 108Final regression results for round tube-to-transverse plate fillet-welded connection

127
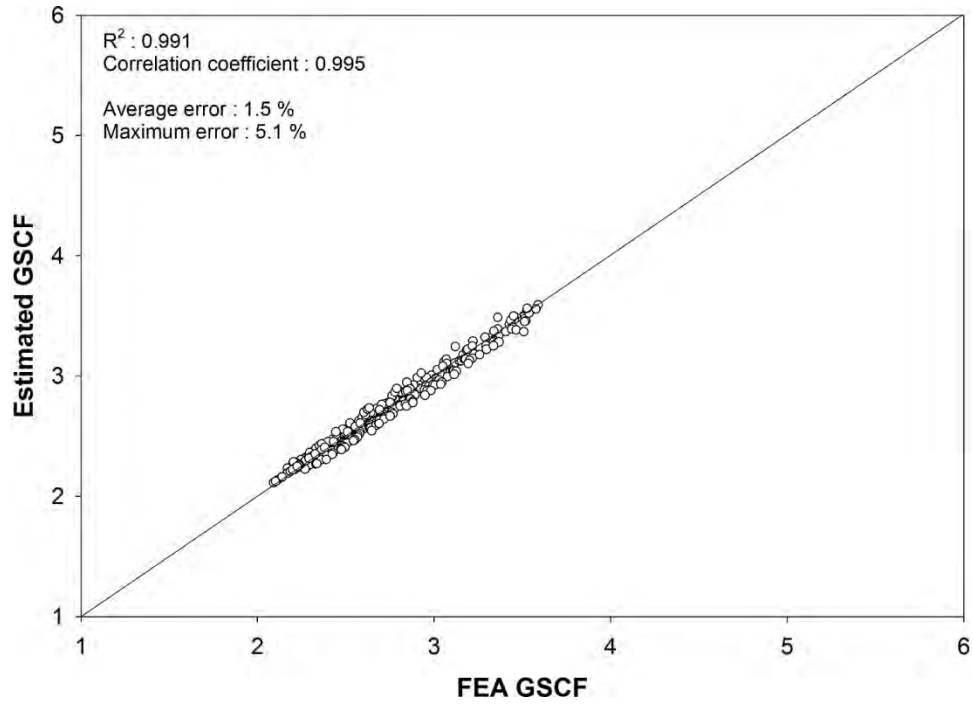
Figure 109Final regression results for round tube-to-transverse plate groove-welded connection
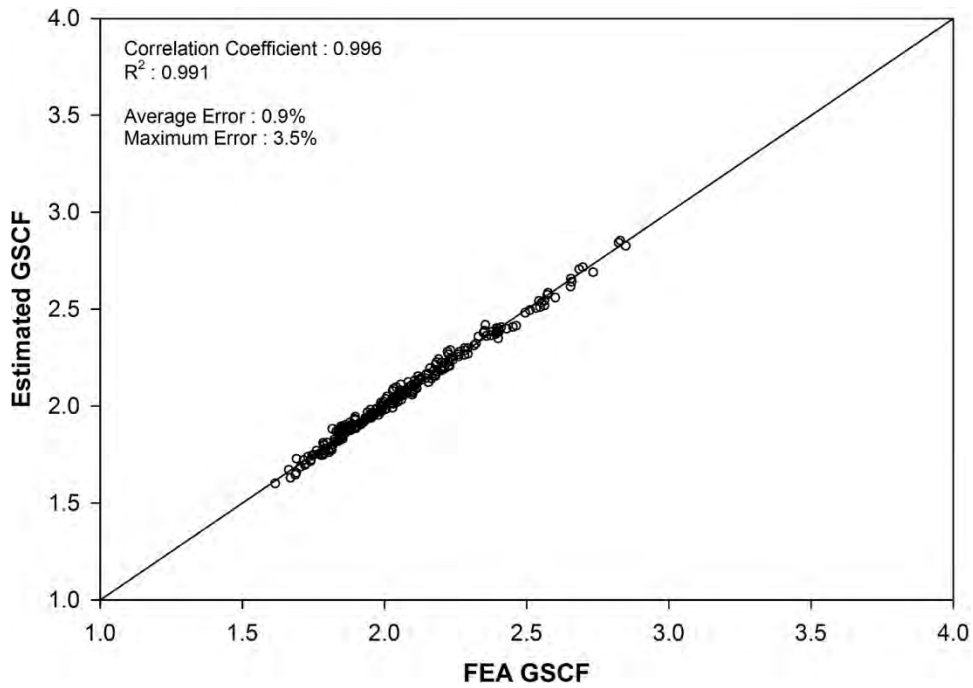
Figure 110Final regression results for stiffened tube-to-transverse plate fillet-welded connections at the stiffener termination on the tube wall

128
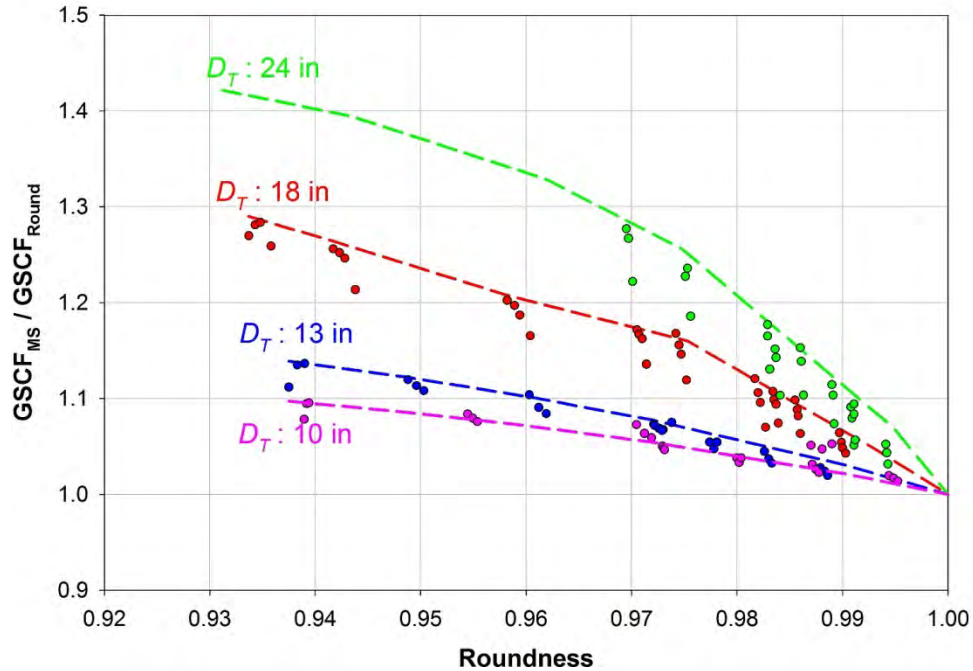
Figure 111 Variation in ratios of GSCFs in multi-sided and round tube-to-transverse plate connections with roundness for various tube diameters
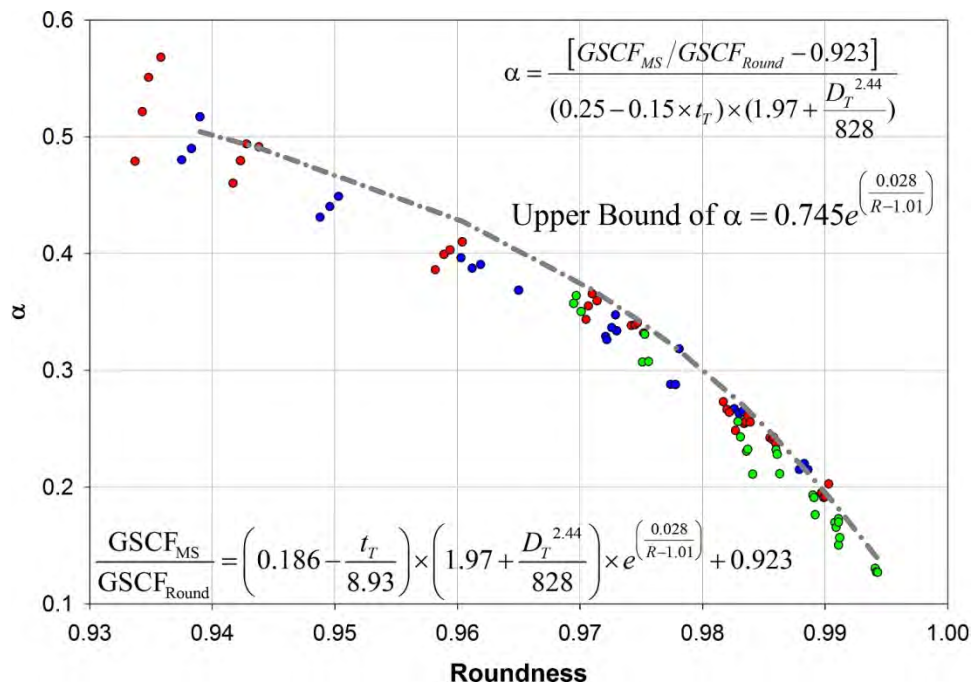
Figure 112 Variation of α with roundness

129
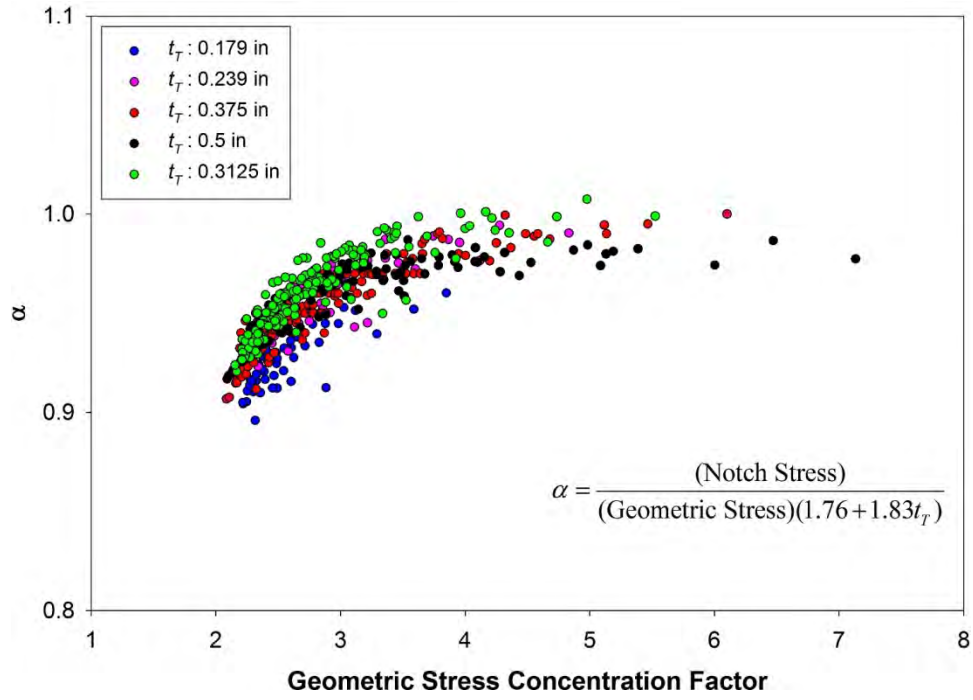
Figure 113 Variation of normalized ratio of notch stress and geometric stress with GSCF

130

Table 1 Details Identified for Investigation
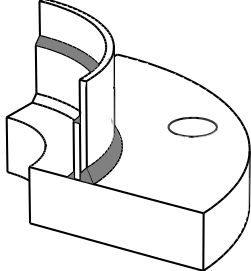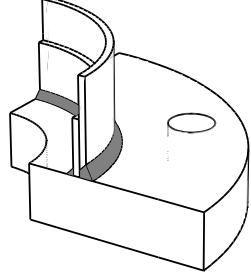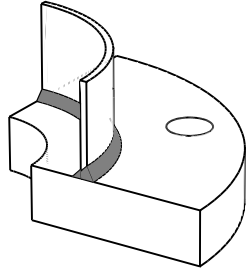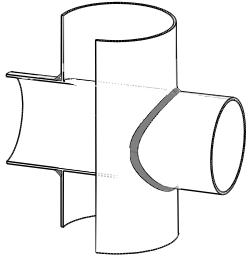
Detail ID	Detail Description	Illustrative Example
GROOVE-WELDED CONNECTIONS		
1	Full penetration groove-welded tube-to-transverse plate connection with a continuous fillet-weld around interior face of backing ring, and backing ring welded to the tube with continuous fillet-weld at top face of backing ring	
2	Full penetration groove-welded tube-to-transverse plate connection with a continuous fillet-weld around interior face of backing ring, and backing ring not welded to the tube	
3	Full penetration groove-welded tube-to-transverse plate connections welded from both sides with back-gouging (without backing ring).	
4	Partial penetration groove-welded mast-arm-to-column pass-through connections	

131

Table 1 Contd.
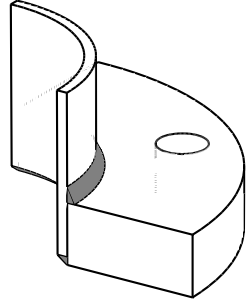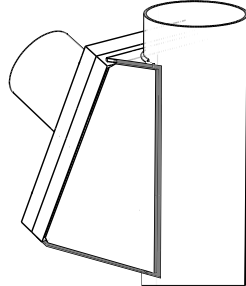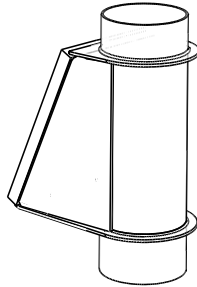
Detail ID	Detail Description	Illustrative Example
	FILLET-WELDED CONNECTIONS	
5	Fillet-welded tube-to-transverse plate connections	
6	Fillet-welded tube-to-rounded transverse plate connections	
7	Fillet-welded connections with one-sided welds normal to the direction of the applied stress	
8	Fillet-welded ring-stiffened box-to-tube connections	

132

Table 1 Contd.
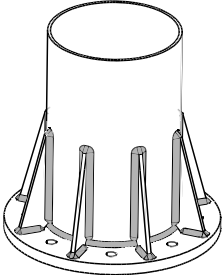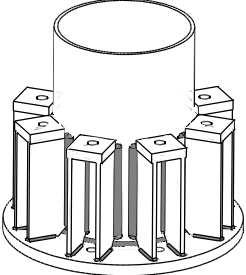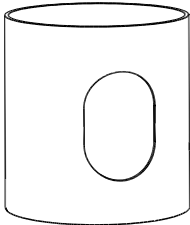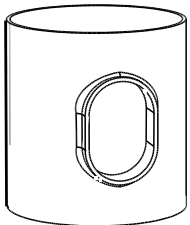
Detail ID	Detail Description	Illustrative Example
ATTACHMENTS		
9	Tube-to-transverse plate connections stiffened by longitudinal attachments with fillet-welds in which the tube is subjected to longitudinal loading and the welds are wrapped around the attachment termination	
10	Tube-to-transverse plate connections stiffened by longitudinal stool type attachments with fillet-welds in which the tube is subjected to longitudinal loading and the welds are wrapped around the attachment termination	
HOLES AND CUTOUTS		
11	Net section of un-reinforced holes and cutouts	
12	Reinforced holes and cutouts	

133

Table 2 Test Matrix

Specimen Type	S_{min} (ksi)	S_r			Section	Distribution of Detail Types#											
		H	L	CAFT		1	2	3	4	5	6	7	8	9	10	11	12
I	16	-	3	4	Round					x			x				x
II	16	-	3	-	Round	x						x					x
III	16	3	3	4	Round		x						x			x	
IV-A	16	-	-	2	Round		x					x					
IV-B	R	-	-	2	Round		x					x					x
V	18	-	2	2	Round		x				x						
VI	10	3	3	4	Round		x		x								
VII	16	-	3	4	MS					x		x					x
IX	R	3	3	4	MS										x		
X	R	-	3	-	MS					x							x
XI	R	3	3	4	MS	x											x
XII	R	3	3	4	MS									x			
Retro	R	-	-	2	MS			x								x	
Total*		15	29	34													

\# For detail type identification refer Tables, Figures, and Sketches

* Total does not include Retrofitted specimens

All specimens are galvanized

Legend:

S_r	Stress Range
S_{min}	Minimum Stress
H	High Level
L	Low Level
CAFT	Constant Amplitude Fatigue Threshold
Round	Rounded Cross Section
MS	Multisided Cross Section
Retro	Retrofitted Detail
R	–S_r/2 due to reversal loading

[shaded box] No tests planned

134

135

Table 3 Distribution of Round Specimens and Details
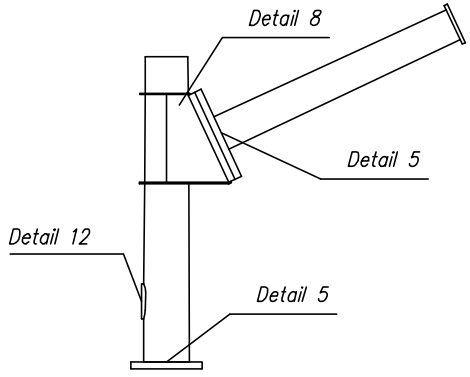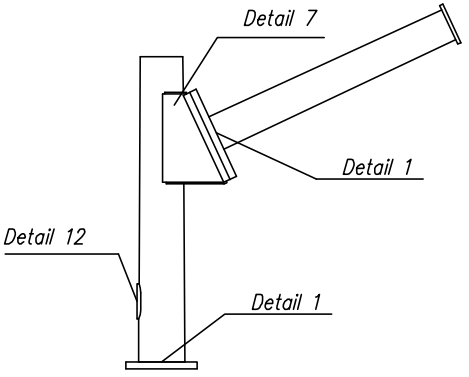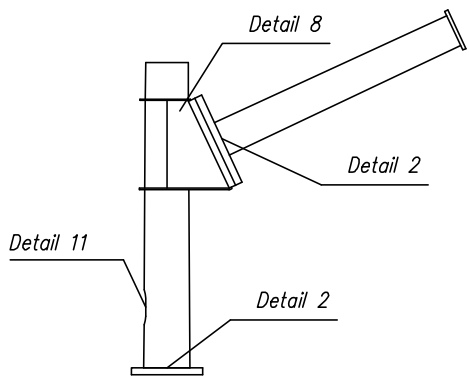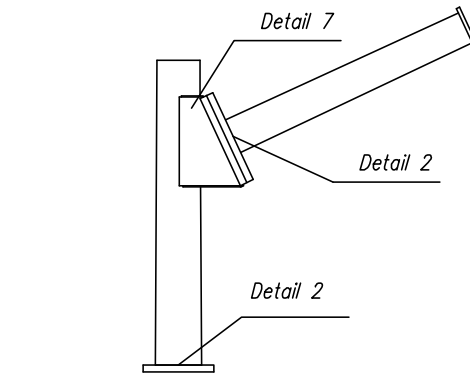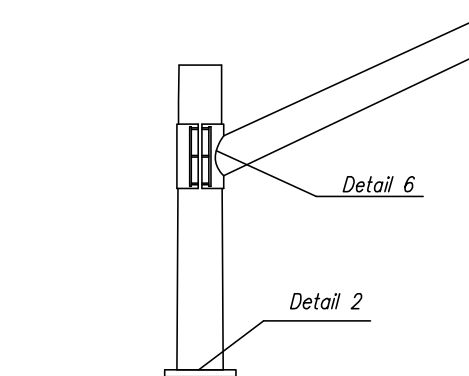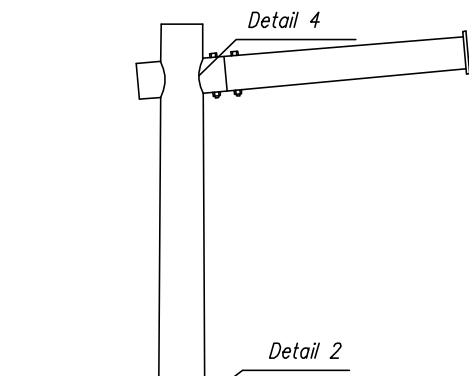
Table 4 Distribution of Multi-sided Specimens and Details
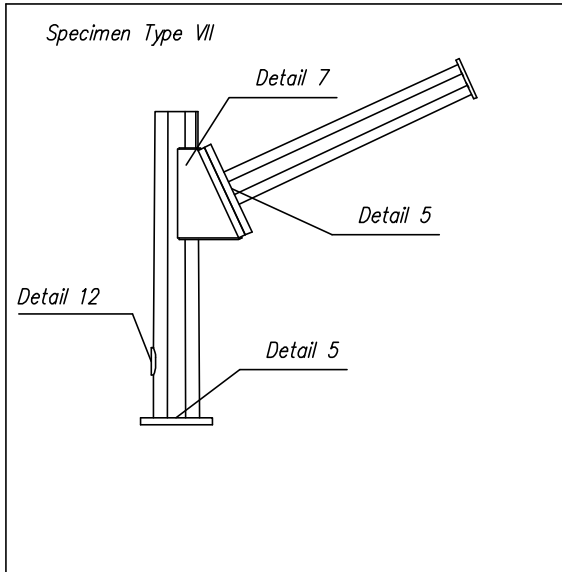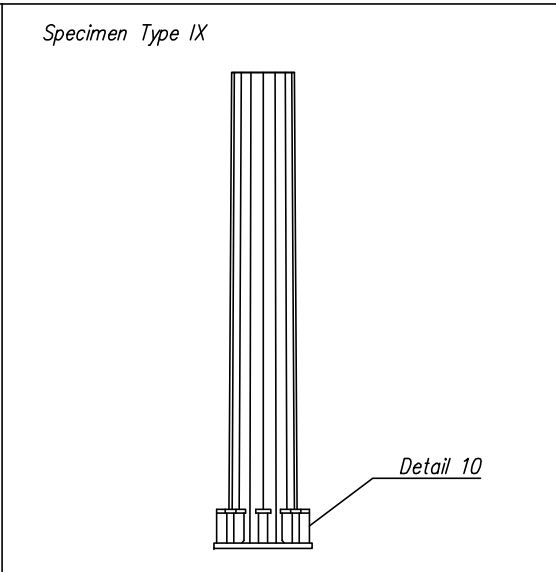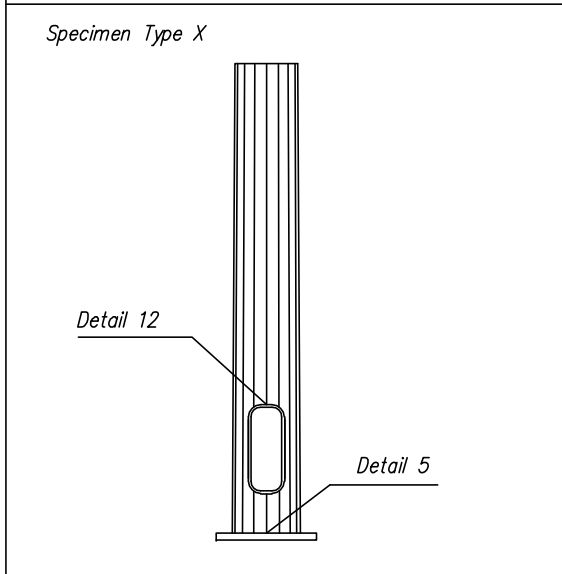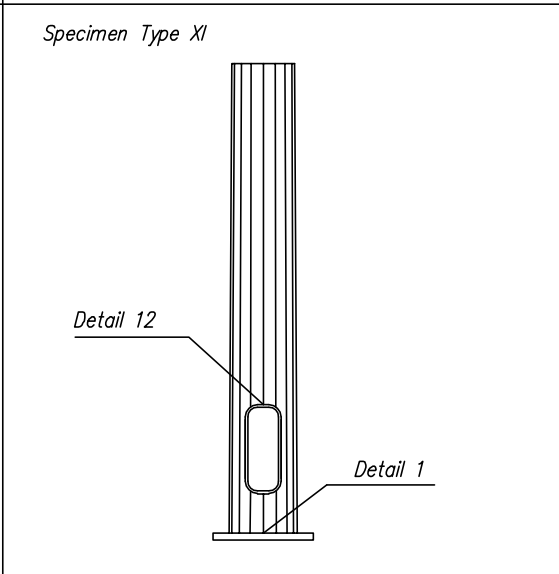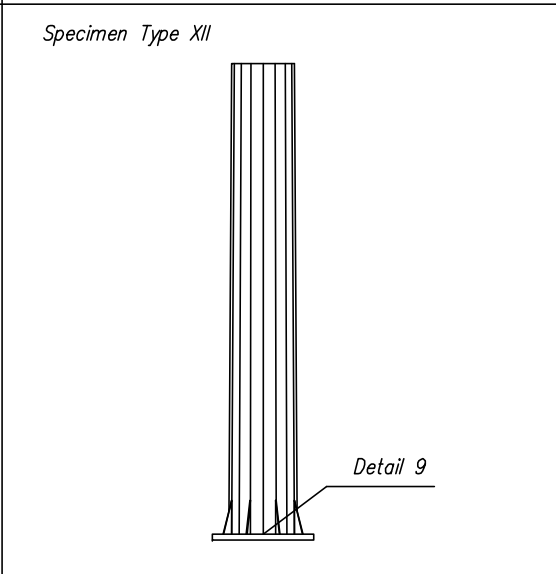
Specimen Type VII

Detail 7

Detail 5

Detail 12

Detail 5

Specimen Type VIII

NOT TESTED

Specimen Type IX

Detail 10

Specimen Type X

Detail 12

Detail 5

Specimen Type XI

Detail 12

Detail 1

Specimen Type XII

Detail 9

137

Table 5 Summary of Fatigue Test Results

Specimen Type	Specimen ID	Detail	Nominal Stress Parameters S_{min} (ksi)	S_r (ksi)	Description of Crack Location and Origin	First Observation Length (in.)	# of Cycles	Crack Length at Half of Diameter Length (in.)	# of Cycles	Final Length (in.)	# of Cycles	Comments
I	1	Arm Base	15.9	12.0	At tube-to-end plate fillet weld toe on the tube wall	9.00	.18E+06	5.00	.18E+06[a]	9.00	.18E+06	Testing continued with Replacement Arms II-R-1 & II-R-3
		Handhole	9.1	7.0	From the root of hand hole frame to pole fillet weld - bottom right corner[d]	0.50	1.78E+06			8.00	2.72E+06	Hole drilled for continuing test; Crack reappeared from arrest hole; Crack terminated the fatigue test
		Pole Base	8.8	6.8								Did not crack
		Ring Stiffened Box Connection	9.8	7.5								Did not crack
	2	Arm Base	15.9	12.0	At tube-to-end plate fillet weld toe on the tube wall	2.25+1.88[b]	.37E+06	5.00	.41E+06	5.88	.41E+06	Testing continue with Replacement Arm II-R-2 & II-R_3
		Handhole	9.1	7.0	From the root of hand hole frame to pole fillet weld - bottom right corner[d]	0.75	1.55E+06			4.38	3.77E+06	Hole drilled for continuing test; Crack reappeared from arrest hole;
					From the root of hand hole frame to pole fillet weld - top right corner[d]	0.25	2.10E+06			1.75	3.77E+06	Hole drilled for continuing test; Crack reappeared from arrest hole;
		Pole Base	8.8	6.8								Did not crack
		Ring Stiffened Box Connection	9.8	7.5								Did not crack
	3	Arm Base	15.9	12.0	At tube-to-end plate fillet weld toe on the tube wall	1.88	1.26E+06	5.00	1.67E+06	6.00	1.77E+06	Crack terminated the fatigue test
		Handhole	9.1	7.0	From the root of hand hole frame to pole fillet weld - bottom right corner[d]	1.00	2.47E+06			3.00	3.27E+06	Continued with special arm. Hole drilled for continuing test; Crack reappeared from arrest hole;
		Pole Base	8.8	6.8								Did not crack
		Ring Stiffened Box Connection	9.8	7.5								Did not crack
	4	Arm Base	15.9	7.0	At tube-to-end plate fillet weld toe on the tube wall	2.75	2.30E+06	5.00	2.73E+06	5.13	2.73E+06	Testing continued with special arm
		Handhole	9.1	4.1								Did not crack
		Pole Base	8.8	4.0								Run-out at 20.00E+06 cycles
		Ring Stiffened Box Connection	9.8	4.4								Did not crack
	4 Re-run 1	Handhole	9.1	5.8	From the root of hand hole frame to pole fillet weld - top left corner[d]	1.25	7.40E+06	1.25	7.40E+06	1.25	7.40E+06	Continued with special arm. Hole drilled for continuing test. Crack reappeared from arrerst hole. Test terminated
		Pole Base	8.8	5.7								
		Ring Stiffened Box Connection	9.8	6.3								

Table 5 *Continued*

Specimen Type	Specimen ID	Detail	Nominal Stress Parameters S_min (ksi)	S_r (ksi)	Description of Crack Location and Origin	First Observation Length (in.)	# of Cycles	Crack Length at Half of Diameter Length (in.)	# of Cycles	Final Length (in.)	# of Cycles	Comments
I	5	Arm Base	15.9	7.0	At tube-to-end plate fillet weld toe on the tube wall	0.38	3.11E+06	5.00	5.98E+06	5.38	5.98E+06	Testing continued with special arm
		Handhole	9.1	4.1								Did not crack
		Pole Base	8.8	4.0								Run-out at 20.00E+06 cycles
		Ring Stiffened Box Connection	9.8	4.4								Did not crack
	5 Re-run 1	Handhole	9.1	5.8								Did not crack
		Pole Base	8.8	5.7	At tube-to-end plate fillet weld toe on the tube wall	0.88+0.38	1.77E+06	6.50	3.54E+06	7.13	3.64E+06	Crack terminated the fatigue test
		Ring Stiffened Box Connection	9.8	6.3								Did not crack
	6	Arm Base	15.9	4.5								Run-out at 20.00E+06 cycles
		Handhole	9.1	2.6								Did not crack
		Pole Base	8.8	2.6								Did not crack
		Ring Stiffened Box Connection	9.8	2.8								Did not crack
	6 Re-run 1	Arm Base	15.9	7.0	At tube-to-end plate fillet weld toe on the tube wall	1.00	1.40E+06	5.00	2.13E+06	5.75	2.13E+06	Testing continued with special arm.
		Handhole	9.1	4.1	From the root of hand hole frame to pole fillet weld - top left corner[d)]	1.25	20.00E+06			1.25	20.00E+06	Hole drilled for continuing test
		Pole Base	8.8	4.0								Run-out at 20.00E+06 cycles
		Ring Stiffened Box Connection	9.8	4.4								Did not crack
	6 Re-run 2	Handhole	9.1	5.8						2.00	1.04E+06	Crack reappeared from arrerst hole. Test terminated
		Pole Base	8.8	5.7								
		Ring Stiffened Box Connection	9.8	6.3								
	7	Arm Base	15.9	4.5								Run-out at 20.00E+06 cycles
		Handhole	9.1	2.6								Did not crack
		Pole Base	8.8	2.6								Did not crack
		Ring Stiffened Box Connection	9.8	2.8								Did not crack

138

Table 5 *Continued*

Specimen Type	Specimen ID	Detail	S_{min} (ksi)	S_r (ksi)	Description of Crack Location and Origin	First Observation Length (in.)	# of Cycles	Half of Diameter Length (in.)	# of Cycles	Final Length (in.)	# of Cycles	Comments
I	7 Re-run 1	Arm Base	15.9	7.0	At tube-to-end plate fillet weld toe on the tube wall	0.75	1.84E+06	5.00	2.87E+06	5.25	2.87E+06	Testing continued with special arm
		Handhole	9.1	4.1								Did not crack
		Pole Base	8.8	4.0	At tube-to-end plate fillet weld toe on the tube wall	0.44	3.05E+06	6.50	8.20E+06	6.81	8.32E+06	Crack terminated the fatigue test
		Ring Stiffened Box Connection	9.8	4.4								Did not crack
II	1	Arm Base	15.5	11.9	From the toe of seal weld termination on the tube wall at the top of backing ring	1.88	1.61E+06	5.00	1.65E+06	10.00	1.68E+06	Testing continued with Replacement Arm II-R-1
		Handhole	9.1	7.0	From the root of hand hole frame to pole fillet weld - top right corner[d]	1.00	1.72E+06			2.50	2.39E+06	Hole drilled for continuing test; Crack reappeared from arrest hole
		Pole Base	9.0	6.9	At tube-to-end plate full-pen weld toe on the tube wall	4.00	1.98E+06	6.50	2.32E+06	7.00	2.39E+06	Crack terminated the fatigue test
		Gussetted Box Connection	2.5	1.9								Did not crack
	2	Arm Base	12.9	9.9	At tube-to-end plate full-pen weld toe on the tube wall	2.00	1.32E+06			4.50	2.03E+06	
			15.5	11.9	From the toe of seal weld termination on the tube wall at the top of backing ring	1.50	1.88E+06			2.38	2.03E+06	
		Handhole	9.1	7.0	From the root of hand hole frame to pole fillet weld - bottom right corner[d]	5.00	2.03E+06			5.00	2.03E+06	Crack terminated the fatigue test
		Pole Base	9.0	6.9								Did not crack
		Gussetted Box Connection	2.5	1.9								Did not crack
	3	Arm Base	12.9	9.9	At tube-to-end plate full-pen weld toe on the tube wall	1.00	1.41E+06			2.25	2.08E+06	Testing continued with Replacement Arm II-R-2
			15.5	11.9	From the toe of seal weld termination on the tube wall at the top of backing ring	5.00	2.08E+06	5.00	2.08E+06	5.00	2.08E+06	
		Handhole	9.1	7.0	From the root of hand hole frame to pole fillet weld - top right corner[d]	0.50	2.21E+06			7.25	2.97E+06	Hole drilled for continuing test; Crack reappeared from arrest
			9.1	7.0	From the root of hand hole frame to pole fillet weld - bottom right corner[d]	0.25	2.57E+06			4.50	2.97E+06	
		Pole Base	9.0	6.9								Did not crack
		Gussetted Box Connection	2.5	1.9								Did not crack
Replaced Arms Type II-R	1	Arm Base	12.9	9.9	At tube-to-end plate full-pen weld toe on the tube wall	1.25	1.17E+06			3.38	1.81E+06	Failed
			15.5	11.9	From the toe of seal weld termination on the tube wall at the top of backing ring	2.00	1.81E+06			2.00	1.81E+06	
	2	Arm Base	12.9	9.9	At tube-to-end plate full-pen weld toe on the tube wall	1.00	1.29E+06	5.00	3.49E+06	5.25	3.49E+06	Failed
	3	Arm Base	12.9	9.9	At tube-to-end plate full-pen weld toe on the tube wall	1.50	1.49E+06			2.50	2.21E+06	Failed (terminated the fatigue test of specimen I-2)
			15.5	11.9	From the toe of seal weld termination on the tube wall at the top of backing ring	0.50	1.55E+06	5.00	2.21E+06	6.75	2.21E+06	

Table 5 *Continued*

Specimen Type	Specimen ID	Detail	Nominal Stress Parameters		Description of Crack Location and Origin	First Observation		Crack Length at Half of Diameter		Final		Comments
			S_{min} (ksi)	S_r (ksi)		Length (in.)	# of Cycles	Length (in.)	# of Cycles	Length (in.)	# of Cycles	
III	1	Arm Base	16.2	12.0	At tube-to-end plate full-pen weld toe on the tube wall	1.50	.98E+06	5.00	1.36E+06	5.75	1.43E+06	Testing continued with special arm
		Handhole	9.7	6.8								
		Pole Base	9.3	6.5								Run-out at 9.42E+06 cycles
		Ring Stiffened Box Connection	10.0	7.0								
	1 Re-run 1	Handhole	9.7	10.5	Right top corner[d]	0.38	.94E+06			3.50	1.00E+06	Hole drilled to continue test; Crack reappeared from arrest. Test terminated
		Pole Base	9.3	10.0								
		Ring Stiffened Box Connection	10.0	10.8								
	2	Arm Base	16.2	12.0	At tube-to-end plate full-pen weld toe on the tube wall	1.06	1.86E+06	5.00	5.04E+06	5.06	5.09E+06	Testing continued with special arm
		Handhole	9.7	6.8								
		Pole Base	9.3	6.5								Run-out at 9.42E+06 cycles
		Ring Stiffened Box Connection	10.0	7.0								
	2 Re-run 1	Handhole	9.7	10.5								
		Pole Base	9.3	10.0								Run-out at 8.16E+06 cycles
		Ring Stiffened Box Connection	10.0	10.8								
	2 Re-run 2	Handhole	9.7	12.6	Left bottom corner[d]	5.63	.58E+06			5.63	.58E+06	
		Pole Base	9.3	12.0								Crack terminated fatigue test
		Ring Stiffened Box Connection	10.0	12.9								
	3	Arm Base	16.2	12.0	At tube-to-end plate full-pen weld toe on the tube wall	0.63	1.25E+06	5.00	2.05E+06	5.13	2.20E+06	Testing continued with special arm
		Handhole	9.7	6.8								
		Pole Base	9.3	6.5								Run-out at 9.42E+06 cycles
		Ring Stiffened Box Connection	10.0	7.0								

141

Table 5 *Continued*

Specimen Type	Specimen ID	Detail	Nominal Stress Parameters		Description of Crack Location and Origin	First Observation		Crack Length at Half of Diameter		Final		Comments
			S_{min} (ksi)	S_r (ksi)		Length (in.)	# of Cycles	Length (in.)	# of Cycles	Length (in.)	# of Cycles	
III	3 Re-run 1	Handhole	9.7	10.5	Left top corner[d]	5.50	.37E+06			5.50	.37E+06	
			9.7	10.5	Right bottom corner[d]	3.50	.37E+06			3.50	.37E+06	Crack terminated fatigue test
		Pole Base	9.3	10.0								
		Ring Stiffened Box Connection	10.0	10.8								
	4	Arm Base	16.2	7.0								Run-out at 14.70E+06 cycles
		Handhole	9.7	4.0								Did not crack
		Pole Base	9.3	3.8								Did not crack
		Ring Stiffened Box Connection	10.0	4.1								Did not crack
	4 Re-run 1	Arm Base	16.2	10.0								Run-out at 8.16E+06 cycles
		Handhole	9.7	5.7								Did not crack
		Pole Base	9.3	5.4								Did not crack
		Ring Stiffened Box Connection	10.0	5.8								Did not crack
	4 Re-run 2	Arm Base	16.2	12.0								Run-out at 6.95E+06 cycles
		Handhole	9.7	6.8								Did not crack
		Pole Base	9.3	6.5								Run-out at 9.42E+06 cycles
		Ring Stiffened Box Connection	10.0	7.0								Did not crack
	4 Re-run 3	Arm Base	16.2	16.0	At tube-to-end plate full-pen weld toe on the tube wall	1.63	.20E+06	5.00	.28E+06	5.38	.28E+06	Crack terminated the fatigue test
		Handhole	9.7	9.1								Did not crack
		Pole Base	9.3	8.7								Run-out at 9.78E+06 cycles
		Ring Stiffened Box Connection	10.0	9.3								Did not crack

142

Table 5 *Continued*

Specimen Type	Specimen ID	Detail	S_{min} (ksi)	S_r (ksi)	Description of Crack Location and Origin	First Observation Length (in.)	# of Cycles	Crack Length at Half of Diameter Length (in.)	# of Cycles	Final Length (in.)	# of Cycles	Comments
III	4 Re-run 4	Handhole	9.7	10.4								Did not crack
		Pole Base	9.3	10.0								Run-out at 8.16E+06 cycles
		Ring Stiffened Box Connection	10.0	10.7								Did not crack
	4 Re-run 5	Handhole	9.7	12.5								Did not crack
		Pole Base	9.3	12.0								Run-out at 6.95E+06 cycles
		Ring Stiffened Box Connection	10.0	12.9								Did not crack
	4 Re-run 6	Handhole	9.7	16.7	Left bottom corner[d]	1.81	.29E+06			1.81	.29E+06	Crack terminated the fatigue test
			9.7	16.7	Right top corner[d]	0.56	.29E+06			0.56	.29E+06	
		Pole Base	9.3	16.0								Did not crack
		Ring Stiffened Box Connection	10.0	17.2								Did not crack
	5	Arm Base	16.2	10.0	From the toe of tack weld termination on the tube wall at the top of backing ring	2.00	6.96E+06	5.00	7.42E+06	5.31	7.43E+06	Testing continued with special arm
		Handhole	9.7	5.7								
		Pole Base	9.3	5.4								Run-out at 16.7E+06 cycles
		Ring Stiffened Box Connection	10.0	5.8								
	5 Re-run 1	Handhole	9.7	6.8								
		Pole Base	9.3	6.5								Run-out at 9.42E+06 cycles
		Ring Stiffened Box Connection	10.0	7.0								
	5 Re-run 2	Handhole	9.7	9.1								
		Pole Base	9.3	8.7								Run-out at 9.78E+06 cycles
		Ring Stiffened Box Connection	10.0	9.3								

143

Table 5 *Continued*

Specimen Type	Specimen ID	Detail	Nominal Stress Parameters		Description of Crack Location and Origin	First Observation		Crack Length at Half of Diameter		Final		Comments
			S_{min} (ksi)	S_r (ksi)		Length (in.)	# of Cycles	Length (in.)	# of Cycles	Length (in.)	# of Cycles	
III	5 Re-run 3	Handhole	9.7	10.5								
		Pole Base	9.3	10.0								Run-out at 8.16E+06 cycles
		Ring Stiffened Box Connection	10.0	10.8								
	5 Re-run 4	Handhole	9.7	12.6	Left top corner[d]	3.56	.77E+06			3.56	.77E+06	Crack terminated fatigue test
		Pole Base	9.3	12.0								
		Ring Stiffened Box Connection	10.0	12.9								
	6	Arm Base	16.2	10.0	From the toe of tack weld termination on the tube wall at the top of backing ring	1.50	9.23E+06	5.00	9.56E+06	7.13	9.64E+06	Testing continued with special arm
		Handhole	9.7	5.7								
		Pole Base	9.3	5.4								Run-out at 16.7E+06 cycles.
		Ring Stiffened Box Connection	10.0	5.8								
	6 Re-run 1	Handhole	9.7	6.8								
		Pole Base	9.3	6.5								Run-out at 9.42E+06 cycles
		Ring Stiffened Box Connection	10.0	7.0								
	6 Re-run 2	Handhole	9.7	10.5	Left top corner[d]	2.75	.85E+06			2.75	.85E+06	Crack terminated fatigue test
		Pole Base	9.3	10.0								
		Ring Stiffened Box Connection	10.0	10.8								
	7	Arm Base	16.2	10.0								Run-out at 8.16E+06 cycles
		Handhole	9.7	5.7								
		Pole Base	9.3	5.4								
		Ring Stiffened Box Connection	10.0	5.8								

Table 5 *Continued*

Specimen Type	Specimen ID	Detail	Nominal Stress Parameters S_{min} (ksi)	S_r (ksi)	Description of Crack Location and Origin	First Observation Length (in.)	# of Cycles	Crack Length at Half of Diameter Length (in.)	# of Cycles	Final Length (in.)	# of Cycles	Comments
III	7 Re-run 1	Arm Base	16.2	12.0								Run-out at 6.95E+06 cycles
		Handhole	9.7	6.8								
		Pole Base	9.3	6.5								Run-out at 9.42E+06 cycles
		Ring Stiffened Box Connection	10.0	7.0								
	7 Re-run 2	Arm Base	16.2	16.0	At tube-to-end plate full-pen weld throat	2.00	.81E+06	5.00	1.40E+06	5.25	1.47E+06	Testing continued with special arm
			16.2	16.0	At tube-to-end plate full-pen weld toe on the tube wall	0.50	1.29E+06			0.50	1.47E+06	
		Handhole	9.7	9.1								
		Pole Base	9.3	8.7								Run-out at 9.,78E+06 cycles
		Ring Stiffened Box Connection	10.0	9.3								
	7 Re-run 3	Handhole	9.7	10.4								
		Pole Base	9.3	10.0								Run-out at 8.16E+06 cycles
		Ring Stiffened Box Connection	10.0	10.7								
	7 Re-run 4	Handhole	9.7	12.5	Left bottom corner[d]	6.75	.69E+06			6.75	.69E+06	Crack terminated fatigue test
		Pole Base	9.3	12.0								
		Ring Stiffened Box Connection	10.0	12.9								
	8	Arm Base	16.2	16.0	At tube-to-end plate full-pen weld toe on the tube wall	0.25	5.84E+06	5.00	6.70E+06	5.63	6.75E+06	Testing continued with special arm
		Handhole	9.7	9.1								Did not crack
		Pole Base	9.3	8.7								Run-out at 9.78E+06 cycles
		Ring Stiffened Box Connection	10.0	9.3								Did not crack

144

Table 5 *Continued*

Specimen Type	Specimen ID	Detail	Nominal Stress Parameters		Description of Crack Location and Origin	First Observation		Crack Length at Half of Diameter		Final		Comments
			S_{min} (ksi)	S_r (ksi)		Length (in.)	# of Cycles	Length (in.)	# of Cycles	Length (in.)	# of Cycles	
III	8 rerun-1	Handhole	9.7	10.4	Right top corner[d]	3.00	.85E+06			3.00	.85E+06	Crack terminated fatigue test
		Pole Base	9.3	10.0								
		Ring Stiffened Box Connection	10.0	10.7								
	9	Arm Base	16.2	16.0	At tube-to-end plate full-pen weld toe on the tube wall	1.25	.27E+06	5.00	.4E+06	6.69	.47E+06	Crack terminated the fatigue test
		Handhole	9.7	9.1								Did not crack
		Pole Base	9.3	8.7								Did not crack. Preserved for the stability test
		Ring Stiffened Box Connection	10.0	9.3								Did not crack
	10	Arm Base	16.2	16.0	At tube-to-end plate full-pen weld toe on the tube wall	1.13	4.79E+06	5.00	5.18E+06	5.38	5.20E+06	Testing continued with special arm
		Handhole	9.7	9.1								
		Pole Base	9.3	8.7								Run-out at 9.78E+06 cycles
		Ring Stiffened Box Connection	10.0	9.3								
	10 rerun-1	Handhole	9.7	10.4	Left top corner[d]	7.50	.48E+06			7.50	.48E+06	Crack terminated fatigue test
			9.7	10.4	Right top corner[d]	3.50	.48E+06			3.50	.48E+06	
		Pole Base	9.3	10.0								
		Ring Stiffened Box Connection	10.0	10.7								
IVA	1	Arm Base	16.0	7.0								Run-out at 14.7E+06 cycles
		Pole Base	8.7	3.8								
		Gussetted Box Connection	2.6	1.1								

145

146

Table 5 *Continued*

Specimen Type	Specimen ID	Detail	Nominal Stress Parameters		Description of Crack Location and Origin	First Observation		Crack Length at Half of Diameter		Final		Comments
			S_{min} (ksi)	S_r (ksi)		Length (in.)	# of Cycles	Length (in.)	# of Cycles	Length (in.)	# of Cycles	
IVA	1 Rerun-1	Arm Base	16.0	10.0								Run-out at 8.16E+06 cycles
		Pole Base	8.7	5.4								
		Gussetted Box Connection	2.6	1.6								
	1 Rerun-2	Arm Base	16.0	12.0	At tube-to-end plate full-pen weld toe on the tube wall	0.50	3.29E+06	5.00	4.20E+06	5.50	4.25E+06	Testing continued with special arm
		Pole Base	8.7	6.5								Run-out at 9.42E+06 cycles
		Gussetted Box Connection	2.6	2.0								
	1 Rerun-3	Pole Base	8.7	10.0								Run-out at 8.16E+06 cycles
		Gussetted Box Connection	2.6	3.0								
	1 Rerun-4	Pole Base	8.7	12.0		1.50	3.66E+06	6.50	5.03E+06	14.13	5.17E+06	Crack terminated fatigue test
		Gussetted Box Connection	2.6	3.6								
	2	Arm Base	16.0	7.0								Run-out at 14.7E+06 cycles
		Pole Base	8.7	3.8								
		Gussetted Box Connection	2.6	1.1								
	2 Rerun-1	Arm Base	16.0	10.0								Run-out at 8.16E+06 cycles
		Pole Base	8.7	5.4								
		Gussetted Box Connection	2.6	1.6								
	2 Rerun-2	Arm Base	16.0	12.0								Run-out at 6.95E+06 cycles
		Pole Base	8.7	6.5								
		Gussetted Box Connection	2.6	2.0								
	2 Rerun-3	Arm Base	16.0	16.0								Run-out at 12.5E+06 cycles
		Pole Base	8.7	8.7								
		Gussetted Box Connection	2.6	2.6								

147

Table 5 *Continued*

Specimen Type	Specimen ID	Detail	Nominal Stress Parameters S_{min} (ksi)	S_r (ksi)	Description of Crack Location and Origin	First Observation Length (in.)	# of Cycles	Crack Length at Half of Diameter Length (in.)	# of Cycles	Final Length (in.)	# of Cycles	Comments
IVA	2 Rerun-4	Arm Base	16.0	24.0	At tube-to-end plate full-pen weld toe on the tube wall	11.25	.33E+06	5.00	.33E+06[a]	11.25	.33E+06	Testing continued with special arm
		Pole Base	8.7	13.0	At tube-to-end plate full-pen weld toe on the tube wall	2.00	2.67E+06	6.50	3.21E+06	8.50	3.28E+06	Crack terminated fatigue test
		Gussetted Box Connection	2.6	3.9								
IVB	1	Arm Base	-5.0	10.0								Run-out at 8.16E+06 cycles
		Hand hole	-2.9	5.8								
		Pole Base	-2.7	5.4								
		Gussetted Box Connection	-0.8	1.6								
	1 Rerun-1	Arm Base	-6.0	12.0								Run-out at 6.95E+06 cycles
		Hand hole	-3.5	7.0								
		Pole Base	-3.2	6.5								
		Gussetted Box Connection	-1.0	1.9	From the root of left side gusset plate-to-pole fillet weld - bottom left corner[d]	2.00	5.78E+06			2.00	5.78E+06	Hole drilled to continue test.
	1 Rerun-2	Arm Base	-8.0	16.0								
		Hand hole	-4.7	9.3	From the root of hand hole frame to pole fillet weld - bottom left corner[d]	3.00	.7E+06			4.00	1.28E+06	Hole drilled to continue test. Crack reappeared from arrest hole. Test terminated
		Pole Base	-4.3	8.6								
		Gussetted Box Connection	-1.3	2.6								
	2	Arm Base	-5.0	10.0								
		Hand hole	-2.9	5.8	From the root of hand hole frame to pole fillet weld - bottom left corner[d]	1.00	3.48E+06			3.00	4.18E+06	Hole drilled to continue test. Crack reappeared from arrest hole. Test terminated
		Pole Base	-2.7	5.4								
		Gussetted Box Connection	-0.8	1.6								
V	1	Arm Base	18.3	12.0	At tube-to-end plate partial penetration weld toe on the end plate	0.75	.28E+06	5.00	.62E+06	6.00	.69E+06	Crack terminated fatigue test
		Pole Base	9.1	6.0								

Table 5 *Continued*

Specimen Type	Specimen ID	Detail	Nominal Stress Parameters		Description of Crack Location and Origin	First Observation		Crack Length at Half of Diameter		Final		Comments
			S_{min} (ksi)	S_r (ksi)		Length (in.)	# of Cycles	Length (in.)	# of Cycles	Length (in.)	# of Cycles	
V	2	Arm Base	18.3	12.0	At tube-to-end plate partial penetration weld toe on the end plate	0.75	.29E+06	5.00	.54E+06	5.63	.57E+06	Crack terminated fatigue test
		Pole Base	9.1	6.0								
	3	Arm Base	10.7	7.0	At tube-to-end plate partial penetration weld toe on the end plate	2.75	4.99E+06	5.00	6.65E+06	5.63	7.39E+06	Crack terminated fatigue test
		Pole Base	5.3	3.5								
	4	Arm Base	10.7	7.0	At tube-to-end plate partial penetration weld toe on the end plate			5.00	13.5E+06	5.00	13.5E+06	Crack terminated fatigue test
		Pole Base	5.3	3.5								
V Pole	1	Pole Base	9.1	12.0	At tube-to-end plate fulll penetration weld toe on the end plate	8.25	.27E+06	6.50	.27E+06[a]	8.25	.27E+06	Crack terminated the fatigue test
	2	Pole Base	9.1	12.0	At tube-to-end plate fulll penetration weld toe on the end plate	3.25	1.10E+06	6.50	1.25E+06	6.63	1.27E+06	Crack terminated the fatigue test
	3	Pole Base	5.3	12.0	At tube-to-end plate fulll penetration weld toe on the end plate	1.50	1.46E+06	6.50	1.64E+06	8.44	1.68E+06	Crack terminated the fatigue test
	4	Pole Base	5.3	12.0								Test did not finished
VI	1	Arm Sleeve to Pole Connection	10.3	7.7	From sleeve-to-pole partial penetration weld root into sleeve (at 180° ~ 270° quadrant)[d]	2.25	4.51E+06			6.50	5.82E+06	Hole drilled to continue test.
					Crack branched into pole wall	0.50	4.77E+06			2.00	5.82E+06	Hole drilled to continue test.
					At sleeve-to-pole partial penetration weld toe (at 180° ~ 270° quadrant)[d]	2.75	5.82E+06			2.75	5.82E+06	Crack terminated fatigue test
												Arm starter piece crack initiated from alignment bolt hole at top and interface with arm tube at top.
		Pole Base	8.4	6.3								
	2	Arm Sleeve to Pole Connection	10.3	7.7	At sleeve-to-pole partial penetration weld toe initiated from weld start and stop (at 90° ~ 180° quadrant)[d]	0.75	3.61E+06	5.00	5.15E+06	8.00	5.69E+06	Crack terminated fatigue test
					Crack branched into pole wall	0.50	3.61E+06			7.38	5.69E+06	Hole drilled to continue test. Crack reappeared from arrest hole.
					Crack branched into sleeve wall	0.50	4.90E+06			3.00	5.69E+06	Hole drilled to continue test.
		Pole Base	8.4	6.3								

149

Table 5 *Continued*

Specimen Type	Specimen ID	Detail	Nominal Stress Parameters		Description of Crack Location and Origin	First Observation		Crack Length at Half of Diameter		Final		Comments
			S_{min} (ksi)	S_r (ksi)		Length (in.)	# of Cycles	Length (in.)	# of Cycles	Length (in.)	# of Cycles	
VI	3	Arm Sleeve to Pole Connection	10.3	7.7	From sleeve-to-pole partial penetration weld root into sleeve and pole wall (at 180° ~ 270° quadrant)[d]	1.00	11.1E+06					Hole drilled to continue test. Crack reappeared from arrest hole. Hole drilled to continue test.
					At sleeve-to-pole partial penetration weld toe (at 180° ~ 270° quadrant)[d]	1.25	14.9E+06			1.75	20.0E+06	Run-out at 20.0E+06 cycles
												Arm starter piece crack initiated from alignment bolt hole at top.
		Pole Base	8.4	6.3								
	4	Arm Sleeve to Pole Connection	10.3	7.7	At sleeve-to-pole partial penetration weld toe initiated from weld start and stop (at 90° ~ 180° quadrant)[d]	1.50	1.54E+06	1.91	1.70E+06	3.38	1.85E+06	
					Crack branced into pole wall	0.50	1.54E+06			0.75	1.85E+06	
					At sleeve-to-pole partial penetration weld toe (at 180° ~ 270° quadrant)[d]	0.75	1.54E+06	3.09	1.70E+06	4.13	1.85E+06	Crack terminated fatigue test
												Arm starter piece cracked from interface with arm tube at top
		Pole Base	8.4	6.3								
	5	Arm Sleeve to Pole Connection	10.3	4.5								Run-out at 20.0E+6 cycles
		Pole Base	8.4	3.7								
	5 Rerun-1	Arm Sleeve to Pole Connection	10.3	7.7								Run-out at 11.3E+6 cycles
		Pole Base	8.4	6.3								
	5 Rerun-2	Arm Sleeve to Pole Connection	10.3	10.0	At sleeve-to-pole partial penetration weld toe (at 180° ~ 270° quadrant)[d]	2.00	2.41E+06	5.00	4.05E+06	5.25	4.29E+06	Crack terminated fatigue test
					Crack branched into sleeve wall	0.50	3.38E+06			0.50	4.29E+06	Hole drilled to continue test
					Crack branched into pole wall	0.25	4.29E+06			0.25	4.29E+06	
												Arm starter piece cracked from interface with arm tube at top
		Pole Base	8.4	8.2								

Table 5 *Continued*

150

Specimen Type	Specimen ID	Detail	Nominal Stress Parameters		Description of Crack Location and Origin	First Observation		Crack Length at Half of Diameter		Final		Comments
			S_{min} (ksi)	S_r (ksi)		Length (in.)	# of Cycles	Length (in.)	# of Cycles	Length (in.)	# of Cycles	
VI	6	Arm Sleeve to Pole Connection	10.3	4.5								Run-out at 20.0E+6 cycles
		Pole Base	8.4	3.7								
	6 Rerun-1	Arm Sleeve to Pole Connection	10.3	7.7	At sleeve-to-pole partial penetration weld toe (at 90° ~ 180° quadrant)[d]	1.38	.9E+06	5.00	3.46E+06	5.00	3.59E+06	Crack terminated fatigue test
			10.3	7.7	At sleeve-to-pole partial penetration weld toe (at 180° ~ 270° quadrant)[d]	1.75	1.37E+06			3.75	3.59E+06	
												Arm starter piece cracked from interface with arm tube at top
		Pole Base	8.4	6.3								
	7	Arm Sleeve to Pole Connection	10.3	4.5								Run-out at 20.0E+6 cycles
		Pole Base	8.4	3.7								
	7 Rerun-1	Arm Sleeve to Pole Connection	10.3	7.7	At sleeve-to-pole partial penetration weld toe (at 180° ~ 270° quadrant)[d]	2.25	1.37E+06	5.00	3.15E+06	5.00	3.15E+06	Crack terminated fatigue test
					Crack branced into pole wall	0.38	2.69E+06			1.63	3.15E+06	
		Pole Base	8.4	6.3								
	8	Arm Sleeve to Pole Connection	10.3	16.0	At sleeve-to-pole partial penetration weld toe (at 180° ~ 270° quadrant)[d]	4.00	.68E+06	5.00	.82E+06	9.50	.94E+06	Crack terminated fatigue test
					Crack branced into pole wall	4.00	.94E+06			4.00	.94E+06	
					At sleeve-to-pole partial penetration weld toe (at 90° ~ 180° quadrant)[d]	3.00	.68E+06			3.88	.94E+06	
												Arm starter piece crack initiated from alignment bolt hole top. Starter piece replaced. Arm starter piece cracked from interface with arm tube top
		Pole Base	8.4	13.1								

Table 5 *Continued*

Specimen Type	Specimen ID	Detail	Nominal Stress Parameters		Description of Crack Location and Origin	First Observation		Crack Length at Half of Diameter		Final		Comments
			S_{min} (ksi)	S_r (ksi)		Length (in.)	# of Cycles	Length (in.)	# of Cycles	Length (in.)	# of Cycles	
VI	9	Arm Sleeve to Pole Connection	10.3	12.0	At sleeve-to-pole partial penetration weld toe initiated from weld start and stop (at 90° ~ 180° quadrant)[d]	3.00	.43E+06	5.00	.68E+06	6.88	.75E+06	Crack terminated fatigue test
					Crack branched into sleeve wall	0.50	.63E+06			2.75	.75E+06	
					At sleeve-to-pole partial penetration weld toe (at 180° ~ 270° quadrant)[d]	2.50	.55E+06			3.56	.75E+06	
					Crack branched into sleeve wall	0.25	.75E+06			0.25	.75E+06	
		Pole Base	8.4	9.8								
	10	Arm Sleeve to Pole Connection	10.3	16.0	At sleeve-to-pole partial penetration weld toe (at 90° ~ 180° quadrant)[d]	1.75	.14E+06	5.00	.64E+06	5.38	.68E+06	Crack terminated fatigue test
					At sleeve-to-pole partial penetration weld toe (at 180° ~ 270° quadrant)[d]	3.25	.34E+06			4.63	.68E+06	
												Arm starter piece cracked from interface with arm tube top. Starter piece replaced.
		Pole Base	8.4	13.1								
VI Pole	1	Pole Base	8.4	12.0								Test continued at higher stress range. Run-out at 6.95E+06 cycles
	1 Rerun-1	Pole Base	8.4	16.0	At tube-to-end plate full penetration weld toe on tube wall	0.75	4.43E+06	6.50	4.99E+06	7.75	5.03E+06	Crack terminated the fatigue test
	2	Pole Base	8.4	12.0								Test continued at higher stress range. Run-out at 6.95E+06 cycles
	2 Rerun-1	Pole Base	8.4	16.0								Test continued at higher stress range. Run-out at 12.5E+06 cycles
	2 Rerun-2	Pole Base	8.4	24.0								Test stopped. Run-out at 14.7E+06 cycles
	3	Pole Base	8.4	12.0								Test continued at higher stress range. Run-out at 6.95E+06 cycles
	3 Rerun-1	Pole Base	8.4	16.0								Test continued at higher stress range. Run-out at 12.5E+06 cycles

151

Table 5 *Continued*

Specimen Type	Specimen ID	Detail	Nominal Stress Parameters		Description of Crack Location and Origin	First Observation		Crack Length at Half of Diameter		Final		Comments
			S_{min} (ksi)	S_r (ksi)		Length (in.)	# of Cycles	Length (in.)	# of Cycles	Length (in.)	# of Cycles	
VI Pole	3 Rerun-2	Pole Base	8.4	24.0	At tube-to-end plate full penetration weld toe on tube wall	9.50	.76E+06	6.50	.76E+06[a)]	9.50	.76E+06	Crack terminated the fatigue test
	4	Pole Base	8.4	12.0								Test continued at higher stress range. Run-out at 6.95E+06 cycles
	4 Rerun-1	Pole Base	8.4	16.0	At tube-to-end plate full penetration weld toe on tube wall	0.50	12.2E+06	6.50	12.8E+06	8.38	13.0E+06	Crack terminated the fatigue test
	6	Pole Base	8.4	12.0								Test continued at higher stress range. Run-out at 6.95E+06 cycles
	6 Rerun-1	Pole Base	8.4	16.0	At tube-to-end plate full penetration weld toe on tube wall	1.25	.48E+06	6.50	1.00E+06	9.50	1.07E+06	Crack terminated the fatigue test
					Seam weld root	1.25	.48E+06			5.63	1.07E+06	
	7	Pole Base	8.4	12.0	At tube-to-end plate full penetration weld toe on tube wall	5.13	5.08E+06	6.50	5.15E+06	7.75	5.21E+06	Crack terminated the fatigue test
	8	Pole Base	8.4	13.1								Run-out at 6.20E+06 cycles
	8 Rerun-1	Pole Base	8.4	16.0								Run-out at 12.5E+06 cycles
	8 Rerun-2	Pole Base	8.4	24.0	At tube-to-end plate full penetration weld toe on tube wall	1.00	.56E+06	6.50	.88E+06	8.88	.91E+06	Crack terminated the fatigue test
	9	Pole Base	8.4	13.1	At tube-to-end plate full penetration weld toe on tube wall	0.25	1.0E+06	6.50	2.43E+06	12.75	2.56E+06	Crack terminated the fatigue test
	10	Pole Base	8.4	13.1								Run-out at 6.20E+06 cycles
	10 Rerun-1	Pole Base	8.4	16.0	At tube-to-end plate full penetration weld toe on tube wall	0.38	.89E+06	6.50	1.35E+06	8.00	1.44E+06	Crack terminated the fatigue test

153

Table 5 *Continued*

Specimen Type	Specimen ID	Detail	Nominal Stress Parameters		Description of Crack Location and Origin	First Observation		Crack Length at Half of Diameter		Final		Comments
			S_{min} (ksi)	S_r (ksi)		Length (in.)	# of Cycles	Length (in.)	# of Cycles	Length (in.)	# of Cycles	
VII	1	Arm Base	15.3	12.0	At tube-to-end plate fillet weld toe on the tube wall	0.5+0.5[b)	0.04E+06	5.00	0.21E+06	14.88	.44E+06	Crack terminated the fatigue test
		Handhole	8.8	6.9								Did not crack
		Pole Base	8.4	6.6	At tube-to-end plate fillet weld toe on the tube wall	2.00	0.09E+06			2.00+3.25[b)	.44E+06	
	2	Arm Base	15.3	12.0	At tube-to-end plate fillet weld toe on the tube wall	2.00	0.04E+06	5.00	0.20E+06	10.75	.44E+06	Crack terminated the fatigue test
		Handhole	8.8	6.9								Did not crack
		Pole Base	8.4	6.6	At tube-to-end plate fillet weld toe on the tube wall	0.38	0.09E+06			1.25+2.00[b)	.44E+06	
	3	Arm Base	15.3	12.0	At tube-to-end plate fillet weld toe on the tube wall	0.63+0.5[b)	0.01E+06	5.00	0.21E+06	9.25	.53E+06	Crack terminated the fatigue test
		Handhole	8.8	6.9								Did not crack
		Pole Base	8.4	6.6	At tube-to-end plate fillet weld toe on the tube wall	0.50	.10E+06	6.50	.53E+06	3.00+3.63[b)	.53E+06	
	4	Arm Base	15.3	4.5	At tube-to-end plate fillet weld toe on the tube wall	0.50	1.03E+06	.63+.88+3.5[b]	3.40E+06	9.50	4.36E+06	Crack terminated the fatigue test
		Handhole	8.8	2.6	At handhole frame seam weld root	0.75	3.27E+06					Hole drilled. Testing continued.
		Pole Base	8.4	2.5								Test continued with special arm. Run-out at 20.00E+06 cycles
	4 Rerun-1	Handhole	8.8	4.7	At handhole frame seam weld root	2.00	1.18E+06			2.00E+00	1.18E+06	Crack reappeared from arrest hole. Test terminated
		Pole Base	8.4	4.5								
	5	Arm Base	15.3	4.5	At tube-to-end plate fillet weld toe on the tube wall	0.13	.39E+06	5.00	6.41E+06	10.25	7.57E+06	Test continued with special arm
		Handhole	8.8	2.6	At handhole frame seam weld root	0.50	12.5E+06					Hole drilled. Testing continued.
		Pole Base	8.4	2.5								Run-out at 20.00E+06 cycles
	5 Rerun-1	Handhole	8.8	4.7								
		Pole Base	8.4	4.5	At tube-to-end plate fillet weld toe on the tube wall	1.13	.65E+06	6.50	1.78E+06	10.50	2.11E+06	Crack terminated fatigue test
	6	Arm Base	15.3	2.5								Run-out at 20.00E+06 cycles
		Handhole	8.8	1.5								Did not crack
		Pole Base	8.4	1.4								Did not crack

154

Table 5 *Continued*

Specimen Type	Specimen ID	Detail	Nominal Stress Parameters		Description of Crack Location and Origin	First Observation		Crack Length at Half of Diameter		Final		Comments
			S_{min} (ksi)	S_r (ksi)		Length (in.)	# of Cycles	Length (in.)	# of Cycles	Length (in.)	# of Cycles	
VII	6 Re-run 1	Arm Base	15.3	4.5								Run-out at 20.00E+06 cycles
		Handhole	8.8	2.7	At handhole frame seam weld root	0.94	8.91E+06			1.19	10.01E+06	Hole drilled. Testing continued.
		Pole Base	8.4	2.5								Did not crack
	6 Re-run 2	Arm Base	15.3	7.0	At tube-to-end plate fillet weld toe on the tube wall	0.88	.89E+06	5.00	2.20E+06	7.00	2.32E+06	Test continued with special arm
		Pole Base	8.4	3.9	At tube-to-end plate fillet weld toe on the tube wall	1.88	11.50E+06			6.38	15.44E+06	
		Handhole	8.8	3.9	From the root of hand hole frame to pole fillet weld - bottom left corner[d]	5.00	15.44E+06			5.00	15.44E+06	Crack terminated the fatigue test
	7	Arm Base	15.3	2.5	At tube-to-end plate fillet weld toe on the tube wall	0.88	0.07E+06					Run-out at 20.00E+06 cycles
		Handhole	8.8	1.5								Did not crack
		Pole Base	8.4	1.4								Did not crack
	7 Re-run 1	Arm Base	15.3	4.5	At tube-to-end plate fillet weld toe on the tube wall			5.00	5.42E+06	10.00	6.85E+06	Test continued with special arm
		Handhole	8.8	2.7	At handhole frame seam weld root	1.00	2.56E+06			1.13	4.06E+06	Hole drilled. Testing continued.
		Pole Base	8.4	2.5								Run-out at 20.00E+06 cycles
	7 Re-run 2	Pole Base	8.4	3.9	At tube-to-end plate fillet weld toe on the tube wall	0.25	4.62E+06	6.50	14.38E+06	6.63	14.44E+06	Crack terminated the fatigue test
IX	1	Stiffener	-6.0	12.0	At tube-to-stiffener fillet weld toe on the tube wall(at 0°)[d]	1.50	.59E+06			10.88	1.81E+06	
			-6.0	12.0	At tube-to-stiffener fillet weld toe on the tube wall (at 180°)[d]	0.63	.59E+06	12.00	1.41E+06	20.00	1.81E+06	Crack terminated fatigue test
		Pole Base	1.6	3.3	At tube-to-end plate fillet weld toe on the tube wall (at 0°)[d]							
			1.6	3.3	At tube-to-end plate fillet weld toe on the tube wall (at 180°)[d]							
	2	Stiffener	-6.0	12.0	At tube-to-stiffener fillet weld toe on the tube wall(at 0°)[d]	0.75	.27E+06	12.00	.77E+06	14.38	.82E+06	
			-6.0	12.0	At tube-to-stiffener fillet weld toe on the tube wall (at 180°)[d]	1.63	.27E+06	12.00	.76E+06	16.50	.82E+06	Crack terminated fatigue test
		Pole Base	1.6	3.3	At tube-to-end plate fillet weld toe on the tube wall (at 0°)[d]							
			1.6	3.3	At tube-to-end plate fillet weld toe on the tube wall (at 180°)[d]							

155

Table 5 *Continued*

Specimen Type	Specimen ID	Detail	S_min (ksi)	S_r (ksi)	Description of Crack Location and Origin	First Observation Length (in.)	# of Cycles	Crack Length at Half of Diameter Length (in.)	# of Cycles	Final Length (in.)	# of Cycles	Comments
IX	3	Stiffener	-6.0	12.0	At tube-to-stiffener fillet weld toe on the tube wall(at 0°)[d]	1.63	.51E+06	12.00	2.79E+06	20.00	7.14E+06	Crack terminated fatigue test
			-6.0	12.0	At tube-to-stiffener fillet weld toe on the tube wall (at 180°)[d]	1.13	1.07E+06			7.00	7.14E+06	
		Pole Base	1.6	3.3	At tube-to-end plate fillet weld toe on the tube wall (at 0°)[d]							
			1.6	3.3	At tube-to-end plate fillet weld toe on the tube wall (at 180°)[d]							
	4	Stiffener	-5.0	10.0	At tube-to-stiffener fillet weld toe on the tube wall(at 0°)[d]	1.00	.45E+06			8.75	2.38E+06	
			-5.0	10.0	At tube-to-stiffener fillet weld toe on the tube wall (at 180°)[d]	1.13	.52E+06	12.00	2.33E+06	16.00	2.38E+06	Crack terminated fatigue test
		Pole Base	1.4	2.7	At tube-to-end plate fillet weld toe on the tube wall (at 0°)[d]							
			1.4	2.7	At tube-to-end plate fillet weld toe on the tube wall (at 180°)[d]							
	5	Stiffener	-3.5	7.0	At tube-to-stiffener fillet weld toe on the tube wall(at 0°)[d]	1.63	3.08E+06	12.00	5.21E+06	16.75	5.84E+06	Crack terminated fatigue test
			-3.5	7.0	At tube-to-stiffener fillet weld toe on the tube wall (at 180°)[d]	1.63	2.57E+06			3.25	5.84E+06	
		Pole Base	1.0	1.9	At tube-to-end plate fillet weld toe on the tube wall (at 0°)[d]							
			1.0	1.9	At tube-to-end plate fillet weld toe on the tube wall (at 180°)[d]							
	6	Stiffener	-2.3	4.5	At tube-to-stiffener fillet weld toe on the tube wall(at 0°)[d]							
			-2.3	4.5	At tube-to-stiffener fillet weld toe on the tube wall (at 180°)[d]	1.00	2.64E+06	12.00	18.45E+06	13.13	19.43E+06	Crack terminated fatigue test
		Pole Base	-0.6	1.2	At tube-to-end plate fillet weld toe on the tube wall (at 0°)[d]							
			-0.6	1.2	At tube-to-end plate fillet weld toe on the tube wall (at 180°)[d]							
	7	Stiffener	-2.3	4.5	At tube-to-stiffener fillet weld toe on the tube wall(at 0°)[d]	1.00	4.00E+06	12.00	15.98E+06	12.25	15.98E+06	Crack terminated fatigue test
			-2.3	4.5	At tube-to-stiffener fillet weld toe on the tube wall (at 180°)[d]							
		Pole Base	-0.6	1.2	At tube-to-end plate fillet weld toe on the tube wall (at 0°)[d]							
			-0.6	1.2	At tube-to-end plate fillet weld toe on the tube wall (at 180°)[d]							

Table 5 *Continued*

Specimen Type	Specimen ID	Detail	Nominal Stress Parameters		Description of Crack Location and Origin	First Observation		Crack Length at Half of Diameter		Final		Comments
			S_{min} (ksi)	S_r (ksi)		Length (in.)	# of Cycles	Length (in.)	# of Cycles	Length (in.)	# of Cycles	
IX	8	Stiffener	-8.0	16.0	At tube-to-stiffener fillet weld toe on the tube wall(at 0°)[d]	1.38	.12E+06			6.88	.39E+06	
			-8.0	16.0	At tube-to-stiffener fillet weld toe on the tube wall (at 180°)[d]	1.25	.07E+06	12.00	.37E+06	13.13	.39E+06	Crack terminated fatigue test
		Pole Base	2.2	4.4	At tube-to-end plate fillet weld toe on the tube wall (at 0°)[d]							
			2.2	4.4	At tube-to-end plate fillet weld toe on the tube wall (at 180°)[d]							
	9	Stiffener	-8.0	16.0	At tube-to-stiffener fillet weld toe on the tube wall(at 0°)[d]	1.00	.13E+06			5.63	.49E+06	
			-8.0	16.0	At tube-to-stiffener fillet weld toe on the tube wall (at 180°)[d]	1.50	.28E+06	12.00	.45E+06	16.00	.49E+06	Crack terminated fatigue test
		Pole Base	2.2	4.4	At tube-to-end plate fillet weld toe on the tube wall (at 0°)[d]							
			2.2	4.4	At tube-to-end plate fillet weld toe on the tube wall (at 180°)[d]							
	10	Stiffener	-8.0	16.0	At tube-to-stiffener fillet weld toe on the tube wall(at 0°)[d]	1.38	.12E+06	12.00	.32E+06	19.00	.42E+06	Crack terminated fatigue test
			-8.0	16.0	At tube-to-stiffener fillet weld toe on the tube wall (at 180°)[d]	0.75	.12E+06			20.00	.42E+06	
		Pole Base	2.2	4.4	At tube-to-end plate fillet weld toe on the tube wall (at 0°)[d]							
			2.2	4.4	At tube-to-end plate fillet weld toe on the tube wall (at 180°)[d]							
X	1	Pole Base	-2.7	5.4								Run-out at 17.00E+06 cycles
		Handhole										
	1 Re-run 1	Pole Base	-4.0	8.0								Run-out at 13.00E+06 cycles
		Handhole										
	1 Re-run 2	Pole Base	-5.0	10.0	At tube-to-end plate fillet weld toe on the tube wall	1.50	1.38E+06	12.00	1.72E+06	17.00	1.78E+06	Crack terminated fatigue test
		Handhole										Did not crack
	2	Pole Base	-4.0	8.0	At tube-to-end plate fillet weld toe on the tube wall	1.00+1.50[b]	1.75E+06	12.00	2.39E+06	12.00	2.39E+06	Crack terminated fatigue test
		Handhole										Did not crack
	3	Pole Base	-4.0	8.0	At tube-to-end plate fillet weld toe on the tube wall on handhole side and opposite.	3.88	.68E+06	12.00	.98E+06	17.00	1.02E+06	Crack terminated fatigue test
		Handhole										Did not crack

156

Table 5 *Continued*

Specimen Type	Specimen ID	Detail	S_{min} (ksi)	S_r (ksi)	Description of Crack Location and Origin	First Observation Length (in.)	# of Cycles	Crack Length at Half of Diameter Length (in.)	# of Cycles	Final Length (in.)	# of Cycles	Comments
XI	1	Pole Base	-6.0	12.0	At tube-to-end plate weld toe on the tube wall (at 0°)[d]	5.00	.75E+06	12.00	.98E+06	16.06	1.13E+06	
			-5.8	11.6	From the toe of weld termination on the tube wall at the top of backing ring (at 180°)[d]	12.25	1.13E+06	12.00	1.06E+06[a]	12.25	1.13E+06	Backing ring crack terminated fatigue test
		Handhole	-4.5	9.0								Did not crack
	2	Pole Base	-6.0	12.0	At tube-to-end plate weld toe on the tube wall (at 0°)[d]	2.38	1.56E+06	12.00	3.09E+06	14.75	3.49E+06	
			-5.8	11.6	From the toe of weld termination on the tube wall at the top of backing ring (at 0°)[d]	4.38	3.13E+06	12.00	3.43E+06	12.50	3.49E+06	Backing ring crack terminated fatigue test
		Handhole	-4.5	9.0								Did not crack
	3	Pole Base	-6.0	12.0	At tube-to-end plate weld toe on the tube wall (at 0°)[d]	3.13	.33E+06			11.44	.77E+06	
			-6.0	12.0	At tube-to-end plate weld toe on the tube wall (at 180°)[d]	3.25	.33E+06	7.12+4.88[b]	.62E+06	8.38+6.63[b]	.77E+06	
			-5.8	11.6	From the toe of weld termination on the tube wall at the top of backing ring (at 180°)[d]	2.19	.59E+06			10.63	.77E+06	Backing ring crack terminated fatigue test
		Handhole	-4.5	9.0								Did not crack
	4	Pole Base	-3.5	7.0								Run-out at 14.70E+06 cycles
		Handhole	-2.6	5.3								
	4 Re-run 1	Pole Base	-5.0	10.0	At tube-to-end plate weld toe on the tube wall (at 0°)[d]	1.75	.65E+06			11.56	2.15E+06	
			-5.0	10.0	At tube-to-end plate weld toe on the tube wall (at 180°)[d]	2.06	.71E+06	12.00	1.30E+06	19.88	2.15E+06	
			-4.8	9.6	From the toe of weld termination on the tube wall at the top of backing ring (at 180°)[d]	1.13	1.59E+06	12.00	2.15E+06	12.75	2.15E+06	Backing ring crack terminated fatigue test
		Handhole	-3.8	7.5								Did not crack
	5	Pole Base	-3.5	7.0								Run-out at 14.70E+06 cycles
		Handhole	-2.6	5.3								

157

Table 5 *Continued*

Specimen Type	Specimen ID	Detail	S_min (ksi)	S_r (ksi)	Description of Crack Location and Origin	First Observation Length (in.)	# of Cycles	Crack Length at Half of Diameter Length (in.)	# of Cycles	Final Length (in.)	# of Cycles	Comments
XI	5 Re-run 1	Pole Base	-5.0	10.0	At tube-to-end plate weld toe on the tube wall (at 0°)[d]	0.63	.68E+06			15.63	2.86E+06	
			-5.0	10.0	At tube-to-end plate weld toe on the tube wall (at 180°)[d]	1.69+.81[b]	.68E+06	12.00	2.24E+06	15.38	2.86E+06	
			-4.8	9.6	From the toe of weld termination on the tube wall at the top of backing ring (at 180°)[d]	2.75	1.79E+06	12.00	2.86E+06	12.75	2.86E+06	Backing ring crack terminated fatigue test
		Handhole	-3.8	7.5								Did not crack
	6	Pole Base	-3.5	7.0								Run-out at 14.70E+06 cycles
		Handhole	-2.6	5.3								
	6 Re-run 1	Pole Base	-5.0	10.0	At tube-to-end plate weld toe on the tube wall (at 0°)[d]	0.19+0.75[b]	.84E+06	12.00	2.24E+06	24.50	2.51E+06	
			-5.0	10.0	At tube-to-end plate weld toe on the tube wall (at 180°)[d]	0.88	.54E+06	12.00	1.73E+06	20.00	2.51E+06	
			-4.8	9.6	From the toe of weld termination on the tube wall at the top of backing ring (at 180°)[d]	1.13	2.12E+06	12.00	2.45E+06	15.50	2.51E+06	Backing ring crack terminated fatigue test
			-4.8	9.6	From the toe of weld termination on the tube wall at the top of backing ring (at 0°)[d]	1.50	2.29E+06			4.88	2.51E+06	
		Handhole	-3.8	7.5								Did not crack
	7	Pole Base	-3.5	7.0								Run-out at 14.70E+06 cycles
		Handhole	-2.6	5.3								
	7 Re-run 1	Pole Base	-5.0	10.0	At tube-to-end plate weld toe on the tube wall (at 0°)[d]	2.06	.77E+06			9.38	1.80E+06	
			-5.0	10.0	At tube-to-end plate weld toe on the tube wall (at 180°)[d]	1.13+1.5+1.5[b]	.50E+06	7.63+1.19+3.2[b]	1.16E+06	21.19	1.80E+06	
			-4.8	9.6	From the toe of weld termination on the tube wall at the top of backing ring (at 180°)[d]	1+0.69+0.75[b]	1.45E+06	12.00	1.75E+06	13.25	1.80E+06	Backing ring crack terminated fatigue test
		Handhole	-3.8	7.5								Did not crack

Table 5 *Continued*

Specimen Type	Specimen ID	Detail	Nominal Stress Parameters		Description of Crack Location and Origin	First Observation		Crack Length at Half of Diameter		Final		Comments
			S_{min} (ksi)	S_r (ksi)		Length (in.)	# of Cycles	Length (in.)	# of Cycles	Length (in.)	# of Cycles	
XI	8	Pole Base	-7.0	14.0	At tube-to-end plate weld toe on the tube wall (at 0°)d)	0.63	0.10E+06			9.88	0.53E+06	
			-7.0	14.0	At tube-to-end plate weld toe on the tube wall (at 180°)d)	0.50	0.10E+06	12.00	0.29E+06	22.38	0.53E+06	
			-6.8	13.5	From the toe of weld termination on the tube wall at the top of backing ring (at 180°)d)	2.75+.75b)	0.39E+06			9.88	0.53E+06	Backing ring crack terminated fatigue test
			-6.8	13.5	From the throat of weld termination on tube wall at top of backing ring (at 180°)d)	5.63	0.47E+06			9.50	0.53E+06	
			-6.8	13.5	From the center of the backing ring seam weld (at 180°)d)	4.75	0.47E+06			7.88	0.53E+06	
		Handhole	-5.3	10.6								Did not crack
	9	Pole Base	-8.0	16.0	At tube-to-end plate weld toe on the tube wall (at 0°)d)	2.5+2.75b)	.14E+06	12.00	0.37E+06	19.00	.60E+06	
			-8.0	16.0	At tube-to-end plate weld toe on the tube wall (at 180°)d)	7.88+.63b)	.14E+06	12.00	.47E+06	17.06	.60E+06	
			-7.7	15.4	From the toe of weld termination on the tube wall at the top of backing ring (at 0°)d)	25.75	.60E+06			25.75	.60E+06	Backing ring crack terminated fatigue test
		Handhole	-6.0	12.0								Did not crack
	10	Pole Base	-8.0	16.0	At tube-to-end plate weld toe on the tube wall (at 0°)d)	2.25	0.06E+06	12.00	.19E+06	16.31	.34E+06	
			-8.0	16.0	At tube-to-end plate weld toe on the tube wall (at 180°)d)	2.75	.15E+06	6+6b)	.34E+06	6+6.13b)	.34E+06	
			-7.7	15.4	From the toe of weld termination on the tube wall at the top of backing ring (at 0°)d)	12.88+3.94b)	.34E+06	12.00	.34E+06a)	12.88+3.94b)	.34E+06	Backing ring crack terminated fatigue test
		Handhole	-6.0	12.0								Did not crack

Table 5 *Continued*

Specimen Type	Specimen ID	Detail	S_min (ksi)	S_r (ksi)	Description of Crack Location and Origin	First Observation Length (in.)	# of Cycles	Crack Length at Half of Diameter Length (in.)	# of Cycles	Final Length (in.)	# of Cycles	Comments
XII	1	Stiffener	-6.0	12.0	At tube-to-stiffener weld toe on the tube wall (at 0°)[d]	0.50	.23E+06	12.00	.72E+06	14.25	.79E+06	Crack terminated fatigue test
			-6.0	12.0	At tube-to-stiffener weld toe on the tube wall (at 180°)[d]	1.50	.53E+06			8.13	.79E+06	
		Pole Base	-4.3	8.5	At tube-to-end plate fillet weld toe on the tube wall (at 0°)[d]	0.75	.38E+06			4.63	.79E+06	
			-4.3	8.5								
	2	Stiffener	-6.0	12.0	At tube-to-stiffener weld toe on the tube wall (at 0°)[d]	1.00	.40E+06			9.00	.91E+06	Crack terminated fatigue test
			-6.0	12.0	At tube-to-stiffener weld toe on the tube wall (at 180°)[d]	0.50	.40E+06	12.00	.88E+06	13.38	.91E+06	
		Pole Base	-4.3	8.5								
			-4.3	8.5								
	3	Stiffener	-6.0	12.0	At tube-to-stiffener weld toe on the tube wall (at 0°)[d]							Crack terminated fatigue test
			-6.0	12.0	At tube-to-stiffener weld toe on the tube wall (at 180°)[d]	1.00	.58E+06	12.00	1.04E+06	12.88	1.06E+06	
		Pole Base	-4.3	8.5								
			-4.3	8.5								
	4	Stiffener	-3.5	7.0	At tube-to-stiffener weld toe on the tube wall (at 0°)[d]							Run-out at 14.70E+06 cycles
			-3.5	7.0	At tube-to-stiffener weld toe on the tube wall (at 180°)[d]							
		Pole Base	-2.5	5.0								
			-2.5	5.0								

160

161

Table 5 *Continued*

Specimen Type	Specimen ID	Detail	Nominal Stress Parameters		Description of Crack Location and Origin	First Observation		Crack Length at Half of Diameter		Final		Comments
			S_{min} (ksi)	S_r (ksi)		Length (in.)	# of Cycles	Length (in.)	# of Cycles	Length (in.)	# of Cycles	
XII	4 Re-run 1	Stiffener	-5.0	10.0	At tube-to-stiffener weld toe on the tube wall (at 0°)[d]	0.25	.61E+06	12.00	1.59E+06	40.75	2.31E+06	Crack terminated fatigue test
			-5.0	10.0	At tube-to-stiffener weld toe on the tube wall (at 180°)[d]							
		Pole Base	-3.6	7.1								
			-3.6	7.1								
	5	Stiffener	-3.5	7.0	At tube-to-stiffener weld toe on the tube wall (at 0°)[d]							Run-out at 14.70E+06 cycles
			-3.5	7.0	At tube-to-stiffener weld toe on the tube wall (at 180°)[d]							
		Pole Base	-2.5	5.0								
			-2.5	5.0								
	5 Re-run 1	Stiffener	-5.0	10.0	At tube-to-stiffener weld toe on the tube wall (at 0o)[d]	1.13	4.69E+06	12.00	6.04E+06	13.38	6.12E+06	Crack terminated fatigue test
			-5.0	10.0	At tube-to-stiffener weld toe on the tube wall (at 180°)[d]							
		Pole Base	-3.6	7.1								
			-3.6	7.1								
	6	Stiffener	-3.5	7.0	At tube-to-stiffener weld toe on the tube wall (at 0°)[d]							
			-3.5	7.0	From the root of stiffener to pole fillet top weld (at 180°)[d]	0.63	4.06E+06	12.00	5.85E+06	15.13	5.94E+06	Crack terminated fatigue test
		Pole Base	-2.5	5.0								
			-2.5	5.0								

Table 5 *Continued*

Specimen Type	Specimen ID	Detail	S_{min} (ksi)	S_r (ksi)	Description of Crack Location and Origin	First Observation		Crack Length at Half of Diameter		Final		Comments
						Length (in.)	# of Cycles	Length (in.)	# of Cycles	Length (in.)	# of Cycles	
XII	7	Stiffener	-3.5	7.0	At tube-to-stiffener weld toe on the tube wall (at 0°)[d]							Run-out at 14.70E+06 cycles
			-3.5	7.0	At tube-to-stiffener weld toe on the tube wall (at 180°)[d]							
		Pole Base	-2.5	5.0								
			-2.5	5.0								
	7 Re-run 1	Stiffener	-5.0	10.0	At tube-to-stiffener weld toe on the tube wall (at 0°)[d]							
			-5.0	10.0	At tube-to-stiffener weld toe on the tube wall (at 180°)[d]	0.75	6.24E+06	12.00	7.98E+06	12.00	7.98E+06	Crack terminated fatigue test
		Pole Base	-3.6	7.1								
			-3.6	7.1								
	8	Stiffener	-8.0	16.0	At tube-to-stiffener weld toe on the tube wall (at 0°)[d]	0.94	.15E+06	12.00	.43E+06	15.75	.49E+06	Crack terminated fatigue test
			-8.0	16.0	At tube-to-stiffener weld toe on the tube wall (at 180°)[d]	0.75	.05E+06			14.19	.49E+06	
		Pole Base	-5.7	11.3	At tube-to-end plate fillet weld toe on the tube wall left bend (at 0°)[d]	1.38	.05E+06			7.19	.49E+06	
			-5.7	11.3	At tube-to-end plate fillet weld toe on the tube wall right bend (at 0°)[d]	2.00	.30E+06			3.56	.49E+06	
			-5.7	11.3	At tube-to-end plate fillet weld toe on the tube wall left bend (at 180°)[d]	2.56	.09E+06			8.06	.49E+06	
			-5.7	11.3	At tube-to-end plate fillet weld toe on the tube wall right bend (at 180°)[d]	2.63	.30E+06			2.63	.49E+06	
	9	Stiffener	-8.0	16.0	At tube-to-stiffener weld toe on the tube wall (at 0°)[d]	0.88	.20E+06	12.00	.42E+06	12.63	.43E+06	Crack terminated fatigue test
			-8.0	16.0	At tube-to-stiffener weld toe on the tube wall (at 180°)[d]	1.00	.38E+06					
		Pole Base	-5.7	11.3								
			-5.7	11.3								

162

163

Table 5 *Continued*

Specimen Type	Specimen ID	Detail	Nominal Stress Parameters S_{min} (ksi)	S_r (ksi)	Description of Crack Location and Origin	First Observation Length (in.)	# of Cycles	Crack Length at Half of Diameter Length (in.)	# of Cycles	Final Length (in.)	# of Cycles	Comments
XII	10	Stiffener	-8.0	16.0	At tube-to-stiffener weld toe on the tube wall (at 0°)[d]	1.13	.05E+06			16.75	.47E+06	
			-8.0	16.0	At tube-to-stiffener weld toe on the tube wall (at 180°)[d]	1.13	.11E+06	12.00	.37E+06	18.50	.47E+06	Crack terminated fatigue test
		Pole Base	-5.7	11.3	At tube-to-end plate fillet weld toe on the tube wall left bend (at 0°)[d]	1.38	.27E+06			1.75	.47E+06	
			-5.7	11.3								
Jacket Retrofit	Type XI	Jacket Base	-5.0	10.0	At tube-to-end plate weld toe on the tube wall (at 0°)[d]							Run-out at 8.16E+06 cycles
			-5.0	10.0	At tube-to-end plate weld toe on the tube wall (at 180°)[d]							Hand hole cracked at BL[d] and BR[d]
	Type X	Jacket Base	-5.0	10.0	At tube-to-end plate weld toe on the tube wall (at 0°)[d]							Run-out at 8.16E+06 cycles
			-5.0	10.0	At tube-to-end plate weld toe on the tube wall (at 180°)[d]							

* Note

a) Estimated life

b) Seperated cracks

c) Stress range considering contribution of backing ring

d) Identification of crack location

Sign/Signal Pole Base (Plan View)

Sign/Signal Arm Base (Plan View)

Highmast (Plan View)

Hand Hole (Front View)

Type VI (View opposite side of arm)
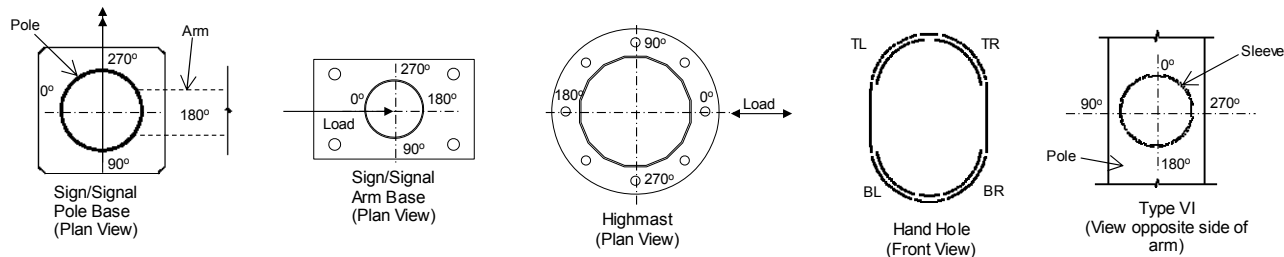
Table 6 Nomenclature of Geometric Parameters

Nomenclature	Parameter
D_{BC}	Diameter of circle through the fasteners in the transverse plate
D_{OP}	Diameter of concentric opening in the transverse plate
D_T	External diameter of a round tube or outer opposite flat-to-flat distance of a multi-sided tube at top of transverse plate
h_{ST}	Height of longitudinal attachment (stiffener)
N_B	Number of fasteners in the transverse plate
N_{ST}	Number of longitudinal attachment (stiffener)
t_{ST}	Thickness of longitudinal attachment (stiffener)
t_T	Thickness of tube
t_{TP}	Thickness of transverse plate
C_{BC}	$\dfrac{D_{BC}}{D_T}$
C_{OP}	$\dfrac{D_{OP}}{D_T}$

Table 7 Range of Parametric Study Variables for Fillet-welded Tube-to-Transverse Plate Connections

N_B	t_{TP} (in)	C_{BC}	D_T (in)	t_T (in)
4	2.0, 2.5, 3.0	1.25, 1.5, 1.75, 2.1	10.0, 13.0, 18.0	0.179, 0.239, $^5/_{16}$, $^3/_8$
6	2.0, 2.5, 3, 3.5	1.25, 1.5, 1.75, 2.1	10.0, 13.0, 18.0	0.179, 0.239, $^5/_{16}$, $^3/_8$
8	2.0, 2.5, 3.0, 3.5, 4.0	1.25, 1.5, 1.75	13.0, 18.0, 24.0	0.239, $^5/_{16}$, $^3/_8$, $^1/_2$
12	2.5, 3.0, 3.5, 4	1.25, 1.5, 1.75	13.0, 18.0, 24.0, 30.0	$^5/_{16}$, $^3/_8$, $^1/_2$
16	2.5, 3.0, 3.5, 4.0	1.25, 1.5	18.0, 24.0, 30.0	$^5/_{16}$, $^3/_8$, ½

164

Table 8 Range of Parametric Study Variables for Groove-welded Tube-to-Transverse Plate Connections

N_B	t_{TP} (in)	C_{OP} (%)	C_{BC}	D_T (in)	t_T (in)
4	2.0, 2.5, 3.0	40, 55, 70, 85, max.[*]	1.25, 1.5, 1.75, 2.1	10.0, 13.0, 18.0	0.179, 0.239, $5/16$, $3/8$
6	2.0, 2.5, 3.0, 3.5	40, 55, 70, 85, max.[*]	1.25, 1.5, 1.75, 2.1	10.0, 13.0, 18.0	0.179, 0.239, $5/16$, $3/8$
8	2.0, 2.5, 3.0, 3.5, 4.0	40, 55, 70, 85, max.[*]	1.25, 1.5, 1.75	13.0, 18.0, 24.0	0.239, $5/16$, $3/8$, $1/2$
12	2.5, 3.0, 3.5, 4.0	40, 55, 70, 85, max.[*]	1.25, 1.5, 1.75	13.0, 18.0, 24.0, 30.0	$5/16$, $3/8$, $1/2$
16	2.5, 3.0, 3.5, 4.0	40, 55, 70, 85, max.[*]	1.25, 1.5	18.0, 24.0, 30.0	$5/16$, $3/8$, ½

* max. = $\max(D_{OP})/(D_T)$; $\max(D_{OP}) = D_T - 2\times$(backing ring thickness + backing ring weld size)

165

Table 9 Range of Parametric Study Variables for Stiffened Tube-to-Transverse Plate Connections

N_{ST}	D_T (in)	h_{ST} (in)	t_T (in)	t_{ST} (in)
6, 8, 12	24.0	12.0, 18.0, 24.0, 30.0	$^5/_{16}$	$^1/_4$, $^5/_{16}$, $^3/_8$, $^1/_2$
			$^3/_8$	$^5/_{16}$, $^3/_8$, $^1/_2$, $^5/_8$
			$^1/_2$	$^3/_8$, $^1/_2$, $^5/_8$, $^3/_4$
			$^5/_8$	$^1/_2$, $^5/_8$, $^3/_4$, $^7/_8$
	30.0	18.0, 24.0, 30.0, 36.0	$^5/_{16}$	$^1/_4$, $^5/_{16}$, $^3/_8$, $^1/_2$
			$^3/_8$	$^5/_{16}$, $^3/_8$, $^1/_2$, $^5/_8$
			$^1/_2$	$^3/_8$, $^1/_2$, $^5/_8$, $^3/_4$
			$^5/_8$	$^1/_2$, $^5/_8$, $^3/_4$, $^7/_8$
	36.0	24.0, 30.0, 36.0, 42.0	$^5/_{16}$	$^1/_4$, $^5/_{16}$, $^3/_8$, $^1/_2$
			$^3/_8$	$^5/_{16}$, $^3/_8$, $^1/_2$, $^5/_8$
			$^1/_2$	$^3/_8$, $^1/_2$, $^5/_8$, $^3/_4$
			$^5/_8$	$^1/_2$, $^5/_8$, $^3/_4$, $^7/_8$

Table 10 Range of Parametric Study Variables for Multi-sided Sections

D_T (in)	r_b (in)	N_S	t_T (in)
10.0	1.0, 2.0, 3.0	8, 12	0.179, 0.239, $^5/_{16}$
13.0	1.0, 2.0, 3.0	8, 12	0.179, 0.239, $^5/_{16}$
18.0	1.0, 2.0, 4.0	8, 12, 16	0.239, $^5/_{16}$, $^5/_8$
24.0	1.0, 4.0, 6.0	12, 16, 20	$^5/_{16}$, $^5/_8$, $^1/_2$

166

CHAPTER 3

INTERPRETATION AND APPRAISAL OF RESULTS

EVALUATION OF FATIGUE TEST RESULTS

S-N plots of the fatigue test results are presented in Figures 114 through 132, against the fatigue design curves of the *AASHTO LRFD Bridge Design Specifications*. Also shown on these plots are the predicted fatigue lives of the various critical details and the estimated CAFT determined by the proposed analytical protocols. All fatigue test results were plotted as nominal stresses versus the life based on the failure criterion defined in the experimental protocol.

Specimen Type I

Fatigue test results of specimen Type I are shown in Figure 114. The fillet-welded tube-to-transverse plate connections at the arm and pole base exhibited a lower bound fatigue resistance of Category E´ in the finite life region consistent with the analytical prediction. Except at the pole base in specimen I-7, tested at a nominal stress range of 4 ksi (28 MPa), no fatigue cracking was observed in the tube-to-transverse plate connections when tested at or below a stress range of 4.5 ksi (31 MPa), the CAFT of AASHTO fatigue Category E, which is defined as the CAFT for this specimen geometry. The analytically predicted CAFT for this detail was 6 ksi (41 MPa).

Specimen Type II

The full-penetration groove-welded connections at the arm base in specimens Type II demonstrated a fatigue resistance exceeding AASHTO Category E against crack growth at the toe of the backing ring-to-tube weld at the top and the tube-to-transverse plate weld on the tube (Figure 115).

Only one of the poles in Type II specimens developed fatigue cracking at the full-penetration groove-welded tube-to- transverse plate weld toe on the tube. This detail exhibited a fatigue resistance slightly less than Category E´.

Specimen Type III

Fatigue test results of Specimen Type III are shown in Figure 116. The full-penetration groove-welded tube-to-transverse plate connections at the arm base in specimen Type III exhibited a lower bound fatigue resistance of AASHTO Category E in the finite life region. The predicted finite life fatigue resistance of this detail was slightly less than Category E. None of the full-penetration groove-welded tube-to-transverse plate connections at the arm base or the pole base developed fatigue cracking when tested at or below a stress range of 10.0 ksi (69 MPa), the CAFT of AASHTO fatigue Category C, which is defined as the CAFT of the groove-welded connections in this test geometry. The predicted CAFT of the mast-arm connection was 7 ksi (48 MPa) and that of the pole connection was 12 ksi (83 MPa).

167

The test results demonstrated significant variability in fatigue performance primarily due to the deviation in the as-fabricated weld shape and angle from the specified weld angle of 30^0. For example, the profiles of welds at the sections of crack initiation are shown in Figure 133 for specimens III-8 and III-9, which demonstrated significantly different lives when tested at identical stress ranges. As is evident in Figure 134, the crack in specimen III-9 initiated at a location where the weld profile changed significantly, causing a higher stress concentration. It appears that the shallow last pass of the weld in specimen III-9 was due to an attempt to produce the specified weld angle of 30^0. The weld angles at the points of crack initiation in specimens III-8 and III-9 were 22.2^0 and 46.1^0 respectively. As was noted during this research, the weld shape and angle has a significant effect on the fatigue performance of welded connections in these thin walled tubular structures. From analytical studies it was evident that the variation in fatigue resistance was more significant for a decrease rather than an increase in the weld angle from the specified value of 30^0.

Seven of the poles in specimens Type III failed by developing fatigue cracks from the edge of the unreinforced handhole when subjected to nominal stress ranges of 10.5 ksi (72 MPa) and 12.5 ksi (86 MPa) at the cracked section. The cracks initiated at the arc transition to the vertical edge of the hand hole opening and progressed into the pole tube normal to the principal stress at the section. Because of the relatively high stress, progression of these cracks through the pole tube was quite fast and most of the fatigue life was expended during the initiation of the cracks. As seen in Figure 117, this unreinforced handhole detail exhibited a fatigue resistance of Category E, although one data point fell along Category E´. When adjusted for the stress concentration effects due to the hand hole opening in the pole tube, which was determined from FEA as approximately 4.0, the fatigue resistance of this detail exceeded that of AASHTO Category A. Since Category A classifies fatigue resistance associated with crack growth in base metal, the finding demonstrated that the handhole details were consistent with AASHTO fatigue classifications.

Specimen Type IV

Fatigue test results of specimens Type IVA and Type IVB are shown in Figures 118 and 119 respectively. The performance of the groove welded connections in the arms and poles of specimens Type IVA were consistent with similar groove welded connections in specimens Type III. None of the groove welded connections developed fatigue cracking when tested at a stress range below 12 ksi (83 MPa). The groove welded connections in the test geometry exhibited a lower bound fatigue resistance of Category E in the finite life and Category C in the infinite life.

None of the groove welded details in the specimens Type IVB developed fatigue cracking. Fatigue test results of specimens Type IVA and IVB are compared in Figure 120. The performance of the groove welded connections in specimens Type IVB under out-of-plane loading was consistent with similar groove welded connections in specimens Type IVA that were tested under in-plane loading, and no effect of out-of-plane loading was evident.

Specimen Type V

All Type V specimens developed fatigue cracks at the fillet-welded arm-to-clamp weld toe on the clamp, which was contrary to the FEA results for this connection. The contour of maximum principal stresses obtained from FEA (Figure 135) showed significantly higher stress

168

at the weld toe on the arm tube, where the fatigue cracking was expected. Stresses measured on the arm and the clamp adjacent to the respective weld toes also confirmed the FEA results (Figure 136). A closer inspection of the weld toe on the clamp at the crack location (Figure 137) indicated a sharper termination and undercut of the weld toe on the clamp, which would explain the unexpected cracking.

The arm-to-clamp connection in specimen Type V exhibited a lower bound fatigue resistance of AASHTO Category E in the finite life (Figure 121). The fatigue resistance of this connection was estimated as E´ as per the analytical protocol, but against crack growth at the fillet weld toe on the arm tube.

As shown in Figure 122, none of the full-penetration groove-welded tube-to-transverse plate connections at the pole base in specimens Type V developed fatigue cracking when tested at a stress range below 12 ksi (83 MPa). The CAFT of this detail is defined is 10.0 ksi (69 MPa) corresponding to the CAFT of AASHTO Category C.

Specimen Type VI

Fatigue cracking of the partial-penetration groove-welded connection between the arm-sleeve and the pole in specimens Type VI occurred at the weld toe on the sleeve in all specimens, which was contrary to the FEA results. The contour of maximum principal stresses obtained from FEA (Figure 138) showed high stress concentration at the toe of the arm-sleeve-to-pole weld on the pole tube in the middle of the lower quadrant. The direction of the principal stress at this location was vertical and therefore was not normal to the weld toe. The maximum stress normal to the weld toe occurred higher up in the quadrant and its position in the quadrant was consistent with the observed cracking at the weld toe, but on the pole tube. Subsequent investigation of the as fabricated weld between the sleeve and the pole revealed a much sharper toe on the sleeve compared to that on the pole (Figure 139). The measured stress normal to the weld at about 0.01 in (4 mm) from the weld toe was of higher on the sleeve compared to the pole. This explained the location of toe cracking on the sleeve rather than on the pole (Figure 140).

The partial-penetration groove-welded connection between the arm-sleeve and the pole in specimens Type VI exhibited a finite life fatigue resistance of AASHTO Category E against crack growth from the toe (Figure 123). Only specimen VI-4 achieved a fatigue resistance slightly less than Category E. None of these groove welded connections developed fatigue cracking when tested at a nominal stress range of 4.5 ksi (31 MPa). When tested at a nominal stress range of 7.7 ksi (53 MPa), all but one of the seven specimens developed fatigue cracks. Accordingly, the CAFT of the partial-penetration groove-welded connections between the arm-sleeve and the pole in specimens Type VI is defined as 4.5 ksi (31 MPa), the CAFT of AASHTO Category E.

Fatigue test results of groove welded pole-to-transverse plate connections in the poles of specimens Type VI are shown in Figure 124. Results of all groove-welded tube-to-transverse plate connections in round sections tested in this project are shown in Figure 125. Fatigue performance of the groove-welded connections in the poles of specimens Type VI was consistent with the respective GSCF.

None of the groove-welded tube-to-transverse plate connections at the pole base in Type VI specimens developed fatigue cracking when tested at a stress range below 12 ksi (83 MPa).

Accordingly, the CAFT of these details in the test geometry is defined as 10.0 ksi (69 MPa), the CAFT of AASHTO Category C.

Specimen Type VII

Fatigue test results of specimen Type VII with multi-sided cross section are shown in Figure 126. The fillet-welded tube-to-transverse plate connections in arms demonstrated a fatigue resistance of AASHTO Category E´ corresponding to a crack length of 5 in (127 mm). These cracks initiated at the outermost bend corners on the tension face and were detected very early into the fatigue tests. Once the cracks developed out of the corners into the flat faces, the crack propagation rate reduced.

The fillet welded tube-to-transverse plate connections in poles also exhibited early cracking at the outermost bend corners on the tension face and exhibited similar crack propagation. Due to higher GSCF in the pole compared to the arm, however, the details in the pole demonstrated a fatigue resistance less than AASHTO Category E´ corresponding to a crack length of 6½ in (165 mm), half the tube diameter (outer opposite flat-to-flat distance).

None of the type VII specimens developed fatigue cracks when tested at or below a stress range of 2.6 ksi (18 MPa), the CAFT of AASHTO fatigue Category E´. It appears that the CAFT of the fillet-welded connection for this specimen geometry is 2.6 ksi (18 MPa). The analytically predicted CAFT for this detail was 2.9 ksi (20 MPa).

Specimen Type IX

Fatigue test results of specimens Type IX are shown in Figure 127. The fillet-welded tube-to-transverse plate connections with stool type stiffeners exhibited a finite life fatigue resistance of Category E, against crack growth from the toe of the wrap-around weld at the termination of the vertical stiffeners on the tube, corresponding to a crack length of half the tube diameter (outer opposite flat-to-flat distance) or 12 in (305 mm). The predicted fatigue resistance of this detail for this cracking mode was AASHTO Category E´. The fatigue resistance corresponding to the first observation of cracking was Category E´. This detail, however, did not exhibit any fatigue threshold, even when tested at a nominal stress range of 4.5 ksi (31 MPa), the CAFT of AASHTO Category E. Accordingly, CAFT of this detail is recommended as 2.6 ksi (18 MPa), the CAFT of AASHTO Category E´.

Specimen Type X

Fatigue test results of specimen Type IX are shown in Figure 128. Two fillet-welded tube-to-transverse plate connections at the pole base in specimens Type X exhibited a fatigue resistance of AASHTO Category E against fatigue cracking at the weld toe on the tube. The other specimen achieved a fatigue resistance of Category E´. One of these specimens was run-out twice, when tested at nominal stress ranges of 5.4 ksi (37 MPa) and 8 ksi (55 MPa) respectively. Due to lack of sufficient data, and to be consistent with the performance of details with similar stress concentration, the CAFT of this detail in the connection geometry was proposed as 4.5 ksi (31 MPa), the CAFT of AASHTO Category E.

Specimen Type XI

The groove-welded tube-to-transverse plate connection in specimens Type XI exhibited a lower bound fatigue resistance exceeding AASHTO Category E´ and approaching Category E (Figure 129), against crack growth at the toe of the fillet reinforcement on the tube. The predicted fatigue resistance of this detail in the finite life region was Category E´. The minimum fatigue resistance of the fillet weld at the top of backing ring against cracking at the weld toe on the tube exceeded AASHTO Category E. The predicted fatigue resistance of this detail was slightly less than Category D. None of the groove welded connections developed fatigue cracking when tested at or below a stress range of 7 ksi (48 MPa). As such, the CAFT for this detail is defined as 7.0 ksi (48 MPa), the CAFT of AASHTO Category D.

Specimen Type XII

Fatigue test results for Type XII specimens are shown in Figures 130 and 131. The stiffened fillet-welded tube-to-transverse plate connections in the test geometry exhibited a lower bound fatigue resistance exceeding AASHTO Category E (Figure 130). These specimens developed fatigue cracking at the stiffener-to-tube weld toe on the tube at the termination of the stiffener, where the predicted fatigue resistance was AASHTO Category E´.

The predicted fatigue resistance against crack growth at the tube-to-transverse plate weld toe on the tube at the pole base was greater than AASHTO Category E´ (Figure 131). Fatigue cracking developed at this detail in only three specimens (XII-1, XII-8, and XII-10). In two of these specimens the crack was first observed near the predicted life. However, the crack growth was inhibited by the fatigue cracking at the stiffener termination, and none of the cracks grew to the failure criteria of 12 in (305 mm), i.e., half the tube diameter. In specimen XII-8, fatigue cracking was observed early at both the stiffener termination and at the fillet weld toe on the tube at the pole base. However, the fatigue life corresponding to a crack length of half the tube diameter (outer opposite flat-to-flat distance) at the stiffener termination exceeded the AASHTO Category E design life. The maximum crack length at the fillet weld toe at the pole base was about 8 in (204 mm), when the test was terminated.

Except for specimen XII-6, none of the stiffener-to-tube weld at the stiffener termination developed fatigue cracking when tested below a stress range of 10.0 ksi (69 MPa), the CAFT of AASHTO Category C (Figure 130). The fatigue crack in Specimen XII-6 initiated at the weld root and proceeded through the weld throat and into the tube wall. The exposed fracture surface (Figure 60) indicated that the fatigue crack grew from a relatively large lack of fusion in the wrap around stiffener-to-tube weld root, causing fatigue cracking at a nominal stress range of 7 ksi (48 MPa). Ignoring this result for an unusually large fabrication defect at the weld root, it is concluded that the CAFT of the stiffener-to-tube weld at the stiffener termination due to fatigue cracking from the weld toe is 7.0 ksi (48 MPa), the CAFT of AASHTO fatigue Category D. The analytically predicted CAFT was about 10 ksi (69 MPa).

Jacket Retrofits JRX and JRXI

Fatigue test results of jacket retrofitted specimens JRX and JRXI are shown in Figure 132. The full-penetration groove-welded jacket tube-to-transverse plate connection demonstrated a CAFT of 10 ksi (69 MPa), the CAFT of AASHTO Category C, for the retrofit jackets of the test geometry. The predicted CAFT of this detail was 12 ksi (83 MPa).

171

FATIGUE RESISTANCE OF UNSTIFFENED POLE-TO-TRANSVERSE PLATE FILLET WELDED CONNECTIONS

Fatigue test results of all fillet welded tube-to-transverse plate connections in round and multi-sided sections tested in this research and reported TPF-5(116) Study (*18*) are presented in Figures 141 and 142. All test results are for transverse plate thickness of 2 (51 mm) or greater. Significant scatter in fatigue performance was evident due to the large variability in weld geometry as discussed earlier.

Fatigue Resistance for Finite Life

In Figure 141, the test results are grouped according to their cross-section and respective GSCF as obtained from the FEA of the specimen models. Also shown on the plot are the stress concentration factors as obtained from Equation 3, which was developed based on parametric study results, and identified as fatigue stress concentration factor for finite life, K_F. The small difference in these two factors is due to the correlation error between the regressed equation and the GSCFs obtained from the FEA. The GSCF for round sections ranges between 2.0 and 2.6, and that for multi-sided sections ranged between 2.3 and 3.0. The plot shows that the multi-sided sections with higher GSCF produced lower fatigue resistance. In the finite life region, all connections having GSCF less than or equal to 2.8 exhibited a lower bound fatigue resistance of AASHTO Category E´. The three multi-sided specimens (Type VII poles) having a GSCF of 3.0 demonstrated a fatigue resistance less than Category E´. Thus, lower bound or design fatigue resistance of fillet-welded tube-to-transverse plate connections in round and multi-sided sections is defined as Category E´ for finite life, with their GSCF limited to 2.8.

Fatigue Resistance for Infinite Life

In Figure 142 the test results are grouped in terms of NSCF, as obtained from the FEA of the specimen models. Also shown on the plot are the stress concentration factors as obtained from Equation 10 (in conjunction with Equation 3), and identified as fatigue stress concentration factor for infinite life, K_I. The NSCF for round sections ranged between 4.5 and 5.6, and that for multi-sided sections ranged between 4.5 and 7.0. The range of NSCF in multi-sided sections is much larger compared to their GSCF and consisted of two distinct data set. One data set belonged to sections having 16 sides and 4 in (102 mm) internal bend radius with NSCF ranging between 4.5 and 5.6 (similar to a round section), and the other data set belonged to sections having eight sides and approximately 0.5 in (13 mm) bend radius with NSCF of about 7.0. The plot shows that the connections having NSCF less than or equal to 5.6 demonstrated a CAFT of 4.5 ksi (31 MPa), the CAFT of AASHTO Category E. The connections having NSCF greater than 5.6 and less than 7.0 exhibited a CAFT of 2.6 ksi (18 MPa), the CAFT of AASHTO Category E´.

Effect of Tube Cross-section

Fatigue performance of fillet-welded tube-to-transverse plate connections in round and multi-sided sections are compared in Figure 143 for identical connection geometry (Type I and Type VII specimens). As the plot shows, fatigue cracking initiated very early in the multi-sided sections, but the life at a crack length of half the tube diameter (the failure criteria used in this

172

research as per the experimental protocol) was similar to that of round tubes. As discussed earlier, the cracks initiated at the outermost bend corner on the tension face and their propagation rate reduced once the cracks developed out of the corners into the flat faces.

Figure 144 shows the distribution of geometric stresses in the longitudinal (meridional) direction around the perimeter at the tube-to-transverse plate fillet-welded connections in the round and multi-sided sections (see Figure 143 for connection geometry) as obtained from FEA. As is evident, a higher geometric stress occurred at the bend corner of multi-sided tube compared to the stress in the round tube at the same circumferential position. The stress in the multi-sided tube then decreased compared to the stress in the round tube, as the circumferential position moved towards the center of flat side. This would explain the reason for decreased crack growth rate in the multi-sided tubes as the crack progressed out of the bend corner. The behavior could be interpreted as the bend corner behaving as a stiffener to the flat face, which would disappear as the multi-sided section approaches round. This stiffening effect also shows the dependence of the GSCF on the geometry of the multi-sided tube.

Figure 145 compares the distribution of maximum principal stresses in the round and multi-sided tubes (see Figure 143 for connection geometry) along a path on the tube surface originating at the highest stressed weld toe location and extending normal to the transverse plate. In the round tube the path is located at the mid plane of the tube and in the multi-sided tube the path in located on the bend corner. As is evident the stress profiles were similar and produced similar GSCF (2.6 for the round tube and 2.8 for the multi-sided tube) at $0.1\sqrt{(r \times t)}$ ahead of the weld toe. This explains the similar finite life performance exhibited by the round and multi-sided tubes.

Figure 146 plots the variation of notch stresses in two multi-sided sections with respect to bend radius. The notch stresses are normalized with respect to the notch stresses in similar round tubes. Also shown on the plots are the respective roundness factors as computed based on Equation 2. The plot shows that the notch stress in the eight-sided tube with about 0.5 in (13 mm) bend radius is significantly higher (~1.5 times) compared to a round tube, which explains the early cracking in these sections. The notch stress decreased significantly for a sixteen-sided tube with 4 in (102 mm) bend radius. In the eight-sided tube similar decrease in notch stress can be achieved with a bend radius of about 2 in (51 mm). Since, the infinite life performance of a connection is dependent on the notch stress, the CAFT of multi-sided tubes with less sides and sharper bend radius (producing smaller roundness) is expected to be lower.

Although the multi-sided sections with eight sides and about 0.5 in (13 mm) bend radius demonstrated similar GSCF as round sections, their NSCF was much higher compared to round sections or multi-sided sections with 16 sides and 4 in (102 mm) internal bend radius, and thus exhibited lower CAFT. This explains the early cracking observed in this tube geometry when tested at a higher stress range. It is evident that the bend radius and number of sides in a multi-sided section have a significant effect on the CAFT of the details. The effects of multi-sided sections are further discussed later in this chapter. The results demonstrated that NSCF characterizes the infinite life fatigue performance of tubular connections; GSCF only captures the geometric effects and is not appropriate for assessing infinite life performance.

173

FATIGUE RESISTANCE OF UNSTIFFENED POLE-TO-TRANSVERSE PLATE GROOVE WELDED CONNECTIONS

Fatigue test results of all full-penetration groove welded tube-to-transverse plate connections in round and multi-sided sections tested in this research and reported TPF-5(116) Study (*18*, *27*, *28*) only the results available at the time of preparing this report) are presented in Figures 147 and 148. All test results are for transverse plate thickness of 2 in (51 mm) or greater. Significant scatter in fatigue performance was evident due to the large variability in weld geometry as discussed earlier.

Fatigue Resistance for Finite Life

In Figure 147, the test results are grouped according to their GSCF as obtained from the FEA of the specimen models. Also shown on the plot are the stress concentration factors as obtained from Equation 4, which was developed based on parametric study results, and identified as K_F. The small difference in these two factors is due to the correlation error between the regressed equation and the GSCFs obtained from the FEA. As is evident, the connections with smaller stress concentration factors exhibited better fatigue performance. In the finite life region, the connections having GSCF in the range of 1.6 to 2.3 exhibited a lower bound fatigue resistance of AASHTO Category E´. The connections having GSCF in the range of 1.2 to 1.6 exhibited a lower bound fatigue resistance of AASHTO Category D. Based on the test results, the GSCF of the groove-welded tube-to-transverse plate connections are limited to 2.3, corresponding to AASHTO Category E´.

Fatigue Resistance for Infinite Life

In Figure 148, the test results are grouped in terms of NSCF, as obtained from the FEA of the specimen models. Also shown on the plot are the stress concentration factors as obtained from Equation 10 (in conjunction with Equation 4), and identified as K_I. The connections having NSCF less than or equal to 5.1 did not develop any fatigue cracking when tested at or below a stress range of 7.0 ksi (48 MPa), the CAFT of AASHTO Category D. None of the connections having NSCF less than or equal to 3.2 developed fatigue cracking when tested at or below a stress range of 10.0 ksi (69 MPa), the CAFT of AASHTO Category C.

Two connections having GSCF of about 2.9 were tested in TPF-5(116) Study (*18*), and demonstrated a finite life fatigue resistance less than Category E´ (Figure 147). Infinite life performance of these connections, having NSCF of about 7.0, was not experimentally determined. Based on analytical assessment, the CAFT of the connections for NSCF in the range of 5.1 and 7.2, is proposed as 4.5 ksi (31 MPa), the CAFT of AASHTO Category E (Figure 148).

Effect of Opening Ratio

Figure 149 shows the effect of opening in the transverse plate on the fatigue performance of groove-welded tube-to-transverse plate connections tested in this research. The results are grouped in terms of % opening ratio, C_{OP}, which is the ratio of opening diameter to the tube diameter. To evaluate only the effect of opening size, the results of connections in round tubes of similar geometry are presented. Also shown on this plot are the results of round fillet-welded tube-to-transverse plate connections of comparable geometry, which represented 100% opening.

174

The data shown are for fatigue cracking at the weld toe on the tube. As the plot shows, with reduced opening ratio the GSCF reduced and the fatigue performance improved. It is evident, that the reduced opening ratio provided significant improvement in the fatigue resistance of the groove-welded tube-to-transverse plate connections by reducing the transverse plate flexibility. As a result, groove-welded connections exhibited significantly better fatigue resistance compared to fillet-welded connections in identical structures.

Figure 157 compares the fatigue test results of fillet- and groove-welded tube-to-transverse plate connections in high-level luminaire support structures with identical cross section — 16 sides, 4 in (102 mm) internal bend radius, and 24 in (610 mm) outer opposite flat-to-flat distance. The fillet welded connection had a 3 in (76 mm) base plate with 16 bolts at a bolt circle ratio of 1.25, producing a GSCF of 2.3. The base plate in the groove-welded connection was 2.5 in (64 mm) thick, and had a 60% opening. Eight bolts were used at a bolt circle ratio of 1.25. The GSCF of this connection was 2.2. As the plot shows, both connections with similar GSCF provided similar performance. The results showed the significance of opening size in reducing the flexibility of the transverse plate. With a 40% reduced opening, the thickness of the transverse plate could be reduced from 3 in (76 mm) to 2.5 in (64 mm), and the number of bolts could be reduced from 16 to eight.

Effect of Backing Ring Weld

Full-penetration groove-welded tube-to-transverse plate connections are usually fabricated with a backing ring. In galvanized structures, the backing ring is often welded to the plate and the tube to avoid ingress of acid in the gaps between the backing ring, the tube and the plate during pickling in the galvanizing process. Any trapped acid in the gaps may cause crevice corrosion or hydrogen related cracking, when exposed to moisture in service. As such, this weld is commonly termed as seal weld. If the backing ring is welded to the plate and the tube, it participates in transferring forces from the tube to the transverse plate, and fatigue cracking can occur both at the backing ring top weld toe on the tube, and the groove weld toe on the tube. The amount of force that is transferred through the backing ring and the resulting stress concentration at the backing ring weld toe depends on the diameter and thickness of the tube, and the height and thickness of the backing ring. When the backing ring is welded to the tube it provides a redundant load path after the tube to transverse plate groove-weld develops fatigue cracking.

Figure 151 shows the fatigue test results of groove welded tube-to-transverse plate connections with the backing ring welded to the tube. All backing rings were specified as 2 in × ¼ in (51 mm × 6 mm). As is evident, fatigue cracking occurred both at the groove-weld toe and the backing ring top weld toe on the tube, exhibiting similar life. Except in one tube of 10 in (254 mm) diameter (specimen II-1 mast-arm), the backing ring weld toe developed fatigue cracking after cracking of the groove-weld toe on the tube. FEA results showed that the GSCF at the backing ring weld toe in an un-cracked specimen was significantly smaller than at the groove weld toe, explaining the sequence of fatigue cracking at these two welds. However, due to cracking of the tube at the groove-weld toe all stresses deviate into the backing ring, increasing the stress concentration at the backing ring weld toe and causing cracking at this weld toe soon after.

The cracking at the backing ring weld prior to the groove-weld was due to inadequate quality of the backing ring-to-tube weld. Figures 152 through 154 show the examples of less than

175

desirable quality of backing ring-to-tube weld in 10 in (254 mm) diameter tubes that would precipitate fatigue cracking at this detail and limit the connection fatigue performance. The primary reason for this inadequate quality is the insufficient access in smaller diameter tubes, which prevents ensuring weld quality between the tube and the backing ring. The other reason is the lack of attention to this weld as it is defined as "seal weld" and therefore perceived as nonstructural. It is recommended that the backing ring be welded to the tube only in larger diameter tubes (16 in [406 mm] or above), where sufficient access can control the quality of this weld adequately. When performed, this weld should be specified and inspected as a structural weld.

In galvanized structures, if the backing ring is not welded to the plate or to the tube wall, all resulting gaps should be sealed by caulking after galvanizing to prevent ingress of moisture and resulting activation of any trapped acid. The backing ring should not be tack-welded to the tube, as premature fatigue cracking from tack welds can limit fatigue performance of the connection. Grinding of tack welds in these thin tubular structures is discouraged.

FATIGUE RESISTANCE OF STIFFENED TUBE-TO-TRANSVERSE PLATE FILLET WELDED CONNECTIONS

Fatigue test results of optimized stiffened fillet-welded tube-to-transverse plate connections tested in this research are presented in Figure 155. These connections had a GSCF of 2.3 and exhibited a fatigue resistance of AASHTO Category E in the finite life region. The NSCF for these connections is 5.3. None of the connections developed fatigue cracking when tested at or below 7.0 ksi (48 MPa), the CAFT of AASHTO Category D. The fatigue resistance of the stiffened tube-to-transverse plate fillet-welded connections for crack growth at the stiffener termination is defined accordingly.

FATIGUE RESISTANCE OF HANDHOLES

Fatigue Resistance of Reinforced Handholes

Fatigue Cracking from Weld Root

Fatigue test results of reinforced handhole due to fatigue cracking from the root of the handhole frame-to-pole fillet-weld are shown in Figure 156.

When plotted against nominal stress computed on the section of the pole including the handhole and the reinforcement, these details exhibited a fatigue resistance of AASHTO Category E´. The opening in the handholes was about 40% of the tube diameter at the section and caused a stress concentration of about 4.0. When plotted against the nominal stress magnified by the stress concentration, the handhole detail exhibited fatigue resistance exceeding that of AASHTO Category A in the finite life. This finding is consistent with the fatigue category of a detail that develops fatigue cracking from the weld root, such as the longitudinal web-flange weld in plain welded beams, which is defined as AASHTO Category B. Only one reinforced handhole developed fatigue cracking from the root of handhole frame-to-pole fillet-weld, when tested at a magnified stress range of about 15 ksi (103 MPa), which is slightly less

than 16.0 ksi (110 MPa), the CAFT of AASHTO Category B. Thus, the fatigue resistance of reinforced handholes against fatigue cracking from the weld root is defined as AASHTO Category B, when the nominal stress is computed on the net section and is magnified by a stress concentration of 4.0.

Fatigue Cracking from Weld Toe

No fatigue cracking was detected from the toe of the handhole frame-to-pole weld. These results are plotted in Figure 157 against nominal stress computed on the section of the pole including the hole and the reinforcement. The maximum performance of this detail exceeded the lower bound fatigue life provided by AASHTO Category D both in the finite and infinite life regions. Thus, the fatigue resistance of reinforced handholes against fatigue cracking from the handhole frame-to-pole weld is defined as AASHTO Category D, when the nominal stress is computed on the net section.

Fatigue Resistance of Unreinforced Handholes

Figure 158 shows the fatigue test results of unreinforced handhole experiencing fatigue cracking from the edge.

When plotted against nominal stress computed on the pole section including the handhole, these details exhibited a fatigue resistance of AASHTO Category E´. The opening in the handholes was about 40% of the tube diameter at the section and caused a stress concentration of about 4.0. When plotted against the nominal stress magnified by the stress concentration, the handhole detail exhibited fatigue resistance exceeding that of AASHTO Category A in the finite life. This finding is consistent with the fatigue category of a detail that develops fatigue cracking from the base metal. None of the unreinforced handhole developed fatigue cracking when tested at a magnified nominal stress range less than 40 ksi (276 MPa), which is greater than 24.0 ksi (165 MPa), the CAFT of AASHTO Category A. Thus, the fatigue resistance of unreinforced handholes against fatigue cracking from the edge is defined as AASHTO Category A, when the nominal stress is computed on the net section and is magnified by a stress concentration of 4.0.

FATIGUE RESISTANCE OF PASS-THROUGH MAST ARM-TO-POLE CONNECTIONS

Fatigue test results of partial-penetration groove-welded arm-sleeve-to-pole connections are shown in Figure 159 in terms of GSCF and NSCF. All connections exhibited a fatigue resistance of AASHTO Category E in the finite life. None of these connections developed fatigue cracking when tested at or below 4.5 ksi (31 MPa), the CAFT of AASHTO Category E.
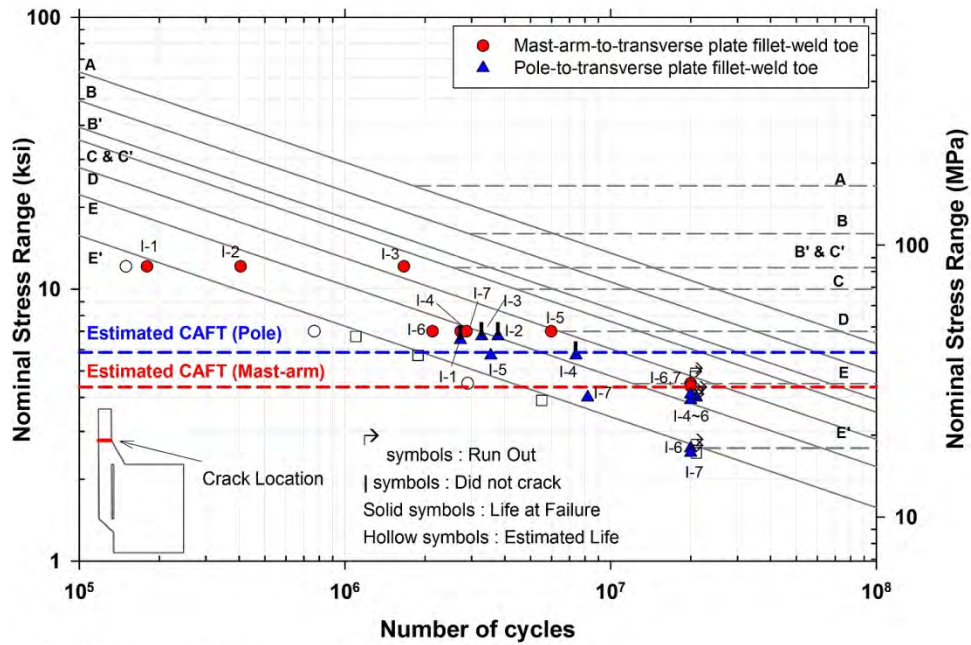
177

Figure 114 Fatigue test results for specimen Type I
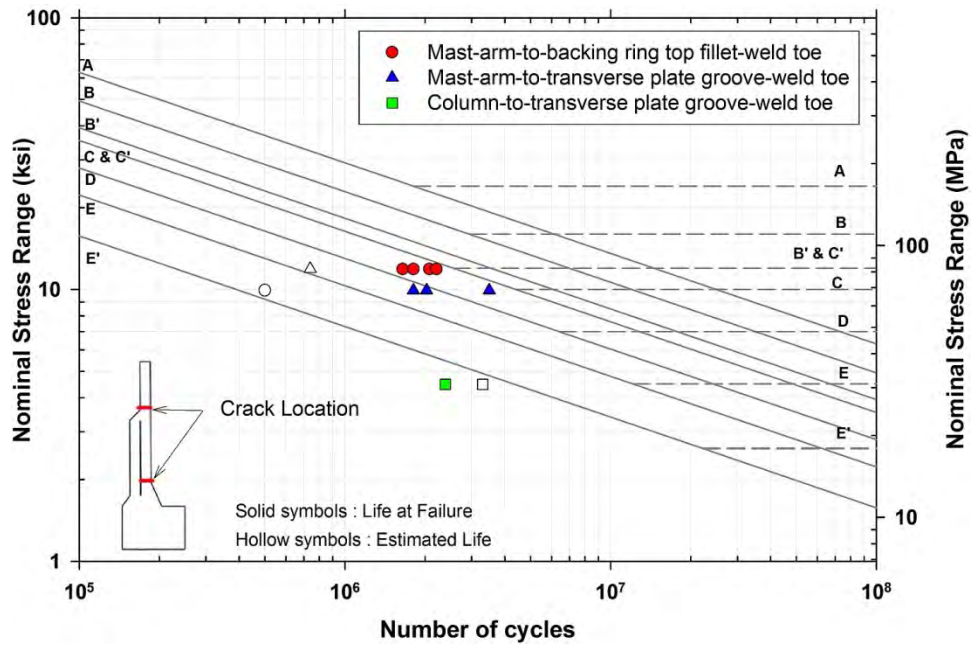

Figure 115 Fatigue test results for specimen Type II

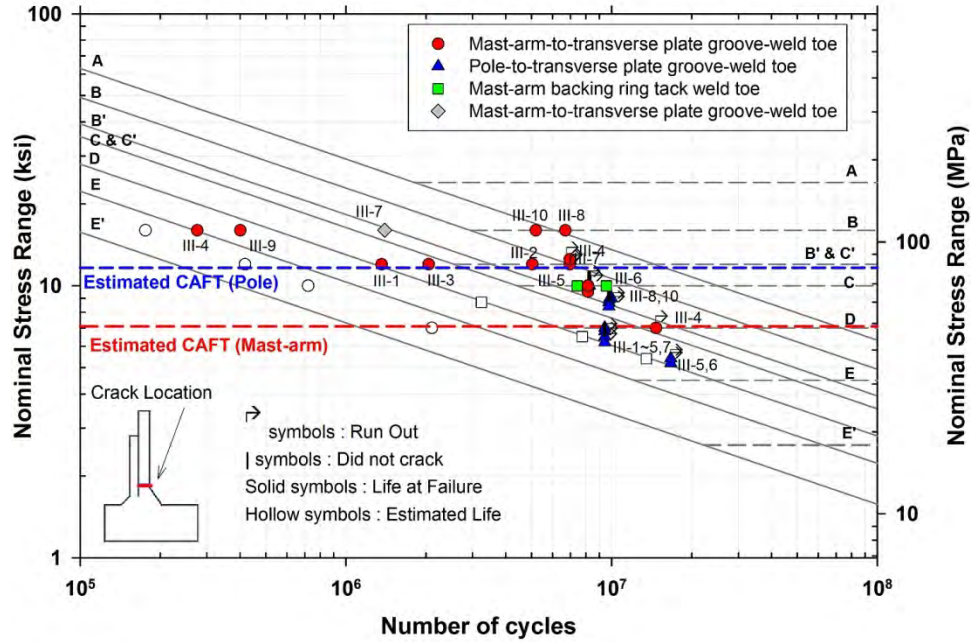178

Figure 116 Fatigue test results for specimen Type III

Figure 117 Fatigue test results for unreinforced handholes

179

Figure 118 Fatigue test results for specimen Type IV-A
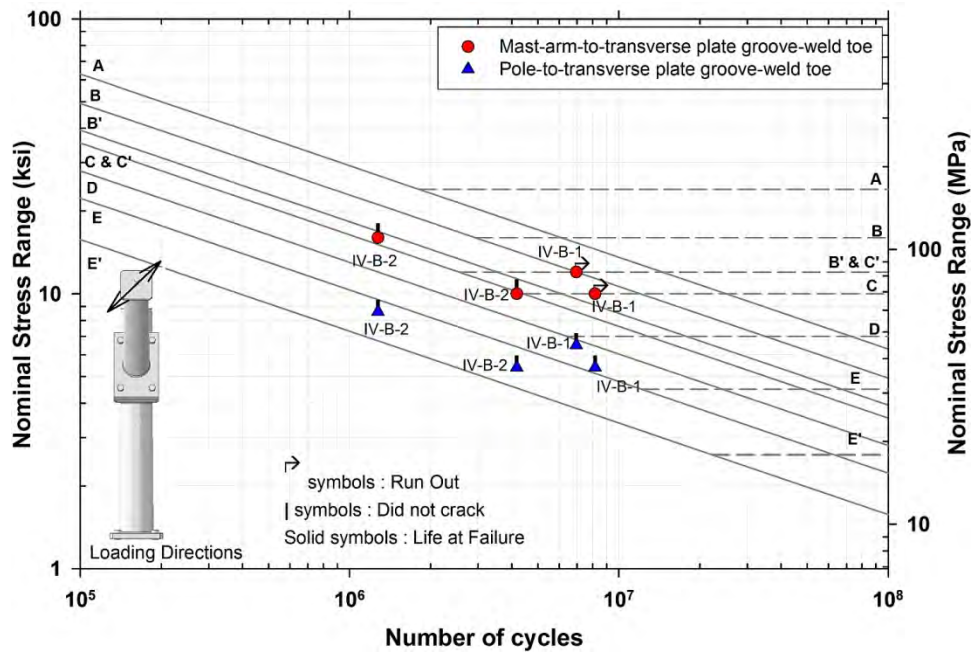
Figure 119 Fatigue test results for specimen Type IV-B

180
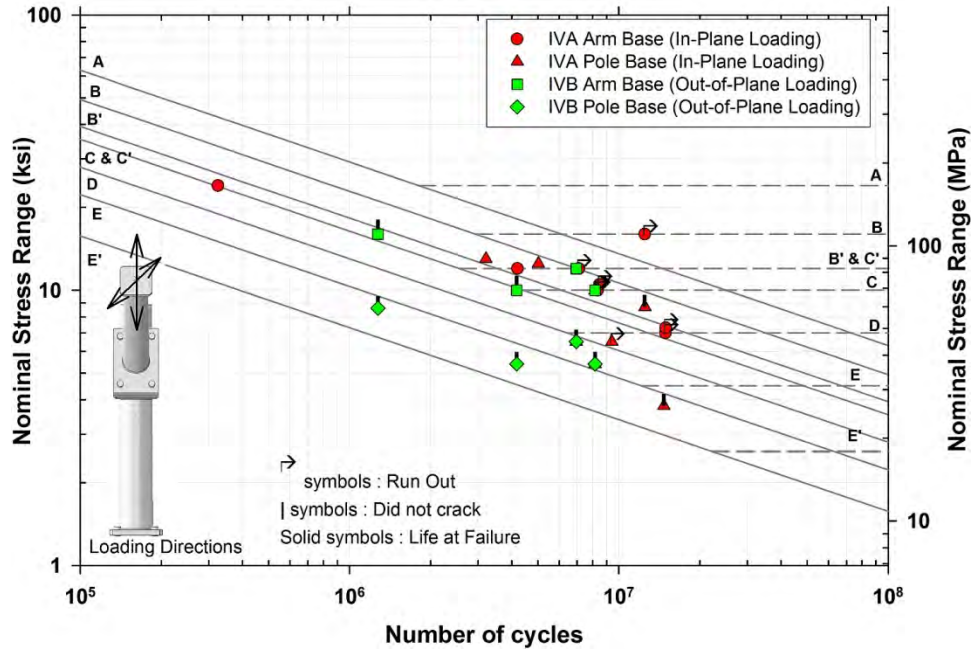
Figure 120 Comparison of fatigue test results for specimens Type IVA and IVB
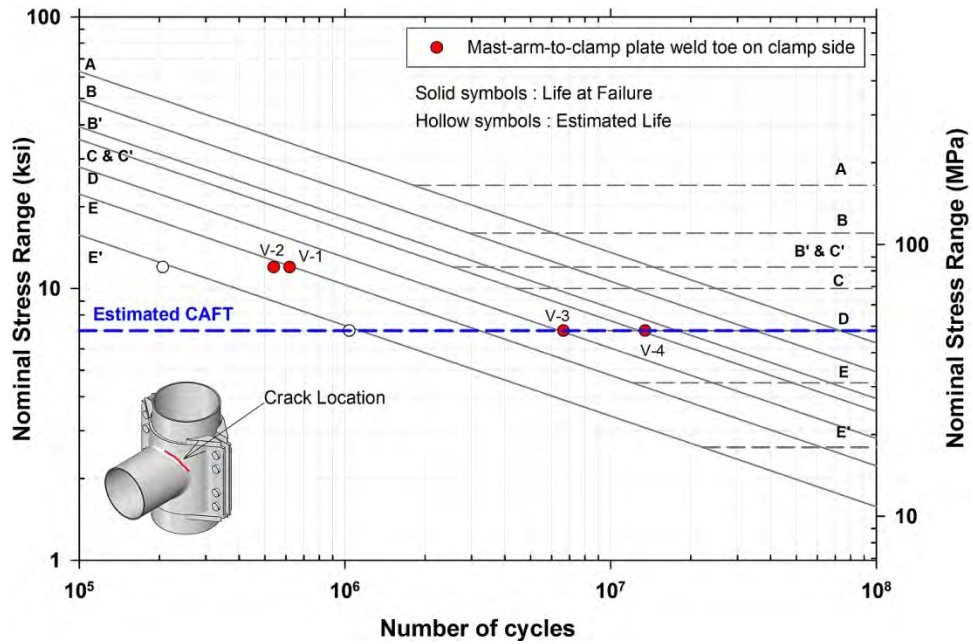
Figure 121 Fatigue test results for specimen Type V arm

181
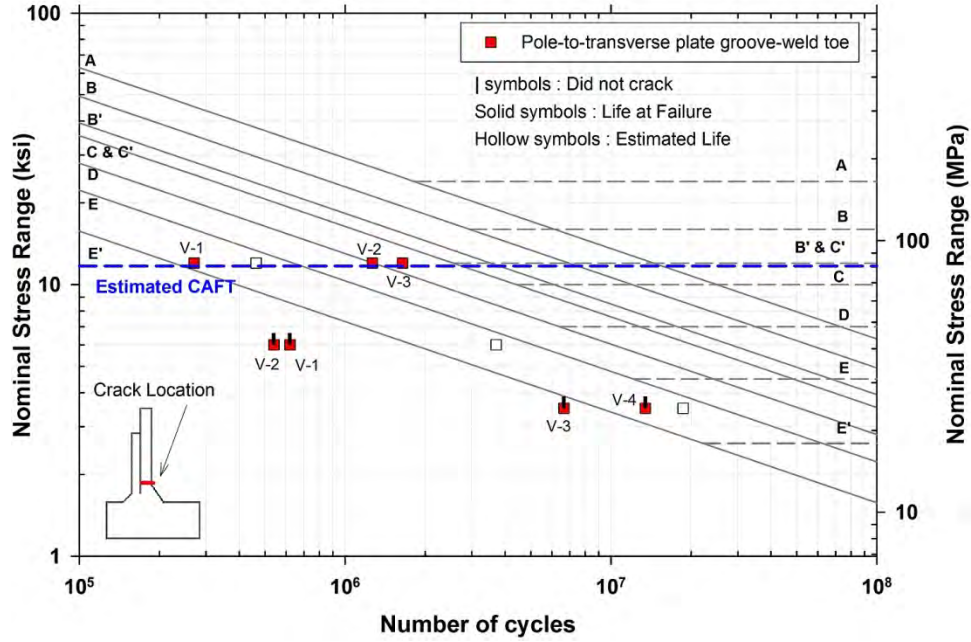
Figure 122 Fatigue test results for specimen Type V pole
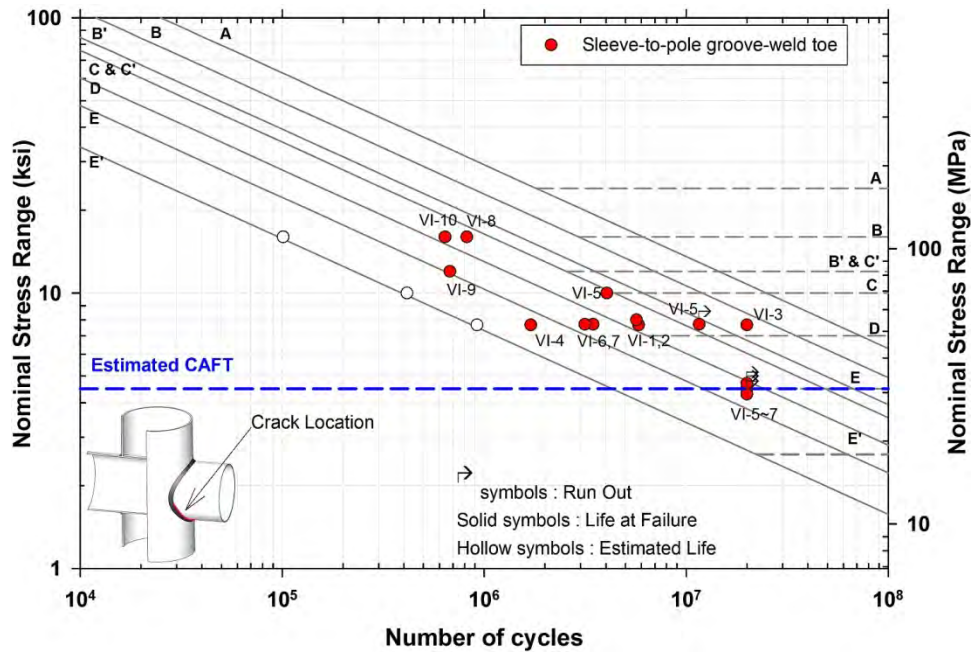
Figure 123 Fatigue test results for specimen Type VI mast arm

182
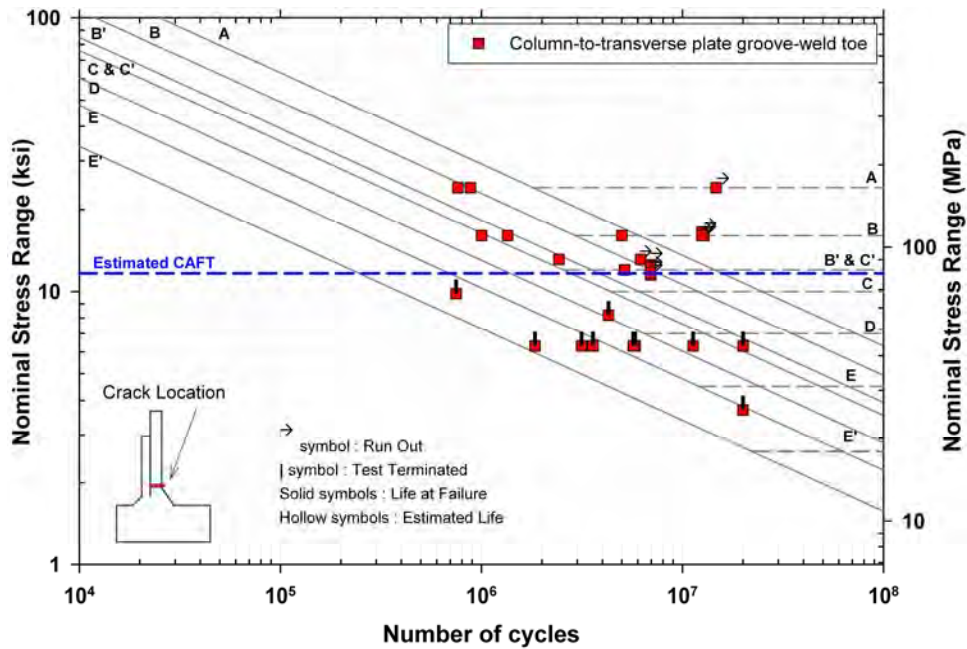
Figure 124 Fatigue test results for specimen Type VI column
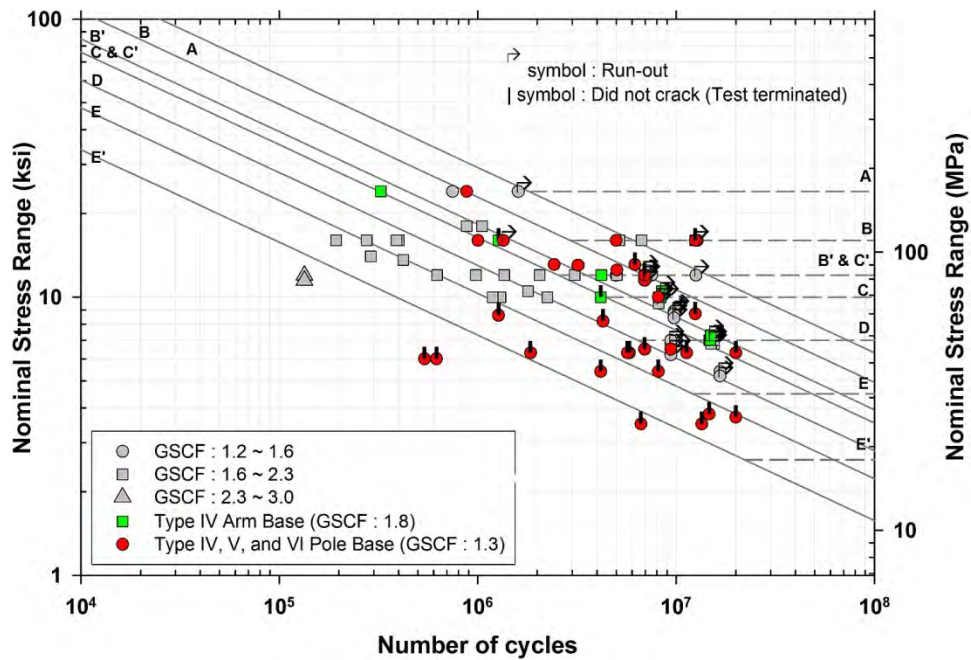
Figure 125 Comparison of fatigue performance of groove welded tube-to-transverse plate connections

183
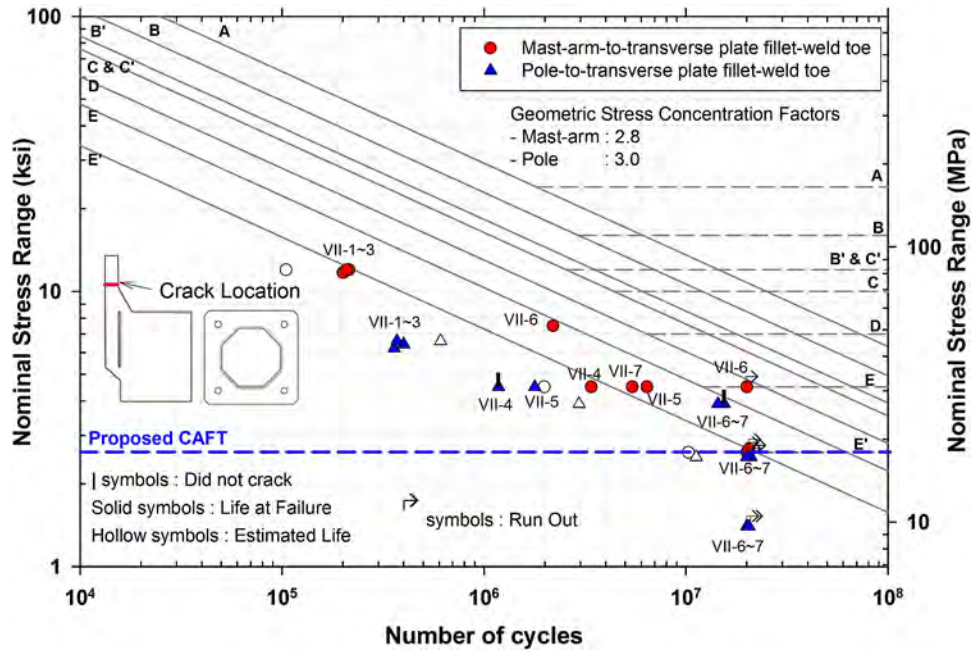
Figure 126 Fatigue test results for specimen Type VII
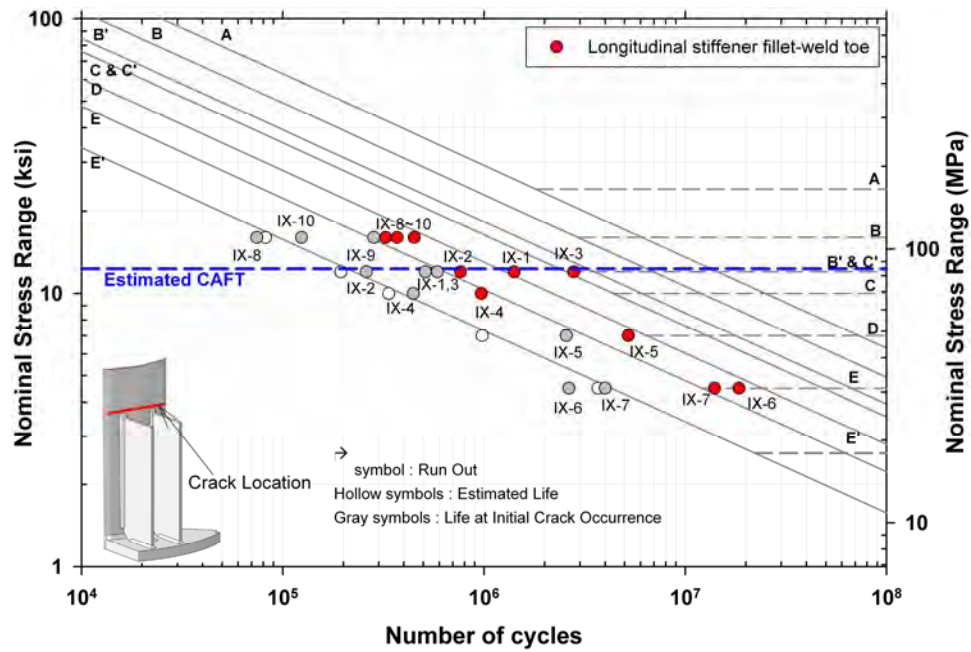
Figure 127 Fatigue test results for specimen Type IX

184
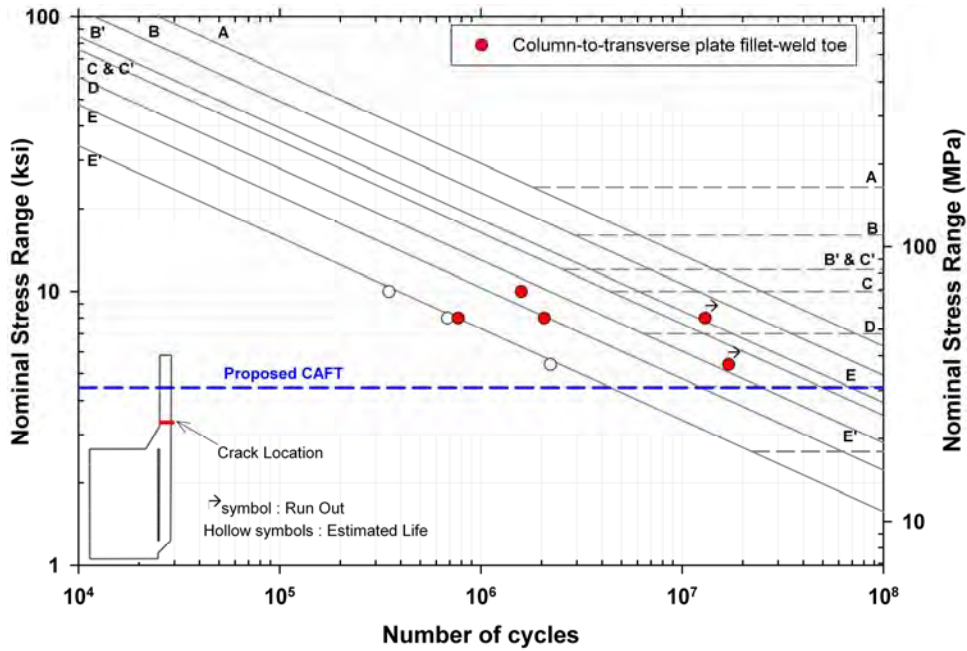
Figure 128 Fatigue test results for specimen Type X
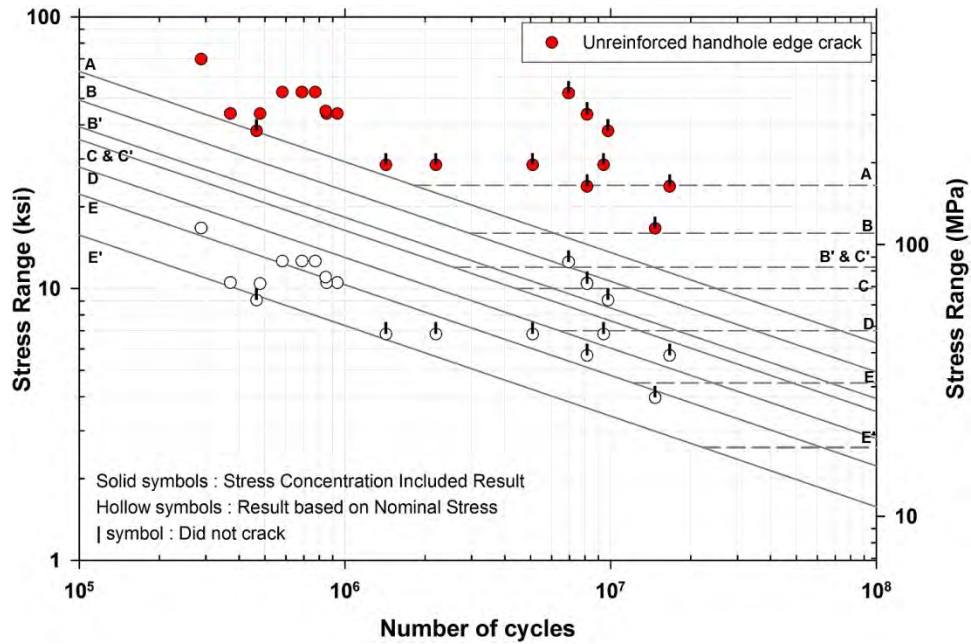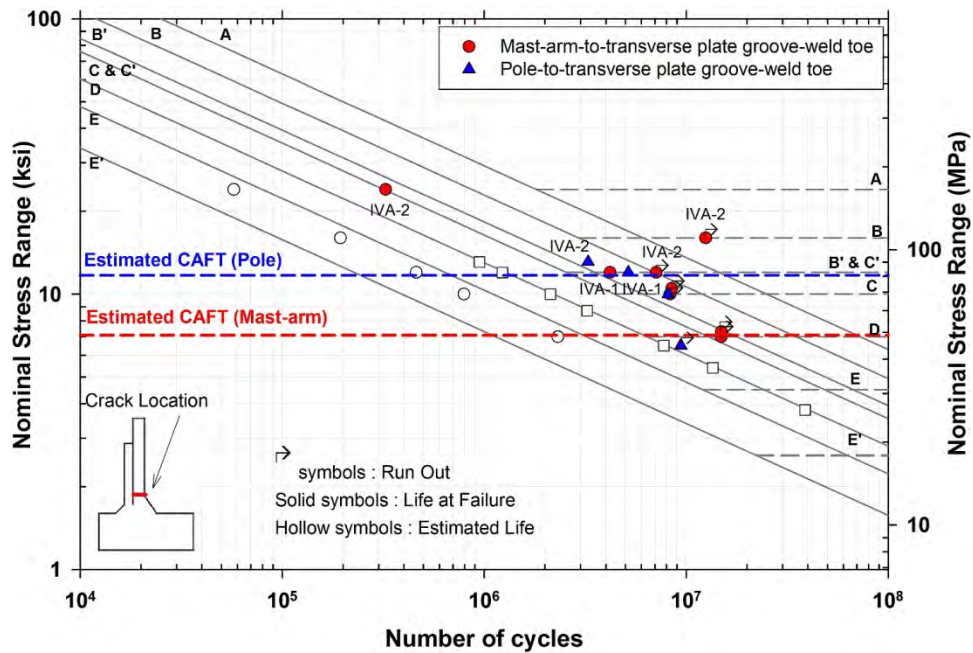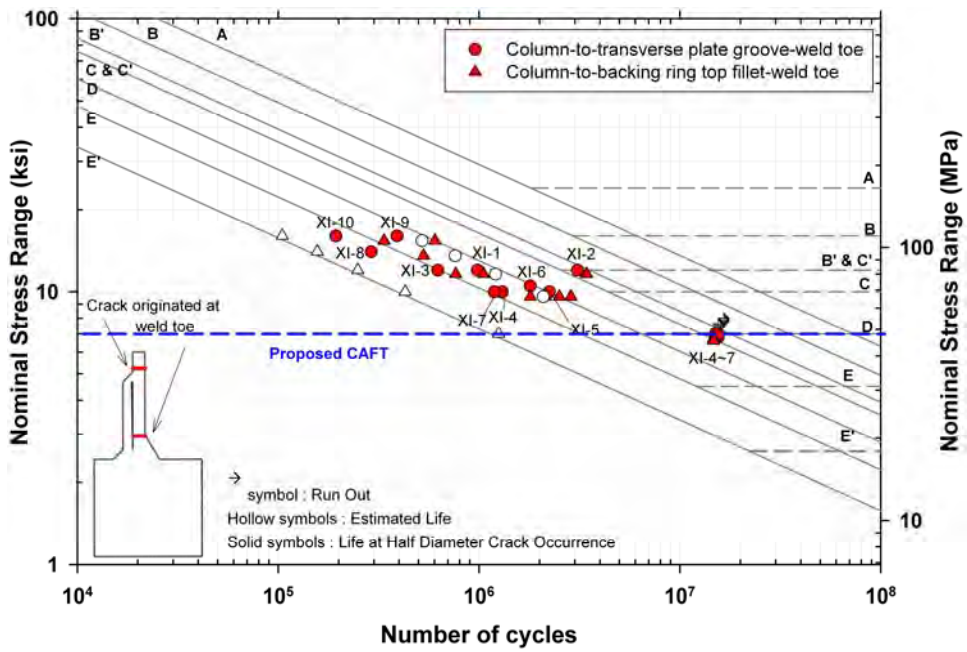

Figure 129 Fatigue test results for specimen Type XI

185
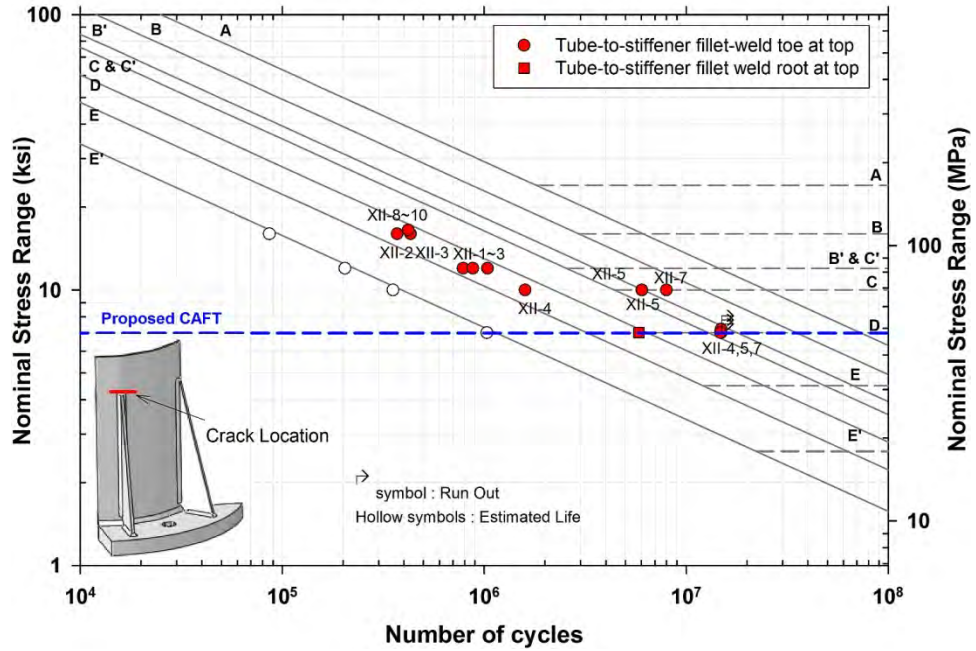
Figure 130 Fatigue test results for specimen Type XII at stiffener top
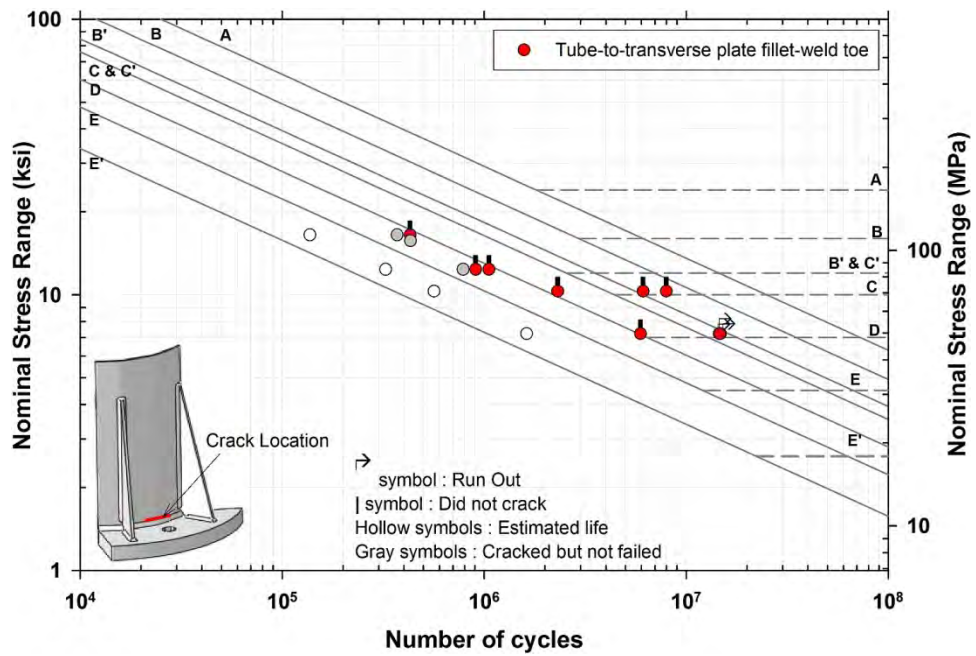
Figure 131 Fatigue test results for specimen Type XII at pole base

186
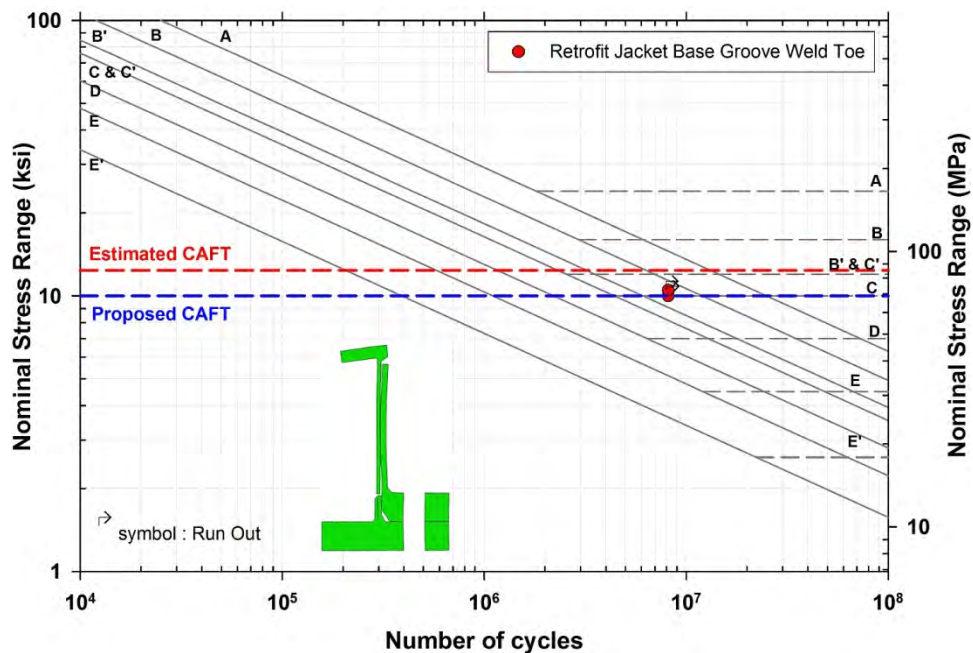
Figure 132 Fatigue test results for specimen retrofit jacket
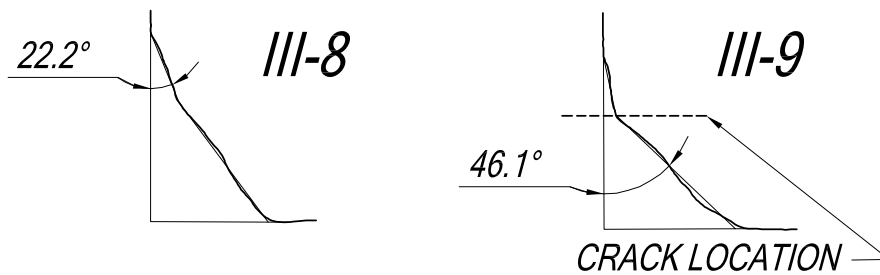
Figure 133 Weld profiles at the sections of crack initiation in specimens III-8 and III-9

187
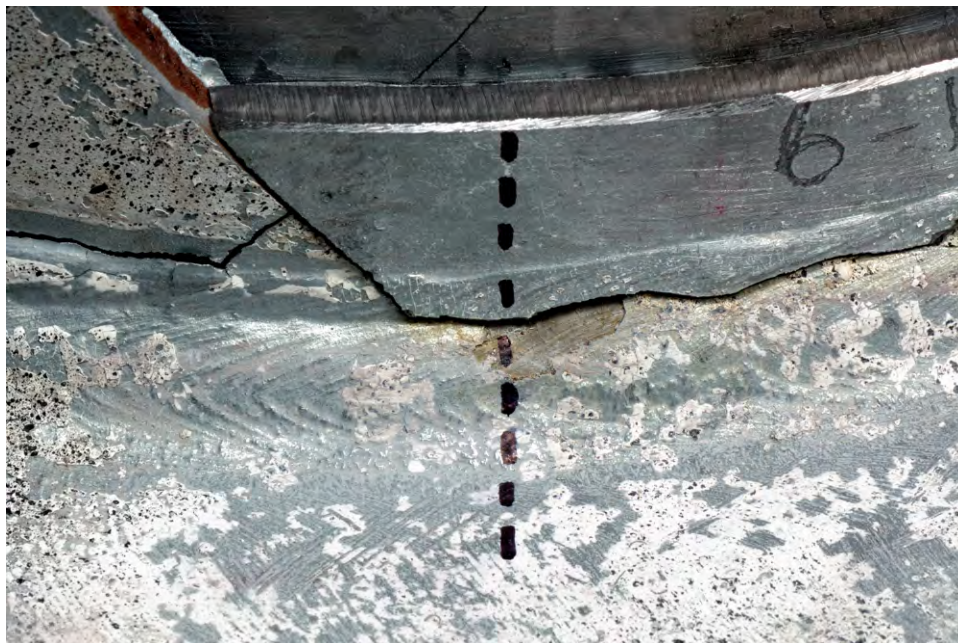
Figure 134 Fatigue crack in the arm of specimen III-9; the broken line indicates the location of the section in Figure 133
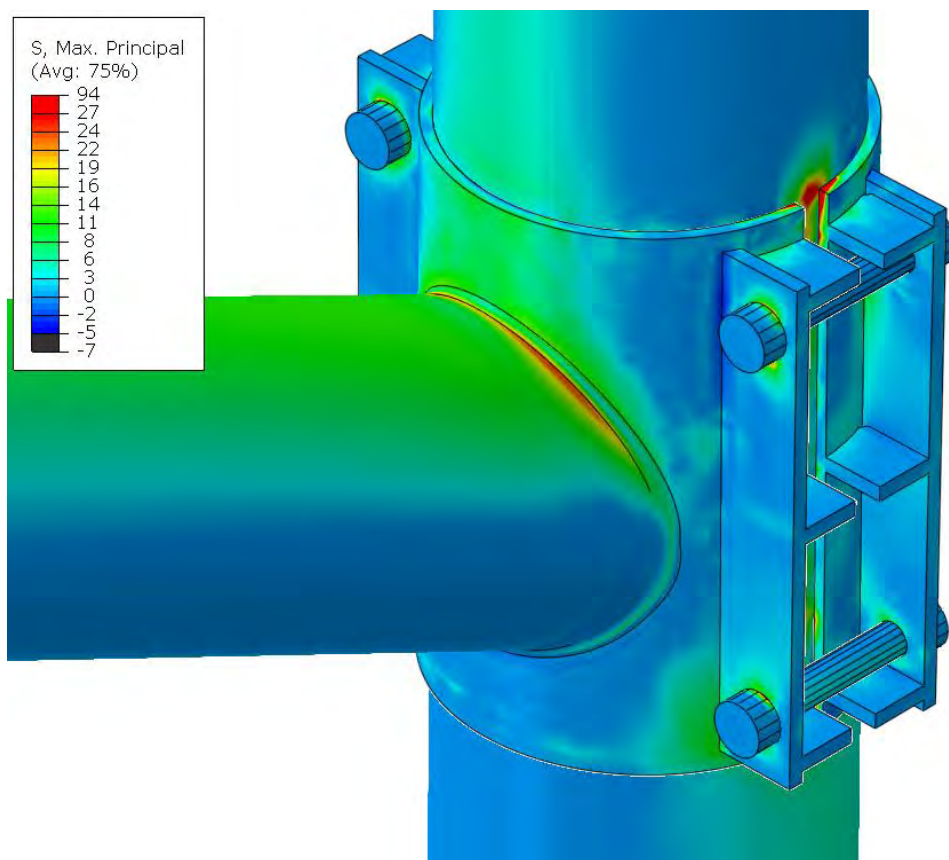
Figure 135 Contour of principal stress in specimen Type V at arm -clamp connection with pole
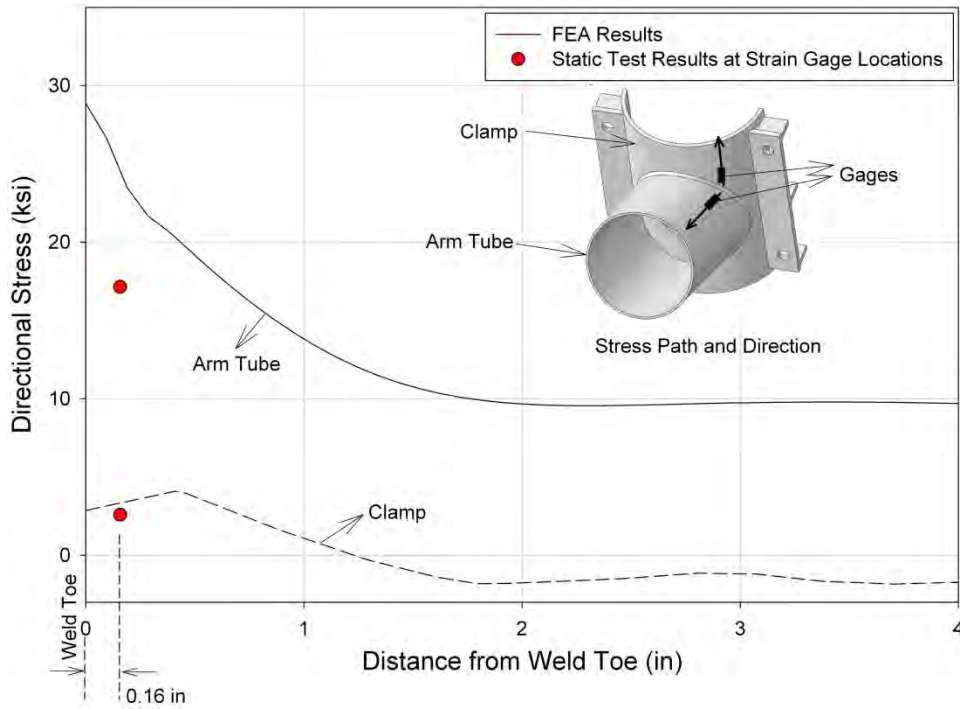
Figure 136 Stress at arm-to-clamp connection in specimen Type V
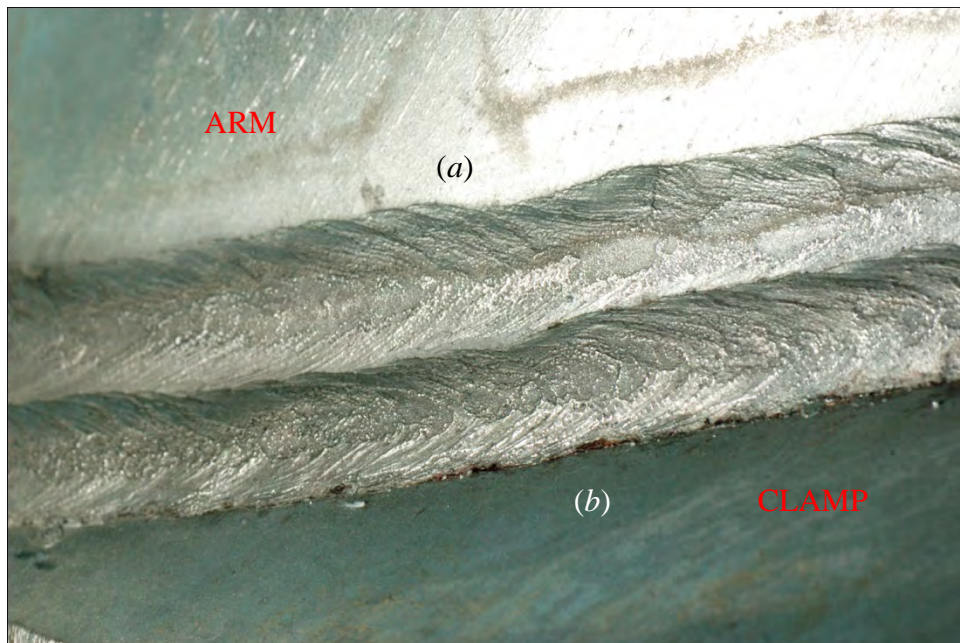
Figure 137 Close-up of weld toe at arm-to-clamp connection in specimen Type V: (a) weld toe on the arm; and (b) cracked weld toe on the clamp

190
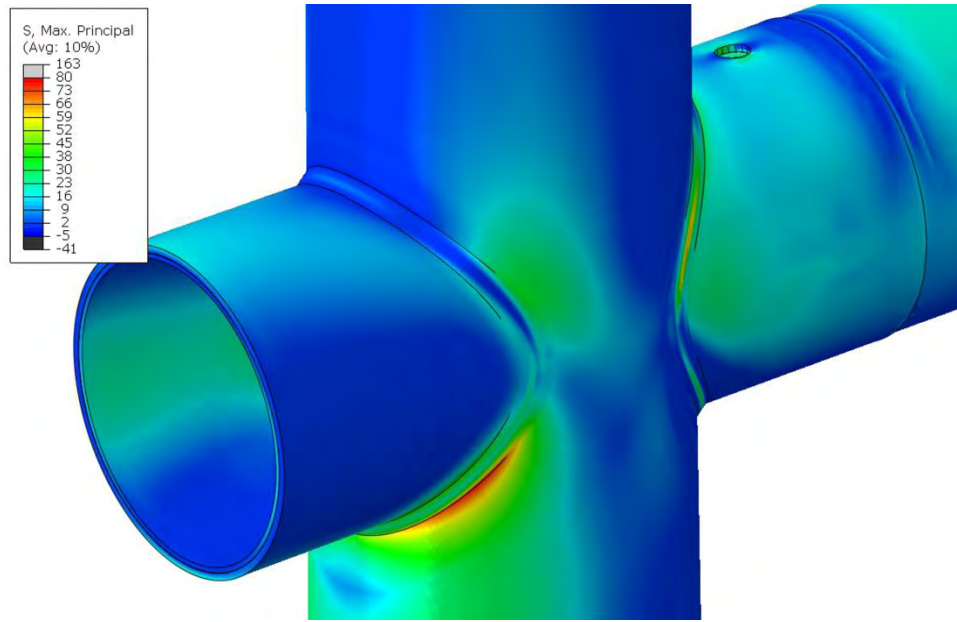
Figure 138 Contour of principal stress in specimen Type VI at arm sleeve to pole connection
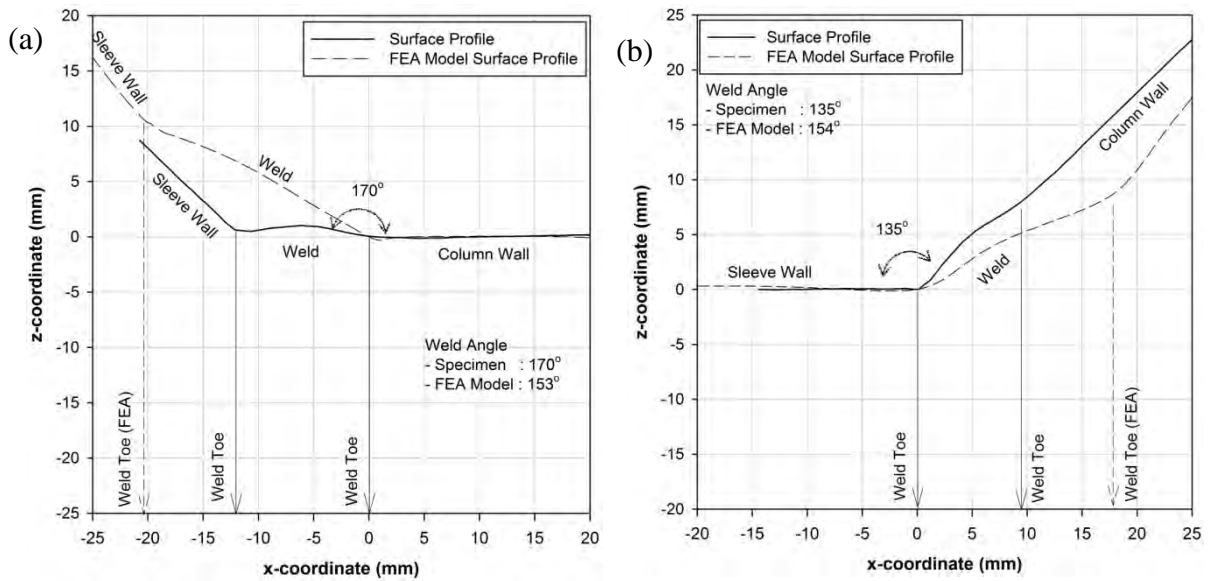
Figure 139 Weld profile : (a) column side weld, (b) sleeve side weld

191
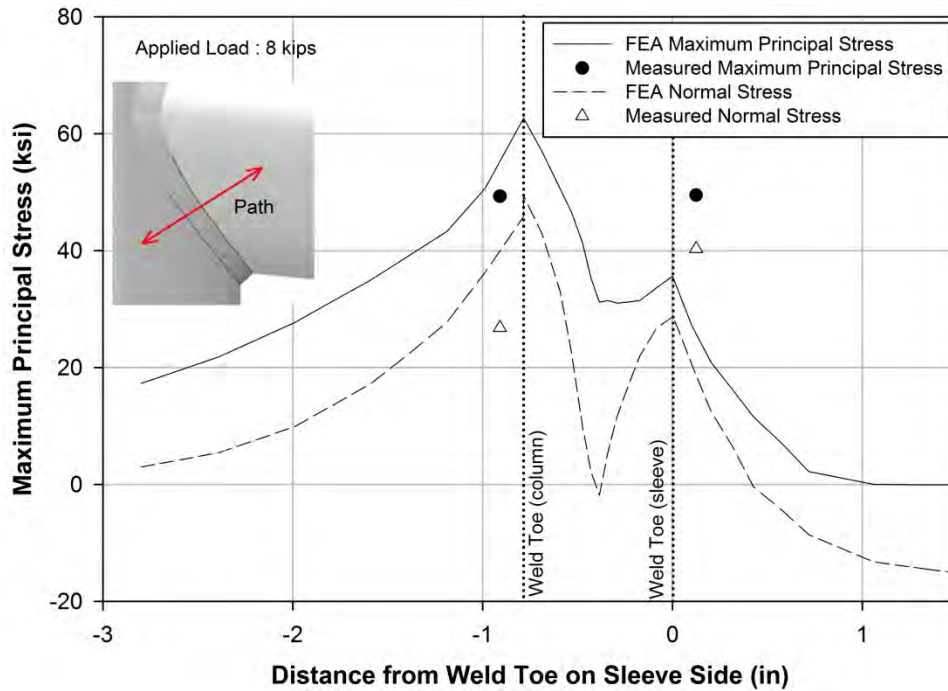
Figure 140 Comparing FEA stresses and strain gauge measured stresses
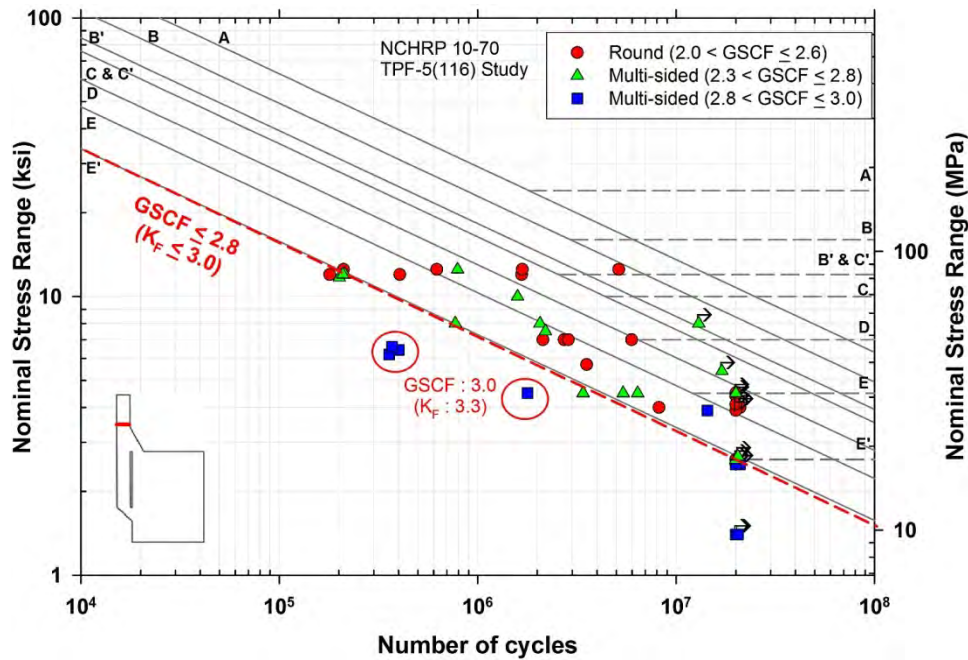
Figure 141 Fatigue resistance of fillet-welded tube-to-transverse plate connections — finite life

192
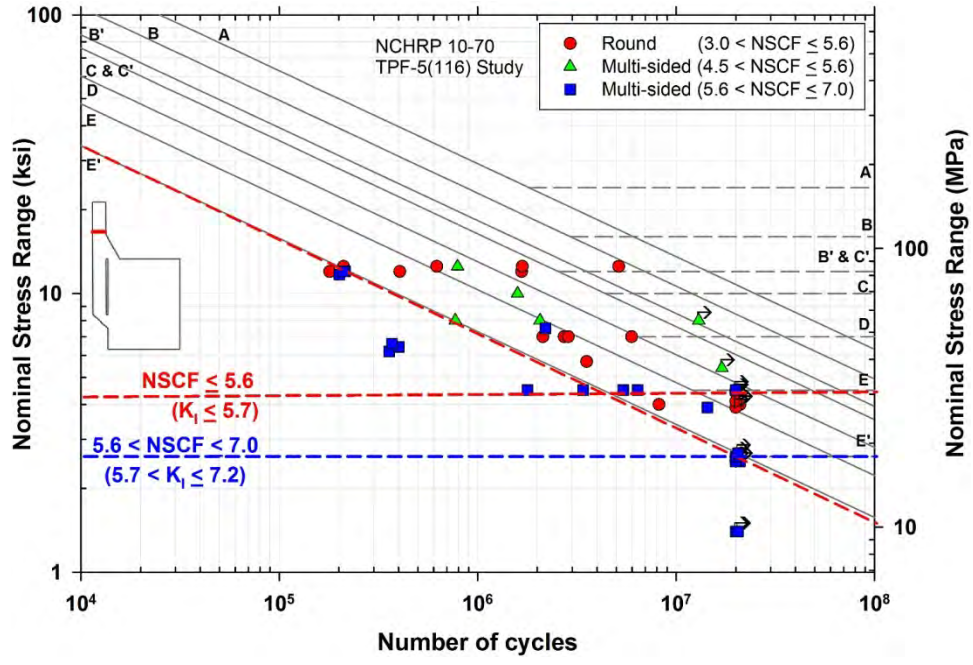
Figure 142 Fatigue resistance of fillet-welded tube-to-transverse plate connections — infinite life
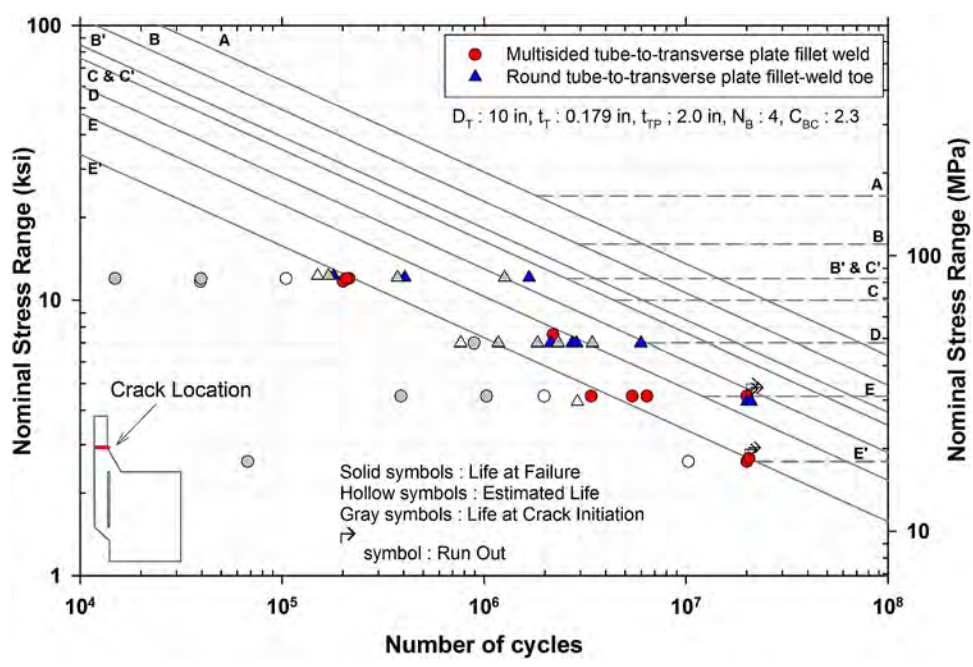
Figure 143 Comparison of fatigue resistance in round and multi-sided sections

193
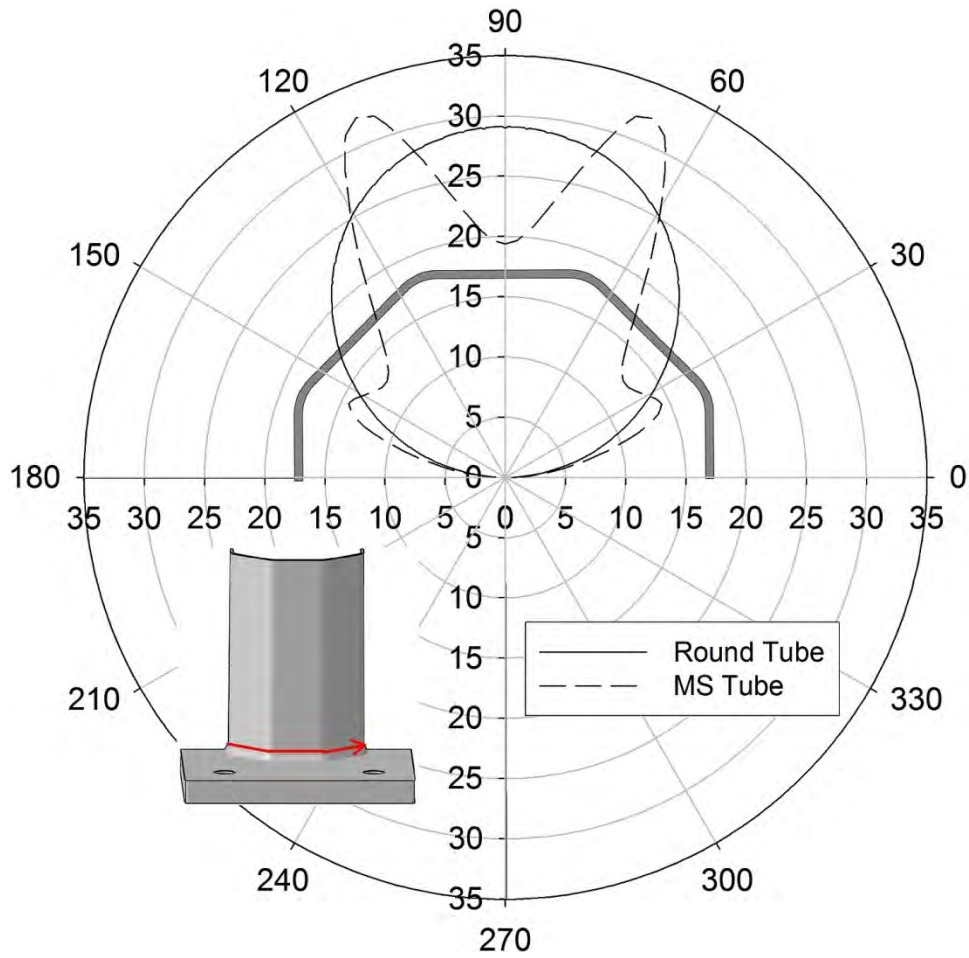
Figure 144 Comparison of geometric stress distribution in round and multi-sided sections — around perimeter
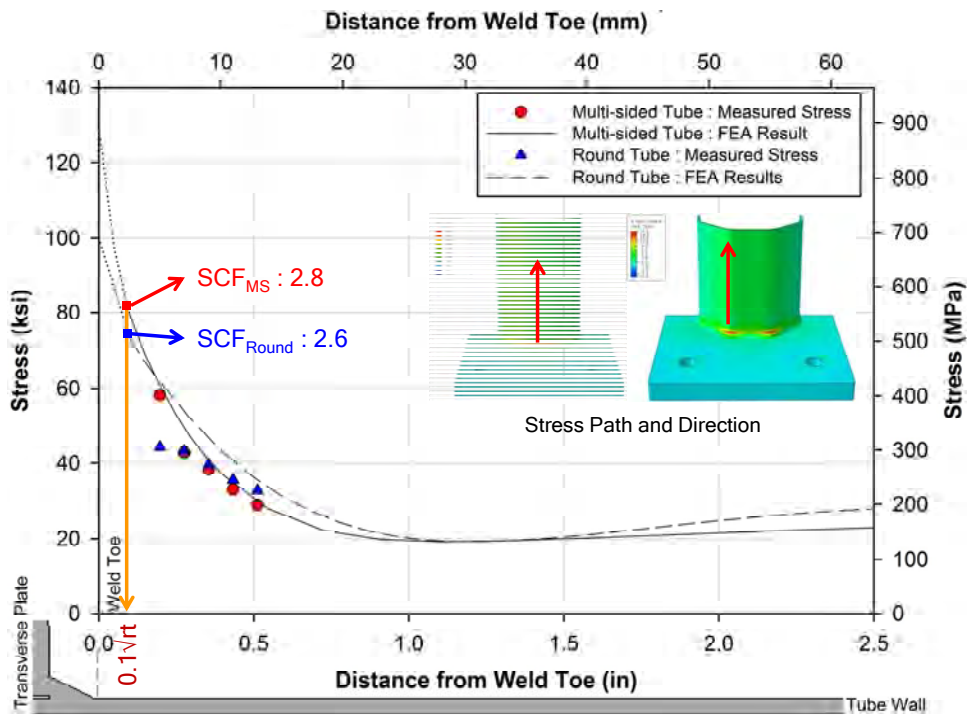
Figure 145 Comparison of geometric stress distribution in round and multi-sided sections — longitudinal direction
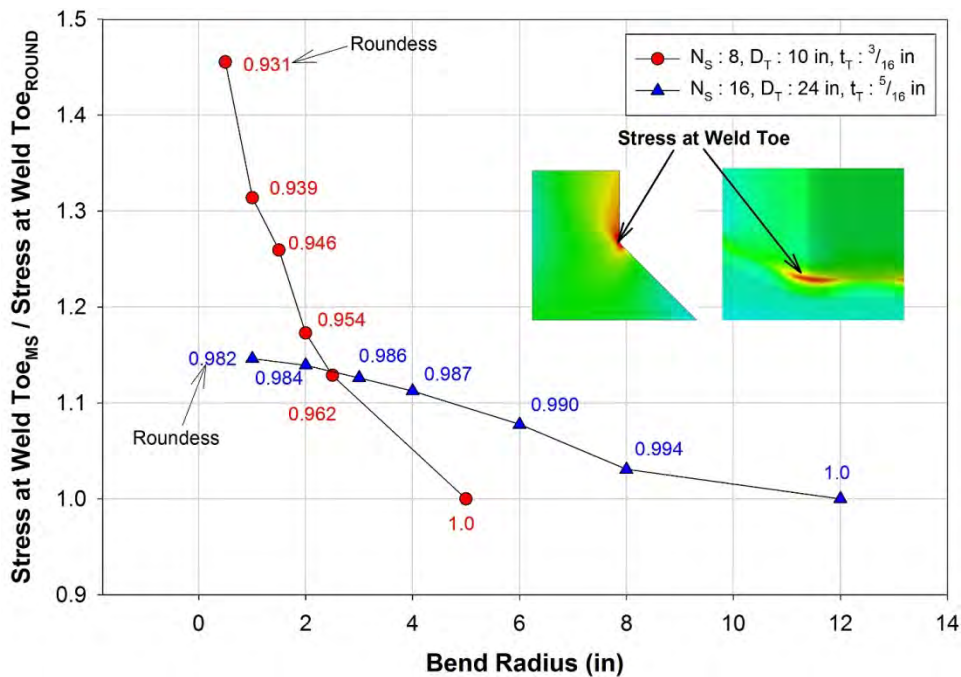
Figure 146 Variation in notch stress in multi-sided sections

195
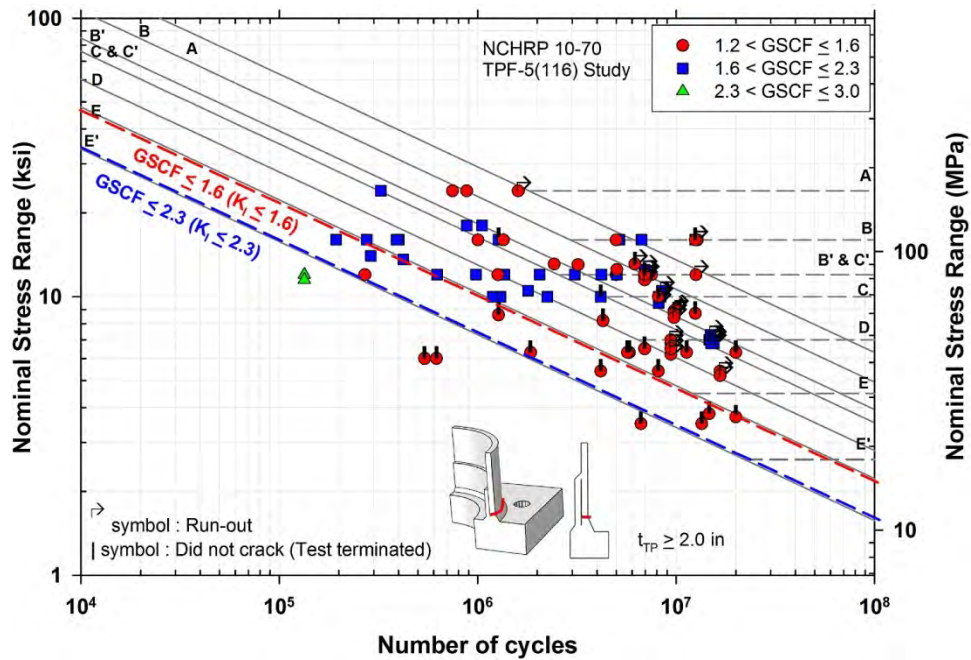
Figure 147 Fatigue resistance of full penetration groove-welded tube-to-transverse plate connections — finite life
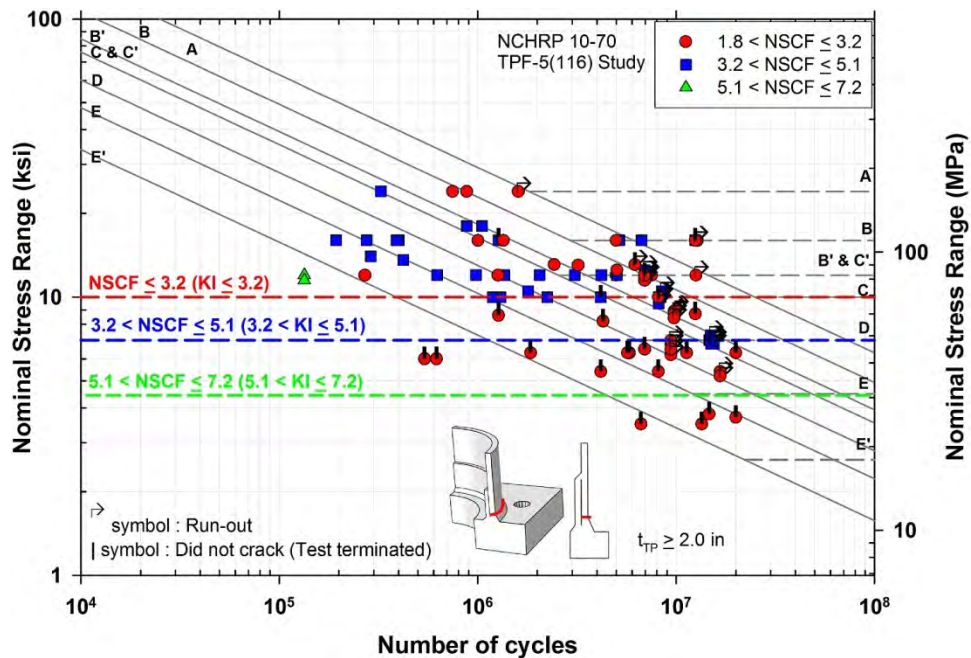
Figure 148 Fatigue resistance of full penetration groove-welded tube-to-transverse plate connections — infinite life

196
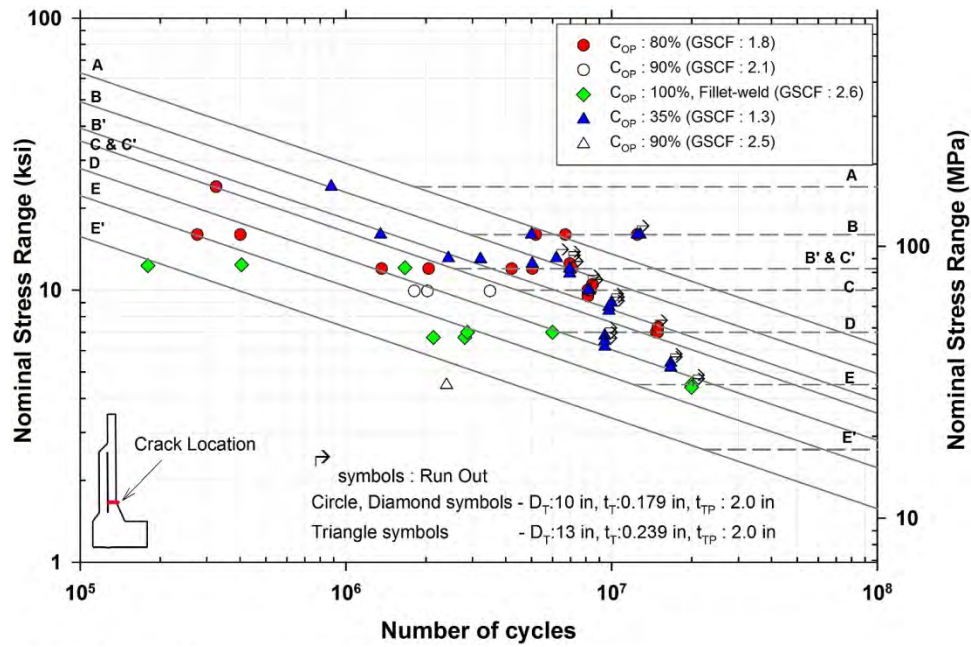
Figure 149 Effect of opening in transverse plate on fatigue resistance of full penetration groove-welded tube-to-transverse plate connections
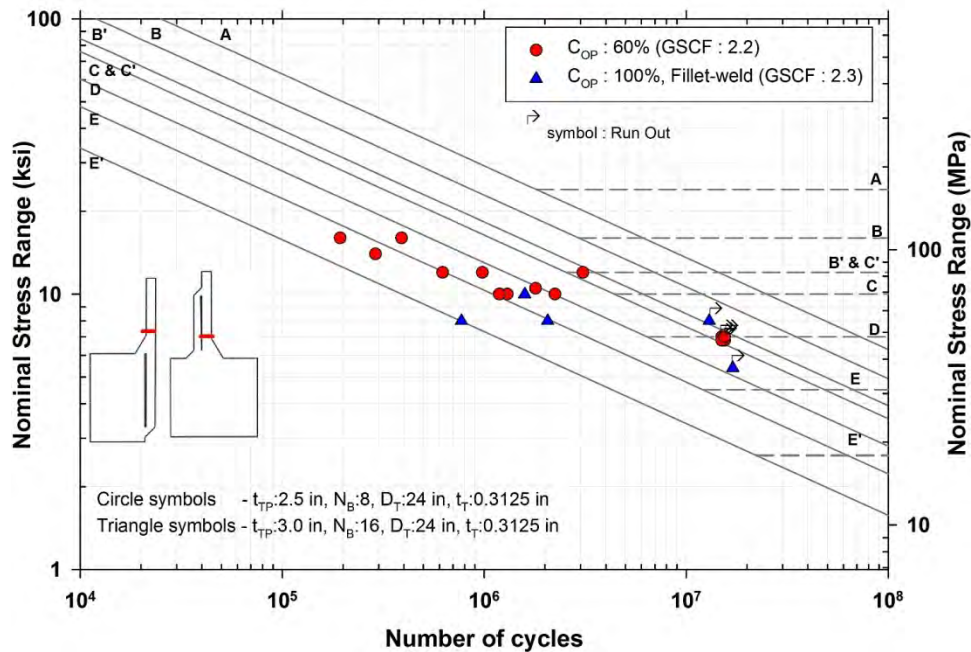
Figure 150 Comparison of fillet- and groove-welded tube-to transverse plate connections with similar GSCF

197
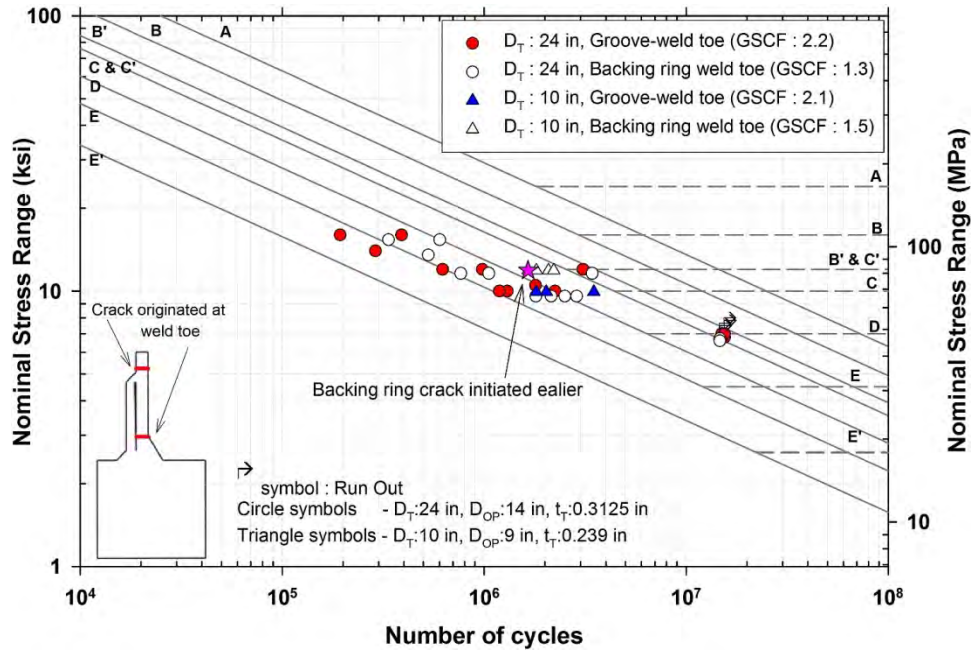
Figure 151 Fatigue resistance of stiffener termination in stiffened fillet-welded connections

Figure 152 Quality of backing ring weld toe and fatigue cracking

198

Figure 153 Lack of fusion at the backing ring-to-tube weld

Figure 154 Polished and etched section showing lack of fusion at the backing ring-to-tube weld (Figure 153)

199
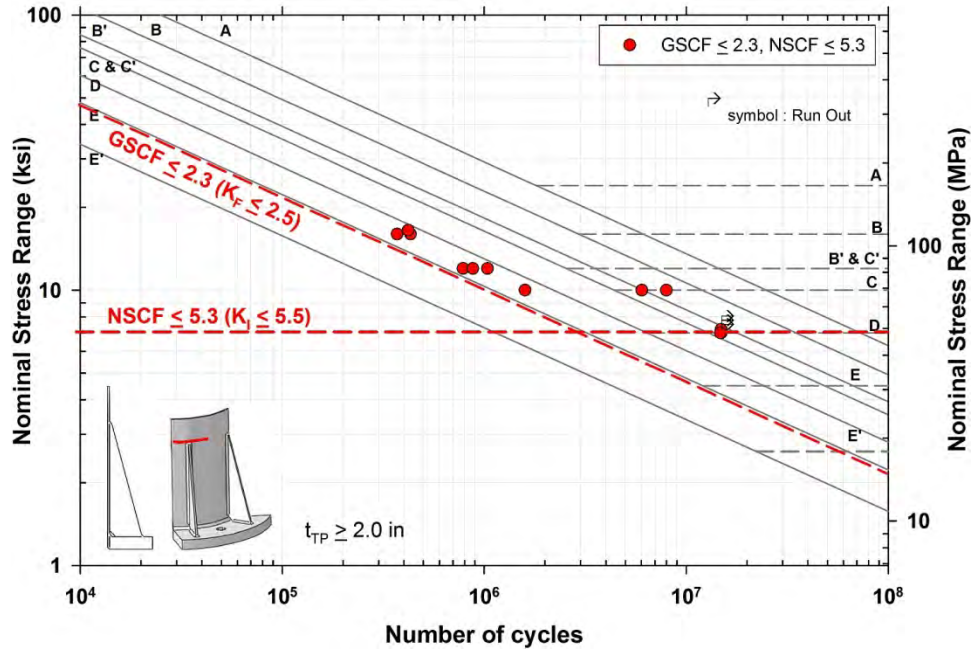
Figure 155 Fatigue resistance of stiffener termination in stiffened fillet-welded connections
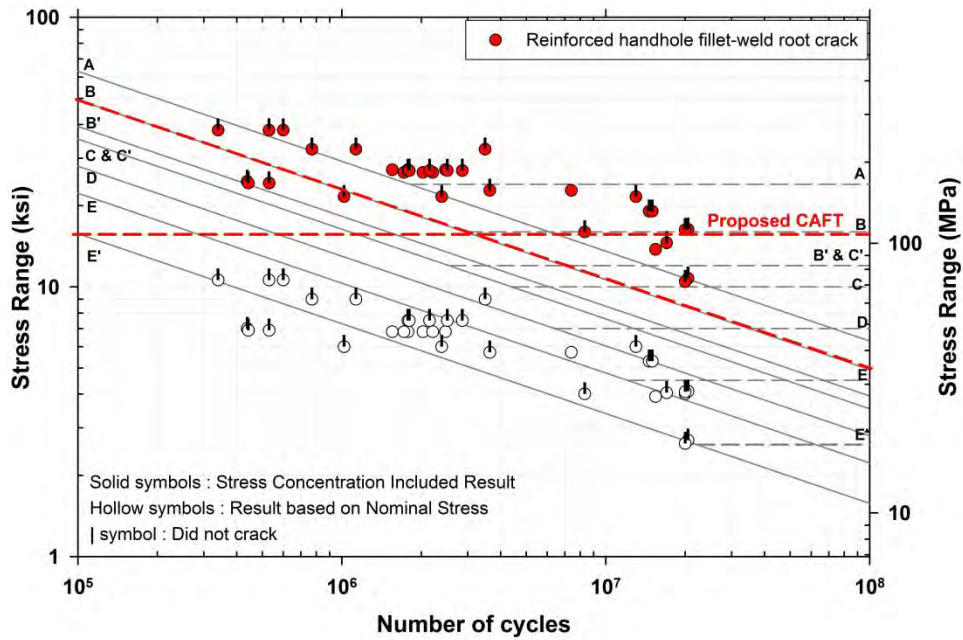
Figure 156 Fatigue resistance of reinforced handholes against cracking from handhole frame-to-pole weld root

200
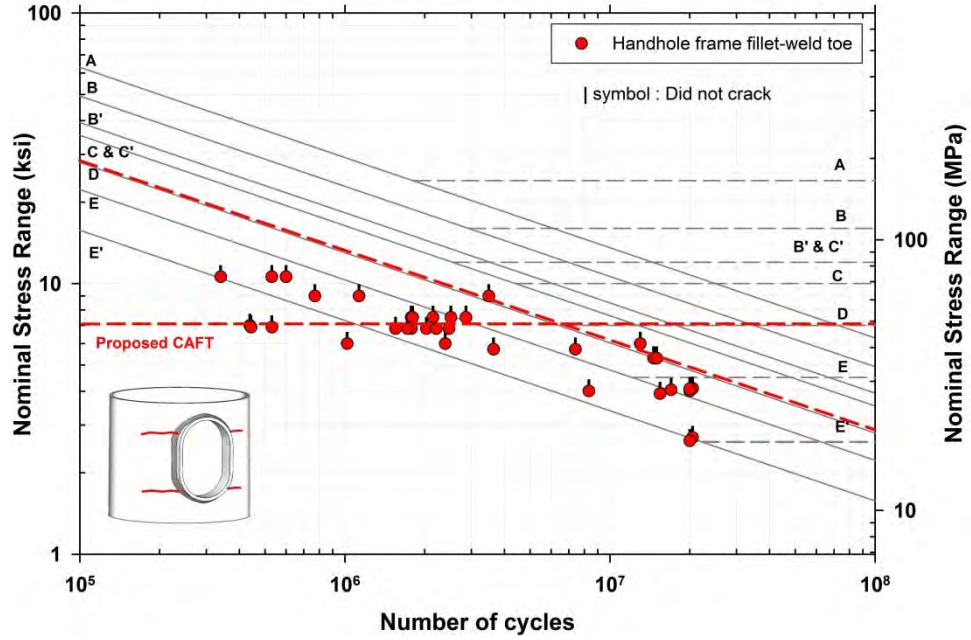
Figure 157 Fatigue resistance of reinforced handholes against cracking from handhole frame-to-pole weld toe
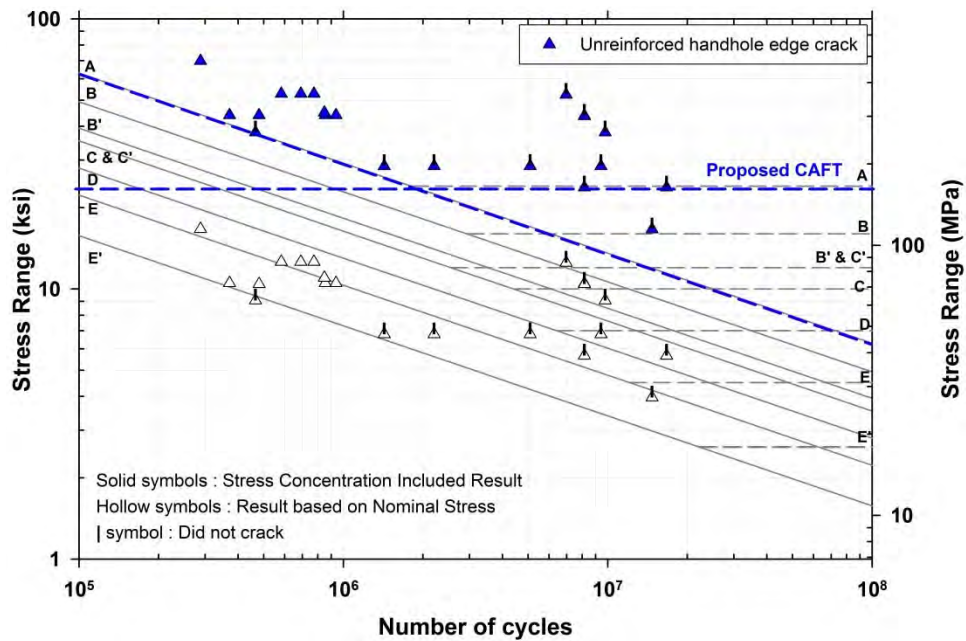
Figure 158 Fatigue resistance of unreinforced handholes

201
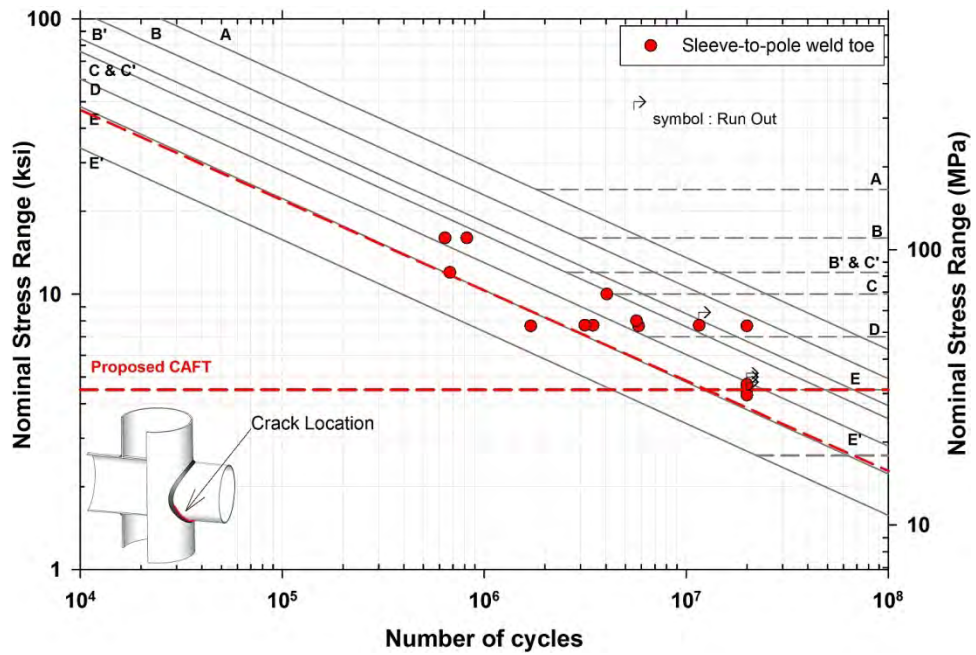
Figure 159 Fatigue resistance of mast-arm-to-pole pass-through connections

202

CHAPTER 4

SPECIFICATION RECOMMENDATIONS AND APPLICATION

RECOMMENDED REVISIONS TO THE AASHTO SPECIFICATION

Based on the findings of this research project, revisions to *Section 11: Fatigue Design* in the *AASHTO Standard Specification for Structural Supports for Highway Signs, Luminaires, and Traffic Signals, 5th Edition, 2009* are proposed in this chapter. The recommended revisions deal with sections 11.5—Design Criteria and 11.9—Fatigue Resistance. The section 11.9 has been eliminated and the relevant provisions of this section have been incorporated in the revised section 11.5.

The proposed specification maintains the infinite life design philosophy for new support structures. For existing support structures, however, a methodology for finite life assessment of the structures has been proposed, which may be used at the discretion of the owner. A nominal stress based design methodology has been retained for the connection details tabulated in Table 11-2. A new *Appendix D: Alternate Methods for Fatigue Design* has been proposed to include the local stress based design provisions and experimental determination of fatigue resistance, which were developed based on the analytical and experimental protocols developed in this project. This alternate approach will provide a tool for evaluating fatigue performance of the details that are not included in Table 11-2.

The specification has been prepared in a two column format following the current *AASHTO LRFD Bridge Design Specification*, with the specifications in the left column and the commentary in the right. In addition, the *Table 11-2: Fatigue Details of Cantilevered Support Structures* has been revised consistent with the *2009 Interim* of the *AASHTO LRFD Bridge Design Specification* to: (1) organize the various welded details in terms of construction; (2) include finite and infinite life classifications; (3) indicate the potential crack locations; and (4) include three dimensional sketches of details with crack locations shown. Table 11-2 was recast in landscape format. For completeness, information on existing details that are beyond the scope of the current project was added to this table from the existing specification. These items are shaded as grey to make a distinction. The foot notes of the table were revised.

A new Table C11-1: Fatigue Details of Support Structures Tested in the Laboratory has been included to assist the Specification users by direct deployment of fatigue resistant cost-effective connections in new structures. In addition, a new Table 11-1 has been added for the Fatigue Stress Concentration Factors in tube-to-transverse plate connections incorporating the geometric parameters of the connection.

203

11.5—DESIGN CRITERIA

Cantilevered and noncantilevered support structures shall be designed for fatigue to resist wind load induced stresses. Stress ranges on all components, mechanical fasteners, and weld details shall be limited to satisfy:

$$(\Delta f) \leq (\Delta F) \qquad (11–1)$$

where Δf is the wind load induced stress range; and ΔF is the fatigue resistance.

Fatigue design of the support structures may be conducted using the nominal stress-based classifications of typical connection details as provided in Article 11.5.1 and Table 11–2, or using the alternate local stress-based and/or experiment-based methodologies presented in Appendix D. Support structures shall be proportioned such that the wind load induced stress is below the constant amplitude fatigue threshold (CAFT) providing infinite life. The remaining fatigue life of existing structures may be assessed based on a finite life.

C11.5

Fatigue design of connection details in support structures may be as per nominal stress- or local stress-based and/or experiment-based methodologies. The nominal stress-based design approach using classification of typical connection details and their fatigue resistances as provided in Article 11.5.1 and Table 11–2 should suffice in most cases. However, if a connection detail is employed that has not been addressed in Table 11–2, an alternate local stress-based and/or experiment-based methodology as provided in Appendix D may be used for fatigue design. It is important that the stresses are calculated in agreement with the definition of stress used for a particular design methodology.

Accurate load spectra and life prediction techniques for defining fatigue loadings are generally not available. Assessment of stress fluctuations and the corresponding number of cycles for all wind-induced events (lifetime loading histogram) is practically impossible. With this uncertainty, the design of sign, high level luminaire, and traffic signal supports for a finite fatigue life is unreliable. Therefore, an *infinite life* fatigue design approach is recommended and is considered sound practice.

The infinite life fatigue design approach should ensure that a structure performs satisfactorily for its design life to an acceptable level of reliability without significant fatigue damage. While some fatigue cracks may initiate at local stress concentrations during the useful life of support structures, there should not be any time dependent propagation of these cracks. This is particularly the case for structural supports where the wind load cycles in 25 years or more are expected to exceed 100 million cycles, whereas typical weld details exhibit Constant Amplitude Fatigue Threshold (CAFT) at 10 to 20 million cycles. It may be noted that in the previous editions of the specification the CAFT was termed as Constant Amplitude Fatigue Limit (CAFL). The terminology in the current specification has been changed to be consistent with the AASHTO LRFD Bridge Design Specifications and considering the movement towards a Load and Resistance Factor Design (LRFD) specification for the support structures.

Where an accurate assessment of the life time wind induced stress range histogram is available, a finite life fatigue design approach may be considered at the discretion of the owner.

The equivalent static wind load effects as specified in Article 11.7 are to be considered for infinite life fatigue design. The wind effects for finite life design should be obtained from analysis based on historical wind records or directly from field measurements on similar structures, as approved by the owner.

204

11.5.1—Nominal Stress-based Design

For nominal stress-based design, Equation 11–1 is rewritten as:

$$(\Delta f)_n \leq (\Delta F)_n \qquad (11\text{–}2)$$

where $(\Delta f)_n$ is the wind induced nominal stress range defined in Article 11.5.1.2; and $(\Delta F)_n$ is the nominal fatigue resistance as specified in Article 11.5.1.3 for the various detail classes identified in Article 11.5.1.1.

11.5.1.1—Detail Classification

All fatigue sensitive details in the connections and components in support structures shall be designed in accordance with their respective detail classifications. Detail classifications for typical components, mechanical fasteners and welded details in support structures are tabulated in Table 11–2.

Tubular structures shall be of round or multi-sided cross-section. Multi-sided tubular sections shall have a roundness factor, R greater than 0.94.

The roundness factor for a multi-sided section is defined as:

$$R = \frac{\cos\left(\dfrac{\pi}{N_S}\right)}{1.0 - \dfrac{r_b}{R_{Ti}}\left(1.0 - \cos\left(\dfrac{\pi}{N_S}\right)\right)} \qquad (11\text{-}3)$$

where N_S is the number of sides; R_{Ti} is the radius of the inner inscribed circle; and r_b is the internal bend radius of the corners.

Multi-sided sections shall have a minimum of eight sides and a minimum internal bend radius of 1 in (25 mm).

C11.5.1

Fatigue-critical details may be designed such that the nominal stress ranges experienced by the details are less than the nominal fatigue resistance of respective detail classes. Fatigue design classification of typical support structure details, the applicable nominal stress ranges and their fatigue resistances are provided in Articles 11.5.1.1, 11.5.1.2, and 11.5.1.3.

C11.5.1.1

Classification of components, mechanical fasteners and welded details in typical support structures that are susceptible to fatigue cracking is provided in Table 11–2. The detail classes are consistent with the detail categories in the fatigue design provisions of the AASHTO LRFD Bridge Design Specifications. The details shown in Table 11–2 are developed based on a review of State Departments of Transportation standard drawings and manufacturers' literature, and are grouped into six sections based on application. The list is not a complete set of all possible connection details; rather it is intended to include the most commonly used connection details in support structures. Any detail that is not listed in Table 11–2 may be categorized based on alternate methodologies provided in Appendix D. Appropriate details can improve the fatigue resistance of these structures, and can help in producing a cost-effective design by reducing the member size required for less fatigue resistant details.

Roundness is a parameter that quantifies the geometric similarity of a multi-sided section relative to a round section. A multi-sided section approaches a round section with increasing number of sides and increasing internal bend radius at the corners. For a perfectly round section this parameter becomes 1.0.

Laboratory fatigue test results demonstrated that fatigue cracking in multi-sided tube-to-transverse plate connections initiated at the bend corners and progressed towards the flat face in between the corners. Analytical studies of Finite Element (FE) models verified by measurements demonstrated existence of high stress concentration at the bend corners, which caused crack initiation very early during the fatigue tests in eight sided tubes with sharper bend radius. Compared to a round tube of similar size, welded connections in multi-sided tubes with lower roundness exhibited significantly less fatigue resistance. Increasing number of sides and/or increasing the internal bend radius can improve fatigue performance of multi-sided sections.

Stiffened and unstiffened tube-to-transverse plate connections, reinforced and unreinforced handholes and anchor rods are the most fatigue critical details in the support structures. Most of the fatigue cracking in service and in laboratory tests under NCHRP Project 10-70 on full size specimens has occurred at these connection details. The details of specimens tested under NCHRP Project 10-70 are shown in Table C11–1.

Unreinforced holes and cutouts shall be detailed as shown in Figure 11–1. The width of opening in the cross sectional plane of the tube shall not be greater than 40% of the tube diameter at that section.

In laboratory fatigue tests under NCHRP Project 10-70, fatigue cracking from unreinforced handholes in sign/signal support structure specimens initiated from the edge of handhole at the point of maximum stress concentration. The handholes in the test specimens were located in the plane of the mast-arm but on the away face to produce the most critical stress condition in the handhole detail for fatigue. It is recommended that in sign/signal support structures the handholes and other holes and cutouts be located in a region of low stress.

Reinforced holes and cutouts shall be detailed as shown in Figure 11–2. The width of opening in the cross sectional plane of the tube shall not be greater than 40% of the tube diameter at that section.

In service fatigue cracks at reinforced handholes have been reported from the toe of the handhole frame-to-pole (reinforcement-to-tube) weld in high-level luminaire support structures. In laboratory fatigue tests under NCHRP Project 10-70, however, fatigue cracking from handhole details in sign/signal support structure specimens initiated only from the lack of fusion at the root of the handhole frame-to-pole (reinforcement-to-tube) fillet-weld. Because of limited access, the handhole frames in sign and signal structures can be welded only from the outside, increasing the possibility of lack of fusion defects at the weld root.

The handholes in the test specimens were located in the plane of the mast-arm but on the away face such as to produce the most critical stress condition in the handhole detail for fatigue. No fatigue cracking at the toe of the handhole frame-to-pole weld was detected. Since the fatigue stress cycles in sign/signal support structures are imparted primarily due to wind induced galloping oscillations in the plane containing the arm, it is recommended that the handholes in these support structures be located on the side normal to that containing the arm.

In high-level luminaire support structure specimens, the handhole details did not develop any fatigue cracking. These specimens were loaded laterally in the plane containing the handhole, simulating vortex shedding oscillation.

In tube-to-transverse plate connections, the plate thickness shall not be less than 2 in (51 mm).

Fatigue resistance of connections in tubular support structures depends on the relative stiffness of the components at a connection or the connection geometry. Experimental and analytical studies demonstrate that the fatigue resistance of tube-to-transverse plate connections is a function of the relative flexibility of the tube and the

In full-penetration groove-welded tube-to-transverse plate connections, the height and thickness of the backing ring shall not exceed 2 in (51 mm) and $^1/_4$ in (6 mm) respectively.

transverse plate. Increasing the thickness of the transverse plate is the most cost-effective means of reducing the flexibility of the transverse plate and increasing the connection fatigue resistance. In-service fatigue cracking in tube-to-transverse plate connections have often occurred where relatively thin plates were used along with a few discrete fasteners.

Reducing the opening size in the transverse plate and/or increasing the number of fasteners are other cost-effective means of reducing the flexibility of the transverse plate and increasing the fatigue resistance of tube-to-transverse plate connections.

Full-penetration groove-welded tube-to-transverse plate connections are usually fabricated with a backing ring. In galvanized structures, the backing ring is often welded to the plate and the tube wall to avoid ingress of acid in the gaps between the backing ring, the tube wall and the plate during pickling in the galvanizing process. Any trapped acid in the gaps may cause crevice corrosion or hydrogen related cracking when exposed to moisture in service.

In galvanized structures, if the backing ring is not welded to the plate or to the tube wall, all resulting gaps should be sealed by caulking after galvanizing to prevent ingress of moisture.

In full-penetration groove-welded tube-to-transverse plate connections with the backing ring welded to the plate and the tube wall, fatigue cracking can occur both at groove-weld toe and the backing ring top weld toe on the tube wall. Depending on the diameter and thickness of the tube, and the height and thickness of the backing ring, the backing ring can participate in transferring forces from the tube to the transverse plate and can provide a redundant load path when the tube to transverse plate groove-weld develops fatigue cracking. In tubes having a diameter smaller than 16 in (406 mm), it is difficult to ensure quality weld between the tube and the backing ring at the top, where premature fatigue cracking from the toe of this weld on the tube wall may limit the fatigue resistance of the connection. It is recommended that the backing ring be welded to the tube wall only in larger diameter tubes, where this weld quality can be adequately controlled. When performed, this weld should be considered as a structural weld and due attention should be paid to the quality of this weld.

In laboratory tests, groove-welded tube-to-transverse plate connections exhibited significantly better fatigue resistance compared to fillet-welded connections in identical structures, because a smaller opening could be used in the transverse plate. Reducing the opening size and/or increasing the plate thickness are the most cost-effective means of reducing the flexibility of the transverse plate and increasing the connection fatigue resistance.

207

Fillet-welds for tube-to-transverse plate connections shall be unequal leg welds, with the long leg of the fillet-weld along the tube. The termination of the longer weld leg should contact the tube surface at approximately 30º angle.

In stiffened fillet-welded tube-to-transverse plate connections (socket connections) only tapered stiffeners having a termination angle of 15^0 on the tube wall shall be used.

The minimum height of stiffeners shall be 12 in (305 mm). At least eight stiffeners shall be used equally spaced around the tube wall. The stiffener spacing shall not exceed 16 in (406 mm).

When stiffened fillet-welded tube-to-transverse plate connections are used, the minimum thickness of the tube wall shall be ¼ in (6 mm). The ratio of the stiffener thickness to the tube wall thicknesses shall not exceed 1.25.

The weld connecting the stiffeners to the tube shall be wrapped around the stiffener termination on the tube wall. The wrapped around weld at the stiffener termination shall not be ground.

Stiffeners having a transition radius shall not be used.

Laboratory test results demonstrated that the fatigue strength of a fillet-welded tube-to-transverse plate connection can be improved by using an unequal leg fillet-weld, compared to equal leg welds. However, significant scatter was observed in the test results, where unequal leg fillet-weld was used. This scatter in test results could be attributed to the variation in the fabricated weld geometry and particularly the weld toe angle from the specified nominal value. In a thin walled tubular support structures, the welds act as tiny stiffeners and affect the geometric stresses and the fatigue resistance of welded connections. The weld geometry should be controlled by tighter tolerance to reduce the scatter in fatigue performance of tube-to-transverse plate connections in the support structures.

In support structures employing larger diameter and thicker tubes, optimized stiffened tube-to-transverse plate fillet-welded connections can provide a cost-effective design compared to an increased transverse plate thickness. Parametric studies demonstrated that the performance of a stiffened connection is a function of the geometric parameters of the connection: the tube thickness, the transverse plate thickness, the stiffener shape and size (thickness, height and angle), and the number of stiffeners (or stiffener spacing). Ideally an optimum solution would render the weld toes on the tube wall at the stiffener termination and at the transverse plate equally susceptible to fatigue cracking. A large stiffener thickness relative to the tube wall can attract more stress into the stiffeners and can increase distortion of the tube wall. On the contrary, relatively thin stiffeners can reduce distortion of the tube wall but fail to sufficiently reduce the stress at the fillet-weld and can cause fatigue cracking through the throat of the stiffener-to-transverse plate weld. A ratio of stiffener thickness to tube thickness of 1.25 provides an optimum solution with equal likelihood of fatigue cracking at the stiffener termination and at the tube-to-transverse plate weld. The fatigue resistance of the stiffener-to-transverse plate fillet or partial joint penetration groove-weld against cracking through the throat should be determined as a transverse load bearing attachment (detail 6.3 in Table 11–2).

Decreasing the ratio of the stiffener height to stiffener spacing reduces protection to the fillet-weld. An optimum solution is obtained when the stiffener height is about 1.6 times the stiffener spacing. Reducing the termination angle of the stiffener on the tube wall improves the fatigue performance of stiffened connections.

Using a stiffener termination angle of 15^0 ensures that the normal stress is linearly distributed over the stiffened cross section and the stiffener sections are fully effective in sharing load.

Fillet-welded tapered stiffeners with wrapped-around weld at the terminus are cost-effective. The wrap-around

208

weld serves as a seal weld for galvanizing. Stiffeners with a transition radius at the termination on the tube wall are fabrication intensive and are expected to be costlier than a tapered alternative. To avoid exposure of the lack of fusion at the weld root in fillet and partial penetration groove-welds, a stiffener termination with a transition radius must be groove-welded, which requires non-destructive inspection in the vicinity of weld termination. It is difficult to grind the weld toe without inadvertently thinning the tube wall at the transition, which is a concern for thin tubes.

The stiffened groove-welded tube-to-transverse plate connection is unlikely to be cost-effective and is excluded from this specification.

Mast-arm-to-pole connections employing fillet-welded gusseted box or ring-stiffened box shall be detailed as shown in Figures 11–3 and 11–4.

Fillet-welded gusseted boxes or ring-stiffened boxes at the mast-arm-to-pole connections tested in the laboratory in full size specimens under NCHRP Project 10-70 did not develop any fatigue cracking under both in-plane and out-of-plane loading. These connections were tested at various load levels and in some specimens were subjected to more than 40 million stress cycles. In all specimens, fatigue cracking occurred in other critical details in the structure, such as the tube-to-transverse plate welds in the mast-arm and/or the pole, and/or handholes. In-service fatigue cracking of these connections has been reported. Failures of the gusseted box connections in Wyoming and Kansas in mid 1990s resulted from wind induced oscillation. No fatigue cracking has been reported in the ring-stiffened box connection in Wyoming or other states that have been employed since.

Fatigue testing has shown the advantage of ring stiffeners that completely encircle a pole relative to a built-up box connection. For built-up box connections, it is recommended that the width of the box be the same as the diameter of the column (i.e., the sides of the box are tangent to the sides of the column).

Ring-stiffened box connections are more fabrication intensive and should be employed in geographic regions where support structures are expected to experience significant wind induced oscillations. In other regions, gusseted-box connections are expected to provide satisfactory performance.

11.5.1.2—Stress Range

C11.5.1.2

Nominal stress range shall be used when fatigue design of connection details is carried out using Table 11–2. Nominal stress shall be calculated at the site of potential fatigue cracking.

The detail categories in Table 11–2 were developed based on nominal stress to be calculated as discussed below.

For unreinforced holes and cutouts in tubes, the

Nominal stress is a stress in a component that can be derived using simple strength of material calculations based on applied loading and nominal section properties. The nominal stress should be calculated considering gross geometric changes at the section, e.g., tapers, handholes, stiffeners, welded backing rings, etc., which locally magnify or decrease the nominal stress.

209

nominal stress shall be calculated considering the net section property of the tube including the hole and magnified by a stress concentration factor of 4.0, where the width of the opening is limited to 40% of the tube diameter.

For reinforced holes and cutouts in tubes, the nominal stress for design against fatigue cracking at the toe of the reinforcement-to-tube weld shall be calculated considering the net section property of the tube including the hole and the reinforcement.

For design against fatigue cracking from the root, the above nominal stress shall be magnified by a stress concentration factor of 4.0, where the width of the opening is limited to 40% of the tube diameter.

In full-penetration groove-welded tube-to-transverse plate connections with the backing ring welded to the plate and the tube wall, the nominal stress at the section through the weld toe at top of the backing ring and at the section through the groove-weld toe on the tube wall shall be calculated based on the section property of the tube at the sections.

In full-penetration groove-welded tube-to-transverse plate connections with the backing ring not welded to the plate or the tube wall, the nominal stress at a section through the groove-weld toe on the tube wall shall be calculated based on the section property of the tube at the section.

For partial penetration groove-welded mast-arm-to-column pass-through connections, the nominal stress shall be calculated on the gross section of the column at the base of the connection.

For fillet-welded tube-to-transverse plate connections (socket connections), nominal stress should be calculated at a section through the weld toe on the tube wall based on the section property of the tube at the section.

In stiffened fillet-welded tube-to-transverse plate connections, the nominal stress at the termination of the stiffener should be calculated based on the section property of the tube at a section through the toe of the wrap around weld.

In stiffened fillet-welded tube-to-transverse plate connections, the nominal stress at the weld toe on the tube wall of the tube-to-transverse plate fillet-weld should be calculated based on the section property of the tube only at that section. The effect of the stiffeners at this section is implicitly included in the computation of fatigue stress concentration factor as given by Equation 11–10 in Table 11–1.

11.5.1.3—Fatigue Resistance   C11.5.1.3

210

Support structures shall be proportioned such that the wind load induced stress is below the CAFT providing infinite life. For infinite life, nominal fatigue resistance shall be taken as:

$$\left(\Delta F\right)_n = \left(\Delta F\right)_{TH} \tag{11–4}$$

The remaining fatigue life of existing structures may be assessed based on a finite life. For finite life, nominal fatigue resistance shall be taken as:

$$\left(\Delta F\right)_n = \left(\frac{A}{N}\right)^{\frac{1}{3}} \tag{11–5}$$

where $(\Delta F)_n$ is the nominal fatigue resistance as specified in Table 11–2; $(\Delta F)_{TH}$ is the constant amplitude fatigue threshold as specified in Table 11–2; A is the constant specified in Table 11–2; and N is the number of wind load induced stress cycles expected during the life time of the structures.

Fatigue resistance of typical fatigue-sensitive connection details in support structures for finite and infinite life designs shall be determined from Table 11–2. The fatigue stress concentration factors as functions of connection geometry in tubular structures shall be determined as given in Article 11.5.1.3.1. Potential location of cracking in each detail is identified in the table. "Longitudinal" implies that the direction of applied stress is parallel to the longitudinal axis of the detail, and "transverse" implies that the direction of applied stress is perpendicular to the longitudinal axis of the detail.

When the wind load induced maximum stress range (determined as static load effects per Article 11.7) experienced by a component or a detail is less than the CAFT, the component or detail can be assumed to have a theoretically infinite fatigue life. Using Equation 11–4 to establish $(\Delta F)_n$ in Equation 11–2 should ensure infinite life performance.

In the finite life regime at stress ranges above the CAFT, the fatigue life is inversely proportional to the cube of the stress range. For example, if the stress range is reduced by a factor of 2, the fatigue life increases by a factor of 2^3. This result is reflected in Equation 11–5. When assessing the finite life of an existing structure, the number of wind load induced stress cycles expected during the life time of the structure should be estimated from analysis based on historical wind records or directly by field measurements on similar structures, as decided by the owner.

The constant A and the constant amplitude fatigue threshold $(\Delta F)_{TH}$ for the detail classes specified in Table 11–2 are consistent with detail categories in the AASHTO LRFD Bridge Design Specifications. Figure C11.5.1.3-1 is a graphical representation of the nominal fatigue resistance for detail categories as per the AASHTO LRFD Bridge Design Specification.
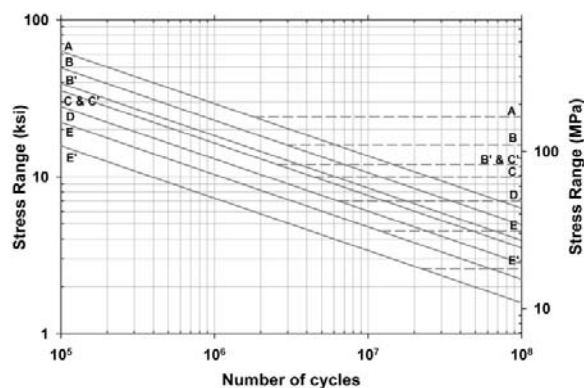
Figure C11.5.1.3-1 Stress Range vs. Number of Cycles.

The fatigue resistance of support structures was established based on laboratory fatigue testing and substantiated by analytical studies. The resistance is based on elastic section analysis and nominal stresses on the cross-section. The resistance includes effects of residual stresses due to fabrication and anchor bolt pretension, which are not to be considered explicitly in the nominal stress computations.

Fatigue resistance of tube-to-transverse plate connections are classified in Table 11–2 in terms of separate fatigue stress concentration factors for finite and infinite life designs, which explicitly incorporate the effects of stress concentration due to the connection geometry and the weld toe notch condition. The effects of

211

weld toe micro-discontinuities are implicitly considered in the experimental results for all connections.

The laboratory test results on support structures substantiated by analytical studies show that the infinite life fatigue resistance of connection details does not always correspond to the respective finite life resistance according to the detail categories of the AASHTO LRFD Bridge Design Specifications.

To assist designers, the details of full size support structure specimens that were tested in the laboratory under NCHRP Project 10-70 are tabulated in Table C11–1 along with their fatigue resistance. The designers are encouraged to directly employ these details in service, wherever applicable, with nominal stress range calculated as per 11.5.1.2.

In laboratory tests, fatigue cracks at the unreinforced handholes initiated from the edge of the hole at the point of maximum stress concentration and grew under the influence of primary normal stress in the tube wall. The maximum principal stress in the tube wall at this section was predominantly in-plane and the stress driving the fatigue crack was magnified by the presence of the hole. Considering this magnified nominal stress, the fatigue performance of the unreinforced handhole in laboratory tests exceeded the lower bound fatigue life provided by the finite life constant A of 250×10^8 ksi^3 (85200×10^8 MPa^3). The fatigue resistance in the infinite life exceeded the CAFT of 24.0 ksi (165 MPa). The fatigue resistance of an unreinforced hole or cutout is accordingly given, considering the magnified nominal stress as defined earlier.

In laboratory tests, fatigue cracks from the lack-of-fusion at the root of the handhole frame-to-pole (hole reinforcement-to- tube) fillet-weld grew under the influence of primary longitudinal stress in the tube wall. Since the maximum principal stress in the tube wall at this section is predominantly in plane and normal to the lack of fusion, the situation is similar to the development of a fatigue crack from the root of longitudinal web to flange weld in built-up beams, which is classified in the AASHTO LRFD Bridge Design Specifications as detail Category B. The difference is that the stress driving the cracking from the lack of fusion in the reinforced hole is magnified by the presence of the reinforced hole. Considering this magnified nominal stress, the fatigue performance of the handhole frame-to-pole weld due to fatigue cracking from the root exceeded the lower bound fatigue life provided by the finite life constant A of 120×10^8 ksi^3 (40900×10^8 MPa^3). The fatigue resistance in the infinite life exceeded the CAFT of 16.0 ksi (110 MPa). The fatigue resistance of reinforcement-to-tube weld at a reinforced hole or cutout due to root cracking is accordingly given, considering the magnified nominal stress as defined earlier.

212

In laboratory tests conducted under NCHRP Project 10-70, no fatigue cracking was detected from the toe of the handhole frame-to-pole weld. The maximum performance of the tube-to-transverse plate welds in poles containing reinforced handholes exceeded the lower bound fatigue life provided by the finite life constant A of 22.0×10^8 ksi³ (7500×10^8 MPa³)and the CAFT of 7.0 ksi (48 MPa). The fatigue resistance of reinforcement-to-tube weld at a reinforced hole or cutout due to toe cracking is accordingly given, considering the nominal stress as defined earlier.

When tested under NCHRP Project 10-70, partial penetration groove-welded mast-arm-to-column pass-through connections developed fatigue cracking both from the weld root and at the weld toe exhibiting a finite fatigue life provided by the finite life constant A of 11.0×10^8 ksi³ (3750×10^8 MPa³) and an infinite life fatigue resistance given by the CAFT of 4.5 ksi (31 MPa). These cracks appeared earlier than expected particularly due to less than acceptable weld quality. Until further research can provide a better estimate of the fatigue resistance of pass-through connections, they shall be classified as indicated in Table 11–2.

The fatigue resistance of the fillet-welded T-, Y-, and K- tube-to-tube, angle-to-tube, and plate-to-tube connections was not established by testing under NCHRP Project 10-70. The fatigue resistance of these connections in Table 11–2 has been retained from the previous edition of the specification, which corresponds to the classification for cyclic punching shear stress in tubular members specified by the *AWS Structural Welding Code D1.1—Steel* based on research in the offshore industry on connections of thicker and larger diameter tubes. Stresses in tubular connections are strongly dependent on their geometric parameters. As such, extrapolation of the fatigue design provisions from the AWS Specification may not be consistent with the performance of these connections in service. Until further research can provide a better estimate of the fatigue resistance of these connections, they shall be classified as indicated in Table 11–2.

Stool-type stiffened fillet-welded tube-to-transverse plate connections, similar to those in-service in Iowa, were tested in the laboratory under NCHRP Project 10-70. These stiffened connections employ a pair of rectangular vertical stiffeners welded to the tube wall and transverse plate and connected by a plate at the top. The top plate serves as an anchorage for the anchor rods, and is not welded to the tube wall. These connection details have performed extremely well in Iowa, where no cracking has been found during 40 years of service. In laboratory tests, however, these connections did not perform well. Fatigue cracks initiated at the termination

213

of the vertical stiffeners and progressed around the perimeter of the tube. The finite life fatigue performance was provided by the finite life constant A of 11.0×10^8 ksi^3 (3750×10^8 MPa^3). However, these details did not exhibit infinite life when tested at the CAFT of 4.5 ksi (31 MPa). The thickness of the tubes in the test specimens was $^5/_{16}$ in (8 mm). This detail may provide better fatigue performance in thicker and larger tubes. Until further research can provide a better estimate of the fatigue resistance these stiffened connections, the fatigue performance of the welds terminating at the end of vertical stiffeners in the stool type stiffened pole-to-transverse plate connections shall be given by the finite life constant A of 3.9×10^8 ksi^3 (1330 MPa^3) and the CAFT of 2.6 ksi (18 MPa).

11.5.1.3.1—Stress Concentration Factors

C11.5.1.3.1

For finite life design of tubular connections, fatigue stress concentration factors in Table 11–2 shall be calculated as per equations given in Table 11–1.

Fatigue resistance of tubular connections in support structures depends on the relative stiffness of the components at a connection or the connection geometry. Geometric stresses arise from the need to maintain compatibility between the tubes and other components at the connections. This geometric stress concentration affects the fatigue resistance of the connections for both finite and infinite life performance. In addition, the resistance of the connections against any fatigue crack growth for infinite life is also affected by the local stress concentration related to local geometry of the weld. The effects of global and local geometric stress concentrations on the fatigue resistance of various connections in the support structures were determined experimentally and analytically under NCHRP Project 10-70.

For infinite life design of tubular connections, the fatigue stress concentration factor in Table 11–2 shall be calculated as:

SI Units

$$K_I = \left[\left(1.76 + \frac{t_T}{13.9} \right) - 4.76 \times 0.22^{K_F} \right] \times K_F$$

$$(11-6)$$

U.S. Customary Units

$$K_I = \left[\left(1.76 + 1.83 t_T \right) - 4.76 \times 0.22^{K_F} \right] \times K_F$$

where K_F is calculated from Table 11–1 for the respective details.

Nomenclature of the parameters used in the expressions for stress concentration factors are:

Equations for fatigue stress concentration factors were determined based on parametric finite element analyses and were verified by test results. The ranges of the parameters describing the connection geometry in the studies covered the ranges determined from state departments of transportation's drawings and manufacturer's literature. Fatigue resistance was determined based on the local stress-based methodology presented in Appendix D. Based on these results, the fatigue resistance of the tube-to-transverse plate connection details were classified in terms of separate fatigue stress concentration factors for finite and infinite life regimes. While the fatigue stress concentration factor for finite life design incorporates the effect of connection geometry, the fatigue stress concentration factor for infinite life design also includes the geometric effect of the weld toe notch condition.

D_{BC} = diameter of circle through the fasteners in the transverse plate (in, mm)

D_{OP} = diameter of concentric opening in the transverse plate (in, mm)

D_T = external diameter of a round tube or outer opposite-to-flat distance of a multi-sided tube at top of transverse plate (in, mm)

h_{ST} = height of longitudinal attachment (stiffener) (in, mm)

N_B = number of fasteners in the transverse plate

N_{ST} = number of longitudinal attachment (stiffener)

t_{ST} = thickness of longitudinal attachment (stiffener) plate (in, mm)

t_T = thickness of tube (in, mm)

t_{TP} = thickness of transverse plate (in, mm)

214

$$C_{BC} = \frac{D_{BC}}{D_{T}}$$

$$C_{OP} = \frac{D_{OP}}{D_{T}}$$

Experimental and analytical studies demonstrated that the fatigue resistance of tube-to-transverse plate connections is a function of the relative flexibility of the tube and the transverse plate. Reducing the relative flexibility of the transverse plate can significantly increase the fatigue resistance of the connection. The relative flexibility of the transverse plate depends on: (1) the thickness of the transverse plate; (2) the opening in the transverse plate (in groove-welded connections); (3) the number of fasteners; (4) the bolt circle ratio, defined as the ratio of the bolt circle diameter to the tube diameter. In addition, the diameter and thickness of the tube affects the relative stiffness. Reducing the opening size and/or increasing the plate thickness are the most cost-effective means of reducing the flexibility of the transverse plate and increasing the connection fatigue resistance.

Fatigue performance of a stiffened tube-to-transverse plate fillet-welded connection is a function of: (1) the thickness of the transverse plate; (2) the thickness of the tube; (3) the stiffener shape and size (thickness, height and angle); and (4) the number of stiffeners (or stiffener spacing). Optimized stiffened tube-to-transverse plate fillet-welded connections can provide cost-effective solution in support structures employing larger diameter and thicker tubes.

The finite life fatigue stress concentration factor for stiffened fillet-welded tube-to-transverse plate connections at the fillet-weld toe on the tube wall as determined from Table 11–1 is to be used with fillet-welded tube-to-transverse plate connection detail in Table 11–1 for determining the fatigue resistance.

Compared to a round tube of similar size, welded tube-to-transverse plate connections in multi-sided sections exhibit less fatigue resistance with decreasing roundness. The deviation in fatigue performance of multi-sided sections from round shapes depend on: (1) outer opposite-to-flat dimension of a multi-sided tube; (2) thickness of the tube; (3) number of sides in the multi-sided section; and (4) internal bend radius. The fatigue stress concentration factors for tube-to-transverse plate connections in multi-sided cross sections shall be obtained by multiplying Equation 11–11 to the fatigue stress concentration factors of respective details in round sections.

215

Table 11–1—Fatigue Stress Concentration Factors, K_F
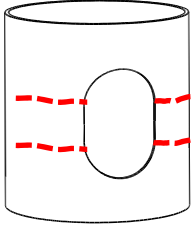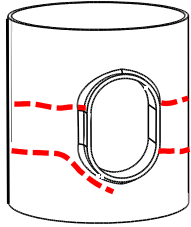
Section Type	Detail	Location	Fatigue Stress Concentration Factor for Finite Life, K_F
Round	Fillet-welded tube-to-transverse plate connections	Fillet-weld toe on tube wall	(11–7) U.S. Customary Units $$K_F = 2.16 + \left(0.908 - 0.924 \frac{C_{BC}^{0.0474}}{N_B^{0.0105}} \right)$$ $$\times \left(4.54 + 52.1 \times t_T \right) \times \left(14.6 - 1.17 \times D_T^{1.15} \right) \times t_{TP}^{-2.36}$$ SI Units $$K_F = 2.16 + 207 \times \left(9.08 - 9.24 \frac{C_{BC}^{0.0474}}{N_B^{0.0105}} \right)$$ $$\times \left(4.54 + 2.05 \times t_T \right) \times \left(14.6 - \frac{D_T^{1.15}}{35.3} \right) \times t_{TP}^{-2.36}$$
	Groove-welded tube-to-transverse plate connections	Weld toe on tube wall	(11–8) U.S. Customary Units $$K_F = 1.35 + \left(0.982 - \frac{C_{BC}^{0.0674}}{N_B^{0.0029}} \right) \times \left(1.0 + 17.3 \times t_T \right)$$ $$\times \left(2.60 - \frac{D_T^{1.12}}{2.24} \right) \times \left(\frac{1.0}{C_{OP}^{-0.689} - 0.764} \right) \times t_{TP}^{-1.95}$$ SI Units $$K_F = 1.35 + \left(2.63 - 2.68 \frac{C_{BC}^{0.0674}}{N_B^{0.0029}} \right) \times \left(12.1 + 8.24 \times t_T \right)$$ $$\times \left(44.1 - \frac{D_T^{1.12}}{4.93} \right) \times \left(\frac{1.0}{C_{OP}^{-0.689} - 0.764} \right) \times t_{TP}^{-1.95}$$
	Fillet-welded tube-to-transverse plate connections stiffened by longitudinal attachments	Weld toe on tube wall at the end of attachment	(11–9) U.S. Customary Units $$K_F = \left(\frac{4.36 \frac{t_{ST}}{t_T^{0.334}} - 1.0}{2.26 \frac{t_{ST}}{t_T^{0.707}}} \right) \times \left(\frac{0.160 + 0.864 \times h_{ST}}{1.0 + 1.12 \times h_{ST}} \right)$$ $$\times \left(0.519 + 0.257 \frac{D_T}{N_{ST}^{1.60} t_T^{1.42}} + \frac{0.870}{t_T^{0.797}} + \frac{0.0293}{t_{ST}^{2.91}} \right)$$
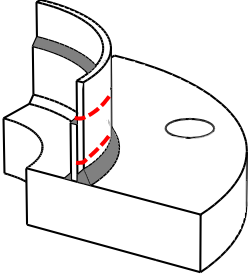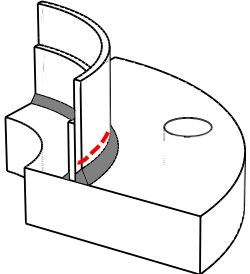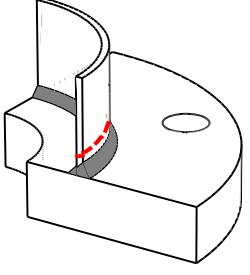
216

Section Type	Detail	Location	Fatigue Stress Concentration Factor for Finite Life, K_F
Round	Fillet-welded tube-to-transverse plate connections stiffened by longitudinal attachments	Weld toe on tube wall at the end of attachment	SI Units $\qquad$ (11–9) $$K_F = \left(\frac{\dfrac{t_{ST}}{t_T^{0.334}} - 1.98}{1.73 \dfrac{t_{ST}}{t_T^{0.707}}} \right) \times \left(\frac{0.160 + \dfrac{h_{ST}}{29.4}}{1.0 + \dfrac{h_{ST}}{22.7}} \right)$$ $$\times \left(0.519 + \frac{D_T}{N_{ST}^{1.60} t_T^{1.42}} + \frac{11.5}{t_T^{0.797}} + \frac{359}{t_{ST}^{2.91}} \right)$$
		Fillet-weld toe on tube wall	U.S. Customary Units $\qquad$ (11–10) $$K_F = \left[\begin{array}{l} \left(9.84 - \dfrac{D_T}{1.82} + 4.89 \dfrac{D_T^{1.03}}{N_{ST}^{0.914}} \right) \times \left(\dfrac{0.129}{h_{ST} + 6.56} \right) \\ \times \left(0.859 + \dfrac{2.79}{t_{ST}^{0.631}} \right) \times \left(0.802 + \dfrac{t_{TP}}{12.9} \right) \\ \times K_F \text{ as per Equation (11-7)} \end{array} \right]$$ SI Units $$K_F = \left[\begin{array}{l} \left(9.84 - \dfrac{D_T}{46.3} + \dfrac{D_T^{1.03}}{5.71 \times N_{ST}^{0.914}} \right) \times \left(\dfrac{1.0}{h_{ST} + 167} \right) \\ \times \left(1.0 + \dfrac{25.0}{t_{ST}^{0.631}} \right) \times \left(2.26 + \dfrac{t_{TP}}{117} \right) \\ \times K_F \text{ as per Equation (11-7)} \end{array} \right]$$
Multi-sided	As above	As above	Multiply respective K_F above by: $\qquad$ (11–11) U.S. Customary Units $$\left[\left(0.186 - \frac{t_T}{8.93} \right) \times \left(1.97 + \frac{D_T^{2.44}}{828} \right) \times e^{\left(\frac{0.028}{R - 1.01} \right)} + 0.923 \right]$$ SI Units $$\left[\left(0.186 - \frac{t_T}{227} \right) \times \left(1.97 + \frac{D_T^{2.44}}{2.22 \times 10^6} \right) \times e^{\left(\frac{0.028}{R - 1.01} \right)} + 0.923 \right]$$

217
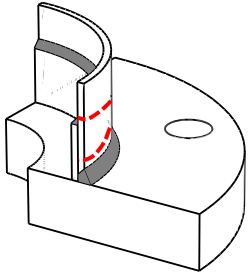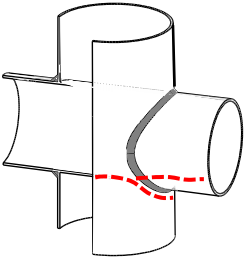
Table 11-2—Fatigue Details of Cantilevered and Noncantilevered Support Structures

Description	Finite Life Constant, $A\times10^8$ $(ksi^3 \ (MPa^3))$	Threshold, $(\Delta F)_{TH}$ (ksi (MPa))	Potential Crack Location	Illustrative Example
SECTION 1 — PLAIN MATERIAL				
1.1 With rolled or cleaned surfaces. Flame-cut edges with ANSI/AASHTO/AWS D5.1 (Article 3.2.2) smoothness of 1000 μ-in. or less.	250.0 (85200)	24.0 (165)		
1.2 Slip-joint splice where L is greater than or equal to 1.5 diameters.	120.0 (40900)	16.0 (110)		High-level lighting poles.
SECTION 2 — MECHANICALLY FASTENED CONNECTIONS				
2.1 Net section of fully tightened, high-strength (ASTM A 325, A 490) bolted connections.	120.0 (40900)	16.0 (110)		Bolted joints.
2.2 Net section of other mechanically fastened connections: a. Steel:	22.0 (7500)	7.0 (48)		
2.3 Anchor bolts or other fasteners in tension; stress range based on the tensile stress area. Misalignments of less than 1:40 with firm contact existing between anchor bolt nuts, washers, and base plate.	22.0 (7500)	7.0 (48)		Anchor bolts. Bolted mast-arm-to-column connections
2.4 Connection of members or attachment of miscellaneous signs, traffic signals, etc. with clamps or U-bolts.	22.0 (7500)	7.0 (48)		

218

Description	Finite Life Constant, $A \times 10^8$ (ksi^3 (MPa^3))	Threshold, $(\Delta F)_{TH}$ (ksi (MPa))	Potential Crack Location	Illustrative Example
SECTION 3 — HOLES AND CUTOUTS				
3.1 Net section of un-reinforced holes and cutouts.	250.0 (85200)	24.0 (165)	In tube wall at edge of unreinforced handhole.	
3.2 Reinforced holes and cutouts. At root of reinforcement-to-tube weld: At toe of reinforcement-to-tube weld:	 120.0 (40900) 22.0 (7500)	 16.0 (110) 7.0 (48)	 In tube wall and hole reinforcement from root of reinforcement-to-tube weld. In tube wall and hole reinforcement from the toe of reinforcement-to-tube weld	
SECTION 4 — GROOVE-WELDED CONNECTIONS				
4.1 Tubes with continuous full- or partial penetration groove-welds parallel to the direction of the applied stress	61.0 (20800)	12.0 (83)		Longitudinal seam welds.
4.2 Full-penetration groove-welded splices with welds ground to provide a smooth transition between members (with or without backing ring removed).	22.0 (7500)	7.0 (48)		Column or mast arm butt-splices.
4.3 Full-penetration groove-welded splices with weld reinforcement not removed (with or without backing ring removed).	11.0 (3750)	7.0 (48)		Column or mast-arm butt-splices.

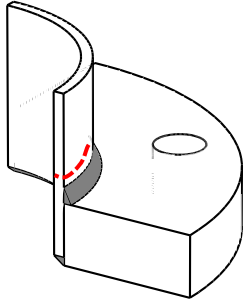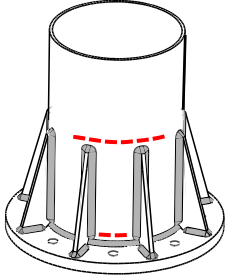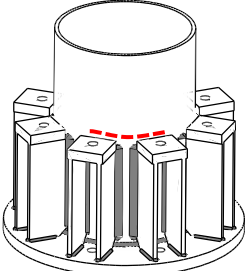| Description	Finite Life Constant, $A \times 10^8$ (ksi³ (MPa³))	Threshold, $(\Delta F)_{TH}$ (ksi (MPa))	Potential Crack Location	Illustrative Example
4.4 Full-penetration groove-welded tube-to-transverse plate connections with backing ring attached to the plate with a full penetration weld, or with a continuous fillet-weld around interior face of backing ring, and the backing ring welded to the tube with a continuous fillet-weld at top face of backing ring.	$K_F \leq 1.6 : 11.0$ (3750) $1.6 < K_F \leq 2.3 : 3.9$ (1330)	$K_I \leq 3.2 : 10.0$ (69) $3.2 < K_I \leq 5.1 : 7.0$ (48) $5.1 < K_I \leq 7.2 : 4.5$ (31)	In tube wall at groove-weld toe or backing ring top weld toe.	
4.5 Full-penetration groove-welded tube-to-transverse plate connections with backing ring attached to the plate with a full penetration weld, or with a continuous fillet-weld around interior face of backing ring, and the backing ring not welded to the tube.	$K_F \leq 1.6 : 11.0$ (3750) $1.6 < K_F \leq 2.3 : 3.9$ (1330)	$K_I \leq 3.2 : 10.0$ (69) $3.2 < K_I \leq 5.1 : 7.0$ (48) $5.1 < K_I \leq 7.2 : 4.5$ (31)	In tube wall at groove-weld toe.	
4.6 Full penetration groove-welded tube-to-transverse plate connections welded from both sides with back-gouging (without backing ring).	$K_F \leq 1.6 : 11.0$ (3750) $1.6 < K_F \leq 2.3 : 3.9$ (1330)	$K_I \leq 3.2 : 10.0$ (69) $3.2 < K_I \leq 5.1 : 7.0$ (48) $5.1 < K_I \leq 7.2 : 4.5$ (31)	In tube wall at groove-weld toe.	

Description	Finite Life Constant, $A \times 10^8$ (ksi³ (MPa³))	Threshold, $(\Delta F)_{TH}$ (ksi (MPa))	Potential Crack Location	Illustrative Example
4.7 Full-penetration groove-welded tube-to-transverse plate connections with the backing ring not attached to the plate, and the backing ring welded to the tube with a continuous fillet-weld at top face of backing ring.	$K_F \leq 1.6 : 11.0$ (3750) $1.6 < K_F \leq 2.3 : 3.9$ (1330)	$K_I \leq 3.2 : 10.0$ (69) $3.2 < K_I \leq 5.1 : 7.0$ (48) $5.1 < K_I \leq 7.2 : 4.5$ (31)	In tube wall at groove-weld toe.	
4.8 Partial penetration groove-welded mast-arm-to-column pass-through connections.	11.0 (3750)	4.5 (31)	In column wall at the mast-arm-to-column weld toe, or in column and mast-arm walls from the mast-arm-to-column weld root.	
SECTION 5 - FILLET-WELDED CONNECTIONS				
5.1 Fillet-welded lap splices.	11.0 (3750)	4.5 (31)		Column or mast-arm lap splices.
5.2 Members with axial and bending loads with fillet-welded end connections without notches perpendicular to the applied stress. Welds distributed around the axis of the member so as to balance welds stresses.	11.0 (3750)	4.5 (31)		Angle-to-gusset connections Slotted tube-to-gusset connections without coped holes (see note d).
5.3 Members with axial and bending loads with fillet-welded end connections with notches perpendicular to the applied stress. Welds distributed around the axis of the member so as to balance weld stresses.	3.9 (1330)	2.6 (18)		Angle-to-gusset connections Slotted tube-to-gusset connections without coped holes.

Description	Finite Life Constant, $A \times 10^8$ (ksi^3 (MPa^3))	Threshold, $(\Delta F)_{TH}$ (ksi (MPa))	Potential Crack Location	Illustrative Example
5.4 Fillet-welded tube-to-transverse plate connections	$K_F \leq 3.0 : 3.9$ (1330)	$K_I \leq 3.0 : 7.0$ (48) $3.0 < K_I \leq 5.7 : 4.5$ (31) $5.7 < K_I \leq 7.2 : 2.6$ (18)	In tube wall at fillet-weld toe.	
5.5 Fillet-welded T-, Y-, and K-tube-to-tube, angle-to-tube, or plate-to-tube connections.		(See notes a and b)		Chord-to-vertical or chord-to-diagonal truss connections (see note a) Mast-arm directly welded to column (see note b)
SECTION 6 - ATTACHMENTS				
6.1 Longitudinal attachments with partial- or full-penetration groove-welds, or fillet-welds, in which the main member is subjected to longitudinal loading: L < 2 in. (51 mm): 2 in (51 mm) ≤ L ≤ 12t and 4 in. (102 mm): L > 12t or 4 in. (102 mm) when t ≤ 1 in. (25 mm):	 44.0 (15000) 22.0 (7500) 11.0 (3750)	 10.0 (69) 7.0 (48) 4.5 (31)		
6.2 Tube-to-transverse plate connections stiffened by longitudinal attachments with partial- or full penetration groove-welds, or fillet-welds in which the tube is subjected to longitudinal loading and the welds are wrapped around the attachment termination.	$K_F \leq 2.5 : 11.0$ (3750)	$K_I \leq 5.5 : 7.0$ (48)	In tube wall at the toe of the attachment to tube weld at termination of attachment, and/or in tube wall at the toe of tube-to-transverse plate weld.	

Description	Finite Life Constant, $A \times 10^8$ (ksi^3 (MPa^3))	Threshold, $(\Delta F)_{TH}$ (ksi (MPa))	Potential Crack Location	Illustrative Example
6.3 Transverse load-bearing partial joint penetration groove-welded or fillet-welded attachments where $t \leq 0.5$ in.(13 mm) and the main member is subjected to minimal axial and/or flexural loads. (When $t > 0.5$ in [13 mm], see note c).	44.0 (15000)	10.0 (69)		Longitudinal stiffeners welded to base plates
6.4 Tube-to-transverse plate connections stiffened by longitudinal stool type attachments with partial- or full penetration groove-welds, or fillet-welds in which the tube is subjected to longitudinal loading and the welds are wrapped around the attachment termination.	11.0 (3750)	2.6 (18)	In tube wall at the toe of the attachment to tube weld at termination of attachment	

Notes:

a   In a branching member with respect to the stress in the branching member:

$(\Delta F)_{TH} = 1.2$ ksi ; when $r/t \leq 24$ for the chord member

$(\Delta F)_{TH} = 8$ MPa ; when $r/t \leq 24$ for the chord member

$(\Delta F)_{TH} = 1.2 \times \left(\dfrac{24}{\frac{r}{t}} \right)^{0.7}$ ksi ; when $r/t > 24$ for the chord member

$(\Delta F)_{TH} = 8 \times \left(\dfrac{24}{\frac{r}{t}} \right)^{0.7}$ MPa ; when $r/t > 24$ for the chord member

In a chord member with respect to the stress in the chord member: $(\Delta F)_{TH} = 4.5$ ksi (31 MPa).

b   In a branching member with respect to the stress in the branching member: $(\Delta F)_{TH} = 1.2$ ksi (8 MPa)

In main member with respect to the stress in the main member (column):

$(\Delta F)_{TH} = 1.0$ ksi ; when $r/t \leq 24$ for the chord member

$(\Delta F)_{TH} = 1.0 \times \left(\dfrac{24}{\dfrac{r}{t}} \right)^{0.7}$ ksi ; when $r/t > 24$ for the chord member

$(\Delta F)_{TH} = 7$ MPa ; when $r/t_c \leq 24$ for the main member

$(\Delta F)_{TH} = 7 \times \left(\dfrac{24}{\dfrac{r}{t_c}} \right)^{0.7}$ MPa ; when $r/t_c > 24$ for the main member

where:

The nominal stress range in the main member equals $(S_R)_{\text{main member}} = (S_R)_{\text{branching member}} (t_b/t_c) \alpha$

where t_b is the wall thickness of the branching member, t_c is the wall thickness of the main member (column), and α is the ovalizing parameter for the main member equal to 0.67 for in-plane bending and equal to 1.5 for out-of-plane bending in the main member. $(S_R)_{\text{branching member}}$ is the calculated nominal stress range in the branching member induced by fatigue design loads. (See commentary of Article 11.5.)

The main member shall also be designed for $(\Delta F)_{TH} = 4.5$ ksi (31 MPa) using the elastic section of the main member and moment just below the connection of the branching member.

224

c   When $t > 0.5$ in. (13 mm), $(\Delta F)_{TH}$ shall be the lesser of 10.0 ksi (69 MPa) or the following:
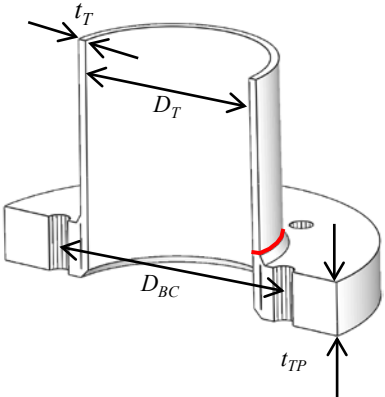
$$(\Delta F)_{TH} = 10.0 \times \left(\dfrac{0.0055 + 0.72\dfrac{H}{t_p}}{t_p^{\frac{1}{6}}} \right) \text{ksi}$$
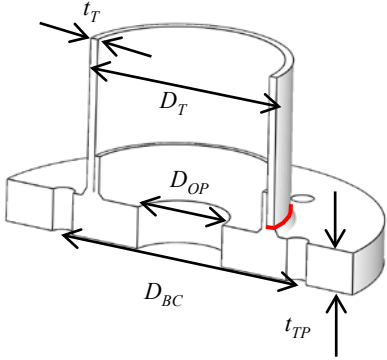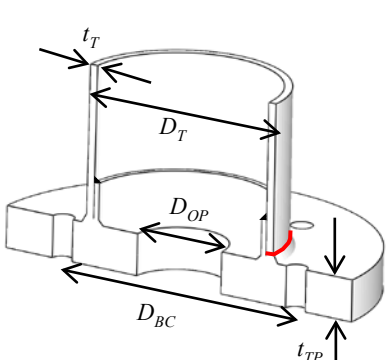
$$(\Delta F)_{TH} = 69 \times \left(\dfrac{0.094 + 1.23\dfrac{H}{t_p}}{t_p^{\frac{1}{6}}} \right) \text{MPa}$$
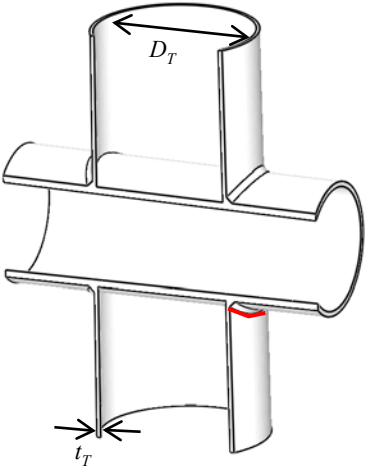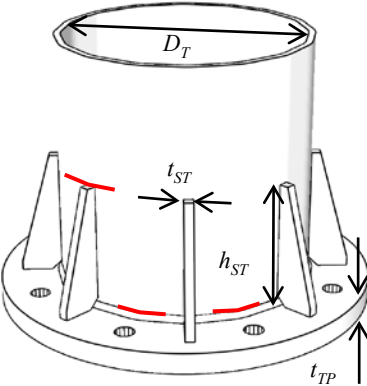
where H is the effective weld throat (in., mm), and t_p is the attachment plate thickness (in., mm).
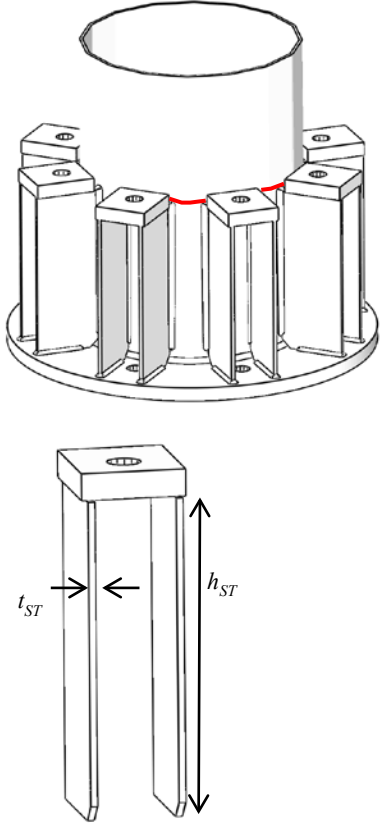
d   The diameter of coped holes shall be the greater of 1 in. (25 mm), twice the gusset plate thickness, or twice the tube thickness.

Table C11–1: Fatigue Details of Support Structures Tested in the Laboratory

Description	Identification of Parameters	Tube Configuration	Detail Parameters	Finite Life Constant, $A \times 10^8$ (ksi^3 (MPa^3))	Threshold, ΔK_{TH} (ksi (MPa))
Fillet-welded tube-to-transverse plate connections		Round	$t_T = 0.179$ in (4.5 mm) $D_T = 10$ in (254 mm) $t_{TP} = 2$ in (51 mm) $D_{BC} = 23.3$ in (592 mm) $N_B = 4$	3.9 (1330) ($K_F = 2.4$)	4.5 (31) ($K_I = 4.6$)
		Round	$t_T = 0.239$ in (6 mm) $D_T = 13$ in (330 mm) $t_{TP} = 2$ in (51 mm) $D_{BC} = 20$ in (508 mm) $N_B = 4$	3.9 (1330) ($K_F = 2.7$)	4.5 (31) ($K_I = 5.7$)
		Multi-sided	$t_T = {}^3/_{16}$ in (5 mm) $D_T = 10$ in (254 mm) $t_{TP} = 2$ in (51 mm) $D_{BC} = 23.3$ in (592 mm) $N_B = 4$ $N_S = 8$ $r_b = 0.5$ in (13 mm)	3.9 (1330) ($K_F = 2.8$)	2.6 (18) ($K_I = 5.8$)
		Multi-sided	$t_T = {}^1/_4$ in (6 mm) $D_T = 13$ in (330 mm) $t_{TP} = 2$ in (51 mm) $D_{BC} = 20$ in (508 mm) $N_B = 4$ $N_S = 8$ $r_b = 0.5$ in (13 mm)	($K_F = 3.3$)	2.6 (18) ($K_I = 7.2$)
		Multi-sided	$t_T = {}^5/_{16}$ in (8 mm) $D_T = 24$ in (610 mm) $t_{TP} = 3$ in (76 mm) $D_{BC} = 30$ in (762 mm) $N_B = 16$ $N_S = 16$ $r_b = 4$ in (102 mm)	3.9 (1330) ($K_F = 2.4$)	4.5 (31) ($K_I = 5.3$)

225

Description	Identification of Parameters	Tube Configuration	Detail Parameters	Finite Life Constant, $A \times 10^8$ (ksi^3 (MPa^3))	Threshold, ΔK_{TH} (ksi (MPa))
Full-penetration groove-welded tube-to-transverse plate connections with backing ring attached to the plate with a full penetration weld, or with a continuous fillet-weld around interior face of backing ring, and the backing ring not welded to the tube.		Round	$t_T = 0.179$ in (4.5 mm) $D_T = 10$ in (254 mm) $t_{TP} = 2$ in (51 mm) $D_{BC} = 23.3$ in (592 mm) $N_B = 4$ $D_{OP} = 7.6$ in (193 mm)	3.9 (1330) ($K_F = 1.9$)	7.0 (48) ($K_I = 3.5$)
		Round	$t_T = 0.239$ in (6 mm) $D_T = 13$ in (330 mm) $t_{TP} = 2$ in (51 mm) $D_{BC} = 20$ in (508 mm) $N_B = 4$ $D_{OP} = 4$ in (102 mm)	11.0 (3750) ($K_F = 1.6$)	10.0 (69) ($K_I = 2.7$)
		Round	$t_T = 0.239$ in (6 mm) $D_T = 13$ in (330 mm) $t_{TP} = 2.5$ in (64 mm) $D_{BC} = 20$ in (508 mm) $N_B = 4$ $D_{OP} = 7$ in (178 mm)	11.0 (3750) ($K_F = 1.6$)	10.0 (69) ($K_I = 2.9$)
Full-penetration groove-welded tube-to-transverse plate connections with the backing ring not attached to the plate, and the backing ring welded to the tube with a continuous fillet-weld at top face of backing ring.		Round	$t_T = 0.179$ in (4.5 mm) $D_T = 10$ in (254 mm) $t_{TP} = 2$ in (51 mm) $D_{BC} = 23.3$ in (592 mm) $N_B = 4$ $D_{OP} = 9.2$ in (244 mm)	3.9 (1330) ($K_F = 2.2$)	Not Tested
		Round	$t_T = 0.239$ in (6 mm) $D_T = 13$ in (330 mm) $t_{TP} = 2$ in (51 mm) $D_{BC} = 20$ in (508 mm) $N_B = 4$ $D_{OP} = 12$ in (305 mm)	3.9 (1330) ($K_F = 2.4$)	Not Tested
		Multi-sided	$t_T = {}^5/_{16}$ in (8 mm) $D_T = 24$ in (610 mm) $t_{TP} = 2.5$ in (64 mm) $D_{BC} = 30$ in (762 mm) $N_B = 8$ $D_{OP} = 14$ in (356 mm) $N_S = 16$ $r_b = 4$ in (102 mm)	3.9 (1330) ($K_F = 2.2$)	7.0 (48) ($K_I = 4.6$)

Description	Identification of Parameters	Tube Configuration	Detail Parameters	Finite Life Constant, $A \times 10^8$ (ksi^3 (MPa^3)	Threshold, ΔK_{TH} (ksi (MPa)
Partial penetration groove-welded mast-arm-to-column pass-through connections.		Round	$t_T = {}^1/_4$ in (6 mm) $D_T = 13$ in (330 mm)	11.0 (3750) ($K_F = 2.1$)	4.5 (31) ($K_I = 2.4$)
Tube-to-transverse plate connections stiffened by longitudinal attachments with partial- or full penetration groove-welds, or fillet-welds in which the tube is subjected to longitudinal loading and the welds are wrapped around the attachment termination.		Multi-sided	$t_T = {}^5/_{16}$ in (8 mm) $D_T = 24$ in (610 mm) $t_{TP} = 2$ in (51 mm) $D_{BC} = 30$ in (762 mm) $N_B = 8$ $N_S = 16$ $r_b = 4$ in (102 mm) $N_{ST} = 8$ $h_{ST} = 18$ in (457 mm) $t_{ST} = {}^3/_8$ in (9.5 mm)	- Cracking at top of stiffener 11.0 (3750) ($K_F = 2.4$) - Cracking at transverse plate fillet-weld toe on tube wall 3.9 (1330) ($K_F = 1.6$)	7.0 (48) ($K_I = 5.2$) 7.0 (48) ($K_I = 3.0$)

227

Description	Identification of Parameters	Tube Configuration	Detail Parameters	Finite Life Constant, $A \times 10^8$ (ksi^3 (MPa^3))	Threshold, ΔK_{TH} (ksi (MPa))
Tube-to-transverse plate connections stiffened by longitudinal stool type attachments with partial- or full penetration groove-welds, or fillet-welds in which the tube is subjected to longitudinal loading and the welds are wrapped around the attachment termination.		Multi-sided	$t_T = {}^5/_{16}$ in (8 mm) $D_T = 24$ in (610 mm) $t_{TP} = 2$ in (51 mm) $D_{BC} = 30$ in (762 mm) $N_B = 8$ $N_S = 16$ $r_b = 1$ in (25 mm) $N_{ST} = 8$ $h_{ST} = 18$ in (457 mm) $t_{ST} = {}^3/_8$ in (9.5 mm)	3.9 (1330) ($K_F = 2.3$)	2.6 (18) ($K_I = 3.2$)
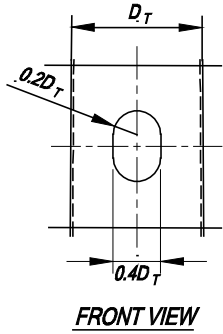
Figure 11-1—Details of unreinforced holes and cutouts
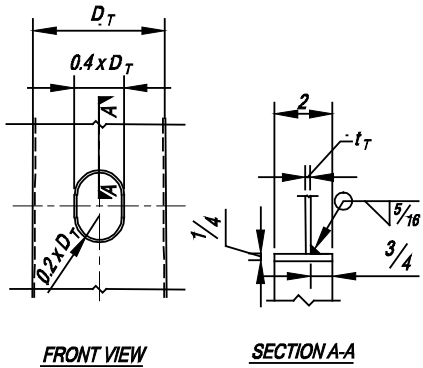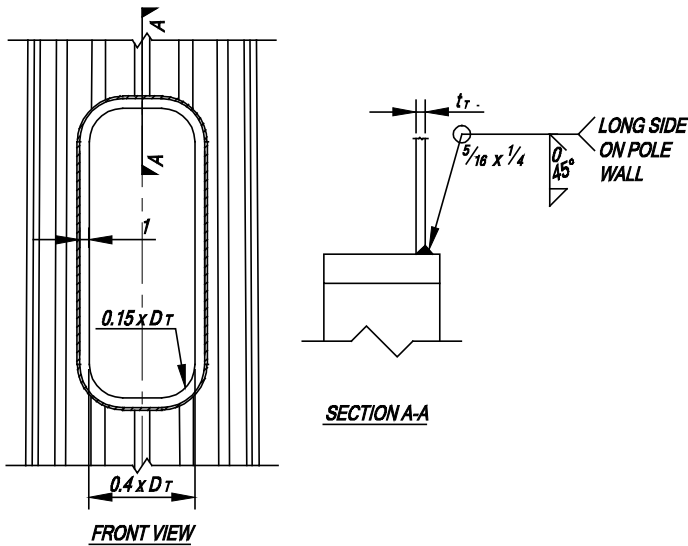
Figure 11-2—Details of reinforced holes and cutouts

229

VIEW A-A
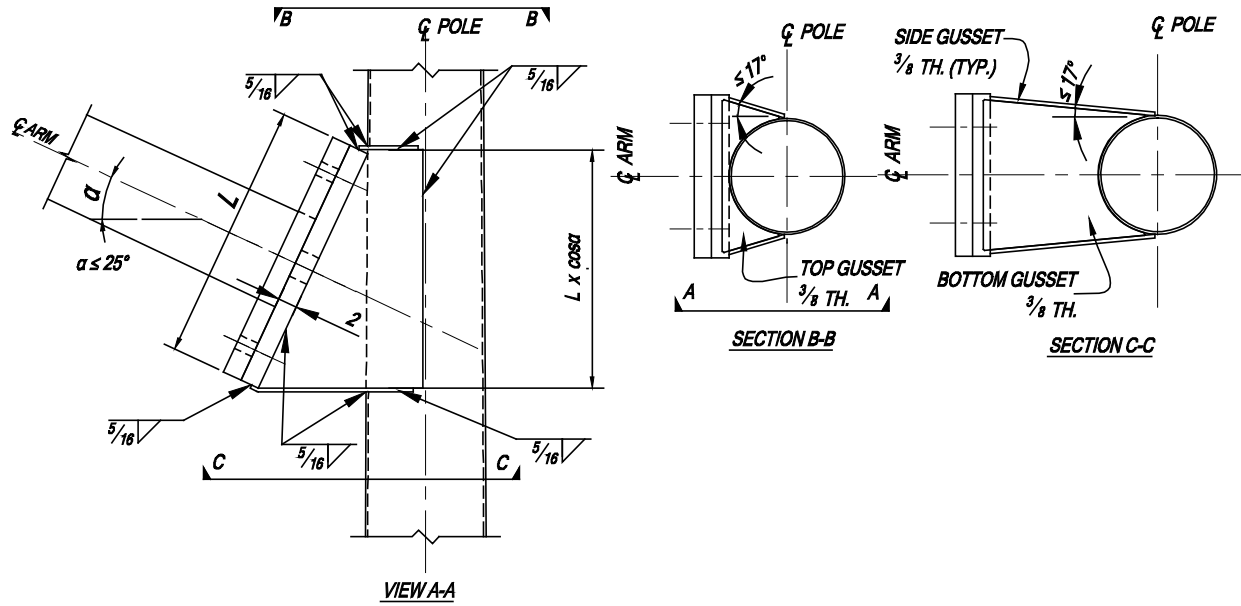
Figure 11-3—Details of fillet-welded gusseted box connections

SECTION B-B

SECTION C-C

VIEW A-A
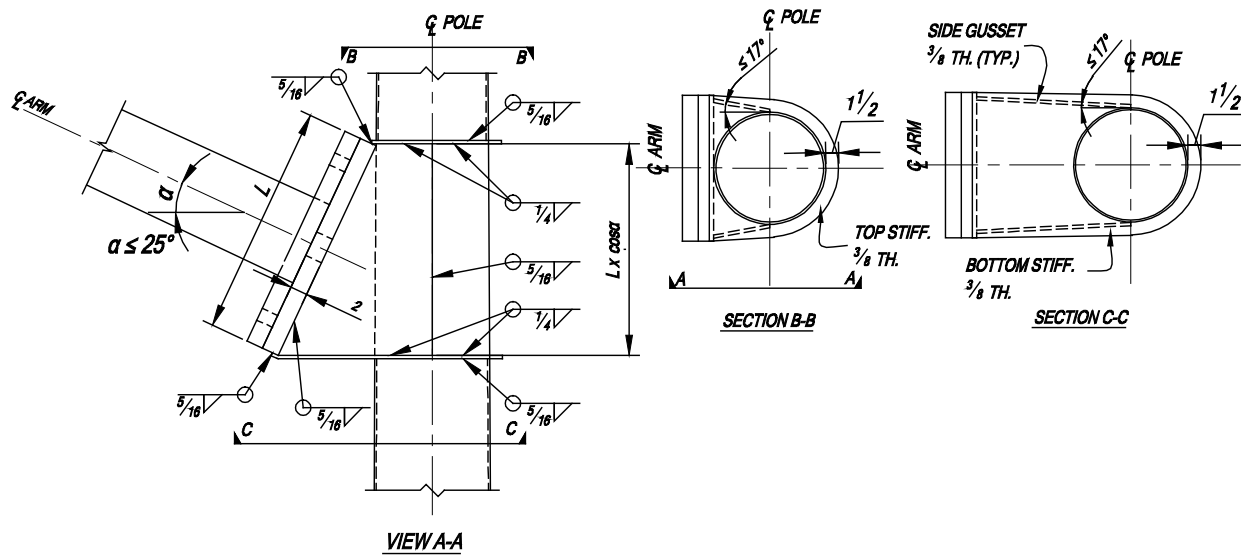
Figure 11-4—Details of fillet-welded ring-stiffened box connections

230

<div style="border:1px solid black">

APPENDIX D:

ALTERNATE METHODS FOR FATIGUE DESIGN

</div>

D1—ALTERNATE METHODS

Section 11, "Fatigue Design," provides a methodology for fatigue design of support structures using nominal stress-based classifications of typical fatigue sensitive connection details as presented in Table 11-2. This appendix provides an alternate local stress-based methodology for fatigue design, and an experimental procedure for establishing fatigue resistance of connections in support structures. Although the methods may be applied to connections that are tabulated in Table 11-2, it is expected that the methods will be more useful for establishing the fatigue resistance of new connection details that are not listed in Table 11–2. Accordingly, these connection details should be designed for infinite life. The analytical and experimental protocols provided in the following articles were verified on connections evaluated under NCHRP Project 10-70, which are listed in Table C11–1. Fatigue resistance of connections determined by the local stress-based methodology, should be verified experimentally.

D2—LOCAL STRESS-BASED DESIGN

As an alternative to the Nominal Stress-based Design of Section 11.5.1, welded connections in support structures may be designed using local stresses obtained from Finite Element (FE) analyses. The FE analyses may be carried out using any available program that has been validated.

For local stress-based design, Equation 11–1 is rewritten as:

$$\left(\Delta f\right)_l \le \left(\Delta F\right)_l \tag{D-1}$$

where $(\Delta f)_l$ is wind induced local stress at the weld toe as defined in Articles D2.1.1 and D2.2.1; and $(\Delta F)_l$ is local fatigue resistance as determined in Articles D2.1.2 and D2.2.2.

It should be noted that the local stress-based method for finite life is only applicable to fatigue design of tubular connections including tube-to-transverse plate and tube-tube connections, where the geometric (out-of-plane distortion induced) stress concentration (see discussion in commentary C11.5.1.3.1) affects the fatigue performance of the connection significantly. For other details that are primarily subjected to in-plane stresses, a nominal stress-based design methodology should be sufficient with due consideration to the magnified nominal stress at a detail if appropriate (as an example see discussion in commentary C11.5.1.3 for handhole details)

The local stress-based design method for finite life is calibrated against fatigue cracking at the weld toe. For infinite life design, however, fatigue crack initiation and crack propagation should be inhibited. Thus the local stress-based design method for finite life is not applicable to infinite life design. Separate methodologies should be used for finite and infinite life designs as provided in Articles D2.1 and D2.2.

D2.1—Design for Finite Life

The remaining fatigue life of tubular connections in existing structures may be assessed based on a finite life.

D2.1.1—Determination of Local Stress

The local stress in welded connections that can experience fatigue cracking at the weld toe shall be determined from detailed linear FE analyses of a three dimensional (3D) model of the connection. The nominal weld geometry shall be included in the model. Because of the steep geometric stress gradient associated with the connection geometry, a three dimensional FE model of the connection should be used. In thin tubular structures, the weld acts like a tiny stiffener and influences the geometric stress concentration. To achieve proper local stiffness and improved stress prediction, the nominal weld geometry should be modeled. The FE model should assume linear material properties.

The model shall be large enough so the calculated results are not significantly affected by the assumptions made for modeling the boundary conditions and the application of loads. If the model is too large to be meshed at the required refinement, an analysis of a refined submodel driven by the analysis results of a less refined global model shall

be performed. Two dimensional (2D) shell elements may be used for modeling other parts of the support structures away from the connections to reduce computation costs.

Reduced integration 20-node solid isoparametric elements shall be used for modeling the connection. 20-node solid hexahedron elements of isoparametric formulation are standard elements used for stress analysis. These elements, also known as serendipity elements, assume an incomplete quadratic polynomial as displacement and geometric shape functions resulting in linear strain and stress distributions. The element stiffness matrix is formed by assuming a reduced number of Gauss integration points for better correlation of FE results with true solution. In tubes a mesh size of $t \times t$ shall be used for at least three rows of elements in front of the weld toe, where t is the tube wall thickness. At least two elements shall be used in the thickness direction. To avoid numerical instabilities and inaccuracy in solutions, the elements should be well shaped and proportioned. All elements in the model shall be limited to a maximum aspect ratio of 1:4. The elements shall be well shaped having corner angles between 30^0 and 150^0.

The maximum (tensile) principal stress on the tube surface at $0.1\sqrt{(r \times t)}$ ahead of weld toe shall be used as the local stress for fatigue design, where r and t are the outer radius and thickness of the tube respectively. For multi-sided cross sections, half of the outer opposite to flat distance shall be substituted for r.

When the weld toe is modeled with zero radius, the stress solution at the weld toe approaches infinity as the element size is decreased to zero. However, the effect of the connection geometry on the stress beyond the influence of the weld toe is of interest. The scatter associated with weld toe micro-discontinuities is included by using experimentally obtained S-N curves. It is well known from theory of thin tubes that the geometric stresses associated with secondary out-of-plane bending deformation at tube boundaries (arising from the need to maintain compatibility at the connections) is a function of the tube geometric parameter $\sqrt{(r \times t)}$. The coefficient to this parameter was determined empirically.

D2.1.2—Fatigue Resistance

The fatigue resistance for design using the local stress shall be taken as:

$$\left(\Delta F\right)_l = \left(\frac{44 \times 10^8}{N}\right)^{\frac{1}{3}} \cdot \text{ksi}$$

$$\left(\Delta F\right)_l = \left(\frac{15 \times 10^{11}}{N}\right)^{\frac{1}{3}} \cdot \text{MPa} \hspace{4cm} \text{(D-2)}$$

The effect of the weld toe discontinuity and the associated variability is included by using the experimentally obtained Category C design curve of the AASHTO LRFD Bridge Design Specifications, which reflects fatigue cracking associated with the weld toe geometry and its inherent variability.

D2.2—Design for Infinite Life

Connection details in support structures shall be designed for infinite life.

D2.2.1—Determination of Local Stress

The requirement for design against infinite life is that fracture due to fatigue must be avoided regardless of the duration of the service life and the possibility of cyclic crack initiation, and that crack propagation must be suppressed. The underlying assumption is that no appreciable damage occurs at the weld toe notch and the notch stresses are purely elastic. This assumption is somewhat simplistic in that cracks may initiate at the weld toe notch but may not propagate, that is, "dormant cracks" may exist with limited damage from cyclic loading. To this end, the local stress at the weld toe notch should be determined.

The local stress for infinite life design against fatigue cracking from weld toe shall be determined by 3D FE analyses considering the local effect of the weld toe notch. A notch of 0.04 in (1 mm) radius shall be introduced at the toe of the nominal weld geometry. Determination of stresses at the weld toe notch is complicated by the significant scatter in local weld geometry and presence of micro discontinuities. Moreover, when the weld toe notch is modeled with zero radius, the stress solution approaches infinity as the element size in the FE model is decreased to zero. To obtain a fatigue effective stress at the weld toe notch, a radius of 0.04 in (1 mm) is introduced at the center of the notch,

232

which has been verified to produce consistent results for structural steel.

The FE model shall be large enough so the calculated results are not significantly affected by the assumptions made for modeling, the boundary conditions and the application of loads. If the model is too large to be meshed at the required refinement, an analysis of a refined submodel driven by the analysis results of a less refined global model shall be performed.

Reduced integration 20-node solid isoparametric elements shall be used for modeling the connection and the weld toe region.

At least eight elements shall be used along the rounded notch perimeter. All elements in the model shall be limited to a maximum aspect ratio of 1:4. To avoid numerical instabilities and inaccuracy in solutions, the elements shall be well shaped having corner angles between 30^0 and 150^0.

The converged maximum (tensile) surface stress at the center of the rounded notch shall be used as the local stress for fatigue design.

D2.2.2—Fatigue Resistance

The fatigue resistance for infinite life design using local stress methodology shall be calculated as:

$$(\Delta F)_l = \frac{1}{3.2}\left[-F_y + \sqrt{F_y^2 + 4 \times F_u^2}\right] \text{ ksi}$$

$$(\Delta F)_l = \frac{1}{22.4}\left[-F_y + \sqrt{F_y^2 + 4 \times F_u^2}\right] \text{ MPa}$$

(D-3)

where F_y is the yield strength of the material (ksi, MPa); and F_u is the tensile strength of the material (ksi ,MPa).

The above equation is simplified from a relationship developed by Roy and Fisher (2005) for assessing the CAFT of welded connections using an effective notch stress. This relationship is a function of the stress ratio (the ratio of the stress range to the minimum stress), welding residual stress, the endurance limit of a smooth specimen and the notch stress concentration factor. In as-welded connections, tensile residual stresses approximately equal to the yield stress of the material exist near the weld, which results in a local stress ratio in excess of 0.5. An endurance limit of 0.5 of the tensile strength is appropriately assumed for structural steel. The fatigue effective notch stress concentration is found to be about 80% of the geometric stress concentration of the rounded weld toe notch. The Roy and Fisher equation is thus simplified to the form of D-3.

D3—EXPERIMENT BASED DESIGN

Fatigue tests should be conducted using minimum stress (S_{min}) and the stress range (S_r) as the two design stress variables. The design stress variables should focus on the particular type of structure in question. The details in the sign and signal support structures should be generally tested under a high level of minimum stress, commensurate with the anticipated dead load effects from the overhanging weights of the signs and signal attachments. The details in the high level luminaire support structures should be tested under the condition of complete stress reversal, which is typically the case in this type of structure.

D3.1—Determination of Finite Life Fatigue Resistance

The remaining fatigue life of connections in existing support structures may be assessed based on finite life.

D3.1.1—Experimental Protocols

The finite life fatigue resistance of the connection details should be determined by full scale laboratory fatigue tests. The fatigue tests should be conducted at two stress range levels separated by at least 4.0 ksi (28 MPa). The stress range levels should be decided based on an analytical assessment of the fatigue performance of the test detail as suggested in Article D2.1. At least three experiments must be conducted at each level of stress range to provide sufficient replicates for a meaningful statistical analysis.

Specimens should be instrumented using encapsulated bonded electrical resistance strain gauges at locations of interest on the specimen surface to measure strains. In steel structures, these strains may be converted to stresses by

233

multiplying with the modulus of elasticity of steel taken as 29000 ksi (200 GPa). The locations of the strain gauges may be decided based on FE analyses of the test specimen in accordance with the guidelines in Article D2.1.1. Uniaxial strain gauges of $^1/_4$ in (6 mm) gauge length may be used for measuring nominal strains away from local stress concentrations such as weld toe. These gauges should be placed a minimum of 5 in (127 mm) away from local stress raisers such as the weld toe of the tested detail, or as determined from the FE results. The strain gauges should be oriented in a direction in which the nominal strain is being measured. Uniaxial strain gauges of 0.04 in (1 mm) grid length may be used near the weld toe to capture local strain peak. At least two strain gauges should be used to measure the variation of the local strain gradient. These strain gauges in tubular connections should be located on the external surface of the tube at $0.1 \sqrt{(r \times t)}$, but not less than 0.16 in (4 mm), and t away from the weld toe, where r is the external radius of the tube, and t is the thickness of the tube. These strain gauges should be oriented perpendicular to the weld toe.

All specimens should be tested under static loading (loading rate less than 1.0 ksi/s (7 MPa/s)) prior to fatigue tests. Static tests will be conducted in a simple up-down pattern by loading the specimen up to the estimated maximum test load and complete unloading. The test will be repeated for at least three times or until the residual strains at the strain gauges upon unloading become negligible. In each test, the strain at each gauge, the applied load, and the displacement at the load point should be recorded.

The fatigue tests should be conducted at a minimum 1 Hz frequency under constant amplitude loading. The tests should be monitored by maximum and minimum strains (or stresses) recorded at control strain gauges. To capture the nominal stresses, the control gauges should be located at a section beyond the influence of local stresses.

The tests should be periodically monitored. The strains (or stresses) at the control and other gauges should be recorded. The test details should be inspected for fatigue crack growth with the aid of 10× magnifying glass and/or dye-penetrant or magnetic particle testing.

Fatigue failure of a detail will be defined by a visible through thickness crack of minimum 5 in (127 mm) length measured tip to tip. This crack length on a tube wall in a tubular connection should be taken as half the diameter of the tube. At an attachment detail on the tube wall (except at stiffeners in stiffened fillet-welded tube-to-transverse plate connections), the failure should be defined when the crack from the toe or the root of the attachment-to-tube weld branches into the tube wall. Failure criteria for stiffened tube-to-transverse plate connections should be the same as tubular connections described above.

D3.1.2—Determination of Fatigue Resistance

The fatigue resistance of the test detail is defined by the nominal stress range and the endured number of cycles at failure. The nominal stress should be extrapolated from the stresses measured at the control gauge to the site of fatigue cracking. The fatigue test results shall be plotted against the AASHTO fatigue design curves (Figure C11.5.1.3-1). The connection detail shall be classified by the fatigue design curve that is exceeded by the fatigue test result exhibiting the least fatigue life. The finite life constant for the connection detail shall be determined accordingly.

Scatter in fatigue test data associated with uncontrolled variables such as the weld toe geometry and the micro discontinuities from the acceptable fabrication practice is expected. However, significantly larger scatter may arise in the fatigue test results owing to the variation in the fabricated weld geometry and particularly the weld angle from the specified nominal value. In the thin walled tubular support structures, the welds act as tiny stiffeners affecting the geometric stresses and contribute to the scatter in the test results. The detail classification based on the least fatigue life is expected to provide a lower bound estimate of the fatigue performance of the tested connection detail.

D3.2—Determination of Infinite Life Fatigue Resistance

Fatigue resistance of connection details in support structures shall be designed to ensure infinite life.

D3.2.1—Experimental Protocols

Connection details should be fatigue tested in a laboratory to establish their respective CAFT. At least four tests must be conducted for each detail type to determine the CAFT.

The first test should be conducted at a nominal stress range corresponding to a CAFT (as tabulated in the AASHTO LRFD Bridge Design Specifications) nearest to the estimated fatigue threshold of the particular detail type assessed by the local stress-based method suggested in D2.2. The nominal stress ranges corresponding to these fatigue thresholds (AASHTO CAFTs) in increasing severity of detail classes are: 16 ksi (110 MPa); 12 ksi (83 MPa); 10.0 ksi (69 MPa); 7.0 ksi (48 MPa); 4.5 ksi (31 MPa); and 2.6 ksi (18 MPa). As an approximation, the nominal stress range

234

may be computed from equation D-3, by dividing the local stress-based fatigue resistance by an approximate stress concentration factor of 6.0.

The "run-out" life shall be taken as: 12.5×10^6 cycles at 16 ksi (110 MPa); 7.0×10^6 cycles at 12 ksi (83 MPa); 8.2×10^6 cycles at 10.0 ksi (69 MPa); 14.7×10^6 cycles at 7.0 ksi (48 MPa); 20×10^6 cycles at 4.5 ksi (31 MPa); and 20×10^6 cycles at 2.6 ksi (18 MPa).

The infinite life tests should be conducted by a "step" method. If a specimen is run-out, it may be tested again at an increased stress range level corresponding to the next CAFT, provided it is verified by magnetic particle and dye-penetrant tests that no fatigue crack has initiated at the weld toe. On the other hand, if the specimen develops fatigue cracking before achieving the target number of cycles for infinite life, the subsequent specimen must be tested at a decreased stress range corresponding to the next lower CAFT.

Other protocols for infinite life tests including instrumentation, static and fatigue testing, and inspection, monitoring and recording, shall be the same as those stipulated in Article D3.1.1 for finite life tests.

D3.2.2—Determination of Fatigue Resistance

The lowest stress range (corresponding AASHTO CAFT) at which the tests are run-out should be defined as the fatigue resistance for the particular test detail.

235

CHAPTER 5

CONCLUSIONS AND FURTHER RESEARCH

CONCLUSIONS

Cost-effective and fatigue resistant connections (details) in highway sign, luminaire and traffic signal structures were developed as part of this research. Fatigue resistance of various critical welded details in the subject structures were established in both finite and infinite life regimes. Seventy eight full size galvanized specimens were fatigue tested. Using parametric FEA verified by test data, fatigue performance of the connections in both finite and infinite life regimes were evaluated and optimized over the range of applicable geometric dimensions. Based on these research findings new specification recommendations and design guidelines were developed that incorporated the effect of connection geometry on fatigue resistance. In addition, experimental and analytical protocols were developed and verified in this research for reliably and consistently assessing finite and infinite life performances of welded connections in the subject structures.

Tube-to-transverse Plate Connections

The research demonstrated that tube-to-transverse plate connection is the most fatigue critical detail in the subject structures. In addition to the conditions inherent to welded connections, fatigue cracking of these connections is precipitated by large out-of-plane bending stresses in the tube that is introduced to maintain compatibility in deformation of the tube and the transverse plate. Accordingly, fatigue performance of these connections is dependent on the connection geometry and particularly on the relative flexibility of the components. The critical geometric parameters of the connections are: the thickness of the transverse plate; the opening in the transverse plate (in groove-welded connections); the number of fasteners; the bolt circle diameter; the tube diameter and thickness; the height and thickness of backing ring (in groove-welded connections); the number of sides and internal bend radius (in multi-sided sections); the stiffener shape and size (thickness, height and angle); and the number of stiffeners or stiffener spacing (in stiffened connections).

Fillet-welded Tube-to-transverse Plate Connection

In an unstiffened fillet-welded tube-to-transverse plate connection, increasing the plate thickness is the most cost-effective means of increasing the connection fatigue performance. For a particular tube geometry, the increase is, however, asymptotic with increasing transverse plate thickness. In larger diameter tubes, the thickness of transverse plate required to achieve the desired fatigue resistance may not be feasible. In such situations, a groove-welded tube-to-transverse plate connections or a stiffened connection should be explored.

Full-penetration Groove-welded Tube-to-transverse Plate Connection

In an unstiffened full-penetration groove-welded tube-to-transverse plate connection, reducing the opening in the transverse plate in addition to increasing the plate thickness provides

236

a cost-effective and fatigue resistant design. The opening size should be sufficient for draining liquid zinc during galvanizing and depositing the weld at the top of backing ring, when the backing ring is welded to the tube.

If the backing ring is welded to the plate and the tube, it participates in transferring forces from the tube to the transverse plate, and fatigue cracking can occur both at groove-weld toe and the backing ring top weld toe on the tube. The amount of force that is transferred through the backing ring and the resulting stress concentration at the backing ring weld toe depends on the diameter and thickness of the tube, and the height and thickness of the backing ring. When the backing ring is welded to the tube it provides a redundant load path after the tube to transverse plate groove-weld develops fatigue cracking.

In tubes having a diameter smaller than 406 mm (16 in), it is difficult to ensure quality weld between the tube and the backing ring at the top, where premature fatigue cracking from the toe of this weld on the tube wall may limit the fatigue resistance of the connection. It is recommended that the backing ring be welded to the tube on the top face only in larger diameter tubes, where this weld quality can be adequately controlled. When performed, this weld should be specified and inspected as a structural weld.

A 2 in × ¼ in backing ring should be sufficient. In galvanized structures, if the backing ring is not welded to the plate or to the tube wall, all resulting gaps should be sealed by caulking after galvanizing to prevent ingress of moisture and resulting activation of any trapped acid. The backing ring should not be tack-welded to the tube unless the tack weld is completely incorporated in subsequent welds. Premature fatigue cracking from tack welds can limit fatigue performance of the connection. Grinding of tack welds in these thin tubular structures is discouraged.

Stiffened Tube-to-transverse Plate Connection

In support structures employing larger diameter and thicker tubes, optimized stiffened tube-to-transverse plate fillet-welded connections can provide a cost-effective design compared to an increased transverse plate thickness. Ideally an optimum solution would render the weld toes on the tube at the stiffener termination and at the transverse plate equally susceptible to fatigue cracking. A large stiffener thickness relative to the tube wall can attract more stress into the stiffeners and can increase distortion of the tube wall. On the contrary, relatively thin stiffeners can reduce distortion of the tube wall but fail to sufficiently reduce the stress at the fillet-weld and can cause fatigue cracking through the throat of the stiffener-to-transverse plate weld. A ratio of stiffener thickness to tube thickness of 1.25 provides an optimum solution with equal likelihood of fatigue cracking at the stiffener termination and at the tube-to-transverse plate weld. Decreasing the ratio of the stiffener height to stiffener spacing reduces protection to the fillet-weld. An optimum solution is obtained when the stiffener height is about 1.6 times the stiffener spacing. Reducing the termination angle of the stiffener on the tube improves the fatigue performance of stiffened connections. Using a stiffener termination angle of 15^0 ensures that the normal stress is linearly distributed over the stiffened cross section and the stiffener sections are fully effective in sharing load.

Fillet-welded tapered stiffeners with wrapped-around weld at the terminus are cost-effective. The wrap-around weld serves as a seal weld for galvanizing. Stiffeners with a transition radius at the termination on the tube wall are fabrication intensive and are expected to be costlier than a tapered alternative. To avoid exposure of the lack of fusion at the weld root in

237

fillet and partial penetration groove-welds, a stiffener termination with a transition radius must be groove-welded, which requires non-destructive inspection in the vicinity of weld termination. It is difficult to grind the weld toe without inadvertently thinning the tube wall at the transition, which is a concern for thin tubes. The stiffened groove-welded tube-to-transverse plate connection is unlikely to be cost-effective.

Multi-sided Tubular Sections

In multi-sided tubular sections, the number of sides and the corner bend radius affect the fatigue resistance of connections. Fatigue cracking in multi-sided tube-to-transverse plate connections initiate early at the bend corners due to high notch stress concentration, which is precipitated with less number of sides and sharper bend radius. Roundness is a parameter that quantifies the geometric similarity of a multi-sided section relative to a round section. A multi-sided section approaches a round section with increasing number of sides and increasing internal bend radius at the corners. For a perfectly round section this parameter becomes 1.0. Compared to a round tube of similar size, the tube-to-transverse plate connection in a multi-sided tube of lower roundness exhibits significantly less fatigue resistance. Increasing the number of sides and/or increasing the internal bend radius can improve fatigue performance of multi-sided sections.

Minimum Plate Thickness

Experimental and analytical studies demonstrated that a minimum 2 in thick plate must be used at a tube-to-transverse plate connection to limit transverse plate flexibility and to increase the connection fatigue performance in a cost-effective manner.

Handholes and Cutouts

Fatigue cracking from unreinforced handholes in specimens of sign/signal support structures initiated from the edge of handhole at the point of maximum stress concentration. In reinforced handholes, fatigue cracking initiated only from the lack of fusion at the root of the handhole frame-to-pole (reinforcement-to-tube) fillet-weld. Because of limited access, the handhole frames in sign and signal structures can be welded only from the outside, increasing the possibility of lack of fusion defects at the weld root. No fatigue cracking at the toe of the handhole frame-to-pole weld was detected. In specimens of high-level luminaire support structures, the handhole details did not develop any fatigue cracking.

Since the fatigue stress cycles in sign/signal support structures are imparted primarily due to wind induced galloping oscillations in the plane containing the arm, the handholes and cutouts in these structures should be located in low stressed areas on the side normal to that containing the arm.

Mast-arm-to-pole Connections

Fillet-welded gusseted boxes or ring-stiffened boxes at the mast-arm-to-pole connections tested in this project did not develop any fatigue cracking under both in-plane and out-of-plane loading. These connections were tested at various load levels and in some specimens were subjected to more than 40 million stress cycles. In all specimens, fatigue cracking occurred in

238

other critical details in the structure, such as the tube-to-transverse plate welds in the mast-arm and/or the pole, and/or handholes.

For built-up box connections, the width of the box should be the same as the diameter of the pole (i.e., the sides of the box are tangent to the sides of the pole).

Ring-stiffened box connections are more fabrication intensive and should be employed in geographic regions where support structures are expected to experience significant wind induced oscillations. In other regions, gusseted-box connections are expected to provide satisfactory performance.

Weld Geometry

Fillet-welds for tube-to-transverse plate connections were specified as unequal leg welds, with the long leg of the fillet-weld along the tube. The termination of the longer weld leg was specified to subtend approximately 30º angle on the tube. Significant scatter was observed in the test results, however, where unequal leg fillet-weld was used. This scatter in test results could be partially attributed to the variation in the fabricated weld geometry and particularly the weld toe angle from the specified nominal value. In a thin walled tubular structure, the weld acts as a tiny stiffener and affects the geometric stresses and the fatigue resistance of welded connections. The weld geometry should be controlled by tighter tolerance to reduce the scatter in fatigue performance of tube-to-transverse plate connections in the support structures.

Assessment of Connection Fatigue Performance

Fatigue cracking in the subject tubular structures mostly precipitate due to magnified (displacement induced) local stresses that are dependent on the geometric parameters of the components at a connection. For adequate assessment of fatigue performance of tubular connections, effect of the geometric parameters must be addressed. A point measure of maximum principal stress on the tube surface at $0.1\sqrt{(r \times t)}$ ahead of the weld toe (where, r is the radius and t is the thickness of the tube), can adequately capture the geometric stress and define the finite life performance of the connections. To achieve infinite life, fatigue cracking at the weld toe or weld root notch must also be contained. The maximum principal stress at a 0.04 in (1 mm) rounded weld toe captures the notch stress and is appropriate for infinite life design against fatigue cracking from the weld toe. Equations for geometric and notch stress concentration factors developed in this research provides an efficient means of defining fatigue resistance of tube-to-transverse plate connections of diverse geometric parameters and weld configuration in both round and multi-sided sections. Fatigue resistance of new connections determined by analytically, should be verified experimentally both in the finite and infinite life regimes.

FURTHER RESEARCH

Although the research performed under NCHRP Project 10-70 developed cost-effective and fatigue resistant solutions for most commonly used connection details in the subject structure, performance of a few connection details could not adequately evaluated due to limited budget. Additional research is recommended to evaluate these details and to address additional parameters that were proven to be critical during the performance of this research.

Clamp-type Mast-arm-to-pole Connection

Four clamp-type mast-arm-to-pole connections tested under this project developed premature cracking from fillet-welded arm-to-clamp weld toe on the clamp A closer inspection of the weld toe on the clamp at the crack location indicated sharper termination and undercut on the clamp. This detail has been reported to be successfully used in New Jersey and other states. A comprehensive evaluation of this connection with proper quality control of the welds may be pursued.

Stool-type Stiffened Tube-to-transverse Plate Connection

Despite encouraging FEA results, the fatigue performance of the stool type stiffened tube-to-transverse plate connections did not perform well. These connections developed fatigue cracking from the toe of wrap around weld at the termination of the vertical stiffeners. The welds were of less than acceptable quality having significant undercutting at the toe. The stool type connections in Iowa have exhibited excellent performance in service, but in larger diameter (22 in [559 mm] to 34½ in [876 mm]) and thicker tubes ($^5/_{16}$ in [8 mm] and $^{11}/_{16}$ in [17 mm]). As such, it is suggested that the fatigue performance of this connection be evaluated in larger diameter and thicker tubes, with tighter quality control of the welds.

Fillet-welded T-, Y-, and K- Connections

Due to limited budget and less application in cantilevered structures, fatigue resistance of the fillet-welded T-, Y-, and K- tube-to-tube, angle-to-tube, and plate-to-tube connections were not established by testing in this research. The fatigue resistance of these connections in Table 11–2 of the AASHTO Specification for Highway Signs, Luminaire and Traffic Signal Structures has been retained from the previous edition of the specification, which corresponds to the classification for cyclic punching shear stress in tubular members specified by the AWS D1.1 based on research in the offshore industry on connections of thicker and larger diameter tubes. Stresses in tubular connections are strongly dependent on their geometric parameters. As such, extrapolation of the fatigue design provisions from the AWS Specification may not be consistent with the performance of these connections in service. The provision of cyclic punching shear stress is also recommended for arm to pole connection in the current specification. The current research, however, showed that the provisions are not applicable to these details. Further research should be conducted to provide a better estimate of the fatigue resistance of these connections.

Effect of Weld Geometry

The effects of weld geometry were not considered as a variable in the current research. All fillet-welds were specified to have a nominal 30^0 angle at the termination on the tube in a tube-to-transverse plate connection. All specimens were tested in as-fabricated condition, to replicate the condition in practice. During execution of this project, the weld geometry appeared to be a significant parameter affecting fatigue performance of the connections. Significant scatter was observed in the test results due to the variation in the fabricated weld geometry and particularly the weld toe angle from the specified nominal value. In a thin walled tubular structure, the weld acts as a tiny stiffener and affects the geometric stress at the connection. The weld toe angle also affects the notch stress and the fatigue resistance of welded connections.

Limited analytical studies performed in this research showed that the variation in fatigue resistance was more significant for a decrease rather than an increase in weld angle from the specified value of 30^0. The results also indicated that the decrease in fatigue resistance due to an increase in weld angle from 30^0 to 45^0 is much less compared to the variability introduced in the weld geometry and the resulting fatigue resistance in an effort to fabricate the unequal weld. Effect of weld geometry on the fatigue performance of the connections should be researched further for developing controlled tolerance to reduce the scatter in fatigue performance of connections in the support structures.

REFERENCES

1. Kaczinski, M.R., Dexter, R.J., and Van Dien, J.P., "Fatigue-Resistant Design of Cantilevered Signal, Sign and Light Supports." *NCHRP Report 412,* Transportation Research Board, Washington, D.C. (1998) 176 pp.

2. Fisher, J.W., Miki, C., Slutter, R.G., Mertz, D.R., and Frank, W., "Fatigue Strength of Steel Pipe-Base Plate Connections." *Engineering Structures,* Vol. 5, No. 2 (1983) p. 90.

3. Koenigs, M.T., Botros, T.A., Freytag, D., and Frank, K.H., "Fatigue Strength of Signal Mast Arm Connections." *FHWA/TX-04/4178-2,* Texas Department of Transportation, Austin, TX (2003) 218 pp.

4. Ocel, J.M., Dexter, R.J., and Hajjar, J.F., "Fatigue-Resistant Design for Overhead Signs, Mast-Arm Signal Poles, and Lighting Standards." *MN/RC-2006-07,* Minnesota Department of Transportation, St. Paul, Minnesota (2006) 190 pp.

5. The International Institute of Welding (IIW/IIS), *Fatigue Design Procedure for Welded Hollow Section Joints,* Zhao, X-L., and Packer, J.A. eds*.,* Abington Publishing, Cambridge, England (2000) 90 pp.

6. Zhao, X.L., Herion, S., Packer, J.A., Puthli, R.S., Sedlacek, G., Wardenier, J., Weynand, K., van Wingerde, A.M., and Yeomans, N.F., *Design Guide for Circular and Rectangular Hollow Section Welded Joints under Fatigue Loading*, TUV-Verlag, Koln, Germany (2000) 121 pp.

7. Alderson, J.L., "Fatigue Study of Cantilevered Traffic Signal Mast Arms." M.S. thesis, University of Missouri-Columbia, Columbia, MO (1999) 120 pp.

8. Deschamp, B., "Fatigue Testing of Traffic Signal Structures." M.S. thesis, University of Wyoming, Laramie, WY (2002) 136 pp.

9. South, J.M., "Fatigue of Tube-to-Plate Fillet Welds and Methods for Their Improvement." *FHWA/IL/PR-118,* Illinois Department of Transportation, Springfield, IL (1997) 43 pp.

10. Xiao, Z.-G. and Yamada, K., "Fatigue Evaluation of Steel Post Structures." *Structural Engineering/Earthquake Engineering,* Vol. 20, No. 2 (2003) p. 119.

11. Miki, C. and Sugimoto, M., "A Study on U-Shaped Rib Configuration with High Fatigue Resistance." *IIW Document No. XIII-1885-01,* International Institute of Welding, Paris, France (2001) 13 pp.

12. Archer, G.L. and Gurney, T.R., "Fatigue Strength of Mild Steel Fillet Welded Tube to Plate Joints." *Metal Constr Brit Weld J,* Vol. 2, No. 5 (1970) p. 207.

242

13. Marshall, P.W., "Designing Tubular Connections with AWS D 1.1." *Welding Journal (Miami, FL),* Vol. 68, No. 3 (1989) p. 45.

14. Marshall, P.W. and Toprac, A.A., "Basis for Tubular Joint Design." *Welding Journal,* Vol. 53, No. 5 (1974) p. 192.

15. Munse, W.H. and Grover, L.M., *Fatigue of Welded Steel Structures*, Welding Research Council (1964) 210 pp.

16. Efthymiou, M., "Development of SCF Formulae and Generalised Influence Functions for Use in Fatigue Analysis." OTJ88: Conference on Recent Developments in Tubular Joints Technology, Englefield Green Near Egham, Surrey, U.K., *Proceedings* Vol. 2 (1988) pp. 1-33.

17. Smedley, P. and Fisher, P., "Stress Concentration Factors for Simple Tubular Joints." First International Offshore and Polar Engineering Conference, Edinburgh, United Kingdom, *Proceedings* Vol. 4 (1991) pp. 475-483.

18. Transportation Pooled Fund Study TPF-5(116): Investigation of the Fatigue Life of Steel Base Plate to Pole Connections for Traffic Structures, *Progress Report* (January 2007) (http://www.pooledfund.org/projectdetails.asp?id=348&status=6)

19. Dexter, R.J. and Ricker, M.J., "Fatigue-Resistant Design of Cantilevered Signal, Sign, and Light Supports." *NCHRP Report 469,* Transportation Research Board, National Research Council, Washington, DC (2002) 76 pp.

20. Peiffer, J.P., Puckett, J.A., and Erikson, R.G., "Fatigue Testing of Ring-stiffened Traffic Signal Structures." *FHWA-WY-08/05F*, Wyoming Department of Transportation, Laramie, WY (2008) 74 pp.

21. Radaj, D. and Sonsino, C.M., *Fatigue Assessment of Welded Joints by Local Approaches*, Abington Publishing, Cambridge (1998) 639 pp.

22. Roy, S. and Fisher, J.W., "Enhancing Fatigue Strength by Ultrasonic Impact Treatment." *Int. J. Steel Structures,* Vol. 5, No. 3 (2005) p. 241.

23. Clayton, A.M., Irvine, N.M., "Stress Analysis Methods for Tubular Connections." European Offshore Research Seminar, Paper 30 (1978) pp. 1-12.

22. Koob, M.J., "Base Connection Retrofits for High Mast Towers and Pole Luminaries." First International Conference on Fatigue and Fracture in the Infrastructure, Philadelphia, PA, *Proceedings* (2006).

23. ABAQUS, *ABAQUS ver. 6.10*, (Province, RI: Dassault Systems Simulia Corp., 2010).

24. SigmaPlot, *SigmaPlot 10 User's Guide*, (San Jose, CA: Systat Software Inc., 2006).

25. Marquardt, D.W., "An Algorithm for Least Squares Estimation of Parameters." *Journal of the Society of Industrial and Applied Mathematics*, Vol. 11 (1963) pp.431-441.

26. Fouad, F.H., Calvert, E. A., and Nunes, E. "Structural Supports for Highway Signs, Luminaries, and Traffic Signals." *NCHRP Report 411*, Transportation Research Board, National Research Council, Washington, D.C. (1999) 114 pp.

27. Richman, N.B., "Fatigue Life Investigation of High Performance Mast Arm Base Plate Connections." M.S. thesis, University of Texas at Austin, Austin, TX (2009) 145 pp.

28. Stam, A.P., "Fatigue Performance of Base Plate Connections Used in High Mast Lighting Towers." M.S. thesis, University of Texas at Austin, Austin, TX (2009) 116 pp.